NONLINEAR STABILITY OF FLOWS OVER RIGID AND FLEXIBLE BOUNDARIES

Michael Dominic Thomas

A Thesis Submitted for the Degree of PhD
at the
University of St Andrews

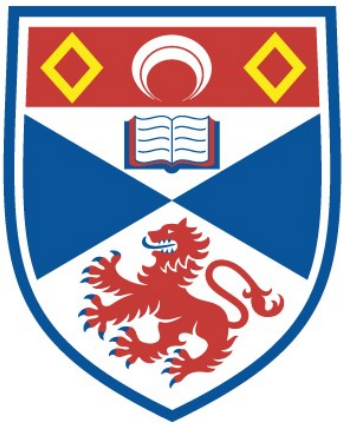

1990

NONLINEAR STABILITY OF FLOWS OVER RIGID AND FLEXIBLE BOUNDARIES

by

Michael Dominic Thomas

Submitted for the degree of Doctor of Philosophy at the University of St. Andrews

ProQuest LLC.
789 East Eisenhower Parkway
P.O. Box 1346
Ann Arbor, MI 48106 – 1346

Abstract

This work assesses the importance of nonlinearity in the stability of flows over compliant and rigid walls, and comprises three main parts. The first part considers inviscid flow with a free surface over a flexible boundary. The dispersion relation is obtained, and the conditions for linear instability investigated. The linear dispersion relation is then used to show that the conditions for nonlinear three-wave resonance are often met. In some circumstances, the resonance may be of 'explosive' sort, involving waves of opposite energy sign; but non-explosive resonant configurations are most common. Next, the wave-amplitude evolution equations for three-wave resonance are derived, firstly by a 'direct' approach, and then via a variational (averaged Lagrangian) method. Results agree with those of Case & Chiu (1977) for capillary-gravity waves, and Craik & Adam (1979), for three-layer fluid flow, on taking the appropriate limits. We also consider a nonlinear model for the flexible boundary.

In the second part, stability of Blasius flow over a compliant surface is studied. This extension of rigid-wall work of Craik (1971) and Hendriks (appendix to Usher & Craik 1975) determines the quadratic interaction coefficients of three-wave resonance, and complements the linear analysis of Carpenter & Garrad (1985, 1986) and others. First, the linear eigenvalue spectrum is investigated for various values of the wall parameters. Then, resonant triads are located and the quadratic interaction coefficients determined numerically. By way of introduction some rigid-wall results are also presented, extending those of Hendriks.

Acknowledgements

The author was supported during this work by a SERC (CASE) Research Studentship, in collaboration with the Procurement Executive, Ministry of Defence. January–March 1988 was spent at the Indian Institute of Technology, Delhi, where the author was under the guidance of Professor P. K. Sen. He is most grateful to Professor Sen for the invaluable assistance he received during this period, and subsequently, and also to the IIT authorities for providing a generous research scholarship. Substantial financial assistance for the visit was also received from the Admiralty Research Establishment. The author would like to thank Dr. D. J. Atkins, Mr. A. V. Yorke and Dr. A. N. Hicks for their help during two profitable summer stays at ARE Teddington.

First and foremost, though, I would like to thank my supervisor, Professor Alex D. D. Craik, without whose expansive knowledge of and great insight into the subject of fluid mechanics this work could not have been possible. I am much indebted to him.

Declaration

I, Michael Dominic Thomas, hereby certify that this thesis has been composed by myself, that it is a record of my own work, and that it has not been accepted in partial or complete fulfilment of any other degree or professional qualification.

Signed Date 21/9/89.

(Michael D. Thomas)

Certificate

I, as supervisor of the candidate, hereby certify that he has fulfilled the conditions of the Resolution and Regulations appropriate to the Degree of Ph.D.

Signed Date 22/9/89

(Alexander D. D. Craik)

Research History

I was admitted as a Research Student to the Faculty of Science of the University of St. Andrews under Ordinance General No. 12 on 1st October 1986, and as a candidate for the degree of Ph.D. on 1st October 1987.

Signed Date 21/9/89.

(Michael D. Thomas)

Nomenclature

Roman

c	phase speed
d	damping coefficent
h	mean fluid depth (Chapter 2), step size (Chapters 3 and 4)
$\mathbf{k}$	wavenumber vector (Chapter 2)
m	wall mass per unit span
R	Reynolds number
S	wall restoring force
F	wall tension
t	time co-ordinate
U,$\bar{u}$	fluid flow speed
x	streamwise co-ordinate
y	transverse co-ordinate
z	vertical co-ordinate

Greek

α	streamwise wavenumber
β	transverse wavenumber
γ	surface tension (Chapter 2), oblique wavenumber (Chapter 3)
δ	boundary layer thickness
ϵ	ordering parameter
ς	free-surface displacement
η	wall displacement
ρ	density
ν	kinematic viscosity
Φ, φ	velocity potential
Φ, ϕ	stream function
ψ	adjoint stream function
ω	frequency

Subscripts

0	reference value
∞	value in free stream
i	imaginary part of complex quantity
m	value pertaining to wall material
r	real part of complex quantity
w	value at wall

Abbreviations

c.c.	complex conjugates
n.l.t.	nonlinear terms

Contents

Chapter 1 Introduction

1.1 Motivation

An understanding of flows over flexible boundaries is of technological and scientific importance, mainly because of the potential benefits of drag and noise reduction for marine craft. Since a fully nonlinear analysis of such problems is presently impossible, previous studies have concentrated on the linear stability of such flows. The present resurgence of interest in this area is largely due to encouraging experimental results by Gaster (unpublished) and Gad-el-Hak (1986). Recent studies by Carpenter (1985), Carpenter & Garrad (1985, 1986) and Yeo (1987) survey the earlier literature at length and present new theoretical and computational results based on linear stability theory.

However, little systematic theoretical work has yet been done on nonlinear aspects of such problems, despite the well-developed state of weakly-nonlinear stability theory, both for fluid flows between rigid boundaries and for interacting interfacial waves (see for example Craik 1986a). In Chapters 2, 3 and 4 of this work we focus on simple weakly-nonlinear models that yield insight into the role of nonlinearity in such flow configurations, and in particular into the potential importance of resonant interactions.

There are several reasons why three-wave resonance can be of importance. Firstly, this weakly-nonlinear interaction occurs at quadratic order in wave amplitude, and therefore can be expected to often be of more significance than the cubic-order interaction studied by Stuart (1960) and Watson (1960). This is particularly likely to be so at smaller wave amplitudes.

Secondly, three-wave resonance provides a mechanism for the development of three- dimensionality in the transition to turbulence of shear flows: the work of Craik (1971) and others has shown that certain forms of resonant triad in viscous shear flows exhibit remarkably large quadratic interaction coefficients, these being $O(R)$ for sufficiently large Reynolds number R. This mechanism has received qualitative support from the experimental investigations of Kachanov & Levchenko (1984), Saric & Thomas (1984) and others.

1.2 The Navier-Stokes equations and the linear approximation

The starting point for all that follows is the incompressible Navier-Stokes

equations

$$\frac{\partial \mathbf{u}}{\partial t} + (\mathbf{u}.\nabla)\mathbf{u} = \mathbf{F} - \frac{1}{\rho}\nabla p + \nu\nabla^2\mathbf{u}, \tag{1.1a}$$

$$\nabla.\mathbf{u} = 0, \tag{1.1b}$$

where $\mathbf{u}$ is the total fluid velocity, and $\mathbf{F}$ is a body force. At rigid boundaries the flow must be exactly zero (no tangential slip, and no normal velocity). The no-slip condition does not obtain for inviscid flows. For flows with deformable boundaries the exact boundary conditions are (i) all velocity components must be continuous, and (ii) shear stress and normal stress must both be continuous across any boundary.

For inviscid, irrotational flow we can define a velocity potential Φ by $\mathbf{u} = \nabla\Phi$; then (1.1b) becomes Laplace's equation

$$\nabla^2\Phi = 0 \tag{1.2}$$

and (1.1a) can be re-expressed as the unsteady Bernoulli equation

$$\frac{\partial \Phi}{\partial t} + \frac{1}{2}\nabla\Phi.\nabla\Phi + gz + \frac{p}{\rho} = f(t), \tag{1.3}$$

on taking $\mathbf{F} = -gz\mathbf{k}$. If we assume that some basic flow $\mathbf{U}$ satisfying (1.1) is perturbed by infinitesimal travelling waves of the form $\exp\{ik(x - ct)\}$, the problem becomes an eigensystem: solutions for Φ at a given wavenumber k will only exist for certain values of the phase speed $c = c_r + ic_i$. Evaluation of (1.3) at boundaries (where we impose conditions on the pressure) yields a linear dispersion relation for the problem. This can be obtained explicitly for many inviscid flow problems. Several distinct solutions for c will in general exist at a given k: these represent different wave modes. For example, in many situations pairs of upstream and downstream propagating waves will be supportable on any deformable boundaries that are present (such as free surfaces or compliant walls).

The dispersion relation can be written generically as

$$D(\omega, k) = 0. \tag{1.4}$$

In simple cases the degree of this equation is equal to the number of wave-modes that the system supports. The dispersion relation (1.4) can often be written in terms of two or more smaller systems that are coupled to some extent:

$$D(\omega,k) = D_1(\omega,k)D_2(\omega,k) - \Lambda^2(\omega,k). \tag{1.5}$$

Here Λ^2 provides a direct measure of the strength of the coupling; in the limit $\Lambda \to 0$ the systems are completely uncoupled, and we may write

$$D_1(\omega_1,k) = D_2(\omega_2,k) = 0, \tag{1.6}$$

In practice Λ is negligible except when ω_1 and ω_2 are almost equal: $\omega_2 = \omega_1 + \delta$, $|\delta| \ll 1$. Cairns (1979) has examined mode coupling using the concept of wave energy; he has shown that, for conservative (non-dissipative) systems, the energy W of a given wave may be expressed as

$$W = \frac{1}{4}\omega_j \frac{\partial D}{\partial \omega_j}|A|^2, \tag{1.7}$$

where A is the wave amplitude. Of course, D has to be suitably defined in some frame of reference in order to be meaningful. The frequency ω will normally be real for non-dissipative systems.

If we suppose that $\omega = \omega_1 + \Delta$, $|\Delta| \ll 1$, then

$$\begin{aligned}
&D_1(\omega_1+\Delta,k)D_2(\omega_2+\Delta-\delta,k) - \Lambda^2 = 0,\\
\Rightarrow &\Delta\frac{\partial D_1}{\partial \omega_1}(\Delta-\delta)\frac{\partial D_2}{\partial \omega_2} - \Lambda^2 \approx 0,\\
\Rightarrow &\Delta^2 - \Delta\delta - \left(\frac{\partial D_1}{\partial \omega_1}\frac{\partial D_2}{\partial \omega_2}\right)^{-1}\Lambda^2 = 0,
\end{aligned}$$

giving

$$\Delta = \frac{1}{2}\left[\delta \pm \sqrt{\delta^2 + 4\Lambda^2\left(\frac{\partial D_1}{\partial \omega_1}\frac{\partial D_2}{\partial \omega_2}\right)^{-1}}\right]. \tag{1.8}$$

It is clear, on remembering that all quantities in the discriminant of (1.8) are real, that if $\frac{\partial D_1}{\partial \omega_1}$ and $\frac{\partial D_2}{\partial \omega_2}$ are both positive then the roots ω_1 and ω_2 will remain real and distinct. If, however, the product $\frac{\partial D_1}{\partial \omega_1}\frac{\partial D_2}{\partial \omega_2}$ is sufficiently negative then ω_1 and ω_2 will form a complex-conjugate pair. In other words, the two roots

coalesce, one of them becoming unstable whilst the other evanesces. The range of wavenumbers over which the instability extends is of course dependent upon the nature of the dispersion curves ω versus k for the two parcipitating wave-modes: the interaction can only occur where these curves are sufficiently near to each other.

The wave energy $W \equiv \frac{1}{4}\omega_j \frac{\partial D}{\partial \omega_j}|A|^2$ can be *negative*, in an appropriately chosen frame of reference: the creation of such a wave results in a reduction of the total energy of the system. For example, an otherwise upstream-propagating wave that is forced to travel downstream by a sufficiently strong basic flow U will possess negative energy. It is clear from the above simple model that interaction of two waves of opposite energy sign will result in instability (due to the negative discriminant), whereas waves of like sign will not: in fact, in the latter case the waves will exchange identities. Both possibilities are well illustrated in Chapter 2 below.

Negative-energy waves have the important property of being driven unstable by dissipative processes, such as viscosity, or damping in a flexible wall. This phenomenon was the subject of a fine theoretical study by Benjamin (1963): he was able to place the possible wave-modes for this combined fluid-solid problem into three classes, according to their behaviour as damping is introduced into the system. Class A consisted of negative-energy waves, and orthodox positive-energy waves were defined as belonging to Class B. The third category, Class C, was reserved for those modes that are not significantly affected by dissipation. Benjamin was able to show that the well-known Tollmien-Schlichting instability waves are in fact Class A. The classical Kelvin-Helmholtz instability is Class C, and modes on flexible walls can also be of this type, although they mainly belong to Class B (see below).

It should be noted that for dissipative systems, such as viscous shear flows, the validity of Cairns' simple interaction model is (as he admits) rather dubious. The presence of a critical layer (that is, the neighbourhood of a point z_c where $\bar{u}(z_c) - c_r = 0$) would unquestionably be of importance, and there is also a difficulty in defining wave energy for non-neutral modes— which are, of course, the norm in such systems. One can nevertheless make tentative deductions,

at least for modes that are in some sense 'near-neutral'. If we allow δ to be complex, then clearly the solutions for Δ will not comprise a conjugate pair, whatever the value of $\mathrm{Re}\{\frac{\partial D_1}{\partial \omega_1}\frac{\partial D_2}{\partial \omega_2}\}$. Hence we do not in general expect to observe modal coalescence in dissipative systems: instead, some form of near-coalescence is likely. This is indeed found to be the case (see Chapter 4 below).

1.3 Nonlinear theories

There are basically two kinds of nonlinear theory. In the first kind, which is the most general, one considers arbitrarily large disturbances in the context of the full, unapproximated Navier-Stokes equations. Integral inequalities are used to provide bounds on various flow properties, for example disturbance energies, and in this way one obtains stability criteria. These take the form of necessary or sufficient conditions for growth or decay with time. The principal advantage, of course, of this approach is the lack of assumptions about the nature of the disturbance. However, for many flow problems, such as shear flows, the stability criteria thus obtained are much too imprecise to provide useful information.

A second type of theory is a rational extension of the fact that linear theory is valid for disturbances which are in some sense sufficiently small; but strictly speaking for any non-zero wave amplitude linear results are nevertheless only an approximation. A sequence of successive approximations is obtained by expanding in powers of a dimensionless wave amplitude. This kind of approach is termed 'weakly-nonlinear', and has proved very fruitful in illuminating underlying physical processes. Not all weakly-nonlinear theories have been developed with full regard to mathematical rigour, but very often this comes later as the fundamental physics becomes more clear. We shall be considering weakly nonlinear theory in chapters 2, 3 and 4 of this work.

Nonlinear interactions may involve one mode only, or several. The former case is known as 'self-interaction', and was the subject of important studies by Stuart (1960) and Watson (1960), using amplitude-expansion techniques. Watson decomposed an initial disturbance into Fourier components— in other words, into a fundamental mode and an infinite series of associated harmonics. This yielded a sequence of ordered equations, which could be then solved suc-

cessively.

Most of the work presented below is concerned with resonant triad interactions. A resonant triad exists if there are three wave-modes of frequencies ω_j and wavenumbers $\mathbf{k}_j$ for which $\sum_{j=1}^{3} \omega_j = 0$, $\sum_{j=1}^{3} \mathbf{k}_j = \mathbf{0}$. The principal importance of the resonant triad interaction is that it is an $O(A^2)$ phenomenon, where A is wave amplitude— other nonlinear effects, such as self-interaction or mean-flow modification, typically occur at $O(A^3)$ or higher, and so only become important at higher amplitude levels. For this reason it has been suggested that the resonant triad interaction can play a major rôle in the transition of flows from the laminar to turbulent regimes.

The interaction equations may be written in their most general form as

$$\left(\frac{\partial}{\partial t} + \mathbf{v}_j.\nabla\right) A_j + \sigma_j A_j = \lambda_j A_{j+1}^* A_{j+2}^*, \qquad j = 1,2,3 \tag{1.9}$$

on truncating at $O(A^3)$. Indices are evaluated modulo three in (1.9), and * represents complex conjugation. The group velocity of the jth wave is represented by $\mathbf{v}_j$, and linear growth or decay by the factors σ_j. These equations are only valid for a finite range of A; at sufficiently large amplitudes, higher-order terms must be retained. Thus in terms of an evolving time t, some time t_0 may arrive at which (1.9) no longer have validity: indeed, A_j may become infinite at some time, in which case we have 'breakdown'.

In seeking ever greater accuracy and validity of solutions, increasing use has been made of the computational facilities that are now available and which indeed continue to be enhanced. The Navier-Stokes equations have been tackled directly by several research groups, following the pioneering work of Fasel (1976). Others have looked to extend the tried and tested weakly-nonlinear theories to ever-higher orders of wave amplitude: indeed, extrapolations to *infinite* order have been accomplished, with some success; the work of Sen and co-workers (Sen & Venkateswarlu 1983; Sen, Venkateswarlu & Maji 1985, etc.) is a good example. Computational fluid dynamics is now viewed by many as comprising a virtually self-contained subject in its own right, and many of the most exciting current developments are occurring in this area, but more traditional approaches will surely always have a place, as it is never easy to gain

understanding from numerical data alone. We believe that the work presented below represents an appropriate blend of theoretical analysis and, where necessary, numerical investigation.

1.4 Solutions of the resonant-triad interaction equations

Since this work is in large measure concerned with resonant triad interactions, it is appropriate to present here a brief summary of the known solutions to the three-wave resonant interaction (3WRI) equations, for later reference. A much fuller account is given in the monograph of Craik (1986a). The equations may be written in the form (1.9).

1.4.1 Conservative systems

Firstly we shall consider conservative systems, for which the quadratic interaction coefficients λ_j can all be taken as real quantities. We shall also take the linear damping/amplification factors σ_j to be all zero, and so (1.9) is simplified to

$$\left(\frac{\partial}{\partial t} + \mathbf{v}_j.\nabla\right) A_j = \lambda_j A_{j+1}^* A_{j+2}^*, \qquad j = 1,2,3 \qquad (1.9)'$$

Exact solutions for the $A_j(t)$ are then known in terms of Jacobi elliptic functions if there is no spatial variation. If the signs of λ_j differ, then the known solutions are mostly periodic, but there are non-periodic limiting cases (see for example Bretherton 1964). If the signs of λ_j are all the same then a singularity may develop at a finite time $t = t_0$; this is often referred to as 'explosive' breakdown. The total energy of the system is conserved, however, and breakdown will in fact only occur if the wave actions E_j/ω_j have the same sign. Numerous examples of this have been found in plasma physics— see Weiland & Wilhelmsson (1977). Craik & Adam (1979) studied three-layer Kelvin-Helmholtz flow, and found that this scenario supported both periodic and explosive sorts of triad, even in linearly stable cases. Ma (1984) studied a simpler Kelvin-Helmholtz flow problem, and found that triads only existed for linearly unstable flows. In Chapter 2 below we present similar findings for inviscid flow over flexible walls.

For near-resonance, we have $\sum_{j=1}^{3} \mathbf{k}_j = \mathbf{0}$ as before but $\sum_{j=1}^{3} \omega_j = \Delta\omega$. This yields interaction equations similar to (1.9)' but with exponential factors

$\exp(-i\Delta\omega t)$ on the right-hand-sides. These too have solutions expressible in terms of elliptic functions, but the total energy is no longer a constant.

An important special case is when one of the waves, say A_1, has a much larger amplitude than the others. Then we have in the linearised approximation

$$\frac{dA_1}{dt} = 0, \qquad \frac{dA_{2,3}}{dt} = \lambda_{2,3} A_1^* A_{3,2}^*, \tag{1.10}$$

or equivalently

$$A_1 = A_1^{(0)} \text{ (constant)}, \quad \frac{d^2 A_{2,3}}{dt^2} = \lambda_2 \lambda_3 |A_1^{(0)}|^2 A_{2,3}. \tag{1.11}$$

If λ_2 and λ_3 have opposite signs then periodic solutions for A_2 and A_3 exist with frequency $|A_1^{(0)}|$. Otherwise, there are solutions with exponential growth/decay rates $\pm|A_1^{(0)}|$. For waves in fluid at rest, each λ_j has the same sign as the corresponding ω_j; and A_2, A_3 remain much smaller than A_1 except when the latter has the largest frequency $|\omega|$. In this case, A_1 is unstable to A_2 and A_3; plasma physicists call A_1 a 'pump-wave' when it is able to boost the amplitudes of the other two waves, and the instability of these others is known as 'parametric resonance'. If the λ_j all have the same sign then the growth of A_2 and A_3 is limited by depletion of A_1 at larger amplitudes, and periodic modulations ensue.

The pump-wave approximation can also be applied to three waves varying in both time and space, with one wave dominant (Craik & Adam 1978). This of course breaks down when the waves become of comparible magnitude, unless the pump-wave is artificially maintained at constant amplitude. In this latter case the governing equations reduce to the Klein-Gordon equation

$$\frac{\partial^2 A}{\partial t^2} - a\frac{\partial^2 A}{\partial x^2} - b\frac{\partial^2 A}{\partial y^2} - dA = 0, \tag{1.12}$$

which is easily solvable.

The conservative 3WRI equations (1.9)′ for undamped waves may be solved by the method of inverse scattering; solutions are known in two, three and four dimensions. The reader is referred to the review articles of Kaup, Reiman & Bers (1979) and Kaup (1981) for details on the inverse-scattering method. The

two-dimensional solutions comprise (i) closed form n-solitons, which only exist if the λ_j have differing signs, and (ii) a continuous spectrum, whose contribution is not time-decaying (because the conservative 3WRI are non-dispersive in the linear limit) and therefore is of equal importance to the soliton solutions.

In three or four dimensions there are 'n-lump' solutions rather like the n-solitons, which however do not arise from discrete bound-state eigenvalues. The one-lump solution is 'phase-locked'. A set of solutions are said to be phase-locked when their collective existence requires that certain quantities, such as linear frequencies, or perhaps the arguments of complex nonlinear interaction coefficients, must be related to each other by some (often simple) condition.

1.4.2 Linearly damped conservative systems

If one or more of the waves is linearly damped or amplified, then the inverse-scattering method cannot be applied and indeed few analytic solutions are known to equation (1.9). If the growth/damping rates are all equal and there is no spatial dependence then (1.9) can be reduced to the undamped system (1.9)′ by a transformation; but if only one wave has non-zero damping then other solutions exist which resemble those for a nonlinear, damped, simple pendulum.

Wersinger, Finn & Ott (1980a,b) examined the 3WRI equations for near-resonant triads with frequency mismatch $\Delta\omega$ for which the wave of greatest frequency is linearly amplified and the others are linearly damped. Temporal evolution only was studied. A remarkably rich solution set was found, comprising periodic orbits that bifurcate through period-doubling to ever more complex forms, and also other solutions exhibiting the chaotic behaviour of a 'strange attractor'.

1.4.3 Non-conservative systems

Craik (1971) gave some particular solutions to the non-conservative 3WRI equations (1.9). If all three waves are linearly damped or linearly amplified then there are periodic solutions, the wave phases being inter-dependent. Further solutions exist if the oblique growth/damping factors σ_1 and σ_2 are equal, for which any two of the wave phases are arbitrary; moreover, if σ_1 and σ_2 are not

too large then sigularities in finite times are possible. Recently some solutions for the case of temporal and spatial variation have been discovered (Craik 1986b, 1987). These have some similarities with the conservative 'one-lump' solutions, and like them are phase-locked. Here again the wave-amplitudes may exhibit finite-time explosion.

1.4.4 Higher-order effects

A more accurate approximation to three-wave resonant-triad interactions is gained by retaining third-order terms: instead of (1.9), we then have

$$\frac{dA_1}{dt} + \sigma_1 A_1 = c_{23} A_3 A_2^* - \mathrm{i} A_1 \sum_{k=1}^{3} d_{1k} |A_k|^2,$$

$$\frac{dA_2}{dt} + \sigma_2 A_2 = c_{13} A_3 A_1^* - \mathrm{i} A_2 \sum_{k=1}^{3} d_{2k} |A_k|^2, \qquad (1.13\mathrm{a,b,c})$$

$$\frac{dA_3}{dt} + \sigma_3 A_3 = c_{12}^* A_1 A_2 - \mathrm{i} A_3 \sum_{k=1}^{3} d_{3k} |A_k|^2.$$

It will be seen that there are nine cubic-order interaction coefficients d_{ij}: the real parts of these give rise to amplitude-dependent frequency shifts, whereas the imaginary parts yield additional growth or damping terms. For conservative cases, $\sigma_j = 0$ and the c_{ij} and d_{ij} are purely real, and there are no unbounded solutions. Cases which are explosive in the absence of third-order terms typically exhibit 'repeated stabilised explosions' when such terms are included. For non-conservative systems, if $c_{ij} \neq 0$ then only approximate analytic solutions are known, though numerical solution is not unduly difficult. Usher & Craik (1975) examined cubic-order three-wave interactions, both resonant and non-resonant, in shear flows, using asymptotic (large Reynolds number) estimates. It was found that the third-order interaction coefficients could be large, and like their second-order counterparts (studied in Chapters 3 and 4 below) could influence the growth of oblique modes in Craik-type triads.

1.5 Review of experimental work on flows over compliant walls

Previous work on stability of flows over flexible walls is reviewed here and in the following section. Several excellent and more detailed reviews are already extant in the literature, and those by Carpenter & Garrad (1985), Riley, Gad-el-Hak & Metcalfe (1988) and Carpenter (1989) are particularly recommended.

The possiblity of compliant-wall induced drag reduction was first experimentally investigated by Kramer (1957, 1960); the stimulus for his work was provided by the idea that the surprising speed capability of the dolphin was due to the particular structure of its skin, which enabled it to maintain laminar flow over its body. Kramer conducted a series of experments (Kramer 1960, 1962, 1965) in open water, towing an axisymmetric body with a flushly-fitting compliant coating. The coatings he used consisted of an array of stubs surrounded by highly viscous damping fluid and enclosed within seamless rubber hose. He claimed to have achieved significant drag reduction for certain of the coatings, and put this down to their supposed property of 'distributed damping'.

Kramer's pioneering work naturally spurred others to take interest in compliant surfaces; however, over the next two decades his results were not validated by subsequent experiments and came to be regarded with considerable scepticism. Puryear (1962) conducted experiments in a towing tank using prolate spheroids partially covered with coatings resembling those of Kramer. Unfortunately his coatings exhibited an increase in drag of 2–6% compared with rigid ones; this was thought by Puryear to be the result of an insufficiently smooth join between the body nose and the coating, since cavitation and separation were wont to occur at the join. Carpenter & Garrad (1985) also infer that none of Puryear's coatings was equivalent to Kramer's best one.

Nisewanger (1964) used bodies of revolution with blunt noses, the first metre of which were covered with compliant coatings. These bodies were released from the bottom of a lake, being propelled to the surface by their own buoyancy. Once again, the compliant coatings showed increased drag compared with a rigid surface, this time about 6–11% more.

Ritter & Messum (1964) employed square flat-plate models for their experiments; they obtained at best only minimal drag reduction. Ritter & Porteous (1965) used a cylindrical body with an ellipsoidal nose, which was immersed in a water tunnel. The compliant coating was situated immediately aft of the nose, and a slot at the join enabled the removal of the boundary layer by suction, thereby ensuring laminar flow at the front of the coated region. Carpenter & Garrad (1985) claim that the coating used was probably comparable

to Kramer's softest coating, which would help to explain why no significant drag reduction was observed. The background turbulence level in the tunnel may also have been a factor.

Grosskreutz (1971, 1975) used flat-plate models with silicone-rubber coatings similar to those of Kramer, except that the stubs were inclined at 45° into the flow direction. A reduction in momentum thickness of 3.6% was obtained for a speed of 1.5 ms^{-1}, but adverse results were obtained for higher speeds.

In recent years their have been a number of experimental studies of the transition process. Gad-el-Hak *et al.* (1984) carried out a comprehensive investigation into laminar, transitional and turbulent flows over compliant surfaces. The apparatus consisted of a flat plate having a working section which could be filled with a soft PVC plastisol. Sophisticated flow-visualisation and measurement techniques were employed. Coatings of various thicknesses and shear moduli of rigidity were used, for various flow speeds $\bar{u}_\infty$. Large-amplitude 'static-divergence' waves appeared on the compliant surfaces in turbulent flow regimes, but not in laminar or transitional ones. Such waves are slow-moving, with speeds no more than 5% of $\bar{u}_\infty$, and have amplitudes of the order of the coating thickness. For the thicker coatings, the amplitudes were 20–40% of the undisturbed boundary-layer thickness, which was increased by the presence of the waves by up to 100%. The static-divergence waves only appeared if $\bar{u}_\infty$ exceeded a certain onset value, which was larger for thinner coatings; they never appeared under a laminar boundary layer, even for flow speeds of twice the onset values for turbulent regimes. Thus they cannot trip laminar flows into turbulent states. As $\bar{u}_\infty$ was increased, so the static-divergence waves exhibited increasing thee-dimensionality, developing significant amplitude modulations along their crests. This resulted in the creation of extra waves with shorter spans.

Gad-el Hak *et al.* conclude that static-divergence waves must be eliminated or at least mitigated in order to reduce drag on the surface. They refer to work of Ash at NASA, wherein the static-divergence waves were suppressed by covering the compliant coating with a thin and tightly stretched layer of Mylar. However, an additional and somewhat detrimental side-effect was a lessening of the dynamic response of the surface. The authors note that in the work of

Hanson & Hunston (1983) on flows over a rotating disc static-divergence waves were observed in laminar flows, provided that the rotational velocity was at least 1.6 times the corresponding onset speed for turbulent regimes.

M. Gaster and G. J. K. Willis have recently conducted a very important series of experiments using a towing tank at British Maritime Technology Ltd. (see Willis 1986). These experiments were conducted in tandem with a numerical investigation based on linear stability theory. The compliant surfaces consisted of silicone rubber or silicone oil compounds over which were stretched a thin latex rubber skin. The skin was an important feature, for it seems that it reduced the magnitude of tangential surface motion whilst permitting relatively free normal motions. (As described below, many theoretical models omit tangential surface motions). The coating was situated in a rectangular well on a flat plate. Flow disturbances were introduced in a controlled manner upstream of the plate and were of harmonic two-dimensional or point-source type. Disturbance growth and decay rates were measured downstream by hot-film probes. Particularly noteworthy of these experiments is the extreme care that was taken at every stage, be it measurement of the surface properties, keeping ambient turbulence levels very low or achieving a smooth coating surface and leading-edge joint.

Tests using a rigid surface gave results agreeing well with theory, particular for the variation of amplication factor with flow speed at given forcing frequencies. For the compliant surface tests, parameters were selected according to theoretical predictions of supression of Tollmien-Schlichting (TS) instabilities. Results were very encouraging, indicating substantial reductions in amplification factors relative to the rigid-wall case; indeed, for some conditions TS wave growth was reduced by an order of magnitude, leading to virtual elimination of this particular form of instability. Strong instabilities were restricted by the presence of a compliant surface to flow-speed regimes so much higher that they tended to take the form of travelling-wave flutter.

1.6 Review of theoretical work on flows over compliant walls

The early experimental works naturally inspired theorists to turn their attention to the analysis of compliant wall boundary-layer stability. The most

important of the pioneering theoretical contributions are those of Benjamin (1960, 1963) and Landahl (1962). Benjamin had previously considered the stability of flows over wavy boundaries (Benjamin 1959), expanding upon the work of Miles on wind-generated water waves (Miles 1957, 1959a,b). In his seminal work of 1960, Benjamin set out some of the fundamental aspects of compliant wall stability theory. He reasoned that the presence of a compliant boundary would certainly affect the thin friction layer adjacent to the wall, thereby influencing the generation there of Tollmien-Schlichting waves (termed Class A waves by Benjamin). Other possible mode-classes were also described (which could also exist in inviscid flows). Class B waves were a surface-resonance phenomenon, travelling at speeds close to the free-wave speed c_0 of the boundary. Class C waves were of Kelvin-Helmholtz type, and included instabilities arising from the coalescence of modes.

Benjamin considered wall models having negligible tangential motion, and introduced a response coefficient Z, characterising the effect of a fluid pressure wave on the wall motion. He expanded upon the linear stability theory of Tollmien (1929), Schlichting (1933) and Lin (1945) and was able to demonstrate that a flexible, non-dissipative wall could stabilise TS waves having velocities lower than c_0. For $Z_r > 0$, the neutral curves are shifted to lower wavenumbers α and higher Reynolds numbers R. Dissipative flexible walls were shown to destabilise TS waves through internal damping (this was also found by Betchov 1960).

Benjamin's analysis suggested that boundary-layer stabilisation could be effected using two very different types of flexible walls, which may be called 'resonant' and 'compliant' surfaces. 'Resonant' surfaces would have c_0 close to the phase speed of the most rapidly growing Class A instability. Hence Class A and Class B waves would have similar phase speeds and any interaction might have a favourable effect on the wall friction layer. It was believed that Kramer's coating was of this type. The present author regards such surfaces as being most unsuitable for transition delay, as linear modal interactions have a strong tendency to produce very severe instability (see Chapter 4 below). 'Compliant' surfaces would be sufficiently flexible to have a large negative value of Z_r, yet

would also have negligible internal damping. Such a surface could stabilise Class A instabilities, but c_0 would have to be large enough to avoid Class B instabilities.

Landahl (1962) utilised the concept of admittance (an acoustical concept) as a characterisation of surface response; he defined it as

$$Y = -\left(\frac{\text{normal wall velocity}}{\text{wall pressure}}\right). \tag{1.4}$$

One advantage of Landahl's formulation is that it is relatively simple to determine whether or not a particular change in wall parameters will be stabilising. He considered an approximate model of the Kramer coating, and was able to confirm Benjamin's conclusions on the effect of internal damping on TS waves. In addition, he reasoned that since the theoretical critical Reynolds number was only marginally increased by a flexible wall, it was improbable that Kramer's drag reductions were due to transition delay. This opinion was held to be corroborated by the fact that Kramer obtained his best results using a highly viscous damping fluid. A disadvantage of Landahl's approach is that when the Reynolds number was varied, the non-dimensional wall parameters were held constant, which meant that he was in fact considering a different membrane for each Reynolds number.

Gyorgyfalvy (1967) used Landahl's methods in a comprehensive investigation of stability and transition of boundary layers for internally-damped spring-backed membranes. The e^9 method of Smith & Gamberoni (1956) was used to calculate the transitional Reynolds number, and it was found that any favourable effects on transition were due to a reduction in amplification rates rather than an increase in critical Reynolds number. Gyorgyfalvy estimated that as much as 90% drag reduction was possible for water flows, albeit only for a limited range of Reynolds numbers. However, it appeared that Kramer's coatings were unsuitable for transition delay.

Landahl & Kaplan (1965) studied a model wherein the wall boundary conditions allowed for a non-zero streamwise component of surface velocity. This was accomplished by introducing a second surface admittance for the streamwise motion. Compliant surfaces composed of non-dissipative elastic media

and viscoelastic media (Voigt bodies) were studied in addition to spring-backed membranes. The importance of pressure-gradient effects was also investigated, as well as secondary instability for flexible walls. It was found that any reduction in secondary instability was non-trivial but small, hence confirming the conclusion Benjamin (1964) had reached using a simpler model. The results of Gyorgyfalvy for spring-backed membranes given above were also confirmed. Landahl & Kaplan reasoned that a light and highly flexible wall would have optimal effect in delaying transition. However, Carpenter & Garrad (1985) place doubt on their results for spring-backed surfaces, though agreeing with their general conclusions.

Among other work on flexible surfaces, Nonweiler (1961) studied flows over non-dissipative elastic walls. Korotkin (1965) presented an alternative formulation of the problem which catered for both normal and tangential compliance, but as pointed out by Carpenter & Garrad (1985) the no-slip condition was incorrect. Korotkin looked at the effect of a streamwise pressure gradient. Amfilokhiev, Droblenkov & Zavordkhina (1972) used Korotkin's method to calculate transitional Reynolds numbers and amplification factors. They obtained reasonable agreement with Gyorgyfalvy (1967).

Some of the most important theoretical work on transition delay for flexible boundaries has been undertaken by Carpenter (1985) and Carpenter & Garrad (1985, 1986), work which has already been referred to several times in this text. Carpenter & Garrad (1985) argue that Kramer's coatings are best modelled by spring-backed plates with finite bending stiffness, and the results of their analysis based on linear stability theory would appear to substantiate this. They also examine the possibilities and effects of coalescence between the various mode-classes. A detailed evaluation of the values to be assigned to the various parameters in order to comply with Kramer's experiments is given. The surface mode classes are studied in Carpenter & Garrad (1986); they are referred to as 'Flow-Induced Surface Instabilities' (FISI), and are investigated using potential flow theory with an energy analysis of the waves (after Landahl 1962). Their results are compared with those of the causal theory evinced by Brazier-Smith & Scott (1984). The main overall conclusions that they reach are:

(i) There are four main instability modes of practical importance, namely Tollmien-Schlichting Instability (TSI, Class A), FISI (travelling-wave flutter, Class B), a coalescence of these two mode-classes (probably Class C) and a slow-moving Kelvin-Helmoltz-like instability which they call 'static divergence' (also probably Class C).

(ii) Any damping will in most cases stabilise FISI and destabilise TSI.

(iii) Modal interaction, and even coalescence are permitted by viscous damping, but not by viscoelastic damping.

(iv) Kramer-type coatings can in theory postpone transition, in the absence of modal interaction.

(v) There may be an optimum value of substrate viscosity, because of (ii).

Yeo (1986, 1988) investigated the linear stability of spatial disturbances in flows over multi-layered compliant surfaces; his work incorporates oblique flow and anisotropic walls. He also studied inviscid flow over passive compliant walls, and extended the classical theorems concerning the range of allowed values of the complex temporal eigenvalue (the phase speed c)— see Yeo & Dowling (1987). For isotropic viscoelastic surfaces, he found the effects of compliance and damping to be consistent with those determined in previous work; he also discovered a long-wave spatial instability which exists even at very low Reynolds numbers, and may be related to similar phenomena reported by Landahl (1962). It has small spatial growth rates, and is considered by Yeo to be irrelevant as far as transition is concerned. Yeo found that wall modes could be significantly stabilised by a two-layer surface, the outer layer being stiffer than the inner and preferably embedded just beneath its surface. Such an arrangement has a small destabilising influence on TSI, but this is outweighed by the much stronger effect on the FISI, or CIFI (compliance-induced flow instabilities) as Yeo calls them. A four-layer wall having a stiff top layer and progressively softer ones underneath, with moderate substrate damping was found to reduce the maximum spatial amplification rate by up to 70%.

For anisotropic walls Yeo finds that the orientation angle of the fibres and the elastic Young's modulus in that direction (related to the concentration of fibres) are important parameters. Large fibre concentration tends to stabilise

the CIFI but destabilise the TSI, and these effects decrease with increasing anisotropy. Yeo finds best results usually for angles of about 45°. The other wall parameters are still critically important for beneficial results, and any such results in general only obtain for a rather narrow speed range.

Three-dimensional instabilities are found by Yeo to be extremely important for flow over isotropic surfaces. This is because oblique modes perceive a stiffer wall, which destabilises TSI (although suppressing CIFI). Hence both the minimum critical Reynolds number and the maximum amplification factor may belong to such modes. However, Yeo makes the reasonable point that for sufficiently compliant surfaces the maximum growth rate may well be less than for the rigid wall, given that such a surface would tend to stabilise TSI.

Sen & Arora (1988) approached the probem from a completely different angle, gaining some valuable new insight. Instead of defining various wall-parameter values, they assigned the eigenfunction a particular value at the wall (relative to its normalisation), and back-calculated the wall-parameter values. In this way they were able to determine parameter values that would be likely to inhibit the development of instabilities. The argument of the eigenfunction at the wall, ϕ_w, was varied through 360° or more at a fixed modulus and the change in the eigenvalue plotted. The periodicities observed enabled the identification of not only Tollmien-Schlichting and Kelvin-Helmoltz mode-classes, but various 'resonant' and 'transitional' mode-classes too. Those classes for which the eigenvalue traces out a closed loop in one 360° cycle are termed 'regular' by Sen and Arora. Three such classes were identified, namely TS, 'Kelvin-Helmholtz' (KH) and 'low-speed stable'. The latter occurs at low values of c_r and high values of $|\phi_w|$, and is relatively uninteresting due to its inherent stability. The KH mode-class exists for low values of $|\phi_w|$, but the limit $|\phi_w| \to 0$ does not correspond to the rigid wall, thereby distinguishing the KH and TS classes. Sen and Arora note that this limit represents a neutrally-stable stationary periodic ripple, but their use of the appellation 'Kelvin-Helmholtz' is rather unfortunate and likely to cause confusion. The classical Kelvin-Helmholtz instability occurs when there is a velocity discontinuity at the interface between two fluids, the more dense being below the less dense; a fundamental characteristic of this in-

stability is the existence of complex conjugate eigenvalue pairs, but such pairs are nowhere in evidence in the study of Sen and Arora.

Another important mode-class identified by Sen & Arora is the 'resonant' (R) class. Modes in this class are periodic over four cycles of $\arg\phi_w$, generally exhibit large c_r (> 0.7), and exist only for large values of $|\phi_w|$. Bifurcation to regular R modes occurs via various transitional modes, periodic over two or three cycles of $\arg\phi_w$. These modes may exhibit characteristics of the regular modes over parts of their cycles. The TS to R bifurcation appears to occur via a singularity, and Sen & Arora conjecture that the concepts of 'modal coalescence' and 'static divergence' (see Carpenter & Garrad 1985) may be related to the behaviour of modes near to this singularity. The appropriateness of the term 'resonant' is manifested by back-calculation of the free-wave speed on the wall, which as Sen & Arora demonstrate is mimicked closely by c_r. The authors conclude, in something of a departure from previous workers, that the TS and R modes should both be avoided rather than any attempt made to stabilise them. They suggest that small values of free-wave speed and damping offer the best prospect (by way of compromise) for flow stabilisation.

In recent years many researchers have investigated fluid dynamical problems by direct numerical integration of the Navier-Stokes equations, rather than considering the Orr-Sommerfeld equation for example. Such an approach has been made possible by the continued increase in computing power, although such large-scale approaches of course incur additional difficulties. Interest has also increased in 'active' walls: as the name suggests, these walls do not just move as a result of pressure perturbations in the fluid above, but are given external forcing of some sort in the hope of favourably influencing the overall fluid-wall motion. A similar but perhaps more subtle approach is the use of so-called 'smart' walls. The idea is that the wall response to flow perturbations is coupled back into the flow field, and the wall is designed or modelled in such a way that its response is tailored to nullify these perturbations. Among the works to have been performed on flows over flexible walls using some of these methods are those of Kleiser & Laurien (1985), Lekoudis & Sengupta (1986), Metcalfe *et al.* (1986) and Domaradzki & Metcalfe (1987). Biringen (1984) con-

sidered periodic suction/blowing, with wall forcing applied at a single time-step. A reduction by half of TS wave amplitudes in a single time-step was attained. No significant transients were generated, but at later times the residual wave was found to grow at the same rate as before the application of forcing. Hence there was only qualified success.

Kleiser & Laurien (1985) considered a system having suction and blowing at the wall with mass forcing and direct manipulation of the Fourier modes. They found that out-of-phase forcing was successful in damping out unstable two-dimensional linear modes, but that if two-dimensional modes exceeded a critical amplitude they became very unstable to three-dimensional disturbances.

Domaradzki & Metcalfe (1987) used direct numerical simulation to study flow over a membrane. The membrane parameters were kept constant in dimensional units, so that variation in Reynolds number did not mean that one was considering different physical membranes. Reynolds number variation was taken to correspond to a variation in boundary layer thickness, and hence in streamwise location. These authors located membrane parameters that doubled the critical Reynolds number over its rigid-wall value, but found that this was offset by a significant increase in growth rates in the unstable region. They also studied the kinetic energy balance equation.

Hall (1988) examined the effect of surface response on TS growth rates using a turbulent wall pressure model, and considering three compliant surfaces: soft PVC, stiffer PVC and a two-layer surface consisting of a thick layer of soft PVC covered with a thin layer of neoprene. The Navier-Stokes equations were solved using a pseudospectral technique, and this was coupled to a finite-element calculation for the compliant wall. The response of each of these walls to an imposed Tollmien-Schlichting wave was calculated, at a displacement thickness Reynolds number of 1000: the soft PVC developed large perturbation amplitudes after a period of time; so did the two-layer surface, though the magnitude of the perturbations was less. The stiffer PVC surface attained a steady state. Unfortunately no comparison was attempted with other work, and the number of calculations performed would appear to be insufficient for any firm conclusions to be drawn.

In summary, then, it may be said that a considerable level of understanding of the linear stability of flows over flexible walls has been reached, both through ever more meticulous experimental work, and through the joint application of analytic and computational methods by an increasing number of theoreticians. The stage is therefore well set for some exploratory forays into the weakly-nonlinear regime, where many topics of great interest await those willing to tackle the formidable difficulties that are entailed. In this work we make such a foray, following the programme summarised below.

1.7 Outline of study topics

In Chapter 2, we study a configuration consisting of an inviscid, constant-velocity, free-surface flow over a simple flexible wall. Linear modal interactions are examined in detail, and resonant triads are located. The possibility of 'explosive' resonance, wherein several interacting wave-modes can grow simultaneously, is revealed. Although no experimental evidence of this phenomenon is yet available for flows over compliant surfaces, such resonance is well-known to play a prominent rôle in boundary-layer stability (see for example Craik 1986a), and so may confidently be expected also to influence the evolution of disturbances in compliant-boundary flows when appropriate conditions are satisfied.

In Chapter 3 we proceed to study resonant-triad interactions in Blasius flow over rigid walls. Numerous triads are located, and their quadratic interaction coefficients calculated. This work agrees with, and considerably extends existing numerical results, thereby providing further evidence for the potential importance of three-wave resonance in shear flows.

Chapter 4 concerns the analogous but coniderably more complex problem of the nonlinear resonant instability of boundary-layer flow over flexible walls. Firstly, linear interactions between Tollmien-Schlichting modes and wall modes are investigated in some detail, complementing the findings of other authors. It is then shown that resonant triads can be formed from various combinations of these modes, and may also comprise higher-order fluid modes. The quadratic interaction coefficients are calculated, and comparisons made with data for the rigid-wall case. In order to highlight the principal phenomena, attention is restricted throughout to relatively simple (but nevertheless realistic) wall

models.

Chapter 2 Inviscid free-surface flows over flexible boundaries

2.1 Introduction

The problem studied here concerns uniform inviscid free-surface flows over flexible boundaries: a deliberate simplification that permits analytic treatment and precise physical insights. In some senses, this problem may be viewed as a simple analogue of the more important boundary-layer flows, in which Tollmien-Schlichting waves interact with a compliant boundary. The study of flows of the latter kind follows in the next chapter. The author hopes that these studies may provide a spur to future experimental work on nonlinear resonances. This work has been published elsewhere (Thomas & Craik 1988).

We consider the following: inviscid irrotational fluid of constant density ρ and mean depth h flows with constant velocity $\mathbf{U} = (U_x, U_y, 0)$ over a flexible boundary, the fluid having a free upper surface. The mean position of the lower boundary is $z = 0$, and that of the free surface is $z = h$. A model dispersion relation incorporates the properties of the lower boundary, and allows for the possibility of some form of substrate material. We consider a small irrotational perturbation $\mathbf{u}' = \nabla\varphi'$, where the complex velocity potential is $\varphi = \mathbf{U}.\mathbf{x} + \varphi'$, which induces waves on the free surface and flexible boundary with normal displacements h and z respectively (see Figure 2.1). For this problem there are four boundary conditions, comprising a kinematic and a pressure condition at each interface. At the upper, air-water interface, these are

$$\eta_t + [\nabla\varphi.\nabla\eta]_{z=h+\zeta}\,, \tag{2.1}$$

$$\left[\varphi_t + \frac{1}{2}\nabla\varphi.\nabla\varphi\right]_{z=h+\zeta} + g(h+\zeta) + \frac{\gamma\kappa}{\rho} = 0, \tag{2.2}$$

where γ is the coefficient of surface tension, κ is the mean surface curvature and g is gravitational acceleration. Without loss, κ is henceforth represented by the approximation $\kappa \approx -\nabla^2\zeta$, which is correct to second order in wave slope.

At the lower boundary of the fluid, where it meets the flexible material, the normal stress N may be represented by a linear model

$$N = m\zeta_{tt} + d\zeta_t - F\nabla^2\zeta + S\zeta, \tag{2.3}$$

such as was used by Benjamin (1963). The parameters may be assigned particular physical identities, for example those characteristic of a stretched membrane:

m would then be the effective membrane mass per unit area, d a damping coefficient due to viscous or frictional effects, F the tension per unit span of the membrane and S its effective spring stiffness.

In practice, the compliant material may be of complex construction. For instance, the 'Kramer surfaces' discussed by Carpenter & Garrad (1985) consisted of a layer of pliable rubber-like material supported on a rigid base by an array of closely-spaced flexible stubs, with viscous fluid in the gap between them. Since detailed mathematical analysis of such composite materials is impracticable, they are best represented by judicious choice of parameters in models like that just introduced. Usually, however, the effective mass, stiffness and so on will not be constants, but will depend on the length-scale of the disturbance. Accordingly, it is best to replace (2.3) by a corresponding representation of the stress $N(\mathbf{k})$ associated with each individual Fourier mode $\zeta(\mathbf{k})$, proportional to $\exp(\mathrm{i}\mathbf{k}.\mathbf{x} - \mathrm{i}\omega t)$, with real wavenumber $\mathbf{k}$ and (perhaps complex) frequency $\omega(\mathbf{k})$; namely

$$N(\mathbf{k}) = [-m\omega^2 - \mathrm{i}d\omega + R]\zeta, \tag{2.4}$$

where R is the restoring force (typically given, as in most of the following, by $Fk^2 + S$) and m, d (and perhaps S) are permitted to be prescribed functions of $k = |\mathbf{k}|$ rather than just constants. Of course, with k-dependent parameters, the total stress N is no longer simply given by (2.3), but by Fourier inversion of $N(\mathbf{k})$.

For example, a simple interface with surface tension F and deep inviscid substrate fluid of density ρ_s yields $m = \rho_s/k$, $d = 0$, $R = Fk^2 + \rho_s g$: clearly, the 'effective mass' per unit area then varies inversely with k. Similarly, a thin stretched membrane under tension T and with mass m_0 per unit area, that lies over a deep inviscid substrate fluid of density ρ_s would have $m(k) = m_0 + \rho_s/k$, where m_0 is the density of the membrane times its thickness. The model considered here is taken to have constant m, and so may be regarded as acting like a thin membrane supported by springs, without a substrate fluid; i.e. $m = \rho_m b$ where ρ_m is the equivalent membrane density and b is its thickness. One could also incorporate the effect of bending stiffness due to a term $b\frac{\partial^4 z}{\partial x^4}$ added to (2.3) (where b is proportional to Young's modulus) by choosing the

'effective stiffness' to be $S(k) = \rho_s g + bk^4$. Likewise, various types of damping may be accommodated by suitable choice of $d(k)$.

It should be noted that the representation (2.4) is designed to model the entire dynamics of the compliant material, and so differs from the formulation of Carpenter & Garrad (1985), who treat the substrate pressure fluctuations separately. There are no procedural difficulties associated with using k-dependent parameters m, d, F, S in (2.3); but particular choices must be made in order to display quantitative results. Here, detailed results are presented for cases with constant m, F and with $d = lmk$, l constant; the last k-dependence being in line with expectations that damping is weaker for long waves than for short. Our main purpose is to establish the conditions for resonantly-interacting wave triads, to derive the corresponding resonance equations and to provide details of specific illustrative cases. Accurate results for particular compliant materials would entail precise k-dependent estimates for the various parameters used in (2.4): but use of a more elaborate model, such as that of Carpenter & Garrad (1985) for a 'Kramer coating', seems premature in the absence of guidelines for simpler models.

Despite our concern with a nonlinear problem, the stress representations (2.3) or (2.4) are linear ones in the wave elavation z or its individual Fourier components. Later, in section 6, we consider how this representation may be altered by additional nonlinear terms. Since the normal stress N is equal to minus the fluid pressure at the interface, the appropriate lower boundary conditions for the fluid are

$$[\eta_t + \nabla\varphi.\nabla\eta]_{z=\eta} = [\varphi_z]_{z=\eta}\,, \tag{2.5}$$

$$\left[\varphi_t + \frac{1}{2}\nabla\varphi.\nabla\varphi\right]_{z=\eta} + gz - \frac{1}{\rho}(m\eta_{tt} + d\eta_t - F\nabla^2\eta + S\eta) = 0. \tag{2.6}$$

if (2.3) is used. Corresponding results hold for the various Fourier modes when the more general model (2.4) is employed; but only those nonlinear terms of appropriate periodicity are then retained.

2.2 Linear Theory

First, assume that φ, η and ζ have the following single-mode forms:

$$\varphi = \mathbf{U}.\mathbf{x} + \frac{1}{2}\epsilon[\{A\cosh(kz) + B\sinh(kz)\}\exp\{\mathrm{i}(\mathbf{k}.\mathbf{x} - \omega t)\} + \text{c.c.}], \tag{2.7}$$

$$\zeta = \frac{1}{2}\epsilon[a\exp\{\mathrm{i}(\mathbf{k}.\mathbf{x} - \omega t)\} + \text{c.c.}], \tag{2.8}$$

$$\eta = \frac{1}{2}\epsilon[b\exp\{\mathrm{i}(\mathbf{k}.\mathbf{x} - \omega t)\} + \text{c.c.}], \tag{2.9}$$

correct to $\mathrm{O}(\epsilon)$, where ϵ is a small dimensionless ordering parameter characteristic of wave slope, c.c. denotes complex conjugation and the scaled amplitudes a, b, A, B are $\mathrm{O}(1)$. The linearised boundary conditions are then

$$\zeta_t + \mathbf{u}.\nabla\zeta = [\varphi'_z]_{z=h}\,, \tag{2.10}$$

$$[\varphi'_t + \mathbf{u}.\nabla\varphi']_{z=h} + gh - \frac{\gamma}{\rho}\nabla^2\zeta = 0, \tag{2.11}$$

$$\eta_t + \mathbf{u}.\nabla\eta = [\varphi'_z]_{z=0}\,, \tag{2.12}$$

$$[\varphi'_t + \mathbf{u}.\nabla\varphi']_{z=0} - \frac{1}{\rho}\{m\eta_{tt} + d\eta_t - F\nabla^2\eta + (S - \rho g)\eta\} = 0. \tag{2.13}$$

Equations (2.10) and (2.11) give the following relation , on elimination of the wave amplitude a:

$$(\omega - \mathbf{U}.\mathbf{k})^2 = gk\left(\frac{A\tanh(kh) + B}{A + B tanh(kh)}\right). \tag{2.14}$$

Likewise, elimination of b from (2.12) and (2.13) yields

$$A(\omega - \mathbf{U}.\mathbf{k})^2 = B\{\frac{mk}{\rho}(\omega^2 - c_0^2k^2 + \mathrm{i}\frac{d}{m}w) - \frac{k}{\rho}(S - \rho g)\}. \tag{2.15}$$

We also have from (2.10) and (2.12) the following amplitude relations:

$$A\sinh(kh) + B\cosh(kh) = -\mathrm{i}k^{-1}(\omega - \mathbf{U}.\mathbf{k})a, \tag{2.16}$$

$$B = -\mathrm{i}k^{-1}(\omega - \mathbf{U}.\mathbf{k})b. \tag{2.17}$$

From (2.14) and (2.15) the dispersion relation is easily obtained as

$$D_1 D_2 = \Lambda^2, \tag{2.18}$$

where

$$D_1 \equiv [(\omega - \mathbf{U}.\mathbf{k})^2 - (gk + \frac{\gamma k^3}{\rho})\tanh(kh)],$$

$$D_2 = [\frac{mk}{\rho}(\omega^2 - c_0^2 k^2 + \mathrm{i}\frac{d}{m}\omega) - \rho^{-1}(S - \rho g)k + (\omega - \mathbf{U}.\mathbf{k})^2 \tanh(kh)], \quad (2.19)$$

$$\Lambda^2 = (\omega - \mathbf{U}.\mathbf{k})^2 (gk + \frac{\gamma k^3}{\rho})\mathrm{sech}^2(kh),$$

and $c_0^2 \equiv F/m$.

The quantity Λ^2 is exponentially small for large values of kh, and in this limit (2.18) has two pairs of roots for ω: those given by $D_1 = 0$ are just deep water capillary-gravity waves, and will be referred to as ω_1 and ω_2; the others correspond to waves on the flexible boundary, and will be called ω_3 and ω_4. As kh is decreased, coupling occurs between the free surface and lower boundary modes, and is particularly important whenever the roots are nearly equal.

Illustrative numerical solutions of (2.18) were obtained and depicted graphically for the case of $\mathbf{U} = U\mathbf{i}$. Initially, S was set equal to ρg, and d to zero. A rather large value of $m/\rho = 5.0$ metres was chosen both to improve the clarity of the graphical displays and to provide, by analogy, some provisional insight into the behaviour of airflow over compliant boundaries. Of course, large values of m/ρ are not possible for liquid flows over an actual membrane, the thickness of which must be small compared with the disturbance wavelength; but such values may be appropriate in models of more complex compliant materials.

It was found that instability of waves on the flexible boundary can occur even in the absence of coupling between these waves and those on the free surface (i.e. when $kh \to 0$). This instability occurs provided U is not too small, and is confined to a small region of (ω, k) space near $k = 0$ (but such that kh is still large). This is just a slow-moving Kelvin-Helmholtz instability of the lower boundary. With kh large, two mode crossings are seen in Figure 2.2a: one with $\omega > 0$ involving ω_2 and ω_3, and another with $\omega < 0$, at smaller wavenumber, involving ω_2 and ω_4. Since surface tension causes ω_2 to become negative again for k sufficiently large, there are in fact two more mode crossings not shown in Figure 2.2a. Figure 2.2b shows the growth rates of the long-wave Kelvin-Helmholtz instability. At smaller h, further regions of instability appear near the erstwhile ω_2–ω_3 crossing points. Only one of these is shown in Figure 2.3, the other being at much larger k. In contrast the ω_2 and ω_4 modes exchange identities near where they previously crossed, no instability

appearing (see Figures 2.3 and 2.4). This is in agreement with expectations, since at the ω_2–ω_3 crossing (but not at the ω_2–ω_4 crossing) ω_2 has negative energy (measured in a stationary frame of reference) and ω_3 has positive energy. In simple terms, a wave has positive energy if its creation results in an increase in the total energy of the sysyem, and negative energy if the energy of the system is decreased. It is known that coalescence of modes of like energy sign always results in an exchange of identities, and coalescence of modes of opposite energy sign always results in linear instability— see e.g. Cairns (1979). When h was decreased yet further, the two regions of instability coalesced into a single, larger region of instability (see Figure 2.5).

The case of S> ρg was also studied: it was discovered that the effect of a greater effective spring stiffness was to displace any regions of instability to larger wavenumbers (see Figure 2.6).

Inclusion of damping (i.e. allowing a non-zero value of d) has the interesting effect of driving any negative-energy waves unstable. This is demonstrated in Figures 2.7 and 2.8 for two separate cases, where $d = lmk$. The modes shown are neutrally stable for $l = 0$ (Figures 2.7a, 2.8a); damping produces instability of the ω_2 mode, which has negative energy (Figures 2.7b,c, 2.8c; see Ball 1964, Landahl 1962). However, this instability is very weak since the ω_2 mode is centred on the upper interface and so experiences little damping. Also, it is seen in Figure 2.7a and 2.7b that modes ω_1 and ω_3 exchange identities near $k = 300\mathrm{m}^{-1}$.

2.3 Three-Wave Resonance

The possibility of finding three-wave resonance in cases of no linear instability and no damping is now investigated. The requisite criteria are

$$\mathbf{k}_1 + \mathbf{k}_2 + \mathbf{k}_3 = \mathbf{0}, \tag{2.20}$$

$$\mathrm{Re}\{\omega_1 + \omega_2 + \omega_3\} = 0. \tag{2.21}$$

It is particularly noteworthy that resonant triads can give rise to explosive instability, wherein all three waves grow simultaneously, provided that the wave of greatest absolute frequency has energy of opposite sign to the other two. But

even when this criterion is not met, resonant interactions remain of interest (see e.g. Craik & Adam 1979).

A graphical technique may be employed to find the approximate locations of resonant triads (Figure 2.9; see e.g. Ball 1964, Craik & Adam 1979). The procedure is as follows: firstly the dispersion curves and axes are copied onto a transparency; then the origin on the transparency is moved along one of the curves on the original graph, the orientation of the axes being maintained. If at any point a curve on the transparency intersects a curve on the original graph, a resonant triad has been located, approximately. The exact position can then be computed numerically.

The procedure outlined above was carried out for the dispersion relation (2.18), taking various physically realistic values of the parameters m, c_0, U, S and restricting wavenumbers to the two-dimensional form $\mathbf{k} = (k, 0)$. Examples of explosive three-wave resonance were found, but only when linear instability was also present at other wavenumbers. When U is so small that there is no linear instability, the model yields numerous examples of non-explosive resonant triads but no explosive ones.

Accordingly, to get two-dimensional explosive instability in the present context one must either accept that linear instability is also present or let one or more of the parameters previously held constant vary with wavenumber in some suitable manner. The latter possibility is illustrated in Figure 2.10 , where c_0 decreases like $k^{-1/2}$ as k increases. (It should be noted that in the former case linear instability is confined to a narrow range of wavenumbers, while the nonlinear instability due to resonance covers a much larger range). We now therefore consider a model with a spring stiffness S that is k-dependent, i.e. may be expanded in powers of k:

$$S = S_0 + S_1 k + S_2 k^2 + \ldots$$

(where S_2 merely supplements the tension term F). Terms of higher order in k are considered to be negligible. If we also put $S_2 = F = 0$, we have a total restoring force $R = S_0 + S_1 k$. Although the previous model yielded no explosive instabilities, this new restoring force does yield examples of such phenomena.

Numerical results for this case are given in Figure 2.11.

The present investigation of the possible existence of explosive three-wave resonance is in accord with the findings of Craik & Adam (1979) for three-layer fluid flows. Indeed, their lower or upper interface may be represented by a suitable stress model (2.3) and their results viewed as further illustrations of the present analysis. Both in their and the present work, resonant triads are ubiquitous; but explosively-unstable configurations are not always present.

The analysis that follows applies equally to resonance of the explosive and non-explosive sorts. We calculate nonlinear evolution equations for resonant triads, involving wave modes on both boundaries. This is accomplished in two ways. Firstly a direct attack is made on the governing equations and the amplitude-evolution equations derived for purely temporal variations. Then, a Lagrangian method similar to those of Whitham (1974) and Simmons (1969) is used to derive the evolution equations for both temporal and spatial variations.

2.4 Derivation by 'direct' method

To proceed, we perform Taylor expansions of equations (2.1), (2.2), (2.3), (2.5) and (2.6) to second order about the mean levels $z = h$ and $z = 0$ of each boundary. This yields

$$\varsigma_t + \mathbf{u}.\nabla\varsigma - [\varphi_z]_{z=h} = \varsigma\,[\varphi_{zz}]_{z=h} - [\nabla\varphi.\nabla\varsigma]_{z=h}\,, \tag{2.22}$$

$$\begin{aligned}[\varphi_t + \mathbf{u}.\nabla\ \varphi]_{z=h} - \frac{\gamma}{\rho}\nabla^2\varsigma + g\varsigma \\ = -\left[\varsigma\varphi_{zt} + \varsigma\mathbf{u}.\nabla\varphi_z + \frac{1}{2}\nabla\varphi.\nabla\varphi\right]_{z=h}\,,\end{aligned} \tag{2.23}$$

$$\eta_t + \mathbf{u}.\nabla\eta - [\varphi_z]_{z=0} = \eta\,[\varphi_{zz}]_{z=0} - [\nabla\varphi.\nabla\eta]_{z=0}\,, \tag{2.24}$$

$$\begin{aligned}[\varphi_t + \mathbf{u}.\nabla\ \varphi]_{z=0} - \frac{m}{\rho}(\eta_{tt} + \frac{d}{m}\eta_t - c_0^2\nabla^2\eta) - \rho^{-1}(S - \rho g)\eta \\ = -\left[\eta\varphi_{zt} + \eta\mathbf{u}.\nabla\varphi_z + \frac{1}{2}\nabla\varphi.\nabla\varphi\right]_{z=0}\,,\end{aligned} \tag{2.25}$$

where φ is the φ' of previous sections, $O(\epsilon^3)$ terms have been neglected, and linear terms have been placed on the left-hand sides of the above equations. Now, on neglecting $O(\epsilon^2)$ second-harmonic and mean-flow terms which do not

contribute to our analysis, φ, ζ and η may be taken in the form

$$\varphi = \frac{1}{2}\epsilon\Bigg[\sum_{j=1}^{3}\{(A_j + \epsilon\hat{A}_j)\cosh(k_j z) + (B_j + \epsilon B_j)\sinh(kz)\} \times \exp\{\mathrm{i}(\mathbf{k}_j.\mathbf{x} - \omega_j t)\} + \mathrm{c.c.}\Bigg] = \epsilon\varphi_1 + \epsilon^2\varphi_2, \tag{2.26}$$

$$\zeta = \frac{1}{2}\epsilon\Bigg[\sum_{j=1}^{3}(a_j + \epsilon\hat{a}_j)\exp\{\mathrm{i}(\mathbf{k}_j.\mathbf{x} - \omega_j t)\} + \mathrm{c.c.}\Bigg] = \epsilon\zeta_1 + \epsilon^2\zeta_2, \tag{2.27}$$

$$\eta = \frac{1}{2}\epsilon\Bigg[\sum_{j=1}^{3}(b_j + \epsilon\hat{b}_j)\exp\{\mathrm{i}(\mathbf{k}_j.\mathbf{x} - \omega_j t)\} + \mathrm{c.c.}\Bigg] = \epsilon\eta_1 + \epsilon^2\eta_2. \tag{2.28}$$

Here, it is supposed that the chosen wavenumbers do not admit quadratic second-harmonic resonance (i.e. $2k_1 \neq k_3$, $2\omega_1 \neq \omega_3$). The latter case is straightforward but would require separate treatment. Setting the right-hand sides of equations (2.22)–(2.25) equal to zero would recover the results of section 2. Now in the weakly nonlinear regime, the amplitudes are assumed to be slowly varying in time in such a way that the derivative of an O(1) quantity is O(ϵ), etc. To obtain the evolution equations for the problem, equations (2.14)–(2.17) and their derivatives are used to reduce equations (2.22)–(2.25) (at O(ϵ^2)) to just two equations, viz.

$$-((\omega - \mathbf{U}.\mathbf{k}))^{-2}\Lambda^{(j)2}\cosh(k_j h)\hat{a}_j + D_2^{(j)}\hat{b}_j = k_j[P^{(j)}(\omega_j - \mathbf{U}.\mathbf{k}_j)^{-2}D_1^{(j)}a_{j,\tau} + Q^{(j)}\mathrm{sech}(k_j h)], \tag{2.29}$$

$$D_1^{(j)}\hat{a}_j - (\omega_j - \mathbf{U}.\mathbf{k}_j)^{-2}\mathrm{sech}(k_j h)\hat{b}_j = -\mathrm{i}(\omega_j - \mathbf{U}.\mathbf{k}_j)^{-1}D_1^{(j)} \times [R_j(\omega_j - \mathbf{U}.\mathbf{k}_j)^{-2}D_1^{(j)}\cosh(k_j h)a_{j,\tau} + S^{(j)}]. \tag{2.30}$$

Here $j = 1,2,3$, $()_{,\tau}$ denotes $\frac{d()}{d\tau}$ where $\tau = \epsilon^{-1}t$, and $P^{(j)}$, $Q^{(j)}$, $R^{(j)}$, $S^{(j)}$ are as given in Appendix A, equations (A1)–(A4). Note from (2.29) and (2.30) that if one sets the right-hand sides equal to zero the O(ϵ^2) amplitudes satisfy the linear dispersion relation, as required. Now (2.29) and (2.30) must be compatible, i.e. must yield a unique solution for each $\frac{da_j}{d\tau}$, and application of this compatibility condition gives the following evolution equations:

$$\frac{da_j}{d\tau} = D_2^{(j)}\cosh(k_j h)(gk_j + \frac{\gamma k_j^3}{\rho}) \times \left(\frac{k_j(\omega_j - \mathbf{U}.\mathbf{k}_j)^3 Q^{(j)} - \mathrm{i}\Lambda^{(j)2}\cosh^2(k_j h)S^{(j)}}{\mathrm{i}\Lambda^{(j)2}\cosh^2(k_j h)R^{(j)} - k_j(\omega_j - \mathbf{U}.\mathbf{k}_j)^3 P^{(j)}}\right) \tag{2.31}$$

where $Q^{(j)}$, $S^{(j)}$ are quadratic functions of the a_i, A_i etc. and $j = 1, 2, 3$. These can be re-expressed, using (2.14)–(2.17), as

$$\mathrm{i}\nu_j \frac{da_j}{d\tau} = \lambda a^*_{j+1} a^*_{j+2}, \tag{2.32}$$

on invoking the linear relationships (2.14)–(2.17) and evaluating subscripts $i+1$ and $j+1$ with modulo 3. Complex conjugation is denoted by *, and ν_j, λ are as given in Appendix A, equations (A5) and (A6). Equation (2.32) can be shown to reduce to the results of Case & Chiu (1977) on taking the limits $U \to 0$, $h \to \infty$, $D_1^{(j)} \to 0$ (with $D_2^{(j)} \neq 0$). It also agrees with the work of Craik & Adam (1979) on three-layer flow with two interfaces if their $\rho_1 \to 0$, $d \to \infty$.

2.5 Derivation by method of averaged Lagrangian

This problem is now tackled from a Lagrangian formulation, and amplitude modulations are allowed to depend on x as well as t. In what follows, the coefficient of damping, d, has been set to zero. This is because the incorporation of terms involving d prevents construction of an appropriate Lagrangian (but see Jimenez & Whitham 1976); for systems with $d \neq 0$ are non-conservative. In the following, as before, we shall assume the symmetric resonance conditions, (2.20) and (2.21). A suitable Lagrangian for the problem is

$$\begin{aligned}
\mathcal{L} = \int_{t_0}^{t_1} \int\int_{All\ x,y} \Big(\int_{\eta}^{h+\varsigma} (\varphi_t + \mathbf{u}.\nabla\varphi + \frac{1}{2}\nabla\varphi.\nabla\varphi + gz) dz \\
+ \frac{\gamma}{\rho}[\sqrt{1+\nabla\varsigma.\nabla\varsigma} - 1] \\
- \frac{1}{2}[\frac{m}{\rho}(\eta_t^2 - c_0^2 \nabla\eta.\nabla\eta) - \frac{S}{\rho}\eta^2] \Big) dx\, dy\, dt \\
\equiv \int_{t_0}^{t_1} \int\int_{All\ x,y} L\, dx\, dy\, dt.
\end{aligned} \tag{2.33}$$

This is a modification of the Lagrangians given by Luke (1967) and Simmons

(1969); it can be transformed to the following (see Miles 1986):

$$\begin{aligned}
\mathcal{L} = \int_{t_0}^{t_1} \int\int_{All\ x,y} \Bigg(& \frac{1}{2}\varphi(\varphi_z - \nabla\varsigma.\nabla\varphi) - \varphi\varsigma_t - \varphi \mathbf{u}.\nabla\varsigma \Big]_{z=h+\varsigma} + \frac{1}{2}g(h+\varsigma)^2 \\
& - \left[\frac{1}{2}\varphi(\varphi_z - \nabla\eta.\nabla\varphi - \varphi\eta_t - \varphi \mathbf{u}.\nabla\eta\right]_{z=\eta} + \frac{\gamma}{\rho}[\sqrt{1+\nabla\eta.\nabla\eta} - 1] \\
& - \frac{1}{2}\left[\frac{m}{\rho}(\eta_t^2 - c_0^2\nabla\eta.\nabla\eta - \left(\frac{S}{\rho} - g\right)\eta^2\right]\Bigg)\, dx\, dy\, dt \\
& - \frac{1}{2}\int_{t_0}^{t_1} \int\int_{All\ x,y} \int_{z=\eta}^{h+\varsigma} \varphi\nabla^2\varphi\, dx\, dy\, dz\, dt \\
& + \int_{t_0}^{t_1} \int_{y=-\infty}^{\infty} \left[\int_{z=\eta}^{h+\varsigma} \varphi(U_x + \frac{1}{2}\varphi_x)dz\right]_{x=-\infty}^{\infty} dy\, dt \\
& + \int_{t_0}^{t_1} \int_{x=-\infty}^{\infty} \left[\int_{z=\eta}^{h+\varsigma} \varphi(U_y + \frac{1}{2}\varphi_y)dz\right]_{y=-\infty}^{\infty} dx\, dt \\
& + \left[\int\int_{All\ x,y} \int_{z=\eta}^{h+\varsigma} \varphi\, dz\, dx\, dy\right]_{t=t_0}^{t_1}.
\end{aligned} \tag{2.34}$$

The last three integrals in the above are evaluated at temporal or spatial endpoints, and so make no contribution to variation of the Lagrangian.

At $O(\epsilon^2)$ the Lagrangian density L simplifies to

$$\begin{aligned}
L = & \left[\frac{1}{2}\varphi_1\varphi_{1z} - \varphi_1\varsigma_{1t} - \varphi_1 \mathbf{u}.\nabla\varsigma_1\right]_{z=h} + \frac{1}{2}g\varsigma_1^2 \\
& - \left[\frac{1}{2}\varphi_1\varphi_{1z} - \varphi_1\eta_{1t} - \varphi_1 \mathbf{u}.\nabla\eta_1\right]_{z=0} + \frac{1}{2}\rho^{-1}\gamma\nabla\varsigma_1.\nabla\varsigma_1 \\
& - \frac{1}{2}\left[\frac{m}{\rho}(\eta_{1t}^2 - c_0^2\nabla\eta_1.\nabla\eta_1) - \left(\frac{S}{\rho} - g\right)\eta_1^2\right]
\end{aligned} \tag{2.35}$$

where φ_1 satisfies Laplace's equation $\nabla^2\varphi_1 = 0$, and φ_1, ς_1, η_1 are as defined in (2.26)–(2.28). This is now averaged over horizontal distances large compared with the fundamental wavelengths $2\pi/k_j$ and periods $2\pi/|\omega_j|$, but short

compared with the modulation length- and time-scales. This gives

$$\begin{aligned}\tilde{L} = \sum_{j=1}^{3}[&\frac{1}{8}k_j(A_j\cosh k_j h - B_j\sinh k_j h)(A_j^*\sinh k_j h - B_j^*\cosh k_j h)\\ &-\frac{1}{4}\mathrm{i}(\omega_j - \mathbf{U}.\mathbf{k}_j)a_j(A_j^*\cosh k_j h - B_j^*\sinh k_j h) - \frac{1}{8}k_j A_j B_j^*\\ &-\frac{1}{4}\mathrm{i}(\omega_j - \mathbf{U}.\mathbf{k}_j)b_j A_j^* + c.c.] + \frac{1}{4}\sum_{j=1}^{3}(g + \frac{\gamma}{\rho}k_j^2)a_j a_j^*\\ &-\frac{1}{4}\sum_{j=1}^{3}[\frac{m}{\rho}(\omega^2 - c_0^2k_j^2) - (\frac{S}{\rho} - g)]b_j b_j^*.\end{aligned} \tag{2.36}$$

The Euler-Lagrange equations, at $\mathrm{O}(\epsilon^2)$ are simply

$$\frac{\partial\tilde{L}}{\partial q} = 0, \tag{2.37}$$

where q represents any of the amplitudes A_j, B_j, a_j, b_j. These result in equations exactly equivalent to (2.14)–(2.17), and give the dispersion relation (2.18) similarly.

At next order, the Lagrangian is supplemented by the additional $\mathrm{O}(\epsilon^3)$ terms

$$\begin{aligned}L' = \Big[&\frac{1}{2}\varsigma_1(\varphi_{1z}^2 + \varphi_1\varphi_{1zz}) + \frac{1}{2}(\varphi_1\varphi_{2z} + \varphi_{1z}\varphi_2) - \frac{1}{2}\varphi_1\nabla\varsigma_1.\nabla\varphi_1\\ &-\varsigma_{1t}\varphi_2 - \varsigma_{2t}\varphi_1 - \varsigma_{1\tau}\varphi_1 - \varphi_{1z}\varsigma_1(\varsigma_{1t} + \mathbf{u}.\nabla\varsigma_1) - \varphi_2\mathbf{u}.\nabla\varsigma_1\\ &-\varphi_1\mathbf{u}.\nabla\varsigma_2\big]_{z=h} + g\varsigma_1\varsigma_2 - \Big[\frac{1}{2}\eta_1(\varphi_{1z}^2 + \varphi_1\varphi_{1zz}) + \frac{1}{2}(\varphi_1\varphi_{2z} + \varphi_{1z}\varphi_2)\\ &-\frac{1}{2}\varphi_1\nabla\eta_1.\nabla\varphi_1 - \eta_{1t}\varphi_2 - \eta_{2t}\varphi_1 - \eta_{1\tau}\varphi_1 - \varphi_{1z}\eta_1(\eta_{1t} + \mathbf{u}.\nabla\eta_1)\\ &-\varphi_2\mathbf{u}.\nabla\eta_1 - \varphi_1\mathbf{u}.\nabla\eta_2\big]_{z=h} + \frac{\gamma}{\rho}(\nabla\varsigma_1.\nabla\varsigma_2 + \nabla\varsigma_1.\tilde{\nabla}\varsigma_1)\\ &-\Big[\frac{m}{\rho}(\eta_{1t}\eta_{2t} + \eta_{1t}\eta_{1\tau} - c_0^2\nabla\eta_1.\nabla\eta_2 - c_0^2\nabla\eta_1.\tilde{\nabla}\eta_1) - \left(\frac{S}{\rho} - g\right)\eta_1\eta_2\Big],\end{aligned} \tag{2.38}$$

where $\nabla^2\varphi_2 = 0$ and φ_2, ς_2, η_2 are as in (2.26)–(2.28). The operator $\tilde{\nabla}$ represents $(\partial/\partial(\epsilon x), \partial/\partial(\epsilon y), \partial/\partial(\epsilon z))$ and yields the slow spatial variations of ς_1 and η_1. Averaging the above Lagrangian as before results in a long expression involving the amplitudes, their temporal and spatial derivatives, and complex conjugates (see Appendix A, equation (A7)).Since we have the amplitude relationships given by (2.14)–(2.17), the averaged Lagrangian may be re-expressed

in terms of just a_j, $\hat{A}_j$, $\hat{B}_j$, $\hat{a}_j$ and $\hat{b}_j$ (plus derivatives and complex conjugates). When this is done all terms involving $\hat{a}_j$ and $\hat{b}_j$ are eliminated, and the coefficients of $\hat{A}_j$ and $\hat{B}_j$ vanish on application of the dispersion relation (2.18). The resultant averaged Lagrangian has the form

$$\begin{aligned}\tilde{L}' = \frac{1}{8}\mathrm{i}\sum_{j=1}^{3}\left[\mathcal{A}_j a_j\left(\frac{\partial}{\partial\tau}+\mathbf{U}.\tilde{\nabla}\right)a_j^* + (\mathcal{B}_j\mathbf{U}+\mathcal{C}_j\mathbf{k}_j).\tilde{\nabla}a_j^*\right] \\ + \frac{1}{8}\lambda a_1 a_2 a_3 + \text{c.c.},\end{aligned} \tag{2.39}$$

where the $\mathcal{A}_j$, $\mathcal{B}_j$, $\mathcal{C}_j$ are as defined in Appendix A, equations (A8)–(A10) and λ is as defined in Appendix A, equation (A6), but with l now taken to be zero; and all summations are modulo 3. The evolution equations for a_j are then found from the appropriate Euler-Lagrange equations, i.e.

$$\frac{\partial\tilde{L}'}{\partial a_j} = \frac{\partial}{\partial t}\frac{\partial\tilde{L}'}{\partial a_{j,t}} + \frac{\partial}{\partial x_i}\frac{\partial\tilde{L}'}{\partial a_{j,x_i}}, \tag{2.40}$$

which yield:

$$\mathrm{i}\left[\mathcal{A}_j\left(\frac{\partial}{\partial\tau}+\mathbf{u}.\nabla\right)(\mathcal{B}_j\mathbf{U}+\mathcal{C}_j\mathbf{k}_j).\tilde{\nabla}\right]a_j = \frac{1}{2}\lambda a_{j+1}^* a_{j+2}^*. \tag{2.41}$$

Now if we define $D^{(j)}$ as

$$D^{(j)} = k_j^{-1}(\omega_j - \mathbf{U}.\mathbf{k}_j)^{-4}D_1^{(j)}(D_1^{(j)}D_2^{(j)} - \Lambda^{(j)2})\cosh^2(k_j h) \tag{2.42}$$

then $\mathcal{A}_j$ is just $\frac{\partial D^{(j)}}{\partial\omega_j}$. Hence we obtain, after a little rewriting,

$$\mathrm{i}\frac{\partial D^{(j)}}{\partial\omega_j}\left[\frac{\partial}{\partial\tau}+\left\{\left(1-\frac{\mathcal{B}_j}{\mathcal{A}_j}\right)\mathbf{U}+\frac{\mathcal{C}_j}{\mathcal{A}_j}\mathbf{k}_j\right\}.\tilde{\nabla}\right]a_j = \frac{1}{2}\lambda a_{j+1}^* a_{j+2}^* \tag{2.43}$$

where $j = 1, 2, 3$ and all subscripts are evaluated modulo 3. In fact, the left hand side of (2.43) is just $\mathrm{i}\frac{\partial D^{(j)}}{\partial\omega_j}\left(\frac{\partial}{\partial\tau}+\mathbf{c}_g.\nabla\right)a_j$ where $\mathbf{c}_g$ denotes the group velocity of each wave.

This result can be reproduced by the following heuristic analysis. In the linear regime, we have the dispersion relation

$$D(\omega,\mathbf{k}) = 0. \tag{2.44}$$

As we move into the weakly nonlinear regime, this is modified to

$$D(\omega + \mathrm{i}\frac{\partial}{\partial \tau}, \mathbf{k} - \mathrm{i}\tilde{\nabla})a_j \approx \mathrm{i}[\frac{\partial D}{\partial \omega}\frac{\partial}{\partial \tau} - \frac{\partial D}{\partial \mathbf{k}}.\tilde{\nabla}]a_j = \text{n.l.t.}, \tag{2.45}$$

where the right-hand side denotes nonlinear terms and $\mathrm{i}\frac{\partial}{\partial \tau}$, $-\mathrm{i}\tilde{\nabla}$ may be identified with small changes $\delta\omega$, $\delta\mathbf{k}$ in frequency and wavenumber. From (2.44) these are related by the dispersion condition

$$\delta\omega\frac{\partial D}{\partial \omega} + \delta\mathbf{k}.\frac{\partial D}{\partial \mathbf{k}} = 0, \tag{2.46}$$

which gives

$$\frac{\partial \omega}{\partial \mathbf{k}} = -\left(\frac{\partial D}{\partial \omega}\right)^{-1}\frac{\partial D}{\partial \mathbf{k}} = \mathbf{c}_g. \tag{2.47}$$

Thus we obtain the generic evolution equation

$$\mathrm{i}\frac{\partial D}{\partial \omega}(\frac{\partial}{\partial \tau} + \mathbf{c}_g.\tilde{\nabla})a_j = \text{n.l.t.}, \tag{2.48}$$

and so (2.43) may finally be written as

$$\mathrm{i}\frac{\partial D^{(j)}}{\partial \omega_j}(\frac{\partial}{\partial \tau} + \mathbf{c}_g^{(j)}.\tilde{\nabla})a_j = \frac{1}{2}\lambda a_{j+1}^* a_{j+2}^*, \tag{2.49}$$

where

$$\mathbf{c}_g^{(j)} = (1 - \frac{\mathcal{B}}{\mathcal{A}})\mathbf{U} + \frac{\mathcal{C}}{\mathcal{A}}k_j. \tag{2.50}$$

As a check, $\mathbf{c}_g$ was calculated explicitly using (2.47), and the form (2.50) was thereby confirmed. Result (2.50) agrees precisely with (2.32) when $l = 0$ in the latter. Note that in both this section and the previous one S has been assumed to be constant; if it is allowed to vary with k the only change is an extra term in the group velocity (2.50), given below:

$$\left(\frac{\partial D^{(j)}}{\partial \omega_j}\right)^{-1} \rho^{-1}k_j^{-1}(\omega_j - \mathbf{U}.\mathbf{k}_j)^{-4}D_1^{(j)2}\cosh^2(k_j h)\frac{dS}{dk_j}\mathbf{k}_j. \tag{2.51}$$

2.6 Nonlinear Model of Flexible Boundary

In all the foregoing, we assumed a linear model for the flexible boundary, given by equation (2.3) or (2.4), and hence the only nonlinearity occuring due to the membrane results from Taylor expansion about the mean position $z = 0$. A possible nonlinear model for a conservative normal reaction N is as follows:

$$N = m(\eta_{tt} - c_0^2\nabla^2\eta[1 - \frac{3}{2}|\nabla\eta|^2]) + K_1\eta + K_2\eta^2 + K_3\eta^3 + \ldots \tag{2.52}$$

All terms of higher than quadratic order in η may be omitted without loss, since they only give rise to terms of $O(\epsilon^4)$ in $\mathcal{L}$. We now replace (2.3) by (2.52) in our Lagrangian formulation.

There are no extra terms resulting at $O(\epsilon^2)$, and so the linear dispersion relation is unaffected (except of course that S is everywhere replaced by K_1). At $O(\epsilon^3)$, however, the Lagrangian has the additional term $\frac{1}{6}\rho^{-1}K_2\eta_1^3$, which on averaging becomes $\frac{1}{8}\rho^{-1}K_2(b_1b_2b_3 + \text{c.c.})$, or equivalently

$$\frac{1}{8}\rho^{-1}K_2\left(\prod_{j=1}^{3}\{(\omega_j - \mathbf{U}.\mathbf{k}_j)^{-2}D_1^{(j)}\cosh(k_jh)\}\right)(a_1a_2a_3 + \text{c.c.}). \qquad (2.53)$$

It is then straightforward to show that this is precisely the term to be added to the interaction coefficient λ in (2.49).

2.7 Conclusions

We have derived the linear dispersion relation for flow with a free surface over a flexible boundary, and studied the linear stability of such a flow, with and without damping. We have shown that three-wave resonance can be of importance in free-surface flows over certain types of flexible boundary, and have derived the wave-amplitude evolution equations for both temporal and spatial variation. These equations have considerable mathematical interest in their own right and have been studied by several authors (e.g. Kaup, Reiman & Bers 1979, Craik 1986a, 1986b, 1987). The nature of solutions is therefore well known. Indeed, it is known that under certain circumstances 'bursting' may occur, i.e. the wave amplitudes may become infinite in a finite time.

The model adopted here is perhaps unrealistically simple in that the fluid flow is uniform and inviscid. However, this simplicity has permitted analytical rather than numerical solution of the problem and so establishes a firm base for future studies of other, more compex flows. In particular, we now proceed to study viscous shear flow over flexible surfaces (in effect, replacing the waves on the free surface with Tollmien-Schlichting waves). Carpenter & Garrad (1985, 1986) and others have considered the linear theory for such configurations, but the corresponding nonlinear problems have not previously been confronted. Firstly, though, we study the problem of Blasius flow over a rigid wall.

Chapter 3 Boundary-layer flow over rigid walls

3.1 Introduction

Boundary-layer flow over a flat plate has long been the subject of research in hydrodynamic stability theory, and the theory is well-developed both for linear and weakly- nonlinear regimes. The linear eigenvalue spectrum has been extensively studied, by Jordinson (1970, 1971), Mack (1976) and Grosch & Salwen (1978) among others. The nonlinear theories studied by Craik (1971), Usher & Craik (1974, 1975), Herbert (1983a,b, 1984, 1988) and other work provide some understanding of the processes causing the onset of three-dimensionality in laminar-turbulent transition through a consideration of subharmonic and resonant modes. Asymptotic, high-Reynolds number triple-deck theory has been used by Smith (1979) to examine the growth of disturbances in a boundary layer and also by Smith & Stewart (1987) for resonant interactions. The experimental work of Klebanoff, Tidstrom & Sargent (1962) was the inspiration for much of the earlier theoretical work, and more recently the studies of Kachanov & Levchenko (1984) have helped to give renewed impetus to the subject. Hendriks (appendix to Usher & Craik 1975) computed some resonant triads and interaction coefficients using the formulation of Craik (1971); he showed that oblique modes experience a remarkably strong resonant interaction at quadratic order, as predicted by Craik (1971). Volodin & Zel'man (1979) considered an analogous formulation for spatially growing disturbances, and had analogous results to those of Hendriks. We shall present an extension of the results of Hendriks (see §3.5).

Smith & Stewart (1987) applied triple-deck theory to resonant-triad interactions in high Reynolds number Blasius flow. They considered high-frequency disturbances asymptotically close to the lower branch of the neutral curve (that is the locus of points in the (α, R)-plane for which disturbances are neutrally stable); both temporal and spatial wave-modes were allowed for. The disturbance frequency Ω was assumed to be less than $R^{\frac{1}{4}}$. In the high Reynolds number regime the oblique constituents of Craik-type triads as defined in (3.9) below have oblique-mode propagation angles θ of exactly 60°. This value is in fair agreement with the experimental data of Kachanov & Levchenko (1984)—

those authors cite values for θ of 56–63°. The interaction coefficients derived by Smith & Stewart have quadratic terms which are of like sign and are also purely imaginary: such forms preclude any finite-time bursting of the solutions— see Chapter 1, §1.4 above.

In this chapter we consider Blasius flow over a rigid wall. The problem formulation is given in full, for completeness, although it has been given elsewhere (Craik 1971). Temporal eigenvalues of the Orr-Sommerfeld equation, resonant triads and interaction coefficients are found by numerical integration. Parallel flow is assumed throughout, although the Blasius solution is in fact only 'nearly parallel'. Previous work (for example Smith 1979) has shown that parallel and non-parallel theories give broadly similar results, the major discrepancy being an extension to the tip of the neutral curve, which gives improved agreement with experiment. Temporal modes are investigated in preference to spatial ones chiefly because they present a slightly more tractable numerical task. For the temporal problem, a real wavenumber α is specified together with a Reynolds number R, and the complex eigenvalue to be found is the phase speed c. The spatial problem requires the specification of R and a real frequency ω, and the eigenvalue is the complex wavenumber α. The two mode types are equivalent only on the curve of neutral stability, but Gaster (1962, 1965) has shown that they can also be related for small spatial and temporal amplification (or damping) rates, by applying the Cauchy-Riemann equations.

3.2 Linear theory

Here we shall consider two-dimensional disturbances only. All physical quantities are non-dimensionalised using appropriate combinations of U_∞, ρ_e and the boundary-layer thickness $\delta \equiv 5\sqrt{\nu x/U_\infty}$. Non-dimensionalisation introduces the Reynolds number R as a flow parameter— here it is defined as $R = U_\infty \delta/\nu$. The basic flow $\bar{u} \equiv U(z)/U_\infty$ is assumed to be quasi-parallel, satisfying the Blasius equation

$$f''' + ff'' = 0, \tag{3.1}$$

where $f'(\chi) = \bar{u}(z)$ and $\chi \equiv \frac{5}{\sqrt{2}}z$; primes denote differentiation of f with

respect to χ. Boundary conditions are

$$f(0) = f'(0) = 0, \qquad f'(\chi) \to 1 \quad \text{as} \quad \chi \to \infty, \tag{3.2a,b,c}$$

corresponding to the physical requirements that the flow should be stationary at the wall and reach some constant value at a certain distance from the wall. A stream function Φ is defined by $u = \frac{\partial \Phi}{\partial z}$, $w = -\frac{\partial \Phi}{\partial x}$. We consider arbitrary small disturbances of the form $\Phi_p = \epsilon\phi(z)\exp(\mathrm{i}\alpha x - \mathrm{i}\alpha ct)$, $\epsilon \ll 1$, and substitute for the total stream function $\Phi = \int \bar{u}\, dz + \Phi_p$ into the vorticity equation

$$\frac{\partial \nabla^2 \Phi}{\partial t} + \frac{\partial \Phi}{\partial y}\frac{\partial \nabla^2 \Phi}{\partial x} - \frac{\partial \Phi}{\partial x}\frac{\partial \nabla^2 \Phi}{\partial y} - \frac{1}{R}\nabla^4 \Phi = 0. \tag{3.3}$$

On neglecting $O(\epsilon^2)$ quantities, this yields the Orr-Sommerfeld equation, the governing equation of the fluid flow in the linear regime:

$$\begin{aligned} L[\phi] \equiv & \mathrm{i}\alpha\left((\bar{u} - c)(\phi'' - \alpha^2\phi) - \bar{u}''\phi\right) \\ & - \frac{1}{R}(\phi'''' - 2\alpha^2\phi'' + \alpha^4\phi) = 0. \end{aligned} \tag{3.4}$$

Primes here and elsewhere denote differentiation with respect to the dependent variable, in this case z (vertical distance from the wall).The boundary conditions for (3.4) are, in terms of the perturbation velocities:

$$u(0) = w(0) = 0; \qquad u, w \to 0 \quad \text{as} \quad z \to \infty. \tag{3.5a,b,c,d}$$

These correspond to requirements of no slip at the wall, and zero perturbation velocities far outside the boundary layer. Rewriting these in terms of ϕ, we have:

$$\phi(0) = \phi'(0) = 0. \tag{3.6a,b}$$

The free-stream boundary conditions in terms of ϕ are

$$\phi(z), \phi'(z) \to 0 \quad \text{as} \quad z \to \infty. \tag{3.7a,b}$$

Equation (3.4) together with the boundary conditions (3.6) and (3.7) constitute an eigenvalue problem for $c = c(\alpha, R)$.

3.3 Nonlinear theory: triad resonance

For the nonlinear analysis we consider a triad of waves defined by

$$\Phi_j = \sum_{i=1}^{\infty} \left(\epsilon^i \phi_j^{(i)}(z) A_j^{(i)}(t) \right) E_j, \qquad j = 1, 2, 3, \tag{3.8}$$

where

$$\begin{aligned} E_1 &= \exp\{\mathrm{i}(\frac{\alpha}{2}x + \beta y - \frac{\alpha}{2}\tilde{c}t)\}, \\ E_2 &= \exp\{\mathrm{i}(\frac{\alpha}{2}x - \beta y - \frac{\alpha}{2}\tilde{c}t)\}, \\ E_3 &= \exp\{\mathrm{i}(\alpha x - \alpha c t)\}. \end{aligned} \tag{3.9}$$

These shall henceforth be termed the '1-wave', '2-wave' and '3-wave'. Exact resonance requires that $\tilde{c}_r = c_r$. Figure 3.1 illustrates the resonant-triad configuration. An ordering parameter ϵ has been introduced, so that all perturbation quantities are $O(\epsilon)$ with $o(\epsilon)$ corrections. The amplitudes are assumed to be slowly varying on an stretched time scale $\tau = \epsilon t$. It is convenient to write (cf. Craik 1968)

$$\begin{aligned} \hat{u}_{1,2} &= \frac{\alpha}{2\gamma} u_{1,2} \mp \frac{\beta}{\gamma} v_{1,2}, \\ \hat{v}_{1,2} &= \pm \frac{\beta}{\gamma} u_{1,2} + \frac{\alpha}{2\gamma} v_{1,2}, \\ \gamma &= \sqrt{\frac{\alpha^2}{4} + \beta^2}. \end{aligned} \tag{3.10}$$

The velocities $\hat{u}_{1,2}$, $\hat{v}_{1,2}$ are defined in the directions $\hat{x}_{1,2}$, $\hat{y}_{1,2}$, which are respectively perpendicular and parallel to the crests of the relevant oblique wave:

$$\begin{aligned} \hat{x}_{1,2} &= \frac{\alpha}{2\gamma} \pm \frac{\beta}{\gamma} y, \\ \hat{y}_{1,2} &= \mp \frac{\beta}{\gamma} x + \frac{\alpha}{2\gamma} y. \end{aligned} \tag{3.11}$$

From the definitions (3.8) and (3.9) it follows that

$$\begin{aligned} \hat{u}_{1,2} &= \sum_{i=1}^{\infty} [\epsilon^i \phi'^{(i)}_j(z) A_j^{(i)}(\tau)] E_{1,2}, \\ w_{1,2} &= -\mathrm{i}\gamma \sum_{i=1}^{\infty} [\epsilon^i \phi_j^{(i)}(z) A_j^{(i)}(\tau)] E_{1,2}. \end{aligned} \tag{3.12}$$

The linearised vorticity equation for the 3-wave gives the Orr-Sommerfeld equation

$$\begin{aligned} L_3[\phi_3] \equiv \mathrm{i}\alpha[(\bar{u} - c)(\phi_3'' - \alpha^2 \phi_3) - \bar{u}'' \phi_3] \\ - R^{-1}(\phi_3'''' - 2\alpha^2 \phi_3'' + \alpha^4 \phi_3) = 0, \end{aligned} \tag{3.13}$$

where $\phi_3 \equiv \phi_3^{(1)}$. We now define an oblique Reynolds number $\tilde{R}$ by

$$\tilde{R} \equiv \frac{\alpha R}{2\gamma}, \tag{3.14}$$

giving for the 1-wave and 2-wave equations equivalent to (3.13), namely

$$\begin{aligned} L_{1,2}[\phi_{1,2}] \equiv\ & \mathrm{i}\gamma[(\bar{u}-\tilde{c})(\phi_{1,2}''-\gamma^2\phi_{1,2})-\bar{u}''\phi_{1,2}] \\ & -\frac{1}{\tilde{R}}(\phi_{1,2}''''-2\gamma^2\phi_{1,2}''+\gamma^4\phi_{1,2})=0, \end{aligned} \tag{3.15}$$

where $\phi_{1,2} \equiv \phi_{1,2}^{(1)}$. (3.10) and (3.14) constitute a Squire transform (Squire 1933). The linearised momentum equations in the $\hat{y}_{1,2}$ directions yield

$$\hat{v}_{1,2}''-[\gamma^2+\mathrm{i}\gamma\tilde{R}(\bar{u}-\tilde{c})]\hat{v}_{1,2}=\pm\mathrm{i}\beta R\bar{u}'. \tag{3.16}$$

The velocity components $\hat{v}_{1,2}$ arise because of the distorting influence of the basic shear flow on oblique wavemodes. The boundary conditions for (3.13) and (3.15) are just (3.6) and (3.7) with appropriate quantities subscripted by 1, 2 or 3. The two boundary conditions for equation (3.16) are

$$\hat{v}_{1,2}(0)=0, \tag{3.17}$$

$$\hat{v}_{1,2}(z)\to 0 \quad \text{as} \quad z\to\infty. \tag{3.18}$$

The first of these results from the requirement that tangential velocity be zero at the wall, and the second follows on remembering that all disturbances must tend to zero outside the boundary layer. As was found by Craik (1971), at $\mathrm{O}(\epsilon^2)$ the nonlinear vorticity equations are

$$\begin{aligned} A_3(t)L_3[\bar{\phi}_3] &= -\frac{dA_3}{dt}(\phi_3''-\alpha^2\phi_3)+F_3 \equiv r^{(3)}, \\ A_{1,2}(t)L_{1,2}[\bar{\phi}_{1,2}] &= -\frac{dA_{1,2}}{dt}(\phi_{1,2}''-\gamma^2\phi_{1,2})+F_{1,2} \equiv r^{(1,2)}, \end{aligned} \tag{3.19}$$

where $\bar{\phi}_j \equiv \phi_j^{(2)}$, $j=1,2,3$, and F_1, F_2, F_3 are as follows:

$$\begin{aligned} F_1 =\ & \frac{1}{4}\mathrm{i}\alpha A_3 A_2^* \exp(\alpha c_i t)\Big(\frac{\alpha^2}{\gamma^2}-2\Big)\phi_3(\phi_2^{*\prime\prime\prime}-\gamma^2\phi_2^{*\prime}) \\ & +\Big(\frac{\alpha^2}{\gamma^2}-3\Big)\phi_3'(\phi_2^{*\prime\prime}-\gamma^2\phi_2^*)-2\phi_2^{*\prime}(\phi_3''-\alpha^2\phi_3) \\ & -\phi_2^{*\prime}(\phi_3'''-\alpha^2\phi_3')-\frac{2\alpha\beta}{\gamma^2}(\phi_3\hat{v}_2^{*\prime\prime}+\phi_3'\hat{v}_2^{*\prime}+\gamma^2\phi_3\hat{v}_2^*) \end{aligned} \tag{3.20a}$$

$$
\begin{aligned}
F_2 = {} & \frac{1}{4}\mathrm{i}\alpha A_3 A_1^* \exp(\alpha c_i t)\left(\frac{\alpha^2}{\gamma^2} - 2\right)\phi_3'(\phi_1^{*\prime\prime\prime} - \gamma^2\phi_1^{*\prime}) \\
& + \left(\frac{\alpha^2}{\gamma^2} - 3\right)\phi_3'(\phi_1^{*\prime\prime} - \gamma^2\phi_1^*) - 2\phi_1^*(\phi_3'' - \alpha^2\phi_3) \\
& - \phi_1^*(\phi_3''' - \alpha^2\phi_3') - \frac{2\alpha\beta}{\gamma^2}(\phi_3\hat{v}_1^{*\prime\prime} + \phi_3'\hat{v}_1^{*\prime} + \gamma^2\phi_3\hat{v}_1)
\end{aligned} \tag{3.20b}
$$

$$
\begin{aligned}
F_3 = {} & \frac{1}{2}\mathrm{i}\alpha A_2 A_1 \exp\{\alpha(c_r - c_i)t\}\left(3 - \frac{\alpha^2}{\gamma^2}\right)\phi_1'(\phi_1'' - \gamma^2\phi_1) \\
& + \phi_1(\phi_1''' - \gamma^2\phi_1') + \frac{2\alpha\beta}{\gamma^2}\left(\hat{v}_1(\phi_1'' - \gamma^2\phi_1) + \phi_1'\hat{v}_1'\right) \\
& - \phi_1^*(\phi_3''' - \alpha^2\phi_1') + \frac{2\beta}{\alpha}(\phi_1''\hat{v}_1 + 2\phi_1'\hat{v}_1' + \gamma^2\phi_1\hat{v}_1'') \\
& - 4\frac{\beta^2}{\gamma^2}\hat{v}_1\hat{v}_1'.
\end{aligned} \tag{3.20c}
$$

In the last equation above we have used the facts that $\phi_2 = \phi_1$ and $\hat{v}_2 = -\hat{v}_1$ for reasons of symmetry. These expressions for F_1, F_2, F_3, identical to Craik's, were re-derived independently by the present author. In the remainder of this section the index j takes the values 1, 2, 3, corresponding to the three constituents of the triad. The wall boundary conditions for (3.19) are similar to those for the $O(\epsilon)$ equation (3.2), that is

$$
\bar{\phi}_j(0) = \bar{\phi}_j'(0) = 0, \qquad j = 1, 2, 3 \tag{3.21a, b}
$$

and

$$
\bar{\phi}_j(z), \bar{\phi}_j'(z) \to 0 \quad \text{as} \quad z \to \infty. \tag{3.22a, b}
$$

In order to solve equations (3.19), we now consider the linear system adjoint to (3.13) and (3.15), viz.

$$
\begin{aligned}
L_j^\dagger[\psi_j] \equiv {} & \mathrm{i}k_j[(\bar{u} - c_j)\psi_j]'' - \mathrm{i}k_j[k_j^2(\bar{u} - c_j) + \bar{u}'']\psi_j \\
& - R_j^{-1}(\psi_j'''' - 2k_j^2\psi_j'' + k_j^4\psi_j) = 0,
\end{aligned} \tag{3.23}
$$

(see e.g. Ince 1956, §9.31), where $k_{1,2} \equiv \gamma$, $k_3 \equiv \alpha$, $R_{1,2} \equiv \tilde{R}$, $R_3 \equiv R$ and $c_{1,2} \equiv \tilde{c}$, $c_3 \equiv c$. The expressions $L_j[\phi_j]$ and $L_j^\dagger[\psi_j]$ are related by the Lagrange identity

$$
\psi_j L_j[\phi_j] - \phi_j L_j^\dagger[\psi_j] = \frac{d}{dz}P_j(\phi, \psi) \tag{3.24}
$$

where $P_j(\phi, \psi)$ is the bilinear concomitant. For an ordinary differential equation of form

$$
p_0\frac{d^n\phi}{dz^n} + p_1\frac{d^{n-1}\phi}{dz^{n-1}} + \ldots + p_{n-1}\frac{d\phi}{dz} + p_n\phi = 0,
$$

with adjoint equation

$$(-1)^n \frac{d^n}{dz^n}(p_0\psi) + (-1)^{n-1}\frac{d^{n-1}}{dz^{n-1}}(p_1\psi) + \ldots - \frac{d}{dz}(p_{n-1}\psi) + p_n\psi = 0,$$

the bilinear concomitant is given by

$$P(\phi,\psi) = \sum_{r=1}^{n}\left[\sum_{j=1}^{r}(-1)^{j-1}\left(\frac{d^{r-j}\phi}{dz^{r-j}}\right)\left(\frac{d^{j-1}}{dz^{j-1}}(p_{n-r}\psi)\right)\right].$$

Thus for our system we have

$$\begin{aligned} P_j(\phi,\psi) = -\frac{1}{R_j}[&\psi_j(\phi_j''' - k_j^2\phi_j') - \phi_j(\psi_j''' - k_j^2\psi_j') + \phi_j'(\psi_j'' - k_j^2\psi_j) \\ &- \psi_j'(\phi_j'' - k_j^2\phi_j) + \mathrm{i}k_jR_j(\bar{u}-c_j)(\phi_j\psi_j' - \psi_j\phi_j') + \mathrm{i}k_jR_j\bar{u}'\phi_j\psi_j]. \end{aligned} \tag{3.25}$$

Integration across the range of the independent variable yields Green's formula

$$\int_0^\infty \{\psi_j L_j[\phi_j] - \phi_j L_j^\dagger[\psi_j]\}dz = \left[P_j(\phi,\psi)\right]_0^\infty. \tag{3.26}$$

The right-hand side of (3.26) contains the boundary conditions both for ϕ_j and for ψ_j. It may be written as eight bilinear terms in ϕ_j and ψ_j, four terms being evaluated at each of the flow boundaries:

$$\left[P_j(\phi,\psi)\right]_0^\infty = \sum_{i=1}^{8} U_i^{(j)}V_{9-i}^{(j)}, \tag{3.27}$$

where

$$\begin{aligned} U_1^{(j)} &\equiv \phi_j(0), \\ U_2^{(j)} &\equiv \phi_j'(0), \\ U_3^{(j)} &\equiv \phi_j(\infty), \\ U_4^{(j)} &\equiv \phi_j'(\infty), \\ U_5^{(j)} &\equiv \phi_j''(0) - (k_j^2 - \mathrm{i}k_jR_jc_j)\phi_j(0), \\ U_6^{(j)} &\equiv \phi_j'''(0) - (k_j^2 - \mathrm{i}k_jR_jc_j)\phi_j'(0) + \mathrm{i}k_jR_j\bar{u}'(0)\phi_j(0), \\ U_7^{(j)} &\equiv \phi_j''(\infty) - (k_j^2 + \mathrm{i}k_jR_j(1-c_j))\phi_j(\infty), \\ U_8^{(j)} &\equiv \phi_j'''(\infty) - (k_j^2 + \mathrm{i}k_jR_j(1-c_j))\phi_j'(\infty); \end{aligned} \tag{3.28}$$

and

$$
\begin{aligned}
V_1^{(j)} &\equiv -\frac{1}{R_j}\psi_j(\infty), \\
V_2^{(j)} &\equiv \frac{1}{R_j}\psi_j'(\infty), \\
V_3^{(j)} &\equiv \frac{1}{R_j}\psi_j(0), \\
V_4^{(j)} &\equiv -\frac{1}{R_j}\psi_j'(0), \\
V_5^{(j)} &\equiv -\frac{1}{R_j}(\psi_j''(\infty) - k_j^2\psi_j(\infty)), \\
V_6^{(j)} &\equiv \frac{1}{R_j}(\psi_j'''(\infty) - k_j^2\psi_j'(\infty)), \\
V_7^{(j)} &\equiv \frac{1}{R_j}(\psi_j''(0) - k_j^2\psi_j(0)), \\
V_8^{(j)} &\equiv -\frac{1}{R_j}(\psi_j'''(0) - k_j^2\psi_j'(0)).
\end{aligned}
\tag{3.29}
$$

Thus the $O(\epsilon^2)$ boundary conditions for ϕ_j may be re-expressed simply in terms of $U_1^{(j)}$, $U_2^{(j)}$, $U_3^{(j)}$ and $U_4^{(j)}$:

$$
\begin{aligned}
U_1^{(j)} &= 0, \\
U_2^{(j)} &= 0, \\
U_3^{(j)} &= 0, \\
U_4^{(j)} &= 0.
\end{aligned}
\tag{3.30a, b, c, d}
$$

The general theory of differential systems (Ince 1956, §9.34) then attests that the boundary conditions for the homogeneous adjoint system must be

$$V_i^{(j)} = 0, \qquad i = 1\text{–}4. \tag{3.31}$$

Furthermore, in order for the principal system given by (3.19), (3.21) and (3.22) to have a solution the following relation must obtain:

$$\int_0^\infty \psi_j r^{(j)}\, dz = 0. \tag{3.32}$$

After a little re-arranging of (3.32), we arrive at the evolution equations

$$
\begin{aligned}
\frac{dA_3}{d\tau} &= a_3 A_1 A_2, \\
\frac{dA_{1,2}}{d\tau} &= a_{1,2} A_{2,1}^* A_3,
\end{aligned}
\tag{3.33a, b}
$$

where

$$a_3 \equiv \frac{\int_0^\infty F_3 \psi_3 \, dz}{A_1 A_2 \int_0^\infty \psi_3 (\phi_3'' - \alpha^2 \phi_3) \, dz}$$

and

$$a_{1,2} \equiv \frac{\int_0^\infty F_{1,2} \psi_{1,2} \, dz}{A_3 A_{2,1}^* \int_0^\infty \psi_{1,2} (\phi_{1,2}'' - \gamma^2 \phi_{1,2}) \, dz}.$$

3.4 Numerical method

3.4.1 Discussion of numerical schemes

There are various computational techniques applicable to equations of Orr-Sommerfeld type, indeed this particular equation has been the principal reason for the development of some of these techniques. There are two main difficulties in its numerical solution: (i) the eigenfunctions and their derivatives vary very rapidly in the vicinity of the critical point z_c, given by $\bar{u}(z_c) = c$; and (ii) the two 'physical' solutions, that decay exponentially in the free stream, tend to become contaminated with the unphysical, rapidly growing viscous solution. The Orr-Sommerfeld equation is therefore an example of what is known as a 'stiff' equation. Among the more frequently-used methods are orthonormalisation (a 'shooting' method), compound matrices and finite differences. The first of these utilises the fact that contamination cannot occur if the solution vectors are made orthogonal to each other at each stage of 'shooting' across the region of integration. One disadvantage of this scheme is that reconstruction of the eigenfunctions subsequent to the integration is a rather awkward process. The method of compound matrices has been used with success by Ng & Reid (1979) and Davey (1980) among others. Its principal disadvantage is that the compound matrix increases vastly in size with the order of the differential equation. Thus it is unsuitable for fully three-dimensional problems for instance, although practicable for Orr-Sommerfeld calculations.

The methods of orthonormalisation and compound matrices have been compared by the present author (Thomas 1988) for boundary layer flows over both heated and unheated flat plates. Fourth- and sixth-order mathematical models were employed. The compound matrix method was found to require four times as many grid-points across the boundary layer to achieve the same accuracy as the orthonormalisation method, and also generally needed a much

more accurate initial guess in order to successfully converge.

The Chebyshev polynomial collocation method was first used by Davey & Nguyen (1971) for pipe flow and by Orszag (1971) for plane Poiseuille flow. Orszag recommended the method on the basis that the truncation error decreases rapidly with the number of polynomials used. This method is more complicated to program than finite differences for example, but of course standard packages are available in program libraries (such as the NAG library).

3.4.2 The finite-difference scheme

The method of finite differences is relatively easy to program, and reconstruction of the eigenfunctions is straightforwward. Accuracy is determined by the choice of finite-difference scheme, by step size and by the number of significant figures of the floating-point arithmetic used. An extension of the finite-difference method of Thomas (1953) was used for the boundary-layer computations presented below. This method utilises a Noumerov auxiliary function to increase the accuracy of the differencing. The principal advantage of finite-difference methods is often said to be their inherent numerical stability, which may be considered more important than the superior speed and accuracy of more sophisticated integration techniques.

The five-point finite difference scheme will now be described. The equations to be solved for the resonant-triad problem are: firstly the Orr-Sommerfeld equation (3.13); then its adjoint, from (3.23); then the oblique Orr-Sommerfeld equation for the 1-wave from (3.15), followed by its adjoint from (3.23); and finally the cross-flow equation for the 1-wave, from (3.16). For the linear problem we only solve (3.13). Let χ represent any of ϕ_j, ψ_j, $j = 1, 2, 3$. We define an auxiliary function g by

$$g = \chi - \frac{1}{6}h^2\chi'' + \frac{1}{90}h^4\chi'''' \tag{3.34}$$

where h is the step size, and χ may be given in terms of g by the Noumerov transform

$$\chi_j = g_j + \frac{1}{6}\delta^2 g_j + \frac{1}{360}\delta^4 g_j \tag{3.35}$$

where δ is the centred difference operator. The coefficients of (3.35) are selected so that the approximations to the derivatives giving $O(h^4)$ accuracy are

simplified (see Thomas 1953). The function and derivative approximations can be shown to be

$$\begin{aligned}
\chi_j &= \frac{1}{360}(g_{j-2} + 56g_{j-1} + 246g_j + 56g_{j+1} + g_{j+2}) + O(h^8), \\
h\chi'_j &= \frac{1}{2}(-g_{j-1} + g_{j+2}) + O(h^4), \\
h^2\chi''_j &= \frac{1}{12}(g_{j-2} + 8g_{j-1} - 18g_j + 8g_{j+1} + g_{j+2}) + O(h^6), \\
h^3\chi'''_j &= \frac{1}{2}(-g_{j-2} + 2g_{j-1} - 2g_{j+1} + g_{j+2}) + O(h^4), \\
h^4\chi''''_j &= g_{j-2} - 4g_{j-1} + 6g_j - 4g_{j+1} + g_{j+2} + O(h^8).
\end{aligned} \tag{3.36}$$

Differencing of the relevant governing equation over n intervals of equal width h yields $n+1$ equations for $g_1, ..., g_{n+1}$, but four fictitious points $g_{-1}, g_0, g_{n+2}, g_{n+3}$ are also created; these are dealt with as follows. The four boundary conditions, two at each end of the integration domain, are finite-differenced at the stations $j = 1$ and $j = n + 1$ as appropriate. This yields four algebraic equations for the unknown quantities $g_{-1}, g_0, g_{n+2}, g_{n+3}$. Hence these unknowns can be re-expressed in terms of the 'known' quantities g_j near to the two end-points of the domain.

The general equation at the jth station is

$$g_{j-2}A(j,1) + g_{j-1}A(j,2) + g_jA(j,3) + g_{j+1}A(j,4) + g_{j+2}A(j,5) = P(j), \tag{3.37}$$

for some $A(j,i)$, i = 1–5 and some $P(j)$. Consider now the first station: we have

$$g_{-1}A(1,1) + g_0A(1,2) + g_1A(1,3) + g_2A(1,4) + g_3A(1,5) = P(1), \tag{3.38}$$

and from the wall boundary conditions we have equations of the form

$$\begin{aligned}
g_{-1} &= X_1g_1 + X_2g_2 + X_3g_3 + X_p, \\
g_0 &= Y_1g_1 + Y_2g_2 + Y_3g_3 + Y_p,
\end{aligned} \tag{3.39}$$

for some $X_j, Y_j, j = 1, 2, 3$ and some X_p, Y_p. Using these we may rewrite (3.38) as

$$A_{11}g_1 + A_{12}g_2 + A_{13}g_3 = p_1, \tag{3.40}$$

where

$$\begin{aligned} A_{11} &\equiv A(1,3) + A(1,1)X_1 + A(1,2)Y_1, \\ A_{12} &\equiv A(1,4) + A(1,1)X_2 + A(1,2)Y_2, \\ A_{13} &\equiv A(1,5) + A(1,1)X_3 + A(1,2)Y_3, \\ p_1 &\equiv P(1) - A(1,1)X_p - A(1,2)Y_p. \end{aligned} \tag{3.41}$$

Similar relations may be obtained for the second and third stations, and thereby all the terms involving g_{-1} and g_0 are absorbed into terms involving non-fictitious points. A similar procedure may also be enacted at the $(n+1)$th station. It follows that the complete system can be re-expressed as a matrix equation of the form

$$[A_{ij}]\mathbf{g} = \mathbf{p} \tag{3.42}$$

where $[A_{ij}]$ is an $(n+1) \times (n+1)$ pentadiagonal band matrix and $\mathbf{g}$ and $\mathbf{p}$ are column vectors of dimension $(n+1)$. The matrix $[A_{ij}]$ is forward-diagonalised into an upper-triangular matrix by Gaussian elimination. For equations (3.13), (3.15) and (3.23) $\mathbf{p}$ is the null vector, and a normalisation condition is required for $\mathbf{g}$, which is taken as $g_{n+1} = 1$. Thus the eigenvalue relation $E(\alpha, R, c) = 0$ is just $A_{n+1,n+1} = 0$. The Orr-Sommerfeld equation and its adjoint must share the same eigenvalues, by the theory of differential systems, and hence no iteration is required for the solution of (3.23). Solution of (3.16) by a three-point scheme is also straightforward since this equation does not have its own eigenvalue, being inhomegeneous.

It is impractical to employ the exact outer boundary conditions (3.7) and (3.18) in any numerical method: clearly we must impose some approximations to these, at some selected finite value z_1 of z. At sufficiently large z, the two physically relevant solutions of the Orr-Sommerfeld equation are those which decay exponentially at the respective rates $(-\alpha z)$ and $(-pz)$, where $p \equiv \sqrt{\alpha^2 + \mathrm{i}\alpha R(1-c)}$, the root with positive real part being taken. The general solution at large z is then simply a linear combination of these two solutions so that

$$\phi \sim Ae^{-\alpha z} + Be^{-pz},$$

where A, B are constants. The simplest differential operator which will annihilate the right-hand side above is $(D+\alpha)(D+p)$ so the most appropriate

numerical forms of the outer boundary conditions (3.7a, b) to be used at $z = z_1$, say, are

$$\phi'' + (\alpha + p)\phi' + \alpha p \phi = 0,$$
$$\phi''' + (\alpha + p)\phi'' + \alpha p \phi' = 0. \qquad (3.43a, b)$$

The above *numerical* idea is due to A. E. Gill, and was first published in Gill & Davey (1969). For the cross-flow velocity $\hat{v}_1$, we approximate (3.18) by $\hat{v}_1'(z_1) = \sqrt{\gamma^2 + \mathrm{i}\gamma\tilde{R}(1-\tilde{c})}\,\hat{v}_1(z_1)$, the root with negative real part being selected.

The integrals appearing in the expressions for the quadratic interaction coefficients a_j, $j = 1, 2, 3$ (equations (3.33) above) are evaluated using Boole's rule:

$$\int_0^{4h} f(r)\,dr \simeq \frac{2h}{45}(7u_0 + 32u_1 + 12u_2 + 32u_3 + 7u_4).$$

This is a five-point rule, and so for successive applications over n intervals n must be a multiple of four (herein we use 1001 grid points, that is 1000 intervals). Boole's rule has good accuracy, the estimated error being $\sim -\frac{2h^6}{945}\{f^{(5)}(b) - f^{(5)}(a)\}$ for an integration range $[a, b]$ (Buckingham 1957).

The program used by the author was developed from one supplied by Professor P. K. Sen, that computes eigenvalues and eigenfunctions for the linear, two-dimensional problem. In the author's program, eigenvalues are located by a combination of Newton-Raphson and regula falsi convergence schemes. The transverse wavenumber β for resonance is determined using the bisection method within the calculation of the eigenvalue $\tilde{c}$ subject to the condition that $\tilde{c}_r = c_r$. The iterative scheme in general requires a reasonably good initial estimate for the eigenvalue in order to converge, but for modes other than Tollmien-Schlichting modes this tended not to be available. Hence the author developed an alternative scheme based on the Principle of the Argument, following the work of Yeo (1986). A closed contour is traced out anticlockwise in the complex phase-speed plane, and the accumulated change in $\arg\{\det[A_{ij}]\}$ is $2n\pi$ if n eigenvalues are enclosed in the contour (assuming there are no singularities). On finding that an eigenvalue is enclosed, the algorithm causes the procedure to be repeated continually using a reduced contour enclosing half the area of the original until at a prescribed limit the iteration procedure is invoked. This method is reliable, but very costly in CPU time since the step-length along

the contour must be sufficiently small to avoid bypassing any loops. Hence the PA scheme was only used in the event of failure of the original initial-guess iteration routine. Yeo (1986) suggests that the step-by-step phase-change should not be permitted to be more than $\pi/4$, but the present author found this generally to be an unnecessarily severe constraint given the large number of modes that had to be located. Problems did however occur in the region of $c_r = 1$ due to the presence of the temporal continuous spectrum there.

All calculations were performed on a VAX 11/785 computer at the University of St. Andrews using double precision arithmetic (64-bit word length for real quantities), which gives a nominal accuracy of about sixteen significant figures. The eigenvalues and discretised eigenfunctions obtained have an estimated accuracy of about five significant figures, which is adequate for most purposes.

3.5 Results and discussion

Linear eigenvalues are compared with the data of Mack (1976) and Gaster (1977) in Table 3.1. The agreement is clearly satisfactory. Differences in the authors' choices of length scales make algebraic transformations of wavenumber and Reynolds number necessary in order to make comparisons, and this accounts for the occasional very small discrepancy between the two sets of data.

Resonant triads for Blasius flow over a rigid wall, encompassing a wide range of wavenumbers α and Reynolds numbers R, are presented in Tables 3.2, 3.3 and 3.4. Here, and below, the domain of integration extended 2.5 boundary-layer thicknesses out from the wall, and 1000 grid-points were used. Table 3.2 presents the present results together with those of Hendriks (appendix to Usher & Craik 1975). Agreement is very good both for the linear data (that is, eigenvalues), and for the nonlinear data (that is, quadratic interaction coefficients), which confirms the soundness of both authors' numerical methods. Plots of the eigenfunctions ϕ_3, ϕ_1, their respective adjoints ψ_3, ψ_1 and the cross-flow velocity $\hat{v}_1$ are presented in Figure 3.2 for the case of $R = 2562.8$ and $\alpha = 0.6$, and are also consistent with equivalent figures of Hendriks.

Considering the linear eigenvalue c (representing a Tollmien-Schlichting

disturbance), the real part c_r at first increases with wavenumber but eventually begins to decrease; c_i for the streamwise mode has a peak, unstable value. For the oblique modes, $\tilde{c}_i$ clearly reaches its peak value at a wavenumber larger than is considered here. Note that the propagation angles θ of these modes are determined by the requirement that resonant triads be formed, and so are different in each case.

It will be seen from Tables 3.3 and 3.4 that the quadratic interaction coefficient a_3 for the streamwise modes always remains O(1) in magnitude, in marked contrast to its oblique counterpart a_1, the modulus of which increases very substantially with both wavenumber and Reynolds number. These results have similarities with those of Volodin & Zel'man (1979) for spatial wave-modes. It would appear from the $\alpha = 1.0$ cases that a_1 decreases for sufficiently large R, although the evidence is only provided by a single data point. Note that by symmetry $a_2 = a_1$, and the a_j are all *complex*.

It is interesting to note the behaviour of the *phases* of a_3 and a_1 as α and R change. It is clear from Tables 3.3 and 3.4 that $\arg a_1$ decreases with both α and R (with the exception of the very last entry in Table 3.4(e)), but in contrast $\arg a_3$ is quite erratic and no general trend can be deduced. The spanwise wavenumber β of the oblique constituents of the triads generally increases with increasing α but decreases with increasing R. The propagation angle θ of these waves decreases with both wavenumber and Reynolds number, as will be shown later.

Comparison of the present results with those of Smith & Stewart (1987) is not straightforward. This is because the latter results assume that the resonating wave-modes lie asymptotically close to the lower-branch neutral curve, which is certainly not in general the case for the triads that are given in Tables 3.2–3.4. However, it must be said that both works are certainly valid in their appropriate contexts.

Since the interaction coefficients a_1, a_3 which are presented in Tables 3.2–3.4 are complex, not real, quantities it follows that finite-time bursting is possible, this being an important difference from the scenario studied by Smith & Stewart. Also, the propagation angles $\theta = \cos^{-1}(\frac{\alpha}{2\gamma})$ for the oblique-mode

triad constituents are never very close to the inviscid value of 60°: they are always less than this, and indeed decrease with increasing α or R.

3.6 Conclusions

In this chapter we have located numerically a large number of resonant triads for Blasius flow, thereby considerably extending the work of Hendriks (appendix to Usher & Craik 1975). The results clearly demonstrate that three-wave resonance can strongly influence participating oblique wave-modes, the streamwise mode being much less affected. The strength of the interaction increases very markedly with both increasing wavenumber and increasing Reynolds number. Thus resonant-triad interactions can be assumed to be extremely relevant in transitional flow regimes, as has indeed been shown experimentally to be the case (in the studies of Kachanov & Levchenko 1984, for example).

Chapter 4 Boundary-layer flow over flexible walls

4.1 Introduction

The possible importance of nonlinear effects in flows over flexible surfaces has hitherto not been considered in theoretical analyses. However, many of the experiments (e.g. those of Gad-el-Hak, Blackwelder & Riley 1984) strongly indicate that three-dimensionality (and hence perhaps nonlinearity) is even more prominent than for rigid-wall flows. Also, the multiplicity of modes in flexible-wall flows suggests that nonlinear modal interaction (in the form of resonant triads, for example) may often be of importance, especially when there is no linear mode-coupling. In this chapter we consider Blasius flow over a simple model wall, similar to that used above in Chapter 2. Temporal eigenvalues of the Orr-Sommerfeld equation, resonant triads and interaction coefficients are found by numerical integration. As in the previous chapter, parallel flow is assumed throughout, although the Blasius solution is in fact only 'nearly parallel'. Much of the following theoretical formulation is the same as for the rigid-wall problem studied in Chapter 3, but we will permit a degree of repetition in the interests of presentational clarity.

We consider a simple wall model, that could for instance be representative of a membrane supported by springs:

$$N = m\frac{\partial^2 \eta}{\partial t^2} + d\frac{\partial \eta}{\partial t} - F\nabla^2 \eta + S\eta, \tag{4.1}$$

The vertical displacement of the wall from its undisturbed position is measured by η, and m, d, F and S are all as defined in (2.3) above. As previously, it is assumed that lateral motion of particles in the surface is zero or negligible. For present purposes it is advantageous to restrict the number of independent wall parameters while retaining a reasonable degree of realism. More complex models may be examined by similar methods, if required.

All quantities, including those pertaining to oblique modes, are non-dimensionalised using appropriate combinations of U_∞, ρ_e and the boundary-layer thickness δ, which we define to be $\delta \equiv 5\sqrt{\frac{\nu x}{U_\infty}}$. The Reynolds number R is defined with respect to δ, i.e. $R \equiv \frac{U_\infty \delta}{\nu}$. The wall parameters are non-dimensionalised in the following way:

$$m = \frac{m_*}{\rho_e \delta},\ c_0^2 = \frac{c_{0*}^2}{{U_\infty}^2},\ d = \frac{d_*}{\rho_e U_\infty},\ S = \frac{S_* \delta}{\rho_e U_\infty^2} \tag{4.2}$$

where $c_0^2 \equiv m^{-1}F$ and $_*$ denotes dimensional quantities. This scheme is akin to that of Domaradzki & Metcalfe (1987). R can be taken to vary with δ, U_∞ or ν: here we assume that $\bar{u}_\infty$ and ν are fixed, and R varies only as δ changes, that is, with x. If allowance is not made for this, different walls will be modelled at different Reynolds numbers. Thus we define reference values $m^{(0)}$ of m and $S^{(0)}$ of S at some Reynolds number R_0, and m and S vary according to

$$m = \frac{m^{(0)}R_0}{R}, \qquad S = \frac{S^{(0)}R}{R_0}. \tag{4.3}$$

Note that R may alternatively be taken to be a function of $\bar{u}_\infty$ rather than of δ, in which case a different scheme is required.

4.2 Linear theory

Here we shall consider two-dimensional disturbances only. The basic flow $\bar{u} \equiv U(z)/U_\infty$ is assumed to be parallel, satisfying the Blasius equation

$$f''' + ff'' = 0 \tag{4.4}$$

where $f'(\chi) = \bar{u}(z)$ and $\chi \equiv \frac{5}{\sqrt{2}}z$; primes here denote differentiation with respect to χ. Boundary conditions are

$$f(0) = f'(0) = 0, \qquad f'(\chi) \to 1 \quad \text{as} \quad \chi \to \infty, \tag{4.5a, b, c}$$

corresponding to the physical requirements that the flow should be stationary at the wall and reach some constant value at a certain distance from the wall. A stream function Φ is defined by $u = \frac{\partial \Phi}{\partial z}$, $w = -\frac{\partial \Phi}{\partial x}$. We consider arbitrary small disturbances of the form $\Phi_p = \epsilon\phi(z)\exp(\mathrm{i}\alpha x - \mathrm{i}\alpha ct)$, $\epsilon \ll 1$, and substitute for the total stream function $\Phi = \int \bar{u}\,dz + \Phi_p$ into the vorticity equation

$$\frac{\partial \nabla^2\Phi}{\partial t} + \frac{\partial \Phi}{\partial y}\frac{\partial \nabla^2\Phi}{\partial x} - \frac{\partial \Phi}{\partial x}\frac{\partial \nabla^2\Phi}{\partial y} - \frac{1}{R}\nabla^4\Phi = 0. \tag{4.6}$$

On neglecting $O(\epsilon^2)$ quantities, this yields the Orr-Sommerfeld equation, the governing equation of the fluid flow in the linear regime:

$$L[\phi] \equiv \mathrm{i}\alpha[(\bar{u} - c)(\phi'' - \alpha^2\phi) - \bar{u}''\phi] - \frac{1}{R}(\phi'''' - 2\alpha^2\phi'' + \alpha^4\phi) = 0. \tag{4.7}$$

The boundary conditions for (4.7) are, in terms of the perturbation velocities:

$$u(\eta) = 0, \quad w(\eta) = \left(\frac{\partial}{\partial t} + \mathbf{u}.\nabla\right)\eta; \quad u, w \to 0 \quad \text{as} \quad z \to \infty. \quad \text{(4.8a, b, c, d)}$$

These correspond to requirements of no slip at the wall, and zero perturbation velocities far outside the boundary layer. Performing Taylor expansions of the first two about the undisturbed wall position yields at first order

$$\phi'(0) + \eta\bar{u}'(0) = 0, \tag{4.9}$$

$$\phi(0) - c\eta = 0. \tag{4.10}$$

Elimination of η gives the homogeneous condition

$$\phi(0) + \frac{\bar{u}'(0)}{c}\phi(0) = 0. \tag{4.11}$$

We require one other boundary condition at the wall, and this is obtained from a consideration of the normal stress:

$$\left[-p + \frac{2}{R}\frac{\partial w}{\partial z}\right]_{z=\eta} = N(\eta). \tag{4.12}$$

From the x-momentum equation,

$$\frac{\partial u}{\partial t} + \mathbf{u}.\nabla u = -\frac{\partial p}{\partial x} + \frac{1}{R}\nabla^2 u, \tag{4.13}$$

and using (4.11) we have

$$p(0) = \frac{1}{\mathrm{i}\alpha R}(\phi'''(0) - \alpha^2\phi'(0)). \tag{4.14}$$

The quantity $N(\eta)$ is as given in (4.1), with appropriate notational changes. From (4.1), (4.10), (4.12) and (4.14) we obtain

$$\phi'''(0) - 3\alpha^2\phi'(0) - B\phi(0) = 0, \tag{4.15}$$

where

$$B \equiv \frac{1}{\mathrm{i}\alpha Rc}[m\alpha^2(c^2 - c_0^2) + \mathrm{i}\alpha cd - S]. \tag{4.16}$$

The free-stream boundary conditions in terms of ϕ are

$$\phi(z),\ \phi'(z) \to 0 \quad \text{as} \quad z \to \infty. \quad \text{(4.17a, b)}$$

Equation (4.7) together with the boundary conditions (4.11), (4.15) and (4.17) constitute an eigenvalue problem for $c(\alpha, R)$.

4.3 Nonlinear theory: triad resonance

The formulation of the resonant-triad problem for flow over a flexible boundary is a reasonably straightforward extension of that for rigid walls given in the preceding chapter: however, care must be taken in deriving the wall boundary conditions for the adjoint system, since these cannot be obtained from any physical considerations. Hence the analysis will be given in detail. We consider a triad of waves defined by

$$\Phi_j = \sum_{i=1}^{\infty} [\epsilon^i \phi_j^{(i)}(z) A_j^{(i)}(t)] E_j, \qquad j = 1, 2, 3, \tag{4.18}$$

where

$$\begin{aligned} E_1 &= \exp\{\mathrm{i}(\frac{\alpha}{2}x + \beta y - \frac{\alpha}{2}\tilde{c}t)\}, \\ E_2 &= \exp\{\mathrm{i}(\frac{\alpha}{2}x - \beta y - \frac{\alpha}{2}\tilde{c}t)\}, \\ E_3 &= \exp\{\mathrm{i}(\alpha x - \alpha c t)\}. \end{aligned} \tag{4.19}$$

These shall henceforth be termed the '1-wave', '2-wave' and '3-wave'. Exact resonance requires that $\tilde{c}_r = c_r$. Figure 3.1 illustrates the resonant-triad configuration. An ordering parameter ϵ has been introduced, so that all perturbation quantities are $O(\epsilon)$ with $o(\epsilon)$ corrections. The amplitudes are assumed to be slowly varying on a stretched time scale $\tau = \epsilon t$. It is convenient to write (cf. Craik 1968)

$$\begin{aligned} \hat{u}_{1,2} &= \frac{\alpha}{2\gamma}\hat{u}_{1,2} \mp \frac{\beta}{\gamma}\hat{v}_{1,2}, \\ \hat{v}_{1,2} &= \pm\frac{\beta}{\gamma}\hat{u}_{1,2} + \frac{\alpha}{2\gamma}\hat{v}_{1,2}, \\ \gamma &= \sqrt{\frac{\alpha^2}{4} + \beta^2}. \end{aligned} \tag{4.20}$$

The velocities $\hat{u}_{1,2}$, $\hat{v}_{1,2}$ are defined in the directions $\hat{x}_{1,2}$, $\hat{y}_{1,2}$, which are respectively perpendicular and parallel to the crests of the relevant oblique wave:

$$\begin{aligned} \hat{x}_{1,2} &= \frac{\alpha}{2\gamma}x \pm \frac{\beta}{\gamma}y, \\ \hat{y}_{1,2} &= \mp\frac{\beta}{\gamma}x + \frac{\alpha}{2\gamma}y. \end{aligned} \tag{4.21}$$

From the definitions (4.18) and (4.19) it follows that

$$\begin{aligned} \hat{u}_{1,2} &= \sum_{i=1}^{\infty} [\epsilon^i \phi_j^{(i)\prime}(z) A_j^{(i)}(t)] E_{1,2}, \\ w_{1,2} &= -\mathrm{i}\gamma \sum_{i=1}^{\infty} [\epsilon^i \phi_j^{(i)}(z) A_j^{(i)}(t)] E_{1,2}. \end{aligned} \tag{4.22}$$

The linearised vorticity equation for the 3-wave gives the Orr-Sommerfeld equation

$$\begin{aligned} L_3[\phi_3] \equiv \mathrm{i}\alpha[(\bar{u}-c)(\phi_3'' - \alpha^2\phi_3) - \bar{u}''\phi_3] \\ - \frac{1}{R}(\phi_3'''' - 2\alpha^2\phi_3'' + \alpha^4\phi_3) = 0, \end{aligned} \tag{4.23}$$

where $\phi_3 \equiv \phi_3^{(1)}$. We now define an oblique Reynolds number $\tilde{R}$ by

$$\tilde{R} \equiv \frac{\alpha R}{2\gamma}, \tag{4.24}$$

giving for the 1-wave and 2-wave equations equivalent to (4.23), namely

$$\begin{aligned} L_{1,2}[\phi_{1,2}] \equiv \mathrm{i}\gamma[(\bar{u}-\tilde{c})(\phi_{1,2}'' - \gamma^2\phi_{1,2}) - \bar{u}''\phi_{1,2}] \\ - \frac{1}{\tilde{R}}(\phi_{1,2}'''' - 2\gamma^2\phi_{1,2}'' + \gamma^4\phi_{1,2)} = 0, \end{aligned} \tag{4.25}$$

where $\phi_{1,2} \equiv \phi_{1,2}^{(1)}$. The linearised momentum equations in the $\hat{y}_{1,2}$ directions yield

$$\hat{v}_{1,2}'' - [\gamma^2 + \mathrm{i}\gamma\tilde{R}(\bar{u}-\tilde{c})]\hat{v}_{1,2} = \pm\mathrm{i}\beta R\bar{u}'\phi_{1,2}. \tag{4.26}$$

The velocity components $\hat{v}_{1,2}$ arise because of the distorting influence of the basic shear flow on oblique wavemodes. The boundary conditions for (4.23) are just (4.11), (4.15) and (4.17) with appropriate quantities subscripted by 3. For equation (4.25), however, the wall boundary conditions depend critically on the type of wall being modelled. In this work we shall consider an idealised anisotropic wall: the effective wall tension experienced by obliquely-propagating wall modes is assumed to be $F\cos\theta$ (that is, $\frac{\alpha}{2\gamma}F$) rather than just F; θ is the angle between the directions of propagation of the oblique wave and the basic flow. More complicated anisotropic models are of course possible, and indeed have been investigated elsewhere in the context of the linear stability problem (for example Yeo 1986), but we feel that our simple model is adequate for this exploratory study. At $\mathrm{O}(\epsilon)$ we have for the 1-wave

$$\phi_1'(0) = -\frac{\alpha}{2\gamma}\bar{u}'(0)\eta_1, \tag{4.27}$$

$$\phi_1(0) = \frac{\alpha}{2\gamma}\tilde{c}\eta_1, \tag{4.28}$$

which gives

$$\phi_1'(0) + \frac{\bar{u}'}{\tilde{c}}(0)\phi_1(0) = 0. \tag{4.29}$$

The normal stress is

$$\left[-p_1 + \frac{2}{R}\frac{\partial w_1}{\partial z}\right]_{z=\eta} = N_1(\eta), \tag{4.30}$$

and the x-momentum equation

$$\frac{\partial u}{\partial t} + \mathbf{u}.\nabla u = -\frac{\partial p}{\partial x} + \frac{1}{R}\nabla^2 u \tag{4.31}$$

yields

$$p_1(0) = \frac{1}{\mathrm{i}\gamma R}(\phi_1'''(0) - \gamma^2\phi_1'(0)). \tag{4.32}$$

Thus we obtain the second wall boundary condition as

$$\phi_1'''(0) - 3\gamma^2\phi_1'(0) - B_1\phi_1(0) = 0, \tag{4.33}$$

where

$$B_1 \equiv \frac{2\mathrm{i}\gamma^2 R}{\alpha\tilde{c}}\Big[\frac{m\alpha^2}{4}(\tilde{c}^2 - \frac{\alpha}{2\gamma}c_0^2) + \mathrm{i}\frac{\alpha\tilde{c}}{2}d - S\Big]. \tag{4.34}$$

Note that in (4.30)–(4.34) the Reynolds number is the original one, not that defined by (4.24). This can be verified by re-deriving the boundary condition in dimensional units, and then non-dimensionalising according to the scheme given above. The two boundary conditions for equation (4.26) are

$$\hat{v}_{1,2}(0) = \pm\frac{\beta}{\gamma}\bar{u}'(0)\eta_{1,2}, \tag{4.35}$$

$$\hat{v}_{1,2}(z) \to 0 \quad \text{as} \quad z \to \infty. \tag{4.36}$$

The first of these results from the requirement that tangential velocity be zero at the wall, and the second follows on observing that $\bar{u} = 1$ outside the boundary layer. As was found by Craik (1971), at $\mathrm{O}(\epsilon^2)$ the nonlinear vorticity equations are

$$\begin{aligned} A_3(t)L_3[\bar{\phi}_3] &= -\frac{dA_3}{d\tau}(\phi_3'' - \alpha^2\phi_3) + F_3 \equiv r^{(3)}, \\ A_{1,2}(t)L_{1,2}[\bar{\phi}_{1,2}] &= -\frac{dA_{1,2}}{d\tau}(\phi_{1,2}'' - \gamma^2\phi_{1,2}) + F_{1,2} \equiv r^{(1,2)}, \end{aligned} \tag{4.37}$$

where $\bar{\phi}_j \equiv \phi_j^{(2)}$, $j = 1, 2, 3$, and F_1, F_2, F_3, bilinear in the first-order disturbance quantities, are exactly as given in Chapter 3, equation (3.20). The expressions for F_1, F_2, F_3, identical to Craik's, were re-derived independently by the present author. In the remainder of this section the index j takes the values 1, 2, 3, corresponding to the three constituents of the triad. The wall boundary conditions for (4.37) are found after a considerable amount of algebraic manipulation to be

$$\begin{aligned} \bar{\phi}_j'(0) + \frac{\bar{u}'}{c_j}\bar{\phi}_j(0) &= \mu_1^{(j)}, \\ \bar{\phi}_j'''(0) - 3k_j^2\bar{\phi}_j'(0) - B_j\bar{\phi}_j(0) &= \mu_2^{(j)}, \end{aligned} \tag{4.38a, b}$$

where the $O(\epsilon^2)$ nonlinear terms μ_j are as given in Appendix B, equations (B1)–(B4) and $k_{1,2} \equiv \gamma$, $k_3 \equiv \alpha$; $c_{1,2} \equiv \tilde{c}$, $c_3 \equiv c$. The three pairs of free-stream boundary conditions are the same as for the linear problem, i.e.

$$\bar{\phi}_j(z), \bar{\phi}_j'(z) \to 0 \quad \text{as} \quad z \to \infty, \quad j = 1, 2, 3. \tag{4.39a, b}$$

In order to solve equations (4.37), we now consider the linear system adjoint to (4.23) and (4.25), viz.

$$\begin{aligned} L_j^\dagger[\psi_j] \equiv\ & \mathrm{i}k_j[(\bar{u} - c_j)\psi_j]'' - \mathrm{i}k_j[k_j^2(\bar{u} - c_j) + \bar{u}'']\psi_j \\ & - \frac{1}{R_j}(\psi_j'''' - 2k_j^2\psi_j'' + k_j^4\psi_j) = 0, \end{aligned} \tag{4.40}$$

(see e.g. Ince 1956, §9.31), where $R_{1,2} \equiv \tilde{R}$ and $R_3 \equiv R$. The expressions $L_j[\phi_j]$ and $L_j^\dagger[\psi_j]$ are related by the Lagrange identity

$$\psi_j L_j[\phi_j] - \phi_j L_j^\dagger[\psi_j] = \frac{d}{dz}[P_j(\phi, \psi)] \tag{4.41}$$

where $P_j(\phi, \psi)$ is the bilinear concomitant, defined by

$$\begin{aligned} P_j(\phi, \psi) = -\frac{1}{R_j}[\psi_j(\phi_j''' - k_j^2\phi_j') - \phi_j(\psi_j''' - k_j^2\psi_j') + \phi_j'(\psi_j'' - k_j^2\psi_j) \\ -\psi_j'(\phi_j'' - k_j^2\phi_j) + \mathrm{i}k_j R_j(\bar{u} - c_j)(\phi_j\psi_j' - \psi_j\phi_j') + \mathrm{i}k_j R_j\bar{u}'\phi_j\psi_j]. \end{aligned} \tag{4.42}$$

Integration across the range of the independent variable yields Green's formula

$$\int_0^\infty \left(\psi_j L_j[\phi_j] - \phi_j L_j^\dagger[\psi_j]\right) dz = [P_j(\phi, \psi)]_0^\infty . \tag{4.43}$$

Note that the range of integration is 0 to ∞. This is because we have eliminated the $O(\epsilon^2)$ wall displacement η_j from the second-order wall boundary conditions (4.38), writing the left-hand-sides in terms of $\bar{\phi}_j$ only, and evaluating at the undisturbed wall position $z = 0$. In order to solve the linear flow equations numerically we of course have to impose outer boundary conditions at some finite value of z, but it is inappropriate to introduce these approximations at this stage (the formulation of the outer boundary conditions for numerical purposes was discussed above, in §3.4; there is no difference between the rigid- and flexible-wall cases).

We now rewrite the right-hand side of (4.43) as

$$[P_j(\phi,\psi)]_0^\infty = \sum_{i=1}^{8} U_i^{(j)} V_{9-i}^{(j)}, \tag{4.44}$$

where

$$\begin{aligned}
U_1^{(j)} &\equiv \phi_j'(0) + \frac{\bar{u}'(0)}{c_j}\phi_j(0),\\
U_2^{(j)} &\equiv \phi_j'''(0) - 3k_j^2\phi_j'(0) - B_j\phi_j(0),\\
U_3^{(j)} &\equiv \phi_j(\infty),\\
U_4^{(j)} &\equiv \phi_j'(\infty),\\
U_5^{(j)} &\equiv \phi_j(0),\\
U_6^{(j)} &\equiv \phi_j''(0) - \left(2k_j^2 - \mathrm{i}k_j R_j c_j\right)\phi_j(0),\\
U_7^{(j)} &\equiv \phi_j''(\infty) - k_j^2\phi_j(\infty),\\
U_8^{(j)} &\equiv \phi_j'''(\infty) - k_j^2\phi_j'(\infty)
\end{aligned} \tag{4.45}$$

and

$$\begin{aligned}
V_1^{(j)} &\equiv -\frac{1}{R_j}\psi_j(\infty),\\
V_2^{(j)} &\equiv \frac{1}{R_j}\psi_j'(\infty),\\
V_3^{(j)} &\equiv -\frac{1}{R_j}\psi_j'(0),\\
V_4^{(j)} &\equiv -\frac{1}{R_j}[\psi_j'''(0) + \frac{\bar{u}'(0)}{c_j}\psi_j''(0) + (\frac{k_j^2\bar{u}'(0)}{c_j} - B_j)\psi_j(0)],
\end{aligned}$$

$$
\begin{aligned}
V_5^{(j)} &\equiv -\frac{1}{R_j}[\psi_j''(\infty) - k_j^2\psi_j(\infty) - \mathrm{i}k_j R_j(1-c_j)\psi_j(\infty)],\\
V_6^{(j)} &\equiv \frac{1}{R_j}[\psi_j'''(\infty) - k_j^2\psi_j'(\infty) - \mathrm{i}k_j R_j(1-c_j)\psi_j'(\infty)],\\
V_7^{(j)} &\equiv \frac{1}{R_j}\psi_j(0),\\
V_8^{(j)} &\equiv \frac{1}{R_j}[\psi_j''(0) + (k_j^2 + \mathrm{i}k_j R_j c_j)]\psi_j(0).
\end{aligned}
\tag{4.46}
$$

These particular forms for the $U_i^{(j)}$ and $V_i^{(j)}$ are only one particular choice: others are also possible. Thus there is some freedom in selecting $U_5^{(j)}$–$U_8^{(j)}$, and since it is these which determine the adjoint boundary conditions $V_i^{(j)} = 0$, $i = 1$–4, it follows that there is not a unique adjoint for this problem.

Thus the $\mathrm{O}(\epsilon^2)$ boundary conditions for ϕ_j may be re-expressed in terms of $U_1^{(j)}$, $U_2^{(j)}$, $U_3^{(j)}$ and $U_4^{(j)}$:

$$
\begin{aligned}
U_1^{(j)} &= \mu_1^{(j)},\\
U_2^{(j)} &= \mu_2^{(j)},\\
U_3^{(j)} &= 0,\\
U_4^{(j)} &= 0.
\end{aligned}
\tag{4.47}
$$

The general theory of differential systems (Ince 1956, §9.34) then attests that the boundary conditions for the homogeneous adjoint system must be

$$
V_i^{(j)} = 0, \qquad i = 1\text{–}4. \tag{4.48}
$$

Furthermore, in order for the principal system given by (4.37), (4.38) and (4.39) to have a solution the following relation must obtain:

$$
\int_0^\infty \psi_j r^{(j)}\,dz = \mu_1^{(j)} V_8^{(j)} + \mu_2^{(j)} V_7^{(j)}. \tag{4.49}
$$

After some re-arrangement of (4.49), we arrive at the evolution equations

$$
\begin{aligned}
\sigma_3 \frac{dA_3}{d\tau} &= \varsigma_3 A_1 A_2,\\
\sigma_{1,2} \frac{dA_{1,2}}{d\tau} &= \varsigma_{1,2} A_{2,1}^* A_3.
\end{aligned}
\tag{4.50a, b}
$$

The quantities σ_j and ς_j are somewhat lengthy and hence are given in Appendix B, equations (B5)–(B8). We define the quadratic interaction coefficients a_j by $a_j = \varsigma_j/\sigma_j$, $j = 1, 2, 3$.

4.4 Numerical method

The numerical scheme for the compliant-wall problem is very similar to that for the rigid-wall problem described above in Chapter 3; the finite-differencing of the boundary conditions is not in itself appreciably more difficult than for the earlier case. A seven-point scheme (supplied by Professor P. K. Sen) was implemented, with the aim of increasing computational accuracy. However, serious difficulties were experienced with this seven-point scheme in attempting to integrate the cross-flow equation (4.26). It was found that a form of numerical instability occured in the region adjacent to the wall, manifesting itself as oscillations in the values of $\hat{v}_1'$ and $\hat{v}_1'''$ on the scale of the step-size h. The problem persisted with different choices of step-size. The author surmised (after some discussions) that the problem was due to the seven-point scheme, for the following reasons.

Any seven-point scheme requires six boundary conditions, three at each extremity, since there are three fictitious points beyond each integration limit. The second-order cross-flow equation (4.26) has only one boundary condition at each end, however, namely (4.35) and (4.36); hence an extra wall condition and an extra free-stream condition must both be decided upon. Such artificial conditions may be obtained by for instance using finite-differencing of lower-order accuracy (giving a *reduced equation*), or by differentiating the field equation. Note that two extra boundary conditions are also required for the Orr-Sommerfeld equations (4.23) and (4.25) and their respective adjoint equations; no numerical problems were encountered regarding these equations. For equation (4.26), the two additional wall equations were chosen as (4.26) itself, evaluated at the wall, and its derivative, again evaluated at the wall.

For the original five-point scheme described in Chapter 3 above, only one extra wall boundary condition is required; this was taken to be the wall-derivative of (4.26). The numerical instability appeared once again, however. Finally, a three-point scheme was implemented, for the cross-flow equation (4.26) only; this gives $O(h^2)$ accuracy. No artificial conditions are here required, (4.35) and (4.36) sufficing. This scheme was found to produce numerically stable results. The seven-point scheme was abandoned, the Orr-Sommerfeld

equations and adjoints being solved via the five-point scheme of Chapter 3. All calculations were performed on a VAX 11/785 computer at the University of St. Andrews using double precision arithmetic (64-bit word length for real quantities), which gives a nominal accuracy of about sixteen significant figures. The eigenvalues and discretised eigenfunctions actually obtained had an estimated accuracy of about five significant figures, which is adequate for most purposes.

4.5 Results for the linear problem

4.5.1 Walls without damping

Eigenvalues for various values of α, R and the wall parameters $m^{(0)}, c_0, S^{(0)}$ are presented in Tables 4.1–4.6. Here streamwise modes only are considered, and there is no wall damping ($d = 0$). As explained above, the quantities $m^{(0)}$ and $S^{(0)}$ are the values of mass per unit area and wall restoring force at a reference value R_0 of R (taken, arbitrarily, to be 2562.8 throughout). Three classes of wave-mode were found, namely Tollmien-Schlichting (TS), wall flutter-modes (which will be labelled F modes, and correspond to free waves on the flexible wall) and a class of slow-moving wall mode typically propagating upstream and having weak rates of amplification or damping (S modes). This latter class corresponds to the 'Kelvin-Helmholtz' (KH) mode-class of Sen & Arora (1988). Examples of the three mode classes are shown in Figure 4.1 and in Tables 4.1 and 4.2.

In the absence of modal interactions, TS mode eigenvalues are typically very similar to their rigid-wall counterparts, having c_r values between about 0.25 and 0.5 for the Reynolds numbers and wavenumbers considered herein. Since this work is principally concerned with resonant interactions, c_0 and S were mainly chosen to give wall modes having similar c_r to those for Tollmien-Schlichting (TS) modes. This was in order to allow the possibility of resonant triads formed from a mixture of mode types. Such values of c_0 and S have a tendency to produce strong linear interactions and ensuing very severe linear instability, as is evidenced in Figure 4.1, where $c_0 = 0.1$ and $S = 0.15$, and also in Tables 4.1–4.3. This is because TS and F modes have opposite energy signs in an appropriate choice of reference frame. As was explained in Chapter 1, if modes of differing energy signs of two uncoupled systems are close to each

other in some parameter space, then on coupling the systems they will interact and produce linear instability.

For the F mode of Figure 4.1, c_r decreases rapidly with wavenumber α. It is in fact easy to show that for the wall model (4.16) the behaviour of streamwise modes in the absence of wall damping is as follows:

$$c \sim \pm\sqrt{c_0^2 + \frac{S}{m\alpha^2}}. \tag{4.51}$$

Thus for small values of c_0, as we have in Figure 4.1, as α increases so c_r decreases as the inverse square of α; this is what is here observed. For the TS mode, c_r at first increases, but abruptly starts to decrease on reaching a certain closeness to the F mode eigenvalue curve. After this point, the TS mode curve mimics the F mode curve. These two modes are in fact interacting, as is demonstrated by the curves for c_i. There is a huge 'bubble' of instability, the F mode being unstable and the TS mode stable, which commences at about the same value of α as the sudden change in the slope of c_r for the TS mode; the instability extends beyond the upper limit of the investigated wavenumbers α. The F and TS modes are analogous to the complex-conjugate pairs of the classical Kelvin-Helmholtz instability, with the important difference that the c_r values for the two modes remain distinct rather than coalescing. The non-coalescence of the modes is due to the dissipative influence of viscosity— see Chapter 1 above.

A stiffer wall ($c_0 = 0.8$ and $S = 0.15$) produces a general increase in c_r for the F mode whilst not affecting the corresponding TS value very much (Figure 4.2, Table 4.1; see also Table 4.3(a)). Thus the TS and F modes do not come as close to each other as for the previous case, and the c_r for the TS wave has no abrupt changes of slope. The interaction is weaker than for the less stiff wall of Figure 4.1, certainly for the range of wavenumbers considered: c_i for the F mode has a smaller maximum value. Another consequence of the weaker interaction is that the TS mode is less damped ($c_i \sim -0.05$ rather than -0.15).

The linear modal interactions behave rather like the modal coalescence of Carpenter & Garrad (1986), and that illustrated in Chapter 2 above, except that the values of c_r for the two interacting modes remain distinct rather than

merging as is the case for true coalescence. The dispersion curves for c_i form upper and lower branches of a 'bubble', just like true coalescence, these typically being unstable and damped respectively (Figures 4.1 and 4.2, Tables 4.1–4.3). The lack of proper coalescence may perhaps be due in part to the particular choices of parameter values used here (for example, the wall being relatively less or more flexible than those considered by Carpenter & Garrad (1986), although it is not very meaningful to make such comparisons since the models are markedly different) or to the basic wall model itself, which is much simpler than that of the earlier authors. However, the main reason that coalescence does not occur is that the system studied herein is dissipative, that is, viscous; the results of Carpenter & Garrad (1986) are for potential flow over a compliant wall— a conservative system.

The eigenfunctions of the TS, F and S classes have distinctive shapes, as can be seen from Figures 4.3–4.7. Here and elsewhere all eigenfunctions ϕ and adjoints ψ are normalised to unity at $z = 1.7208$, that is at five displacement thicknesses from the wall; this normalisation was used by Hendriks (appendix to Usher & Craik 1975). There is much similarity between ϕ for Tollmien-Schlichting waves over rigid walls and for those over flexible walls as can be seen on comparing Figure 4.3 with Figure 3.2. For the two examples compared here, there is however a noticeable difference in the slopes of ϕ_r outside the boundary layer (that is, for $z > 1$). The adjoint functions are very similar also.

The F mode eigenfunction is completely different in shape to that of the TS mode, as can been seen from Figure 4.4. The normal velocity (of which ϕ is a measure) has its maximum at the wall and decreases rapidly with increasing z. This is of course expected for wall modes. The large value of ϕ_w is a consequence of normalisation being imposed in the free-stream rather than at the wall. The F mode adjoint eigenfunction also has a characteristic shape (Figure 4.4), with an extremely small imaginary part.

The S-class mode eigenfunction, illustrated in Figure 4.5, has a real part which bears some resemblance to ϕ_r for TS modes, although there is a 'kink' near the wall. The shape of the S-class eigenfunction is in fact just like that of the KH mode class eigenfunction given in Sen & Arora (1988), and we may

therefore state with confidence that these classes are equivalent. Note that the S-mode adjoint eigenfunction bears no resemblance to that for the TS mode.

Figures 4.6 and 4.7 depict an F mode and a TS mode at a wavenumber of $\alpha = 0.6$, larger than that for Figures 4.3 and 4.4. Here the TS and F modes are interacting linearly. The most remarkable feature is that ϕ_r for the F mode has changed drastically in shape from that of Figure 4.4, and now is indistinguishable from a TS mode. The imaginary part ϕ_i has retained its profile, albeit reflected about the z-axis and considerably increased in magnitude. Comparison of Figures 4.7 and 4.3 reveals much less dramatic changes for the TS mode— the main one being an increase in the size of ϕ_i. The dramatic change in character of the F-mode eigenfunction is solely due to its linear interaction with the TS mode. Here we do not have the straightforward phenomena of exchange of identities or Kelvin-Helmholtz instability that were so well illustrated in Chapter 2: viscosity has a greatly complicating influence. The principal physical effect of this behaviour is that the wall mode extends its influence (as measured by its normal velocity) much further out into the fluid.

4.5.2 Walls with damping

Introduction of linear damping d to the wall model can have a significant effect on these modal interactions, as we shall now see. In Figures 4.8 and 4.9 c_0 has a value of 0.6, less than Figure 4.2 but more than Figure 4.1; the restoring-force parameter $S = 0.15$ is however the same as for the previous cases. Thus the instability due to modal interaction has a strength intermediate to those earlier examples. The plots of c_r and c_i for the TS and F modes in Figure 4.8, where $d = 0.05$, are similar to that for Figure 4.1, except that the TS mode is now less damped than the F mode for wavenumbers α less than about 0.6. The F mode again forms the upper branch of the 'bubble' which is however displaced to wavenumbers a little higher than that shown in Figure 4.1. The maximum value of c_i for the F mode is about 0.08— indicating a moderately strong instability.

A larger damping factor $d = 0.1$ radically alters the characteristics of the dispersion curves, as is demonstrated by Figure 4.9. The c_r curves for the TS and F modes now cross one another, at $\alpha \approx 1.0$, and the region of instability

extends to smaller wavenumbers. It is now the TS mode which is unstable— it has exchanged rôles with the F mode, which is now damped. This reversal of the modal stability characteristics is due to the fundamentally different effects of damping on the TS and F modes: the former are Class A and hence destabilised by damping, whilst the latter being Class B are stabilised. These energy classes were postulated by Benjamin (1962) and Landahl (1962), and are discussed in Chapter 1. Note that the maximum value of c_i (for the range of wavenumbers considered) is reduced from $\sim$ 0.07 to $\sim$ 0.05 by the increase in damping; but this beneficial effect must be weighed against the increase in the range of wavenumbers for which there are unstable eigenmodes.

The S mode-class waves are rendered less stable by wall damping, suggesting that they are Class A, (and hence probably upstream-propagating TS waves): however, the eigenvalues for these waves are more sensitive to changes in the wall parameters than is expected for fluid modes, to such an extent that the author was unable to keep track of them or to find rigid-wall analogues (hence fewer S modes were located than TS and F modes). This indicates that they might be upstream-propagating wall modes (which we however expect to be stabilised by wall damping). Sen & Arora (1988) clearly hold the latter view, since they regard their KH modes as 'stationary periodic ripples' in the limit of $|c| \to 0$. There has been very little work done on upstream-propagating TS waves for any Orr-Sommerfeld problem, other than the derivation of formal bounds for the eigenvalues (Joseph 1968, 1969), although Mack (1984) does briefly mention them in the context of the spatial stability problem. Thus the true nature of these modes must be considered to be uncertain at present.

4.5.3 Other fluid modes

In addition to the three mode types already described, there also exist higher-order fluid modes (see for example Mack 1976, where these are discussed for the rigid-wall configuration) and oblique Squire modes of $\hat{v}$. The former category falls into two distinct groups, comprising discrete and continuous parts of the eigenvalue spectrum. These are in general heavily damped and hence often considered to be of little practical interest, although as α or R increases they migrate towards $c = 0$ in the (complex) phase-speed plane (that is, they

become less damped). It has been suggested that the continuous spectrum plays a role in the transfer of energy between the boundary layer and the free stream (Corner, Houston & Ross 1976), because the associated perturbation velocities can remain significant at the edge of the boundary layer and beyond. An example of a higher-order (HO) mode belonging to the discrete part of the spectrum is depicted in Figure 4.10, where a damping level $d = 0.2$ applies; see also Table 4.6(c). The HO eigenfunction and adjoint and those of the F mode are shown in Figures 4.11 and 4.12 respectively, for a wavenumber of 0.6. The TS and F eigenmodes (real parts) cross at $\alpha \approx 0.86$, as do the F and HO eigenmodes at $\alpha \approx 0.65$, just larger than the value at which we have sample plots of the eigenfunctions. The TS mode is unstable, with c_i having a maximum value of ~ 0.05. The F mode is strongly damped due to the presence of wall damping, with $c_i \approx -0.1$; and the HO is rather more heavily damped, having $c_i \approx -0.2$. The F mode strongly resembles a typical TS mode, as was the case in Figure 4.6. The HO mode also has some similarity with TS modes, but there are distinctive 'wobbles' in the profile of ϕ_r. The peaks in ϕ_i for the two modes are located at the critical point, where $c_r = \bar{u}$. Examination of the adjoints reveals remarkable similarities between them (and considerable differences from any previously considered). It seems that these modes are interacting in some way, although there is no evidence of this in the behaviour of c_i for these modes in Figure 4.10. We are in no doubt that the F mode has been correctly identified— an examination of Figure 4.13, where there is no wall damping, reveals that for $d = 0$ the dispersion curves are qualitatively very similar, in both real and imaginary parts, to those cases already considered in Figures 4.1 and 4.2.

Squire modes are solutions to the homogeneous version of (4.26), that is

$$\hat{v}''_{sq} - [\gamma^2 + i\gamma\tilde{R}(\bar{u} - c_{sq})]\hat{v}_{sq} = 0. \tag{4.52}$$

The outer boundary condition is the same as for the cross-flow velocities $\hat{v}_{1,2}$, that is (4.36), but at the wall we have the simple condition $\hat{v}_{sq}(0) = 0$. This is because Squire modes have no vertical velocity component, and hence cannot induce any displacement of the wall from its undisturbed position. Thus *in the*

linear limit there is no difference between Squire modes over flexible walls and their rigid-wall counterparts, at the same values of α and R. The Squire-mode problem is an eigensystem in its own right, with a spectrum of eigenvalues c_{sq}. It is known that these are all damped (see Davey & Reid 1977, where the mathematically equivalent problem of temperature modes in a stratified fluid is studied; and also Murdock & Stewartson 1977, where the plane Poiseuille problem is investigated via a model equation). However, they may resonate linearly or nonlinearly with the eigenvalues of the Orr-Sommerfeld system, either exactly or approximately, and therefore should not be overlooked.

Solutions to the Squire-mode equation are somewhat similar to the two viscous solutions of the Orr-Sommerfeld equation. There is a continuous spectrum of damped modes with $c_r = 1$, together with a set of discrete modes having smaller c_r. Interactions between TS and Squire modes in boundary-layer flow have been examined for the case of spatial disturbances by Nayfeh (1985): he found that the interactions could be strong, hence suggesting that they represent an additional means of amplifying three-dimensional effects. Herbert (1983a,b) has studied forms of secondary instability in rigid-wall flows (that is, three-dimensional effects that follow the Tollmien-Schlichting instability); he found that near-resonant triads can be formed between a TS wave and a pair of (highly damped) Squire modes.

The present author experienced difficulty in locating Squire modes: in the absence of initial guesses, the iterative convergence scheme was unsuccessful, and the Principle of the Argument (PA) method proved inadequate; this is because, as for the Orr-Sommerfeld S-modes, the eigenvalues are located in very narrow troughs of the eigenvalue function $E(c_r, c_i; \alpha, R)$. Hence a substantial amount of cpu time is required for the PA algorithm to reduce the initial contour in the (c_r, c_i)-plane to a size comparable to the diameter of the trough.

4.6 Results for the resonant-triad problem

4.6.1 Resonant triads of three TS waves

Resonant triads comprising three TS waves were located mainly for one set of wall parameters, but considering a wide range of wavenumbers α and Reynolds numbers R, and are presented in Tables 4.7 and 4.8. The wall pa-

rameters were selected to emulate a wall that is stiff enough to preclude linear modal interactions. The real part of phase speed, c_r, is generally higher than for the equivalent rigid-wall case. It is difficult to make any firm observations on the effect of surface compliance on linear stability from these results, except to say that in the main both the streamwise and oblique modes are a little more amplified (or less damped) than their rigid-wall analogues; this indicates that the wall parameters selected here are not beneficial in promoting transition delay.

Quadratic interaction coefficient moduli are plotted against wavenumber at constant R in Figure 4.14a, along with the corresponding rigid-wall values. It will be seen that the difference between the two cases in terms of these coefficients is only small, although the compliant-wall values are usually larger. A comparison of the propagation angles θ of the oblique constituents of the triads for the two configurations (Figure 4.14b) reveals that the obliquity is consistently greater for compliant wall flow than for rigid wall flow. The phases of a_1 and a_3 are given in Table 4.7: as for the rigid-wall case (Table 3.3), $\arg a_1$ exhibits a general decrease with increasing α, whilst $\arg a_3$ is much more erratic. Quadratic interaction coefficient moduli and propagation angles are plotted against Reynolds number for (fixed) $\alpha = 0.29056$ in Figure 4.15, and for $\alpha = 1.0$ in Figure 4.16. Here differences between the rigid and compliant cases are a little more apparent, although they remain broadly similar. For $\alpha = 1.0$, the oblique coefficients at first increase in magnitude with R, but eventually begin to decrease; the behaviour of their respective arguments (Table 4.8) is similar to the previous case (Table 4.7). The propagation angles θ decrease with R as they do with α, but more markedly.

A few results are also given for a slightly stiffer wall in Table 4.7. Once again, there is no consistent trend in the linear stability data, although c_i is smaller than for the less stiff wall and larger than for the rigid wall (which is as expected, since the rigid wall corresponds to the limit of infinite stiffness).The quadratic interaction coefficients are however clearly always a little smaller in magnitude than for the less stiff wall; this indicates that wall flexibility has a reinforcing effect on the strength of resonant triad interactions, even though no

wall modes are participating.

4.6.2 Mixed-mode resonant triads

It was envisaged at the outset that resonant triads comprising a mixture of TS and other modes would be of particular interest. However, as has already been mentioned, location of such triads was hampered by the presence of modal coalescence or near-coalescence. Indeed, the author was unable to locate any clear example of this sort of resonant triad. This does not imply that such triads do not exist, because an exhaustive search of wall parameter space would require to be undertaken before such an assertion could be made, and would be a daunting task. However, it is undoubtedly true that the existence of such triads is crucially dependent on the particular wall model considered.

It is quite difficult to locate any triads with oblique wall (F) mode constituents: this is because the the eigenvalue $\tilde{c}$ for such modes (the free-wave speed on the wall) varies with α according to

$$\tilde{c}_r \sim \pm\sqrt{\frac{\alpha}{2\gamma}c_0^2 + \frac{4S}{m\alpha^2}}, \tag{4.53}$$

in the absence of wall damping. Note the differences between (4.53) and (4.51): the factor $\frac{\alpha}{2\gamma}$ is due to the particular form of tension we have selected; but the extra 4 in the restoring-force term arises from the particular form of periodicity $\exp\{\mathrm{i}(\frac{1}{2}\alpha x \pm \beta y - \frac{1}{2}\alpha\tilde{c}t)\}$ that is required for Craik-type resonance. The effect is generally to make $\tilde{c}$ much larger than c, which obviously is detrimental to the location of resonant triads.

Triads comprising three wall modes have nevertheless been located, and two examples are given in Table 4.9. The oblique interaction coefficients $|a_1|$ are large, being O(100) whilst the streamwise coefficient $|a_3|$ remains O(1). (Note that in each case there is some linear instability, and for the second wall-mode triad presented c_i and $\tilde{c}_i$ are both rather large at $O(10^{-2})$. A TS-mode triad at the same values of α, R and wall parameters as one of the wall triads is also given, and it will be observed that a_1 for the TS triad is substantially less than for the wall-mode triad (note also the comparative smallness of the propagation angles θ for the oblique modes in both cases). The eigenfunctions, their adjoints and the cross-flow velocity are presented in Figure 4.17.

Triads formed of a streamwise TS wave and a pair of oblique higher-order modes have been located at a Reynolds number of 15000, and are presented in Table 4.9 for both rigid-wall and compliant-wall configurations. The oblique modes are significantly damped in the linear regime ($c_i \approx 0.1$) but nevertheless have remarkably large oblique quadratic interaction coefficients a_1, these being O(8000) in modulus for the compliant wall and O(6000) for the rigid wall; the a_3 remain O(1) in magnitude. These particular triads could be written off as of no practical significance because of their rather strong linear damping, but examples exhibiting less severe damping may well be possible.

4.6.3 Mixed-mode resonant triads with wall damping

The presence of linear modal interaction has a strong influence on the nature of resonant triad interactions. Figure 4.18 shows dispersion curves for three modes, namely a TS, an F and a higher-order fluid mode. A damping coefficient $d = 0.2$ applies here. The TS and F mode phase speeds (real parts) cross at $\alpha \approx 0.86$, and strong linear interaction is indicated by the presence of a 'bubble' in Figure 4.10b (c_i versus α). This particular scenario admits a wide variety of resonant triad configurations, involving all three of the different mode-types here present. Triads have been located at the various points marked on the curves. Points A, B, C, D, E indicate the eigenvalues of streamwise constituents of resonant triads, where all three participating modes are of TS type. In each case the streamwise mode is undergoing a strong linear interaction with the streamwise F-mode (the interaction occurs over a wide range of wavenumbers α, as can be seen from Figure 4.10b). It is the TS mode which is driven unstable ($c_i \approx 0.05$ at most), but the wall damping mitigates the severity of the instability (cf. Figure 4.13, where $c_i \approx 0.088$ at most for the F mode). Points X, Y, Z correspond to a streamwise wall mode interacting resonantly with a pair of oblique TS modes. All the triads located are tabulated in Table 4.10. The various points A–E, X–Z just represent particular examples of the triads that may be constructed: there are in fact two continua of points representing triads, each of which extends some distance along the TS and F mode dispersion curves (we have not determined these distances).

The quadratic interaction coefficients for the heterogeneous TS triads are

highly interesting as can be seen from Figure 4.19: $|a_1|$ has a sharp spike centred at about $\alpha = 1.0$, with maximum magnitude of approximately 2000. The streamwise coefficient a_3 behaves much less spectacularly, being O(10) in magnitude and having its maximum in the region $\alpha = 0.8$–0.9. Note however that $|a_3|$ is an order of magnitude larger than has hitherto been normal for TS triads. It is clear from Table 4.10 that the phases $\arg a_3$, $\arg a_1$ of the interaction coefficients are markedly different from earlier cases: $\arg a_1$ is typically $\sim 30°$ rather than roughly 90°; and the smallness of $\arg a_3$ indicates that a_3 is almost a pure real number. The propagation angles θ are somewhat larger than previously, decreasing with α from $\sim 69°$ to about 57°.

The eigenfunctions, their associated adjoints and the cross-flow velocity are presented in Figure 4.20: the cross-flow velocity and its derivatives are large in magnitude relative to other triads, and it is these functions which give rise to the unusually large value of $|a_1|$. It was considered a possibility that the large values of $\hat{v}$ are due to resonance or near-resonance with Squire modes; but a search for Squire modes with appropriate values of c_r (that is, close to 0.5012) proved unsuccessful.

The interactions at points X, Y, Z are no less interesting (Table 4.10, Figure 4.18): at point X, the streamwise triad component experiences a *stronger* resonant interaction than its oblique counterparts ($|a|_3 > |a|_1$), though as α increases this interaction weakens rapidly unlike the oblique ones. The phases $\arg a_3$, $\arg a_1$ and the oblique-wave propagation angle θ also change substantially as α increases from 0.8 to 1.0.

Points 1–4 of Figure 4.18 and Table 4.10 designate the linear eigenvalues of the streamwise constituents of four different resonant triads that have been located for a streamwise wavenumber $\alpha = 1.2$. For points 1 and 2 the streamwise mode is a higher-order fluid mode, whereas for points 3 and 4 the streamwise mode is a TS mode. The two oblique constituents of these four triads are of the following mode-classes: for point 1, wall (F); for point 2, TS; for point 3, TS; for point 4, wall (F). For each of the triads the oblique modes experience strong resonant interaction, as indicated by the values of $|a_1|$, which are all O(100). The triad at point 3, comprising three TS waves, has the largest value of $|a_1|$,

but by contrast also has the smallest value of the streamwise coefficient $|a_3|$.It will be seen from Table 4.10 that the phases $\arg a_3$ are again small, indicating that a_3 is almost pure real; no trend can be discerned in the values of $\arg a_1$.

Dispersion curves of $\tilde{c}$ versus the transverse wavenumber β, at fixed values 0.9, 1.0 and 1.2 of α are given in Figures 4.21, 4.22 and 4.23 respectively. Both oblique TS and oblique F mode eigenvalues are shown, and the locations of computed resonant triads are shown. A linear interaction is taking place between the TS and F modes, which increases with increasing α. The mode-crossing phenomenon that is a feature of linear interactions in the presence of wall damping is observed to occur at $\alpha = 1.2$ (Figure 4.23), but not at the smaller values of α (Figures 4.21, 4.22). One may speculate that this linear interaction is in some way responsible for the curious spike in $|a_1|$ described earlier, although the nature of the underlying mechanism is at present unclear. Eigenfunctions, adjoints and cross-flow velocities for the triads at points 1–4 are given in Figures 4.24–4.27.

In Figure 4.24, we see that ϕ_3 has the distinctive profile of higher-order fluid modes; and ϕ_{3i} has a strong peak, which is in fact located at the critical point z_c. The oblique F mode ϕ_1 looks like a TS mode, but the maximum value is in fact at the wall. The cross-flow velocity $\hat{v}_1$ is very much like those of Figures 3.2 and 4.20, and is like them almost entirely located within the third quadrant of the complex plane.

From Figure 4.25 we see that the oblique TS mode ϕ_1 has the profile expected, with its maximum amplitude well away from the wall; but the imaginary part resembles an F mode. (Note that points 1 and two share a common streamwise mode, as do points 3 and 4). The cross-flow velocity is noticably bigger than that for point 1, though of very similar shape.

At point 3 we have a triad composed of three TS waves. The eigenfunction profiles are as expected, with maxima away from the wall (Figure 4.26). The cross-flow velocity has similar magnitude to that for point 1.

From Figure 4.27 we see that the oblique F mode eigenfunction ϕ_{1r} has maximum amplitude both at the wall and at a certain distance from it. The cross-flow velocity $\hat{v}_1$ resembles that for point 2 in magnitude, but the definite

'kink' at $z \approx 0.8$ is similar to that occuring in $\hat{v}_1$ for point 1 (and also evident in Figure 4.20).

When considering the relative magnitudes of quadratic interaction coefficients a_3, a_1 for different resonant triads, and even within the same triad, it must be remembered that these magnitudes are dependent on the normalisations employed for ϕ_j and ψ_j. This is particularly important when comparing wall modes (F or S) with fluid modes (TS or HO). The obvious normalisation to employ for wall modes is to set ϕ_w equal to some constant, say unity, but this is not very suitable for fluid modes, especially when one is also considering the rigid-wall problem. We have imposed normalisation at a point away from the wall because this permits investigation of both basic scenarios.

4.7 Conclusions

4.7.1 The linear regime

We have found and examined four distinct classes of wave-mode for the problem of Blasius flow over flexible walls, which we labelled TS, HO, F and S. The Tollmien-Schlichting (TS) class has very similar properties to its rigid-wall counterpart, as does the HO class of discrete higher-order wave-modes. The class of wall modes which we have termed F modes is identifiable with the FISI of Carpenter & Garrad (1986), and the CIFI of Yeo (1986); the S class corresponds to that of Sen & Arora (1988).

The stability of TS modes is determined in the absence of modal interaction principally by the values of wavenumber α and Reynolds number R, being much less dependent on wall parameter-values. The F modes, being fundamentally inviscid in character, are typically very close to a state of neutral stability, again provided they are not participating in modal interaction. The S modes that have been located for various walls have a tendency to be very slow-moving ($c_i \approx 0$), usually in the upstream direction, and have small to moderate ($-0.05 < c_i < 0$) rates of linear damping. We believe these to be wall modes, although this has not been definitely established. The HO modes tend not to be especially interesting, at least in the linear regime, as they are strongly damped except for large values of α and/or R.

Modal interaction between TS waves (Class A) and F waves (Class B) al-

most invariably produces strong instability of one or other of the participating modes. Such interactions have some similarity to the classical Kelvin-Helmholtz instability— the c_i versus α curves for the two modes have the familiar 'bubble' shape, the extent of this bubble indicating the range of wavenumbers over which linear interaction is occurring. There are important differences, however: the c_r values of the modes do not coincide during the interaction but remain distinct, that is there is no *coalescence*; and the phenomena of quasi-Kelvin-Helmholtz instability and modal exchange of identities are not mutually exclusive, unlike non-dissipative cases such as that studied earlier in Chapter 2. F-mode eigenfunctions are often transformed by modal interaction into forms indistinguishable from TS-mode eigenfunctions, but the converse has not been observed.

Clearly such instabilities are most undesirable, and they are best avoided by choosing walls which have sufficient stiffness to render c_r for the F modes appreciably larger than c_r for TS modes at all relevant values of α and R.

[In this work we have not investigated the linear instability of oblique wave-modes for preselected propagation angles θ, being principally interested in nonlinear resonant interactions. Such problems have been admirably studied elsewhere, for example in the work of Yeo (1986).]

4.7.2 Resonant triad interactions

We have searched for and located numerous examples of Craik-type resonant triads (Craik 1971), for various values of α, R and of the wall parameters m, c_0, d, S. The located triads comprise a variety of combinations of TS, F and HO modes. Triads composed of three TS waves show nontrivial but small differences from rigid-wall analogues regarding both the magnitudes of the quadratic interaction coefficients a_3 and a_1 and their respective variations with α and R. It has been demonstrated that triads of three wall modes (that is, F modes) are possible for our spring-backed tensioned membrane wall model. These triads are not found at such low values of α as TS triads, because of differences in the α-variation of c_r and $\tilde{c}_r$. Constructive comparison of quadratic interaction coefficients for wall-mode triads with those for TS triads is difficult due to the difficulty in defining a mutually satisfactory normalisation of the respective

eigenfunctions.

Triads comprising a streamwise TS mode and two oblique (strongly linearly damped) HO modes have been found for both rigid and compliant wall cases. These are notable principally for the remarkably large magnitudes of the quadratic interaction coefficients : $|a_1| \sim O(1000)$. The streamwise, reasonably near-neutral TS mode has a less exceptional interaction coefficient, though: $|a_3| \sim O(1)$. It is known (Mack 1976) that for HO modes c_i and c_r both approach zero with increasing α or R, implying that such resonant-triad interactions may well be of physical significance at large wavenumbers. Large values of R are unlikely to be practically important however, as they tend to imply turbulent flow regimes.

A particular situation involving linear modal interactions in the presence of wall damping was found to support an abundance of resonant triads of varying composition. There are a number of curious aspects to the data obtained for these triads, most notably the spike in the graph of oblique interaction coefficient modulus $|a_{1,2}|$ versus α for the case of triads composed of three TS waves. It is most unlikely that normalisation has much to do with this particular effect, which is related to the α-variation of the cross-flow velocities $v_{1,2}$. Linear resonance with Squire modes may be responsible, but we did not manage to prove this.

In conclusion, then, it is clear that flexible walls greatly enrich the possibilities for the formation of resonant triads, but linear instabilities in the form of modal interactions tend often to be present for the required parameter values. The strength of these often vigorous instabilities can be reduced by the introduction of judicious amounts of wall damping, but this tends to further complicate the phenomenology of the interactions.

We believe that our understanding of this very complex problem would be significantly enhanced by a re-examination of it from the standpoint of nonlinear, high Reynolds number triple-deck theory, in tandem with further, carefully selected numerical investigations.

Chapter 5 Overall conclusions

5 Overall conclusions

In this work we have made what is to our knowledge the first investigation of resonant interactions in flows over flexible walls. This being so, it was endeavoured to restrict attention to relatively simple problems using simple wall models. Firstly, in Chapter 2 free-surface inviscid flow over a flexible wall was studied: this could be described as a model problem, a preliminary foray into this area of hydronamic stability theory. The phenomenology of linear modal interactions was examined in detail, giving valuable insight and complementing the work of other authors for different (but in some sense analogous) flow configurations. The amplitude evolution equations for resonant triad interactions were derived both by a multiple scales approach and by an averaged Lagrangian technique, the forms of the interaction coefficients being given explicitly.

Chapter 3 was concerned with Blasius flow over a rigid wall. Our main aim was to extend the work of Hendriks (appendix to Usher & Craik 1975) on resonant-triad interactions. The original formulation of Craik (1971) was re-derived, and a considerable number of resonant triads together with their associated quadratic interaction coefficients was computed. The coefficients were found to increase substantially both with increasing wavenumber and with increasing Reynolds number, as broadly predicted by Craik (1971).

In Chapter 4 we proceeded to study the topical subject of Blasius flow over flexible walls. Some illustrative linear results were given, showing the severe and generally detrimental effects of linear modal interactions. Three-dimensional resonant triads were then sought and located, and the quadratic interaction coefficients determined numerically. As had been anticipated, the multiplicity of mode-types was shown to give rise to many interesting phenomena; these can be expected to be of importance in selecting and designing compliant surfaces with optimal transition-delaying properties, although it is recognised that further work is necessary to explain all the characteristics of the resonant interactions reported herein.

References

Amfilokhiev, V. B., Droblenkov, V. V. & Zavordkhina, A. S. (1972) Growth of small disturbances in a boundary layer on an elastic surface. [In Russian.] *PMTF-Zh. Prikl. Mekh. i Tekh. Fiz.*, March–April, 137–139

Ball, F. K. (1964) Energy transfer between external and internal gravity waves. *J. Fluid Mech.* **19**, 465–78

Benjamin, T. B. (1959) Shearing flow over a wavy boundary. *J. Fluid Mech.* **6**, 161–205

Benjamin, T. B. (1960) Effects of a flexible boundary on hydrodynamic stability. *J. Fluid Mech.* **9**, 513–532

Benjamin, T. B. (1963) The threefold classification of unstable disturbances in flexible surfaces bounding inviscid flows. *J. Fluid Mech.* **16**, 436–450

Benjamin, T. B. (1964) Fluid flow with flexible boundaries. In *Proc. 11th Intl. Congr. Appl. Mech., Munich* (ed. H. Görtler), p109. Springer.

Biringen, S. (1984) Active control of transition by periodic suction blowing. *Phys. Fluids* **27**(6), 1345

Brazier-Smith, P. R. & Scott, J. F. (1984) Stability of fluid flow in the presence of a compliant surface. *Wave Motion* **6**, 547–560

Bretherton, F. P. (1964) Resonant interactions between waves. The case of discrete oscillations. *J. Fluid Mech.* **20**, 457–479

Buckingham, R. A. (1957) *Numerical Methods.* London: Pitman

Cairns, R. A. (1979) The role of negative energy waves in some instabilities of parallel flows. *J. Fluid Mech.* **92**, 1–14

Case, K. M. & Chiu, S. C. (1977) Three-wave resonant interactions of gravity-capillary waves. *Phys. Fluids* **20**, 742–745

Carpenter, P. W. (1985) The optimization of compliant surfaces for transition delay, *University of Exeter Technical note* 85/2

Carpenter, P. W. (1989) Status of transition delay using compliant walls. In *Viscous Drag Reduction* (eds. D. M. Bushnell, J. N. Heffner), *AIAA* (to appear)

Carpenter, P. W. & Garrad, A. D. (1985) The hydrodynamic stability of flow over Kramer-type compliant surfaces. Part 1. Tollmien-Schlichting instabilities.

J. Fluid Mech. **155**, 465–510

Carpenter, P. W. & Garrad, A. D. (1986) The hydrodynamic stability of flow over Kramer-type compliant surfaces. Part 2. Flow-induced surface instabilities. *J. Fluid Mech.* **170**, 199–232

Corner, D., Houston, D. J. R. & Ross, M. A. S. (1976) Higher eigenstates in boundary- layer stability theory. *J. Fluid Mech.* **77**, 81–103

Craik, A. D. D. (1968) Resonant gravity-wave interactions in a shear flow. *J. Fluid Mech* **34**, 531–549

Craik, A. D. D. (1971) Non-linear resonant instability in boundary layers. *J. Fluid Mech.* **50**, 393–413

Craik, A. D. D. (1986a) *Wave Interactions And Fluid Flows.* Cambridge: C.U.P.

Craik, A. D. D. (1986b) Exact solutions of non-conservative equations for three-wave and second-harmonic resonance. *Proc. Roy. Soc.* **A 406**, 1–12

Craik, A. D. D. (1987) A note on the exact solutions for non-conservative three-wave resonance. *Proc. Roy. Soc. Edin.* **106A**, 205–207

Craik, A. D. D. & Adam, J. A. (1978) Evolution in space and time of resonant wave triads. I. The 'pump-wave approximation'. *Proc. Roy. Soc.* **A 363**, 243–255

Craik, A. D. D. & Adam, J. A. (1979) 'Explosive' resonant wave interactions in a three-layer fluid flow. *J. Fluid Mech.* **92**, 15–33

Davey, A. (1980) On the numerical solution of difficult boundary-value problems. *J. Comp. Phys.* **35**(1), 36–47

Davey, A. & Nguyen, H. P. F. (1971) Finite-amplitude stability of pipe flow. *J. Fluid Mech.* **45**, 701–720

Davey, A. & Reid, W. H. (1977) On the stability of stratified viscous plane Couette flow. Part 1: Constant buoyancy flow. *J. Fluid Mech.* **80**, 509–525

Domaradzki, J. & Metcalfe, R. W. (1987) Stabilization of laminar boundary layers by compliant membranes. *Phys. Fluids* **30**(3), 695–705

Fasel, H. (1976) Investigation of the stability of boundary layers by a finite-difference model of the Navier-Stokes equations. *J. Fluid Mech.* **78**, 355–383

Gad-el-Hak, M. (1986) Compliant coatings research: a guide to the experimentalist. *J. Fluids and Structures* **1**(1), 55–70

Gad-el-Hak, M., Blackwelder, R. F. & Riley, J. J. (1984) On the interaction of compliant coatings with boundary-layer flows. *J. Fluid Mech.* **140**, 257–280

Gaster, M. (1962) A note on the relation between temporally-increasing and spatially-increasing disturbances in hydrodynamic stability. *J. Fluid Mech.* **14**, 222–224

Gaster, M. (1965) On the generation of spatially growing waves in a boundary layer. *J. Fluid Mech.* **22**, 433–441

Gaster, M. (1977) Series representation of the eigenvalues of the Orr-Sommerfeld equation. *Laminar-turbulent transition: AGARD conference proceedings No. 224*

Gill, A. E. & Davey, A. (1969) Instabilities of a buoyancy-driven system. *J. Fluid Mech.* **35**, 775–798

Grosch, C. E. & Salwen, H. (1978) The continuous spectrum of the Orr-Sommerfeld equation. Part 1. The spectrum and the eigenfunctions. *J. Fluid Mech.* **87**, 33–54

Grosskreutz, R. (1971) Wechselwirkungen zwischen turbulenten Grenzschichten und weichen Wänden. *MPI für Strömungsforschung und der AVA, Göttingen, Mitt. No. 53*

Grosskreutz, R. (1975) An attempt to control boundary-layer turbulence with nonisotropic compliant walls. *University Science Journal (Dar es Salaam)* **1**, 67–73

Gyorgyfalvy, D. (1967) Possibilities of drag reduction by the use of flexible skin. *J. Aircraft* **4**, 186–192

Hall, M. S. (1988) The interaction between a compliant material and an unstable boundary layer flow. *J. Comp. Phys.* **76**, 33–47

Hansen, R. J. & Hunston, D. L. (1983) Fluid-property effects on flow-generated waves on a compliant surface. *J. Fluid Mech.* **133**, 161–177

Herbert, T. (1983a) Subharmonic three-dimensional disturbances in unstable shear flows. *AIAA Paper* **83**–1759

Herbert, T. (1983b) Modes of secondary instability in plane Poiseuille flow.

Proc. IUTAM Symp. 'Tubulence and Chaotic Phenomena in Fluids', Kyoto 1983

Herbert, T. (1984) Analysis of the subharmonic route to transition in boundary layers. *AIAA Paper* 84–0009

Herbert, T. (1988) Secondary instability in boundary layers. *Ann. Rev. Fluid Mech.* **20**, 487–526

Ince, E. L. (1956) *Ordinary Differential Equations.* Dover

Jimenez, J. & Whitham, G. B. (1976) An averaged Lagrangian method for dissipative wavetrains. *Proc. Roy. Soc.* **A 349**, 277–287

Jordinson, R. (1970) The flat-plate boundary layer. Part 1. Numerical integration of the Orr-Sommerfeld equation. *J. Fluid Mech.* **43**, 801–811

Jordinson, R. (1971) Spectrum of eigenvalues of the Orr-Sommerfeld equation for Blasius flow. *Phys. Fluids* **14**, 2535–7

Joseph, D. D. (1968) Eigenvalue bounds for the Orr-Sommerfeld equation. *J. Fluid Mech.* **33**, 617–621

Joseph, D. D. (1969) Eigenvalue bounds for the Orr-Sommerfeld equation. Part 2. *J. Fluid Mech.* **36**, 721–734

Kachanov, Yu. S. & Levchenko, Ya. V. (1984) The resonant interaction of disturbances at laminar-turbulent transition in a boundary layer. *J. Fluid Mech.* **138**, 209–247

Kaup, D. J. (1981) The lump solutions of the Bäcklund transformation for the three-dimensional three-wave resonant interaction. *J. Math. Phys.* **22**, 1176–1181

Kaup, D. J., Reiman, A. & Bers, A. (1979) Space-time evolution ofnonlinear three-wave interactions. I. Interactions in a homogeneous medium. *Rev. Mod. Phys.* **51**, 275–310 [Errata, in *Rev. Mod. Phys.* **51**, 915, are corrected in reprints.]

Klebanoff, P. S., Tidstrom, K. D. & Sargent, L. M. (1962) The three-dimensional nature of boundary-layer instability *J. Fluid Mech.* **12**, 1–34

Kleiser, L. & Laurien, E. (1985) Numerical investigation of interactive transition control. *AIAA Paper* 85–0566

Korotkin, A. I. (1965) The stability of laminar boundary layers in the presence

of compliant boundaries. M.I.T. Sc.D. Thesis

Kramer, M. O. (1957) Boundary-layer stabilisation by distributed damping. *J. Aero. Sci.* **24**,459

Kramer, M. O. (1960) The dolphins' secret. *New Scientist* **7**, 1118–1120

Kramer, M. O. (1962) Boundary-layer stabilisation by distributed damping. *J. Am. Soc. Naval Engrs.* **74**, 341–348

Kramer, M. O. (1965) Hydrodynamics of the dolphin. *Adv. in Hydrosci.* **2**, 111–130

Landahl, M. T. (1962) On the stability of a laminar incompressible boundary layer over a flexible surface *J. Fluid Mech.* **13**, 609–632

Landau, L. D. (1944) On the problem of turbulence. *C.R. Acad. Sci. U.R.S.S.* **44**,311–314 (Also *Collected Papers* (1965), pp. 387–391)

Landahl, M. T. & Kaplan, R. E. (1965) Effect of compliant walls on boundary layer stability and transition. *AGARDograph* **97**-1-353

Lekoudis, S. G. & Sengupta, T. K. (1986) Two-dimensional turbulent boundary layers over rigid and moving swept wavy surfaces. *Phys. Fluids* **29**, 964–970

Lin, C. C. (1945) On the stability of two-dimensional parallel flows, Parts I, II and III. *Q. Appl. Maths* **3**, 117–142, 218–234, 277–301

Luke, J. C. (1967) A variational principle for a fluid with a free surface. *J. Fluid Mech.* **27**, 395–397

Ma, Y.-C. (1984) Resonant triads and direct resonance for Kelvin-Helmholtz waves. *Phys. Fluids* **27**, 571–578

Mack, L. M. (1976) A numerical study of the temporal eigenvalue spectrum of the Blasius boundary layer. *J. Fluid Mech.* **73**, 497–520

Mack, L. M. (1984) Boundary-layer stability theory. *AGARD special course on stability and transition of laminar flow*

Metcalfe, R. W., Rutland, C.J., Duncan, J.H. & Riley, J. J. (1986) Numerical simulations of active stabilizations of laminar boundary layers. *AIAA J.* **24**, 1494–1501

Miles, J. W. (1957) On the generation of surface waves by shear flows. *J. Fluid Mech.* **3**, 185–199

Miles, J. W. (1959a) On the generation of surface waves by shear flows. Part

2. *J. Fluid Mech.* **6**, 568–582

Miles, J. W. (1959b) On the generation of surface waves by shear flows. Part 3. Kelvin-Helmholtz instability. *J. Fluid Mech.* **6**, 583–598

Miles, J. W. (1962) On the generation of surface waves by shear flows. Part 4. *J. Fluid Mech.* **13**, 433–448

Miles, J. W. (1986) Weakly nonlinear waves in a stratified fluid: a variational formulation. *J. Fluid Mech.* **172**, 499–512

Murdock, J. W. & Stewartson, K. (1977) Spectrum of the Orr-Sommerfeld equation. *Phys. Fluids* **20**, 1404–1411

Nayfeh, A. H. (1985) Three-dimensional spatial secondary instability in boundary-layer flows. *AIAA Paper* **85**–1697

Ng, B. S. & Reid, W. H. (1979) An initial value method for eigenvalue problems using compound matrices. *J. Comp. Phys.* **30**(1), 125–136

Nisewanger, C. R. (1964) Flow noise and drag measurements of vehicle with compliant coating. *U.S. Naval Ordnance Test Station, China Lake, California. NAVWEPS Rep.* 8518

Nonweiler, T. (1961) Qualitative solutions of the stability equation for a boundary layer in contact with various forms of flexible surface. *A.R.C. Rep. No.* **22**, 670

Orszag, S. A. (1971) Accurate solution of the Orr-Sommerfeld stability equation. *J. Fluid Mech.* **50**, 689–703

Puryear, F. W. (1962) Boundary layer control drag reduction by compliant surfaces. *U.S. Dept. of Navy, David Taylor Model Basin. Report* 1668

Riley, J. J., Gad-el-Hak, M. & Metcalfe, R. W. (1988) Compliant coatings. *Ann. Rev. Fluid Mech.* **20**, 393–420

Ritter, H. & Messum, L. T. (1964) Water tunnel measurements of turbulent skin friction on six different compliant surfaces of one foot length. *Admiralty Research Laboratory Report* ARL/G/N9

Ritter, H. & Porteous, J S. (1965) Water tunnel measurements of skin friction on a compliant coating. *Admiralty Research Laboratory Report* ARL/N3/G/HY/9/7

Saric, W. S. & Thomas, A. S. W. (1984) Experiments on the subharmonic

route to turbulence in boundary layers. *Proc. IUTAM Symp. 'Turbulence and Chaotic Phenomena in Fluids', Kyoto* 1983

Schlichting, H. (1933) Zur Entstehung der Turbulenz bei der Plattenströmung. *Z. angew. Math. Mech.* **13**, 171–174

Sen, P. K. & Arora, D. S. (1988) On the stability of laminar boundary-layer flow over a flat-plate with a compliant surface. *J. Fluid Mech.* **197**, 201–240

Sen, P. K. & Venkateswarlu, D. (1983) On the stability of plane-Poiseuille flow to finite-amplitude disturbances, considering the higher-order Landau coefficients. *J. Fluid Mech.* **133**, 179–206

Sen, P. K., Venkateswarlu, D. & Maji, S. (1985) On the stability of pipe-Poiseuille flow to finite-amplitude axisymmetric and non-axisymmetric disturbances. *J. Fluid Mech.* **158**, 289–316

Simmons, W.F. (1969) A variational method for weak resonant wave interactions. *Proc. Roy. Soc.* **A 309**, 551–575

Smith, F. T. (1979) On the non-parallel flow stability of the Blasius boundary layer. *Proc. Roy. Soc.* **A 366**, 91–109

Smith, F. T. & Stewart, P. A. (1987) The resonant-triad nonlinear interaction in boundary-layer transition. *J. Fluid Mech.* **179**, 227–252

Squire, H. B. (1933) On the stability for three-dimensional disturbances of viscous fluid flow between parallel walls. *Proc. Roy. Soc.* **A 142**, 621–628

Stuart, J. T. (1960) On the non-linear mechanics of wave disturbances in stable and unstable parallel flows. Part 1. The basic behaviour in plane Poiseuille flow. *J. Fluid Mech.* **9**, 353–370

Thomas, L. H. (1953) The stability of plane Poiseuille flow. *Phys. Rev.* **91**, 780–784

Thomas, M. D. (1988) Comparison of the compound matrix and orthonormalisation methods for calculating the stability of heated water boundary layers. *Admiralty Research Establishment Tech. Memo.* ARE(UHA) 88505

Thomas, M. D. & Craik, A. D. D. (1988) Three-wave resonance for free-surface flows over flexible boundaries. *J. Fluids and Structures* **2**, 323–338

Tollmien, W. (1929) Über die Entstehung der Turbulenz. *1. Mitt., Nachr. Ges. Wiss. Göttingen, Math. Phys. Klasse*, pp. 21–44

Usher, J. R. & Craik, A. D. D. (1974) Nonlinear wave interactions in shear flows. Part 1. A varational formulation. *J. Fluid Mech.* **66**, 209–221

Usher, J. R. & Craik, A. D. D. (1975) Nonlinear wave interactions in shear flows. Part 2. Third-order theory. *J. Fluid Mech.* **70**, 437–461

Volodin, A. G. & Zel'man, M. B. (1979) Three-wave resonance interaction of disturbances in a boundary layer. *Fluid Dyn.* **13**, 698–703 [Translation of *Mekh. Zhid. i Gaza* **5**, 78–84]

Watson, J. (1960) On the non-linear mechanics of wave disturbances in stable and unstable parallel flows. Part 2. The development of a solution for plane Poiseuille flow and for plane Couette flow. *J. Fluid Mech.* **9**, 371–389

Weiland, J. & Wilhelmsson, H. (1977) *Coherent nonlinear interaction of waves in plasmas.* Oxford: Pergamon

Wersinger, J-M., Finn, J. M. & Ott, E. (1980a) Bifurcations and strange behaviour in instability saturation by nonlinear mode coupling. *Phys. Rev. Lett.* **44**, 453–456

Wersinger, J-M., Finn, J. M. & Ott, E. (1980b) Bifurcation and 'strange' behaviour in instability saturation by nonlinear three wave mode coupling. *Phys. Fluids* **23**, 1142–1154

Whitham, G. B. (1974) *Linear and Nonlinear Waves.* Wiley

Willis, G. J. K. (1986) Hydrodynamic stability of boundary layers over compliant surfaces. Ph.D. Thesis, University of Exeter

Yeo, K. S. (1986) The stability of flow over flexible surfaces. Ph.D. Thesis, University of Cambridge

Yeo, K. S. (1988) The stability of boundary-layer flow over single- and multi-layer viscoelastic walls. *J. Fluid Mech.* **196**, 359–408

Yeo, K. S. and Dowling, A. P. (1987) The stability of inviscid flows over passive compliant walls. *J. Fluid Mech.* **183**, 265–292

Appendix A

$$P^{(j)} = -2i\left\{\frac{(\omega_j - \mathbf{U}.\mathbf{k}_j)}{k_j}\sinh(k_j h) + \frac{m}{\rho}(\omega_j + \frac{1}{2}ilk_j)\cosh(k_j h)\right\} \qquad \text{(A1)}$$

$$\begin{aligned}
Q^{(j)} =& \frac{1}{2}\{\mathrm{i}(\omega_{j+1} - \mathbf{U}.\mathbf{k}_{j+1})k_{j+1}(A^*_{j+1}\sinh(k_{j+1}h) + B^*_{j+1}\cosh(k_{j+1}h))a^*_{j+2} \\
&+\mathrm{i}(\omega_{j+2} - \mathbf{U}.\mathbf{k}_{j+2})k_{j+2}(A^*_{j+2}\sinh(k_{j+2}h) + B^*_{j+2}\cosh(k_{j+2}h))a^*_{j+1} \\
&+k_{j+1}k_{j+2}(A^*_{j+1}\sinh(k_{j+1}h) + B^*_{j+1}\cosh(k_{j+1}h)) \\
&\times(A^*_{j+2}\sinh(k_{j+2}h) + B^*_{j+2}\cosh(k_{j+2}h)) - \mathbf{k}_{j+1}.\mathbf{k}_{j+2} \\
&\times(A^*_{j+1}\cosh(k_{j+1}h) + B^*_{j+1}\sinh(k_{j+1}h)) \\
&\times(A^*_{j+2}\cosh(k_{j+2}h) + B^*_{j+2}\sinh(k_{j+2}h)) - \cosh(k_j h) \\
&\times[\mathrm{i}(\omega_{j+1} - \mathbf{U}.\mathbf{k}_{j+1})k_{j+1}B^*_{j+1}b^*_{j+2} \\
&+\mathrm{i}(\omega_{j+2} - \mathbf{U}.\mathbf{k}_{j+2})k_{j+2}B^*_{j+2}b^*_{j+1} + k_{j+1}k_{j+2}B^*_{j+1}B^*_{j+2} \\
&-\mathbf{k}_{j+1}.\mathbf{k}_{j+2}A^*_{j+1}A^*_{j+2}] - \mathrm{i}k_j^{-1}(\omega_j - \mathbf{U}.\mathbf{k}_j)\sinh(k_j h) \\
&\times[\mathbf{k}_j.\mathbf{k}_{j+2}b^*_{j+1}A^*_{j+2} + \mathbf{k}_j.\mathbf{k}_{j+1}A^*_{j+1}b^*_{j+2}]\}
\end{aligned} \qquad \text{(A2)}$$

$$\begin{aligned}
R^{(j)} =& -2\sinh(k_j h)\left\{\frac{mk_j}{\rho}(\omega_j - \mathbf{U}.\mathbf{k}_j)^{-1}(\omega_j + \frac{1}{2}\mathrm{i}k_j)\right. \\
&\left.-(\omega_j - \mathbf{U}.\mathbf{k}_j)^{-2}\left[\frac{mk_j}{\rho}(\omega_j^2 - c_0^2k_j^2 + ilk_j\omega_j) - \frac{1}{\rho}(S - \rho g)k_j\right]\right\}
\end{aligned} \qquad \text{(A3)}$$

$$\begin{aligned}
S^{(j)} =& \frac{1}{2}\{\mathbf{k}_j.\mathbf{k}_{j+2}a^*_{j+1}(A^*_{j+2}\cosh(k_{j+2}h) + B^*_{j+2}\sinh((k_{j+2}h) \\
&+\mathbf{k}_j.\mathbf{k}_{j+1}a^*_{j+2}(A^*_{j+1}\cosh(k_{j+1}h) + B^*_{j+1}(\sinh(k_{j+1}h) \\
&+\mathrm{i}(\omega_j - \mathbf{U}.\mathbf{k}_j)^{-1}k_j\sinh(k_j h)[\mathrm{i}(\omega_{j+1} - \mathbf{U}.\mathbf{k}_{j+1})k_{j+1}B^*_{j+1}b^*_{j+2} \\
&+\mathrm{i}(\omega_{j+2} - \mathbf{U}.\mathbf{k}_{j+2})k_{j+2}B^*_{j+2}b^*_{j+1}] + k_{j+1}k_{j+2}B^*_{j+1}B^*_{j+2} \\
&-\mathbf{k}_{j+1}.\mathbf{k}_{j+2}A^*_{j+1}A^*_{j+2} - \cosh(k_j h) \\
&\times[\mathbf{k}_j.\mathbf{k}_{j+1}A^*_{j+1}b^*_{j+2} + \mathbf{k}_j.\mathbf{k}_{j+2}A^*_{j+2}b^*_{j+1}]\}
\end{aligned} \qquad \text{(A4)}$$

$$\nu_j = 4\left\{\frac{D_1^{(j)2}\cosh^2(k_j h)}{(\omega_j - \mathbf{U}.\mathbf{k}_j)^5}\left[\frac{m}{\rho}\left(\omega_j + \frac{1}{2}\mathrm{i}lk_j\right)(\omega_j - \mathbf{U}.\mathbf{k}_j)\right.\right.$$
$$\left.-\left\{\frac{m}{\rho}(\omega_j^2 - c_0^2 k_j^2 + \mathrm{i}lk_j\omega_j) - \left(\frac{S}{\rho} - g\right)\right\}\right]$$
$$\left.+(\omega_j - \mathbf{U}.\mathbf{k}_j)^{-1}\left(g + \frac{\gamma k_j^2}{\rho}\right)\right\} \tag{A5}$$

$$\lambda = \sum_{i=1}^{3}\left\{(\omega_i - \mathbf{U}.\mathbf{k}_i)(\omega_{i+1} - \mathbf{U}.\mathbf{k}_{i+1}) + \frac{\left(g + \frac{\gamma k^2}{\rho}\right)\left(g + \frac{\gamma k^2}{\rho}\right)\mathbf{k}_i.\mathbf{k}_{i+1}}{(\omega_i - \mathbf{U}.\mathbf{k}_i)(\omega_{i+1} - \mathbf{U}.\mathbf{k}_{i+1})}\right\}$$
$$-\left[\prod_{r=1}^{3}\frac{D_1^{(r)}\cosh(k_j h)}{(\omega_r - \mathbf{U}.\mathbf{k}_r)^2}\right]\sum_{i=1}^{3}\left\{(\omega_i - \mathbf{U}.\mathbf{k}_i)(\omega_{i+1} - \mathbf{U}.\mathbf{k}_{i+1})\right.$$
$$+\mathbf{k}_i\mathbf{k}_{i+1}\left[\frac{m}{\rho}(\omega_i^2 - c_0^2 k_i^2 + \mathrm{i}lk_i\omega_i) - \frac{S}{\rho} + g\right]$$
$$\left.\times\frac{[\rho^{-1}m(\omega_{i+1}^2 - c_0^2 k_{i+1}^2 + \mathrm{i}lk_{i+1}\omega_{i+1}) - \rho^{-1}S + g]}{(\omega_i - \mathbf{U}.\mathbf{k}_i)(\omega_{i+1} - \mathbf{U}.\mathbf{k}_{i+1})}\right\} \tag{A6}$$

$$\tilde{L}' = \frac{1}{8}\sum_{j=1}^{3}\{[k_j(\hat{A}_j\cosh(k_j h) + \hat{B}_j\sinh(k_j h))(A_j^*\sinh(k_j h) + B_j^*\cosh(k_j h))$$
$$+k_j(A_j\cosh(k_j h) + B_j\sinh(k_j h))(\hat{A}_j^*\sinh(k_j h) + \hat{B}_j^*\cosh(k_j h))$$
$$+k_{j+1}k_{j+2}a_j(A_{j+1}\sinh(k_{j+1}h) + B_{j+1}\cosh(k_{j+1}h))$$
$$\times(A_{j+2}\sinh(k_{j+2}h) + B_{j+2}\cosh(k_{j+2}h)) + \frac{1}{2}\mathbf{k}_{j+1}.\mathbf{k}_{j+2}$$
$$\times(A_j\cosh(k_j h) + B_j\sinh(k_j h))$$
$$\times\{a_{j+1}(A_{j+2}\cosh(k_{j+2}h) + B_{j+2}\sinh(k_{j+2}h))$$
$$+a_{j+2}(A_{j+1}\cosh(k_{j+1}h) + B_{j+1}\sinh(k_{j+1}h))$$
$$+2(\omega_j - \mathbf{U}.\mathbf{k}_j)\{\mathrm{i}a_j(\hat{A}_j^*\cosh(k_j h) + \hat{B}_j^*\sinh(k_j h))$$
$$+\mathrm{i}\hat{a}_j(A_j^*\cosh(k_j h) + B_j^*\sinh(k_{j+1}h))\}$$
$$+\mathrm{i}k_{j+2}(\omega_{j+1} - \mathbf{U}.\mathbf{k}_{j+1})a_j a_{j+1}$$
$$\times(A_{j+2}\sinh(k_{j+2}h) + B_{j+2}\cosh(k_{j+2}h))$$
$$+2\left(g + \frac{\gamma k^2}{\rho}\right)a_j\hat{a}_j^* - 2a_{j,r}(A_j^*\cosh(k_j h) + B_j^*\sinh(k_j h))$$

$$
\begin{aligned}
&- k_j(\hat{A}_j B_j^* + A_j \hat{B}_j^*) - k_{j+1}k_{j+2}b_j B_{j+1}B_{j+2} \\
&- \frac{1}{2}(k_{j+1}^2 + k_{j+2}^2)b_j A_{j+1}A_{j+2} - 2\mathrm{i}(\omega_j - \mathbf{U}.\mathbf{k}_j)(b_j \hat{A}_j^* + \hat{b}_j A_j^*) \\
&- \frac{1}{2}\mathbf{k}_{j+1}.\mathbf{k}_{j+2}A_j(b_{j+1}A_{j+2} + b_{j+2}A_{j+1}) \\
&- \mathrm{i}(\omega_{j+1} - \mathbf{U}.\mathbf{k}_{j+1})b_j b_{j+1}B_{j+2}k_{j+2} \\
&- 2\Big[\frac{m}{\rho}(\omega_j^2 - c_0^2 k_j^2) - \Big(\frac{S}{\rho} - g\Big)\Big]b_j \hat{b}_j^* \\
&+ 2b_{j,\tau}A_j^* - 2\mathrm{i}\frac{m}{\rho}\omega_j b_{j,\tau}b_j^* \\
&- 2(A_j^* \cosh(k_j h) + B_j^* \sinh(k_j h))\mathbf{U}.\tilde{\nabla}a_j \\
&+ 2\mathrm{i}\frac{\gamma}{\rho}a_j \mathbf{k}_j.\tilde{\nabla}a_j^* + 2A_j^*\mathbf{U}.\tilde{\nabla}b_j + 2\mathrm{i}\frac{m}{\rho}c_0^2 b_j \mathbf{k}_j.\tilde{\nabla}b_j^* \\
&- \frac{\mathrm{i}}{k_j}\{(\frac{1}{2}\sinh(2k_j h) + k_j h)A_j^*\mathbf{k}_j.\tilde{\nabla}A_j \\
&+ (\frac{1}{2}\sinh(2k_j h) - k_j h)B_j^*\mathbf{k}_j.\tilde{\nabla}B_j \\
&+ \sinh^2(k_j h)(B_j^*\mathbf{k}_j.\tilde{\nabla}A_j + A_j^*\mathbf{k}_j.\tilde{\nabla}B_j)\Big] + \mathrm{c.c}\}
\end{aligned}
\tag{A7}
$$

$$
\begin{aligned}
\mathcal{A}_j =& 2\left\{\frac{(g + \rho^{-1}\gamma k_j^2)}{(\omega_j - \mathbf{U}.\mathbf{k}_j)} - \left[\frac{D_1^{(j)2}\cosh^2(k_j h)}{(\omega_j - \mathbf{U}.\mathbf{k}_j)^5}\right]\right. \\
&\left.\times\left[\frac{m}{\rho}(\omega_j \mathbf{U}.\mathbf{k}_j - c_0^2 k_j^2) - \frac{S}{\rho} + g\right]\right\}
\end{aligned}
\tag{A8}
$$

$$
\mathcal{B}_j = -2\left\{\frac{m\omega_j}{\rho}\frac{D_1^{(j)2}\cosh^2(k_j h)}{(\omega_j - \mathbf{U}.\mathbf{k}_j)^4}\right\}
\tag{A9}
$$

$$
\begin{aligned}
\mathcal{C}_j =& \left\{\frac{2}{\rho}[\gamma + mc_0^2(\omega_j - \mathbf{U}.\mathbf{k}_j)^{-4}D_1^{(j)2}\cosh^2(k_j h)]\right. \\
&+ \left\{\frac{D_1^{(j)2}\cosh^3(k_j h)\sinh(k_j h)}{k_j^3(\omega_j - \mathbf{U}.\mathbf{k}_j)^6} + \frac{hD_1^{(j)2}\cosh^2(k_j h)}{k_j^2(\omega_j - \mathbf{U}.\mathbf{k}_j)^6}\right\} \\
&\times\left[\frac{mk_j}{\rho}(\omega_j^2 - c_0^2 k_j^2) - \left(\frac{S}{\rho} - g\right)k_j\right\}^2 + (\omega_j - \mathbf{U}.\mathbf{k}_j)^4\Big] \\
&+ \left[\frac{2D_1^{(j)2}\cosh^2(k_j h)\sinh^2(k_j h)}{k_j^3(\omega_j - \mathbf{U}.\mathbf{k}_j)^4}\right] \\
&\times\left.\left[\frac{mk_j}{\rho}(\omega_j^2 - c_0^2 k_j^2) - \left(\frac{S}{\rho} - g\right)k_j\right]\right\}
\end{aligned}
\tag{A10}
$$

Appendix B

$$\mu_1^{(3)} = f_1 + \frac{\bar{u}'(0)}{\mathrm{i}\alpha c} f_2 \tag{B1}$$

$$\mu_2^{(3)} = -R\{\mathrm{i}\alpha c \mu_1^{(3)} + f_3 - \mathrm{i}\alpha f_4 + c^{-1}[m\alpha^2(c^2 - c_0^2) + \mathrm{i}\alpha c d - S] f_2\} \tag{B2}$$

$$\mu_1^{(1)} = \frac{\alpha}{2\gamma}\lambda_1 + \frac{\beta}{\gamma}\lambda_2 + \frac{\bar{u}'(0)}{\mathrm{i}\gamma\tilde{c}}\lambda_3 \tag{B3}$$

$$\begin{aligned}\mu_2^{(1)} =& R\{\mathrm{i}\gamma\lambda_4 - \frac{\alpha}{2\gamma}\lambda_5 - \frac{\beta}{\gamma}\lambda_6 - \frac{1}{2}\mathrm{i}\alpha\tilde{c}\mu_1^{(1)} \\ & - 2\frac{\gamma}{\alpha\tilde{c}}[\frac{1}{4}m\alpha^2(\tilde{c}^2 - \frac{\alpha}{2\gamma}c_0^2) + \mathrm{i}\frac{\alpha}{2}\tilde{c}d - S]\lambda_3\}\end{aligned} \tag{B4}$$

$$\begin{aligned}\sigma_3 =& \frac{1}{\mathrm{i}\alpha c R}\phi_3'(0)[\psi_3''(0) + (\alpha^2 + \mathrm{i}\alpha R c)\psi_3(0)] \\ & - \frac{1}{\bar{u}'(0)R}\phi_3'(0)\psi_3(0)[\mathrm{i}\alpha R(2\mathrm{i}\alpha c m - d) - \frac{\mathrm{i}}{\alpha}B_3] \\ & + \int_0^\infty (\phi_3'' - \alpha^2\phi_3)\psi_3\, dz\end{aligned} \tag{B5}$$

$$\begin{aligned}\sigma_1 =& \frac{2}{\mathrm{i}\alpha\tilde{c}R'}\phi_1'(0)[\psi_1''(0) + (\gamma^2 + \mathrm{i}\gamma R'\tilde{c})\psi_1(0)] \\ & - \frac{2\gamma}{\alpha\bar{u}'(0)\tilde{R}}\phi_1'(0)\psi_1(0)[\mathrm{i}\gamma R(\mathrm{i}\alpha c m - d) - \frac{\mathrm{i}}{\gamma}B_1] \\ & + \int_0^\infty (\phi_1'' - \gamma^2\phi_1)\psi_1\, dz\end{aligned} \tag{B6}$$

$$\begin{aligned}\varsigma_3 =& \int_0^\infty F_3\psi_3\, dz + \psi_3(0)[\mathrm{i}\alpha c f_1 + \bar{u}'(0)f_2 + f_3 - \mathrm{i}\alpha f_4 + \frac{1}{\mathrm{i}\alpha R}B_3 f_2] \\ & - \frac{1}{R}[f_1 + \frac{\bar{u}'(0)}{\mathrm{i}\alpha c}f_2][\psi_3''(0) + (\alpha^2 + \mathrm{i}\alpha R c)\psi_3(0)]\end{aligned} \tag{B7}$$

$$\begin{aligned}\varsigma_1 =& -\frac{1}{R'}[\frac{\alpha}{2\gamma}\lambda_1 + \frac{\beta}{\gamma}\lambda_2 + \frac{\bar{u}'(0)}{\mathrm{i}\gamma\tilde{c}}\lambda_3][\psi_1''(0) + (\gamma^2 + \mathrm{i}\gamma R'\tilde{c})\psi_1(0)] \\ & + \int_0^\infty F_1\psi_1\, dz - \frac{R}{R'}\psi_1(0)\{\mathrm{i}\gamma\lambda_4 - \frac{\alpha}{2\gamma}\lambda_5 - \frac{\beta}{\gamma}\lambda_6 \\ & - \mathrm{i}\frac{\alpha}{2\gamma}[\frac{\alpha}{2}\tilde{c}\lambda_1 + \beta\tilde{c}\lambda_2 - \mathrm{i}\bar{u}'(0)\lambda_3] - \frac{1}{\mathrm{i}\gamma R}B_1\lambda_3\}\end{aligned} \tag{B8}$$

where

$$f_1 = \eta_1 \left(\frac{\beta}{\gamma} \hat{v}_1'(0) - \frac{\alpha}{2\gamma} \phi_1''(0) \right) \tag{B9}$$

$$f_2 = \mathrm{i}\alpha\eta_1 \left(\frac{\beta}{\gamma} \hat{v}_1(0) - \frac{\alpha}{2\gamma} \phi_1'(0) - \frac{1}{2} \bar{u}'(0)\eta_1 \right) \tag{B10}$$

$$\begin{aligned} f_3 =& \frac{\mathrm{i}\alpha}{2\gamma} \tilde{c}\eta_1 \left(\frac{\alpha}{2} \phi_1''(0) - \beta \hat{v}_1'(0) \right) - \mathrm{i}\frac{\alpha}{2} \eta_1 p_1'(0) + \mathrm{i}\frac{\beta}{\gamma} \bar{u}'(0)\eta_1 \left(\beta\phi_1'(0) + \frac{\alpha}{2} \hat{v}_1'(0) \right) \\ & - \frac{\mathrm{i}}{\gamma^2} \left(\left(\frac{\alpha^3}{8} - \frac{\alpha\beta^2}{2} \right) {\phi_1'}^2(0) + \alpha\beta^2 {\hat{v}_1'}^2(0) + \left(\beta^3 - \frac{3\alpha^2\beta}{4} \right) \phi_1'(0)\hat{v}_1(0) \right. \\ & \left. - \gamma\phi_1(0) \left(\frac{\alpha}{2} \phi_1''(0) - \beta \hat{v}_1'(0) \right) \right) \\ & + \frac{1}{\gamma R} \eta_1 \left(\frac{\alpha}{2} \left(\phi_1''''(0) - \gamma^2 \phi_1''(0) \right) - \beta \left(\hat{v}_1'''(0) - \gamma^2 \hat{v}_1'(0) \right) \right) \end{aligned} \tag{B11}$$

$$\begin{aligned} f_4 =& -\frac{1}{R} \eta_1 \left(Rp_1'(0) + \mathrm{i} \left(\frac{3\alpha^2 + 4\beta^2}{\gamma} \right) \phi_1''(0) \right. \\ & \left. - \mathrm{i}\frac{\alpha\beta}{\gamma} \hat{v}_1'(0) + \mathrm{i}\gamma \left(\frac{\alpha^2}{4} - \beta^2 \right) \phi_1(0) \right) \end{aligned} \tag{B12}$$

$$\lambda_1 = -\frac{1}{2} \left(\frac{\alpha}{2\gamma} \eta_3 \phi_1^{*\prime\prime}(0) - \frac{\beta}{\gamma} \eta_3 \hat{v}_1^{*\prime}(0) + {\eta_1}^* \phi_3''(0) \right) \tag{B13}$$

$$\lambda_2 = \frac{1}{2} \eta_3 \left(\frac{\beta}{\gamma} \phi_1^{*\prime\prime}(0) + \frac{\alpha}{2\gamma} \hat{v}_1^{*\prime}(0) \right) \tag{B14}$$

$$\lambda_3 = -\mathrm{i}\frac{\alpha}{4} \left(\bar{u}'(0)\eta_1^* \eta_3 - 2\frac{\beta}{\gamma} \hat{v}_1^*(0)\eta_3 + \phi_3'(0)\eta_1^* + \left(\frac{\alpha^2 - 2\gamma^2}{\gamma\alpha} \right) \phi_1^{*\prime}(0)\eta_3 \right) \tag{B15}$$

$$\begin{aligned} \lambda_4 =& -\frac{1}{2} (\eta_1^* p_3'(0) + \eta_3 p_1^{*\prime}(0)) + \mathrm{i}\gamma\eta_3 \phi_1^{*\prime\prime}(0) - \mathrm{i}\alpha\eta_1^* \phi_3''(0) \\ & - \frac{1}{2} \mathrm{i}\alpha\eta_3 \left(\frac{\alpha}{2\gamma} (\phi_1^{*\prime\prime}(0) + \gamma^2 \phi_1^*(0)) - \frac{\beta}{\gamma} \hat{v}_1^{*\prime}(0) \right) \\ & + \mathrm{i}\frac{\alpha}{4} \eta_1^* (\phi_3''(0) + \alpha^2 \phi_3(0)) \end{aligned} \tag{B16}$$

$$\lambda_5 = -\frac{1}{2R}\left(\eta_1^*(\phi_3^{*\prime\prime\prime\prime}(0) - \alpha^2\phi_3^{*\prime\prime}(0))\right.$$
$$\left.+\frac{\alpha}{2\gamma}\eta_3(\phi_1^{*\prime\prime\prime\prime}(0) - \gamma^2\phi_1^{*\prime\prime}(0)) - \frac{\beta}{\gamma}\eta_3(\hat{v}_1^{*\prime\prime\prime}(0) - \gamma^2\hat{v}_1^{*\prime}(0))\right)$$
$$+\mathrm{i}\frac{\alpha}{4}\left(\eta_3 p_1^{*\prime}(0) - 2\eta_1^* p_3'(0) - \tilde{c}^*\eta_3(\frac{\alpha}{2\gamma}\phi_1^{*\prime\prime}(0) - \beta\hat{v}_1^{*\prime}(0)) - 2c\eta_1^*\phi_3''(0)\right)$$
$$-\frac{\mathrm{i}}{2}\left(\frac{\alpha^2}{4\gamma}\phi_1^{*\prime}(0)\phi_3'(0) - \frac{\alpha\beta}{2\gamma}\hat{v}_1^*(0)\phi_3'(0) + \gamma\phi_1^*(0)\phi_3''(0) - \frac{\alpha^2}{2\gamma}\phi_1^{*\prime\prime}(0)\phi_3(0)\right.$$
$$\left.+\frac{\alpha\beta}{\gamma}\hat{v}_1^{*\prime}(0)\phi_3(0) + \frac{\beta^2}{\gamma}\bar{u}'(0)\eta_3\phi_1^{*\prime}(0) + \frac{\alpha\beta}{2\gamma}\bar{u}'(0)\eta_3\hat{v}_1^*(0)\right) \qquad \text{(B17)}$$

$$\lambda_6 = \mathrm{i}\frac{\alpha}{4\gamma}\left(\tilde{c}^*\eta_3(\beta\phi_1^{*\prime\prime}(0) + \frac{\alpha}{2}\hat{v}_1^{*\prime}(0)) - 2\phi_3(0)(\beta\phi_1^{*\prime\prime}(0) + \frac{\alpha}{2}\hat{v}_1^{*\prime}(0))\right)$$
$$-\frac{1}{2}\eta_3\left(\mathrm{i}\beta p_1^{*\prime}(0) + \frac{\beta}{\gamma R}(\phi_1^{*\prime\prime\prime\prime}(0) - \gamma^2\phi_1^{*\prime\prime}(0))\right.$$
$$\left.+\frac{\alpha}{2\gamma R}(\hat{v}_1^{*\prime\prime\prime}(0) - \gamma^2\hat{v}_1^{*\prime}(0))\right) \qquad \text{(B18)}$$

α	R	(c_r, c_i) [Gaster]	(c_r, c_i)	(a)
0.87169	1452.8	(0.39768, -0.00093)	(0.39768, -0.00093)	
0.58113	4358.4	(0.31561, 0.01578)	(0.31562, 0.01578)	
0.43584	8716.9	(0.26813, 0.01854)	(0.26813, 0.01854)	

α	R	(c_r, c_i) [Mack]	(c_r, c_i)	(b)
0.895	2900.0	(0.3641, 0.0080)	(0.3641, 0.0080)	
0.895	5000.0	(0.3383, 0.0048)	(0.3383, 0.0048)	
0.895	10000.0	(0.3089, -0.0166)	(0.3089, -0.0166)	

TABLE 3.1 Rigid wall, linear eigenvalues: (a) first column, data of Gaster (1977); (b) first column, data of Mack (1976); second column in both cases, data of present author.

α	β	γ	R	c_r	c_i	c_i	$\lvert a_3 \rvert$	$\lvert a_1 \rvert$	
0.29056	0.1792	0.2307	1613.7	0.2860	-0.0461	-0.0888	0.825	0.949	(a)
0.58113	0.3512	0.4558	1633.7	0.3394	0.0041	-0.0295	0.242	3.82	
0.73803	0.4303	0.5669	1668.2	0.3569	0.0101	-0.0122	0.452	6.02	
0.87169	0.4955	0.6599	1692.7	0.3685	0.0083	-0.0034	0.536	8.72	
1.1623	0.6069	0.8403	1772.4	0.3847	-0.0108	0.0035	0.642	19.13	
1.4528	0.5560	0.9148	2035.0	0.3835	-0.0446	0.0048	0.977	30.22	
0.29056	0.1793	0.2307	1613.7	0.2859	-0.0461	-0.0888	0.824	0.890	(b)
0.58113	0.3513	0.4559	1633.4	0.3394	0.0041	-0.0294	0.247	3.92	
0.73803	0.4300	0.5666	1669.1	0.3570	0.0102	-0.0122	0.455	6.12	
0.87169	0.4954	0.6598	1692.9	0.3685	0.0083	-0.0033	0.537	8.83	
1.1623	0.6096	0.8422	1768.4	0.3846	-0.0107	0.0035	0.642	19.24	
1.4528	0.5553	0.9143	2036.1	0.3834	-0.0444	0.0047	0.971	30.20	

TABLE 3.2 Rigid wall, resonant triads, R = 2562.8: (a) present author, (b) Hendriks. $|a_1|$, $|a_3|$ are given (in this table only) in the nondimensional form used by Hendriks.

α	β	γ	$\tilde{R}$	c	$\tilde{c}_i$	θ^*	$\lvert a_3 \rvert$	$\lvert a_1 \rvert$	$\arg a_3$	$\arg a_1$
0.29056	0.1792	0.2307	1613.7	0.2860 −0.0888i	−0.0461	50.97	0.439	0.802	−47.54	156.33(a)
0.4	0.2543	0.3235	1584.2	0.3111 −0.0611i	−0.0197	51.81	0.392	2.213	9.5	134.72
0.5	0.3095	0.3979	1610.3	0.3282 −0.0419i	−0.0038	51.08	0.155	4.246	93.21	119.36
0.58113	0.3512	0.4558	1633.7	0.3394 −0.0295i	0.0041	50.40	0.251	6.46		
0.6	0.3608	0.4692	1638.5	0.3418 −0.0269i	0.0055	50.25	0.294	7.065	−168.87	108.19
0.7	0.4113	0.5401	1660.9	0.3531 −0.0157i	0.0096	49.61	0.502	11.01	−143.01	99.96
0.73803	0.4303	0.5669	1668.2	0.3569 −0.0122i	0.0101	49.39	0.571	12.91		
0.8	0.4610	0.6104	1679.5	0.3626 −0.0076i	0.0099	49.06	0.672	16.62	−130.92	93.58
0.87169	0.4955	0.6599	1692.7	0.3685 −0.0034i	0.0083	48.66	0.777	22.10		
1.0	0.5524	0.7451	1719.8	0.3772 +0.0013i	0.0021	47.85	0.941	36.12	−122.37	84.26
1.1623	0.6069	0.8403	1772.4	0.3847 +0.0035i	−0.0108	46.24	1.13	64.61		
1.2	0.6147	0.8590	1790.1	0.3858 +0.0037i	−0.0145	45.69	1.183	73.22	−131.52	78.41
1.4528	0.5560	0.9148	2035.0	0.3835 +0.0048i	−0.0446	37.43	1.64	127.6		
0.29056	0.1836	0.2341	2482.1	0.2712 −0.0273i	−0.0649	51.64	0.360	1.054	−22.01	148.02(b)
0.4	0.2473	0.3181	2515.2	0.2937 −0.0032i	−0.0394	51.04	0.137	2.704	56.97	126.52
0.5	0.2989	0.3897	2566.1	0.3090 +0.0093i	−0.0217	50.09	0.208	4.926	−171.80	112.86
0.6	0.3512	0.4619	2598.2	0.3216 +0.0150i	−0.0084	49.50	0.401	8.140	−143.93	103.17
0.7	0.4043	0.5347	2618.2	0.3323 +0.0159i	0.0008	49.11	0.557	12.96	−131.94	95.81
1.0	0.5479	0.7417	2696.4	0.3548 −0.0020i	0.0110	47.61	0.987	47.59	−127.80	81.20

TABLE 3.3 Rigid wall, resonant triads. (a) $R = 2562.8$, (b) $R = 4000$

R	β	γ	$\tilde{R}$	c	$\tilde{c}_i$	θ°	$\lvert a_3 \rvert$	$\lvert a_1 \rvert$	$\arg a_3$	$\arg a_1$	
2562.8	0.1792	0.2307	1613.7	0.2860 −0.0461i	−0.0888	50.97	0.439	0.802			(a)
4000	0.1836	0.2341	2482.1	0.2712 −0.0273i	−0.0649	51.64	0.360	1.054	−22.01	148.02	
5000	0.1831	0.2337	3108.0	0.2636 −0.0190i	−0.0548	51.56	0.291	1.197	−8.21	143.73	
10000	0.1749	0.2274	6389.3	0.2395 +0.0017i	−0.0291	50.29	0.063	1.651	54.36	131.14	
15000	0.1692	0.2230	9771.1	0.2254 +0.0103i	−0.0169	49.35	0.059	1.892	173.70	124.77	
20000	0.1662	0.2207	13164.8	0.2156 +0.0148i	−0.0093	48.83	0.099	2.057	−161.58	120.65	
4350	0.2641	0.3424	2768.3	0.2961 +0.0045i	−0.0290	50.47	0.104	3.514	144.26	119.74	(b)
8716.9	0.2527	0.3337	5692.3	0.2681 +0.0185i	−0.0046	49.23	0.236	4.367	−149.14	110.36	
13050	0.2512	0.3326	8551.7	0.2528 +0.0225i	0.0061	49.07	0.275	5.017	−138.94	105.57	
4358.4	0.3398	0.4471	2832.3	0.3156 +0.0158i	−0.0075	49.47	0.382	7.646	−144.23	103.85	(c)
2900	0.5048	0.6746	1923.7	0.3641 +0.0080i	0.0016	48.44	0.811	25.68	−124.17	87.79	(d)
5000	0.5043	0.6742	3318.6	0.3383 +0.0048i	0.0137	48.41	0.855	35.46	−126.06	83.43	
10000	0.5150	0.6822	6559.3	0.3089 −0.0166i	0.0180	49.01	1.507	65.40	−144.97	77.59	
2562.8	0.5524	0.7451	1719.8	0.3772 +0.0021i	0.0013	47.85	0.941	36.12	−122.37	84.26	(e)
4000	0.5479	0.7417	2696.4	0.3548 −0.0020i	0.0110	47.61	0.987	47.59	−127.80	81.20	
6000	0.5446	0.7393	4057.9	0.3354 −0.0129i	0.0152	47.44	1.23	65.39	−140.26	78.42	
10000	0.3967	0.6382	7834.1	0.2971 −0.0460i	0.0196	38.42	1.85	63.99	144.09	86.15	

TABLE 3.4 Rigid wall, resonant triads. (a) $\alpha = 0.29056$, (b) $\alpha = 0.43584$, (c) $\alpha = 0.58113$, (d) $\alpha = 0.895$, (e) $\alpha = 1.0$

α	c_{TS}	c_F	c_S	
0.29056	(0.4071, -0.0198)	(1.1914, 0.0009)		(a)
0.4	(0.4619, -0.0220)		(-0.1506, -0.0342)	
0.5	(0.4995, -0.0572)	(0.7902, 0.0220)	(-0.0955, -0.0450)	
0.6	(0.4776, -0.1166)	(0.6846, 0.0856)	(-0.1122, -0.0413)	
0.7	(0.4394, -0.1251)	(0.6435, 0.1226)		
0.8	(0.4159, -0.1226)	(0.6191, 0.1364)	(-0.0830, -0.0481)	
0.2	(0.3321, -0.0492)	(1.5065, 0.0009)		(b)
0.29056	(0.3821, -0.0207)	(1.2736, 0.0007)		
0.4	(0.4138, -0.0097)	(1.1000, 0.0004)		
0.6	(0.4335, -0.0147)	(0.9265, 0.0008)		
0.7	(0.4348, -0.0214)	(0.8784, 0.0033)		
0.8	(0.4331, -0.0296)	(0.8454, 0.0058)		
0.9	(0.4294, -0.0387)	(0.8227, 0.0079)		
1.2	(0.4046, -0.0675)	(0.7872, 0.0111)		
0.2	(0.3498, -0.0446)	(1.429, 0.0012)	(-0.0896, -0.0446)	(c)
0.29056	(0.4294, -0.0210)	(1.133, 0.001)	(-0.0492, -0.0535)	
0.35	(0.4784, -0.0277)		(-0.0399, -0.0544)	
0.4	(0.5269, -0.0598)	(0.8263, 0.0165)	(-0.0359, -0.0541)	
0.44	(0.5358, -0.1415)	(0.7254, 0.0779)		
0.47	(0.4895, -0.1697)	(0.6909, 0.1255)		
0.5	(0.4588, -0.0572)	(0.6688, 0.1578)	(-0.0327, -0.0523)	
0.6	(0.4050, -0.1647)	(0.6178, 0.2132)	(-0.0324, -0.0501)	
0.7	(0.3747, -0.1549)	(0.5804, 0.2330)	(-0.0333, -0.0478)	

TABLE 4.1 Compliant wall. $R = R_0 = 2562.8$, $m^{(0)} = 1.1$, $d = 0$, $S^{(0)} = 0.15$:

(a) $c_0 = 0.5$, (b) $c_0 = 0.8$, (c) $c_0 = 0.1$

α	c_{TS}	c_F	c_S	
0.4	(0.3855, -0.0076)	(1.2210, 0.0003)		(a)
0.6	(0.4348, -0.0154)			
0.7		(0.8142, 0.0108)		
0.8	(0.4499, -0.0647)	(0.7311, 0.0316)		
0.29056	(0.3411, -0.0276)	(1.2877, 0.0005)		(b)
0.4	(0.3818, -0.0078)			
0.5	(0.4085, -0.0050)			
0.6	(0.4282, -0.0132)	(0.7574, 0.0136)		
0.7	(0.4398, -0.0310)	(0.6745, 0.0324)		
0.8	(0.4376, -0.0532)	(0.6232, 0.0554)		
0.29056	(0.3870, -0.0203)	(1.2554, 0.0008)	(-0.1217, -0.0441)	(c)
0.29056	(0.5263, -0.0443)			
0.29056		(0.7384, 0.2171)		
0.87169	(0.5506, 0.2122)		(-0.0709, -0.0401)	(d)

TABLE 4.2 Compliant wall. $R = R_0 = 2562.8$, $d = 0$:

(a) $m^{(0)} = 1.1$, $c_0 = 0.5$, $S^{(0)} = 0.3$; (b) as (a) but $m^{(0)} = 2$; (c) $m^{(0)} = 1.1$, $c_0 = 0.1$, $S^{(0)} = 0.2$, 0.1, 0.05; (d) as (b) but $S^{(0)} = 0.2$

α	c_{TS}	c_F	
0.4	(0.3823, -0.0197)		(a)
0.5	(0.4299, -0.0545)		
0.6	(0.4600, -0.0614)		
0.7	(0.4731, -0.0737)	(0.7900, 0.0137)	
0.8	(0.4782, -0.0895)	(0.7506, 0.0222)	
0.9	(0.4804, -0.1075)	(0.7252, 0.0292)	
0.4	(0.4228, -0.0430)		(b)
0.5	(0.4963, -0.0641)		
0.55	(0.5205, -0.0834)		
0.6	(0.5342, -0.1154)		
0.65	(0.5356, -0.1547)		
0.7	(0.5446, -0.1781)	(0.6606, 0.0911)	
0.8	(0.5379, -0.1900)	(0.6351, 0.1096)	
0.9		(0.6189, 0.1156)	
1.0		(0.6077, 0.1155)	
1.2		(0.5939, 0.1066)	
1.4		(0.5864, 0.0935)	

TABLE 4.3 Compliant wall. $R = R_0 = 10000$, $m^{(0)} = 1.1$, $d = 0$, $S^{(0)} = 0.15$:

(a) $c_0 = 0.7$, (b) $c_0 = 0.55$

α	c_{TS}	c_F	
0.29056	(0.3932,-0.0535)	(0.8919, 0.0029)	(a)
0.4	(0.4448,-0.0377)	(0.6926, 0.0238)	
0.5	(0.4749,-0.0506)	(0.5897, 0.0556)	
0.6	(0.4733,-0.0686)	(0.5483, 0.0832)	
0.7	(0.4637,-0.0743)	(0.5317, 0.0925)	
0.8	(0.4550,-0.0752)	(0.5238, 0.0934)	
0.9	(0.4477,-0.0747)	(0.5200, 0.0904)	
0.29056	(0.3921,-0.0456)	(0.8910,-0.0272)	(b)
0.4	(0.4469,-0.0227)	(0.6870,-0.0127)	
0.5	(0.4994,-0.0341)	(0.5615, 0.0192)	
0.6	(0.4912,-0.0720)	(0.5273, 0.0685)	
0.7	(0.4755,-0.0796)	(0.5172, 0.0814)	
0.8	(0.4636,-0.0805)	(0.5129, 0.0838)	
0.9	(0.4543,-0.0796)	(0.5116, 0.0817)	
0.29056	(0.3895,-0.0379)	(0.8921,-0.0576)	(c)
0.4	(0.4436,-0.0072)	(0.6875,-0.0503)	
0.5	(0.4916, 0.0198)	(0.5663,-0.0551)	
0.6	(0.5035, 0.0594)	(0.5122,-0.0814)	
0.7	(0.5019, 0.0726)	(0.4886,-0.0875)	
0.8	(0.5016, 0.0754)	(0.4730,-0.0873)	
0.9	(0.5028, 0.0738)	(0.4615,-0.0855)	
1.0	(0.5049, 0.0700)		

TABLE 4.4 Compliant wall. $R = 1500$, $R_0 = 2562.8$, $m^{(0)} = 2$, $c_0 = 0.5$, $S^{(0)} = 0.3$:

(a) $d = 0$, (b) $d = 0.05$, (c) $d = 0.1$

α	c_{TS}	c_F	
0.2	(0.3354,-0.0418)		(a)
0.29056	(0.3935,-0.0097)		
0.4	(0.4377, 0.0005)		
0.5	(0.4640,-0.0045)		
0.6	(0.4826,-0.0195)		
0.7	(0.4925,-0.0471)	(0.7227,-0.0268)	
0.8	(0.4159,-0.1226)	(0.6733,-0.0003)	
0.9	(0.5620,-0.1554)	(0.6525, 0.0218)	
1.0	(0.5594 -0.1565)	(0.6437, 0.0330)	
0.2	(0.3325,-0.0362)		(b)
0.29056	(0.3904, 0.0005)		
0.4	(0.4357, 0.0155)		
0.5	(0.4635, 0.0155)		
0.6	(0.4851, 0.0075)		
0.7	(0.5052,-0.0081)	(0.7305,-0.0965)	
0.8	(0.5355,-0.0364)	(0.6613,-0.0928)	
0.9	(0.5963,-0.1253)	(0.6004,-0.0201)	
1.0	(0.5827,-0.1445)	(0.6101, 0.0036)	
1.1		(0.6147, 0.0135)	
1.2		(0.6181, 0.0180)	
1.3		(0.6211, 0.0197)	

TABLE 4.5 Compliant wall. $R = R_0 = 2562.8$, $m^{(0)} = 1.1$, $c_0 = 0.65$, $S^{(0)} = 0.15$:

(a) $d = 0.05$, (b) $d = 0.1$

α	c_{TS}	c_F	c_{HO}	
0.29056	(0.3636,-0.0374)			(a)
0.4	(0.4086,-0.0178)			
0.5	(0.4383,-0.0168)	(0.7246, 0.0180)		
0.55	(0.4499,-0.0219)			
0.6	(0.4582,-0.0309)	(0.6329, 0.0419)		
0.7	(0.4594,-0.0526)	(0.5843, 0.0688)		
0.8	(0.4488,-0.0657)	(0.5625, 0.0831)		
0.9	(0.4374,-0.0721)	(0.5511, 0.0878)		
1.0	(0.4272,-0.0756)	(0.5446, 0.0873)		
1.1	(0.4180,-0.0779)	(0.5407, 0.0842)		
0.29056	(0.3608,-0.0285)			(b)
0.4	(0.4068,-0.0024)			
0.5	(0.4399, 0.0069)	(0.7201,-0.0519)		
0.6	(0.4728, 0.0072)	(0.6130,-0.0413)		
0.7	(0.5238, 0.0284)			
0.75	(0.5260, 0.0465)			
0.8	(0.5257, 0.0562)			
0.9	(0.5246, 0.0648)			
1.0	(0.5243, 0.0664)			
1.1	(0.5248, 0.0647)			
0.29056	(0.3558,-0.0205)			(c)
0.4	(0.3996, 0.0111)			
0.5	(0.4294, 0.0268)			
0.6	(0.4531, 0.0362)	(0.6316,-0.1197)	(0.6044,-0.2638)	
0.7	(0.4719, 0.0432)	(0.5589,-0.1144)	(0.5933,-0.2463)	
0.8	(0.4853, 0.0484)	(0.5115,-0.1087)	(0.5810,-0.2345)	
0.9	(0.4944, 0.0508)	(0.4803,-0.1046)	(0.5689,-0.2237)	
1.0	(0.5012, 0.0504)	(0.4579,-0.1012)	(0.5581,-0.2135)	
1.1	(0.5069, 0.0481)	(0.4405,-0.0985)	(0.5489,-0.2039)	
1.2	(0.5117, 0.0446)	(0.4262,-0.0964)	(0.5412,-0.1951)	

TABLE 4.6 Compliant wall. $R = 2000$, $R_0 = 2562.8$, $m^{(0)} = 2$, $c_0 = 0.5$, $S^{(0)} = 0.3$;

(a) $d = 0$, (b) $d = 0.1$, (c) $d = 0.2$

α	β	θ°	$\tilde{R}$	c_r	c_i	$\tilde{c}_i$	$\lvert a_3 \rvert$	$\lvert a_1 \rvert$	$\arg a_3$	$\arg a_1$	
0.29056	0.2139	55.82	1439.9	0.3016	-0.0399	-0.0847	0.631	1.095	-26.88	94.40	(a)
0.4	0.3082	57.02	1395.2	0.3322	-0.0135	-0.0548	0.573	2.70	54.98	79.06	
0.5	0.3841	56.94	1398.0	0.3532	-0.0003	-0.0349	0.514	4.59	149.1	73.52	
0.6	0.4573	56.73	1405.8	0.3697	0.0048	-0.0208	0.805	7.25	-154.0	72.36	
0.7	0.5281	56.46	1415.8	0.3829	0.0042	-0.0115	1.13	11.39	-126.5	72.59	
0.8	0.5942	56.05	1431.2	0.3934	-0.0008	-0.0060	1.41	17.97	-110.8	72.85	
1.0	0.6889	54.03	1505.4	0.4063	-0.0210	-0.0026	1.50	43.2	-105.1	73.33	
1.2	0.6237	46.11	1776.8	0.4035	-0.0508	-0.0012	1.03	78.1	-174.2	78.58	
0.29056	0.2052	54.70	2311.5	0.2813	-0.0230	-0.0616	0.439	1.14	-4.18	108.3	(b)
0.4	0.2825	54.70	2311.3	0.3073	0.0004	-0.0346	0.234	2.76	102.6	94.74	
0.5	0.3499	54.45	2325.4	0.3255	0.0106	-0.0166	0.399	4.91	-167.0	88.49	
0.6	0.4186	54.37	2330.1	0.3403	0.0132	-0.0043	0.641	8.26	-135.5	84.74	
0.7	0.4869	54.29	2334.8	0.3525	0.0103	0.0032	0.851	13.71	-119.1	81.83	
0.8	0.5513	54.04	2349.0	0.3623	0.0029	0.0068	1.02	22.6	-110.4	79.25	
1.2	0.4326	35.79	3244.6	0.3597	-0.0610	0.0098	1.29	66.4	147.7	86.15	
0.29056	0.1956	53.41	3577.3	0.2640	-0.0010	-0.0448	0.252	1.32	20.09	116.4	(c)
0.4	0.2635	52.80	3627.6	0.2867	0.0100	-0.0196	0.180	3.08	167.9	102.3	
0.5	0.3279	52.67	3637.7	0.3030	0.0173	-0.0033	0.388	5.59	-145.5	94.56	
0.6	0.3955	52.82	3626.3	0.3167	0.0174	0.0070	0.569	9.77	-127.2	88.99	
0.7	0.4629	52.91	3618.5	0.3283	0.0119	0.0125	0.729	16.9	-117.6	84.38	
0.8	0.5263	52.77	3630.4	0.3377	0.0016	0.0142	0.884	29.05	-115.9	80.43	
1.0	0.5801	49.24	3917.2	0.3456	-0.0361	0.0121	1.66	73.8	-169.5	78.40	
0.29056	0.1914	52.80	3023.4	0.2676	-0.0173	-0.0534	0.313	1.180	-0.10	129.2	(d)
0.29056	0.1885	52.38	3662.9	0.2607	-0.0114	-0.0461	0.240	1.298	11.59	128.7	(e)
0.6	0.3710	51.04	3772.7	0.3104	0.0187	0.0059	0.498	9.600	-131.0	93.88	
0.8	0.4923	50.90	3783.4	0.3306	0.0066	0.0148	0.796	27.26	-120.7	83.12	

TABLE 4.7 Compliant wall, resonant triads comprising three TS modes. $R_0 = 2562.8$, $m^{(0)} = 2.0$, $c_0 = 0.5$, $d = 0$, $S^{(0)} = 1.0$: (a) $R = 2562.8$, (b) $R = 4000$, (c) $R = 6000$, (d) $R = 5000$, $S^{(0)} = 2.0$, (e) $R = 6000$, $S^{(0)} = 2.0$

R	β	γ	$\tilde{R}$	c	$\tilde{c}_i$	$\theta°$	$\lvert a_3 \rvert$	$\lvert a_1 \rvert$	$\arg a_3$	$\arg a_1$	
2562.8	0.2139	0.2586	1439.9	0.3016 −0.0399i	−0.0847	55.82	0.631	1.095			(a)
4000.0	0.2052	0.2514	2311.5	0.2813 −0.0230i	−0.0616	54.70	0.439	1.14			
6000.0	0.1956	0.2437	3577.3	0.2640 −0.0010i	−0.0448	53.41	0.252	1.32			
10000	0.1833	0.2339	6211.7	0.2434 +0.0032i	−0.0274	51.60	0.076	1.62	74.96	119.22	
15000	0.1750	0.2275	9580.7	0.2254 +0.0103i	−0.0169	50.31	0.072	1.87	171.41	117.98	
20000	0.1707	0.2242	12962.5	0.2175 +0.0154i	−0.0084	49.61	0.107	2.04	−162.84	116.13	
4350	0.3018	0.3722	2546.7	0.3097 +0.0071i	−0.0243	54.16	0.247	3.51	158.69	94.04	(b)
8716.9	0.2733	0.3495	5434.4	0.2749 +0.0191i	−0.0020	51.43	0.282	4.35	−148.19	101.15	
13050	0.2658	0.3437	8274.2	0.2574 +0.0225i	0.0076	50.65	0.301	5.05	−137.32	100.51	
4358.4	0.3998	0.4942	2562.4	0.3325 +0.0145i	−0.0035	53.99	0.580	7.74	−137.10	86.78	(c)
2900	0.6347	0.7766	1671.0	0.3918 −0.0079i	0.0002	54.81	1.40	29.53	−104.14	74.68	(d)
5000	0.5871	0.7382	3031.0	0.35520.0113 −0.0097i		52.68	1.05	41.72	−118.34	77.72	
10000	0.5298	0.6935	6452.6	0.3142 −0.0357i	0.0162	49.81	2.46	70.42	−179.93	79.19	
2562.8	0.6889	0.8512	1505.4	0.4063 −0.0210i	−0.0026	54.03	1.50	43.2	−105.08	73.33	(e)
5000	0.6127	0.7908	3161.4	0.3587 −0.0289i	0.0101	50.78	1.32	66.7	−148.06	77.01	
6000	0.5801	0.7658	3917.2	0.3456 −0.0361i	0.0121	49.24	1.66	73.8	−169.48	78.40	
10000	0.2442	0.5564	8985.5	0.2884 −0.0543i	0.0208	26.02	1.07	29.2	131.54	93.66	

TABLE 4.8 Compliant wall, resonant triads comprising three TS modes. $R_0 = 2562.8$, $m^{(0)} = 2.0$, $c_0 = 0.5$, $d = 0$, $S^{(0)} = 1.0$: α = (a) 0.29056, (b) 0.43584, (c) 0.58113, (d) 0.895, (e) 1.0

α	β	γ	θ°	$\tilde{R}$	c	$\tilde{c}_i$	$\lvert a_3 \rvert$	$\lvert a_1 \rvert$	arg a_3	arg a_1	
0.8	0.3310	0.5192	39.61	1974.4	0.3824 +0.0039i	-0.0068	0.31	15.55	-128.92	86.09	(a)
0.8	0.2508	0.4721	32.08	2171.3	1.1577 -0.0002i	0.0001	2.39	89.48	45.27	54.09	
1.2	0.8729	1.0592	55.50	1451.7	0.7872 +0.111i	0.0128	1.39	130.45	48.32	-132.04	(b)
1.0	0.5317	0.7299	46.76	10276.0	0.3525 -0.0390i	-0.1125	0.60	6373.	135.47	157.55	(c)
1.0	0.8101	0.9520	58.32	7878.4	0.3635 -0.0418i	-0.0904	4.22	8544.	-52.54	152.95	

TABLE 4.9 Compliant wall, resonant triads. $R_0 = 2562.8$. (a) $R = 2562.8$, $m^{(0)} = 2.0$, $c_0 = 1.2$, $d = 0$, $S^{(0)} = 0.1$: first row is a triad of three TS modes, second row is a triad of three F modes; (b) $R = 2562.8$, $m^{(0)} = 1.1$, $c_0 = 0.8$, $d = 0$, $S^{(0)} = 0.15$: triad of three F modes; (c) $R = 15000$, first row is rigid wall, for second row $m^{(0)} = 2.0$, $c_0 = 0.5$, $d = 0$, $S^{(0)} = 1.0$: in both cases triad comprises a streamwise TS mode and two oblique HO modes. Oblique-wave propagation angle θ in degrees.

	α	β	γ	$\tilde{R}$	c	$\tilde{c}_i$	θ°	$\lvert a_3 \rvert$	$\lvert a_1 \rvert$	$\arg a_3$	$\arg a_1$	
A	0.6	0.7829	0.8384	715.6	0.4531 +0.0362i	-0.0279	69.03	10.00	29.05			(a)
B	0.8	1.0668	1.1392	702.2	0.4853 +0.0484i	-0.0275	69.44	24.8	92.1			
C	0.9	1.1386	1.2243	735.1	0.4944 +0.0508i	-0.0309	68.43	25.2	218.6	-4.77	29.9	
-	0.95	1.1407	1.2356	768.9	0.4980 +0.0509i	-0.0323	67.39	21.98	429.5	-2.05	31.11	
-	0.975	1.1284	1.2292	793.2	0.4996 +0.0508i	-0.0325	66.63	19.46	732.4	-1.80	32.27	
D	1.0	1.1041	1.2120	825.1	0.5012 +0.0504i	-0.0323	65.64	16.4	2020.0	-2.30	36.90	
-	1.05	1.0093	1.1376	923.0	0.5041 +0.0495i	-0.0291	62.52	9.62	997.2			
E	1.1	0.8582	1.0193	1079.2	0.5068 +0.0481i	-0.0208	57.34	4.18	477.8	-8.04	-161.3	
X	0.8	1.4693	1.5228	525.4	0.5115 -0.1087i	-0.0482	74.77	72.32	50.63	-11.4	15.4	(b)
Y	0.9	0.9286	1.0318	872.2	0.4803 -0.1046i	-0.0203	64.14	4.00	85.15	5.15	76.8	
Z	1.0	0.4571	0.6774	1476.1	0.4579 -0.1012i	-0.0015	42.43	0.4	76.1	46.59	-100.9	
1	1.2	0.5698	0.8274	1450.3	0.5412 -0.1951i	-0.0576	43.52	2.59	205.1	3.05	-59.62	(c)
2	1.2	1.0075	1.1726	1023.4	0.5412 -0.1951i	0.0112	59.22	7.23	107.9	8.80	-162.0	
3	1.2	0.5704	0.8278	1449.6	0.5117 +0.0446i	0.0011	43.55	0.41	338.1	-2.20	175.9	
4	1.2	0.8752	1.0611	1130.9	0.5117 +0.0446i	-0.0754	55.57	4.87	266.1	3.91	-88.05	

TABLE 4.10 Compliant wall, resonant triads. $R = 2000$, $R_0 = 2562.8$, $m^{(0)} = 2.0$, $c_0 = 0.5$, $d = 0.2$, $S^{(0)} = 0.3$: (a) TS resonant triads, (b) triads formed of one streamwise wall mode and two oblique TS waves, (c) case 1: HO wave and two oblique wall waves; case 2: HO wave and two oblique TS waves; case 3: three TS waves; case 4: TS wave and two oblique wall waves.

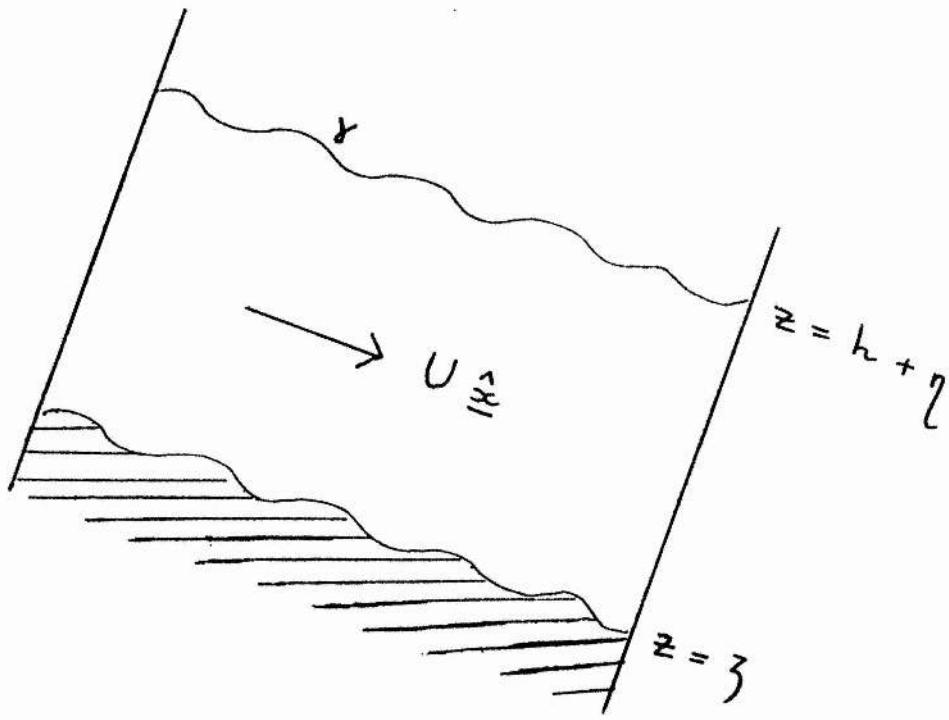

Figure 2.1 The model.

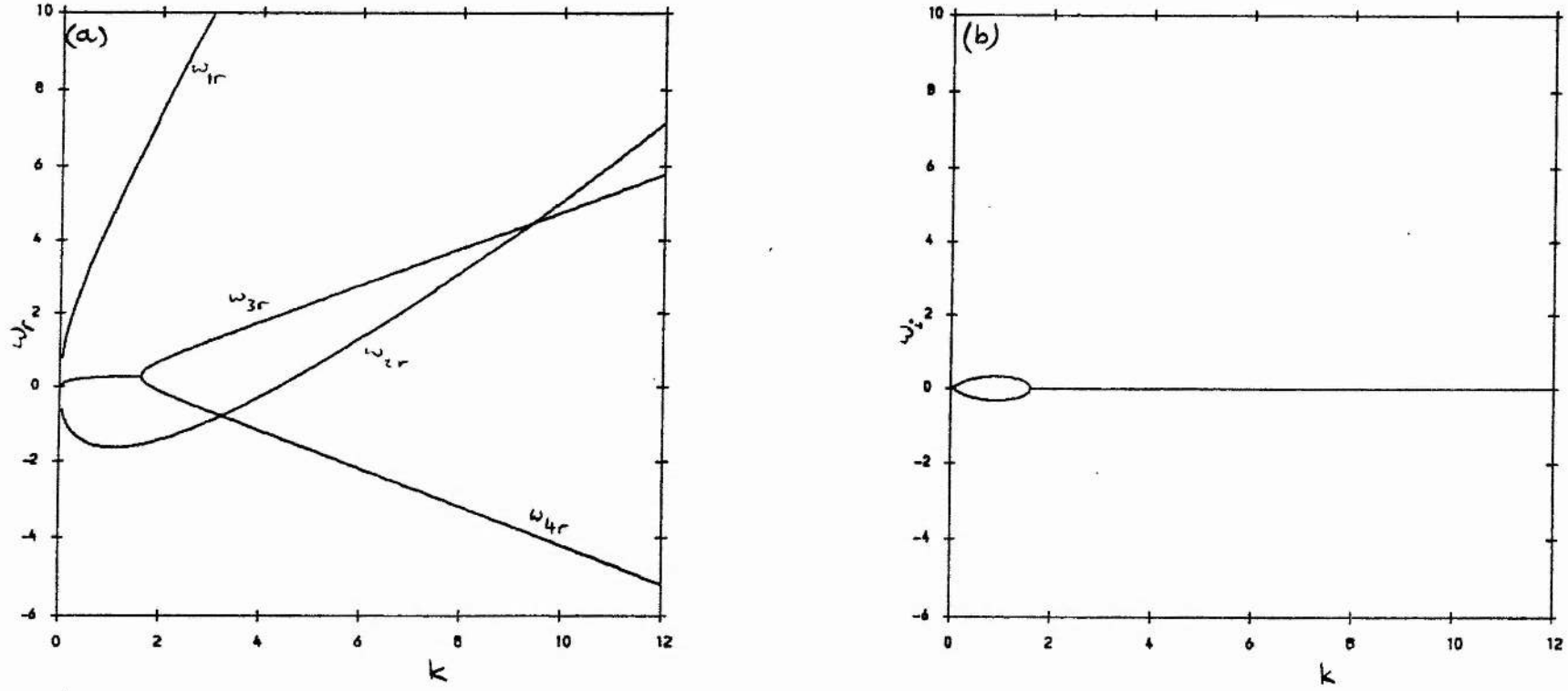

Figure 2.2 Real and imaginary parts, ω_r and ω_i (rad s^{-1}) of angular frequency, versus wavenumber k (m^{-1}). Only non-zero values of ω_i are shown. $U = 1.5$ ms^{-1}, $c_0 = 0.5$ ms^{-1}, $\rho^{-1}m = 5.0$ metres, $I = 0$ ms^{-1}, $S = \rho g$, $h = 100.0$ m: effectively no coupling.

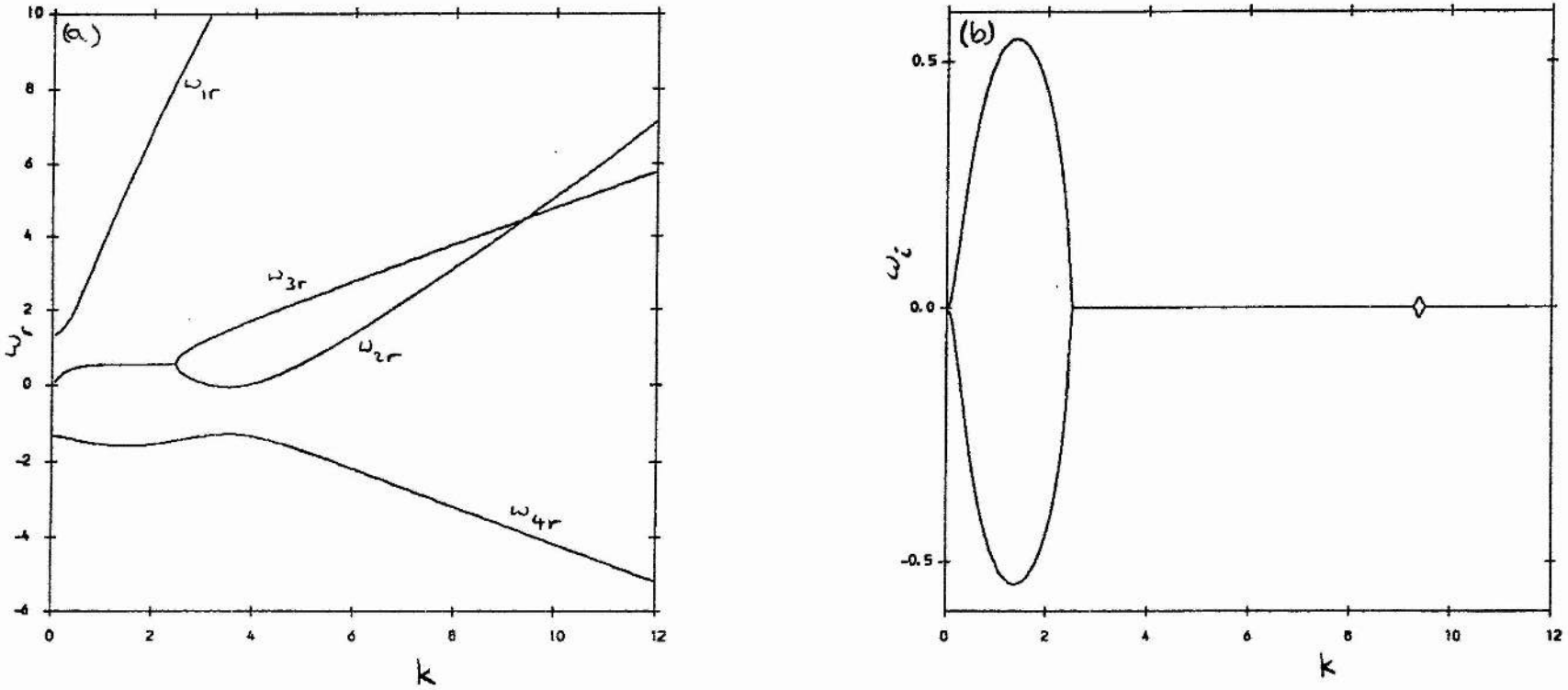

Figure 2.3 As Figure 1, except $h = 1.0$ m: weak coupling.

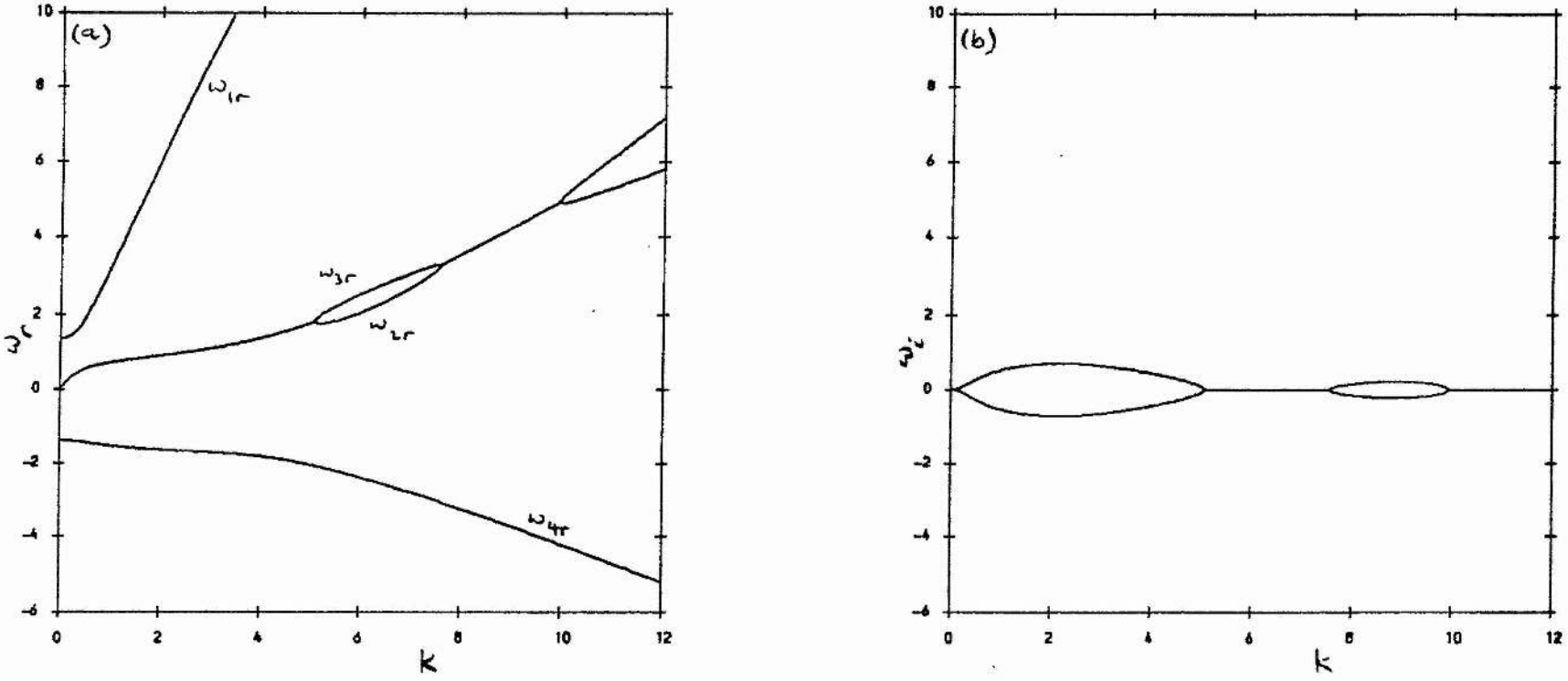

Figure 2.4 As Figure 1, except $h = 0.25$ m: stronger coupling.

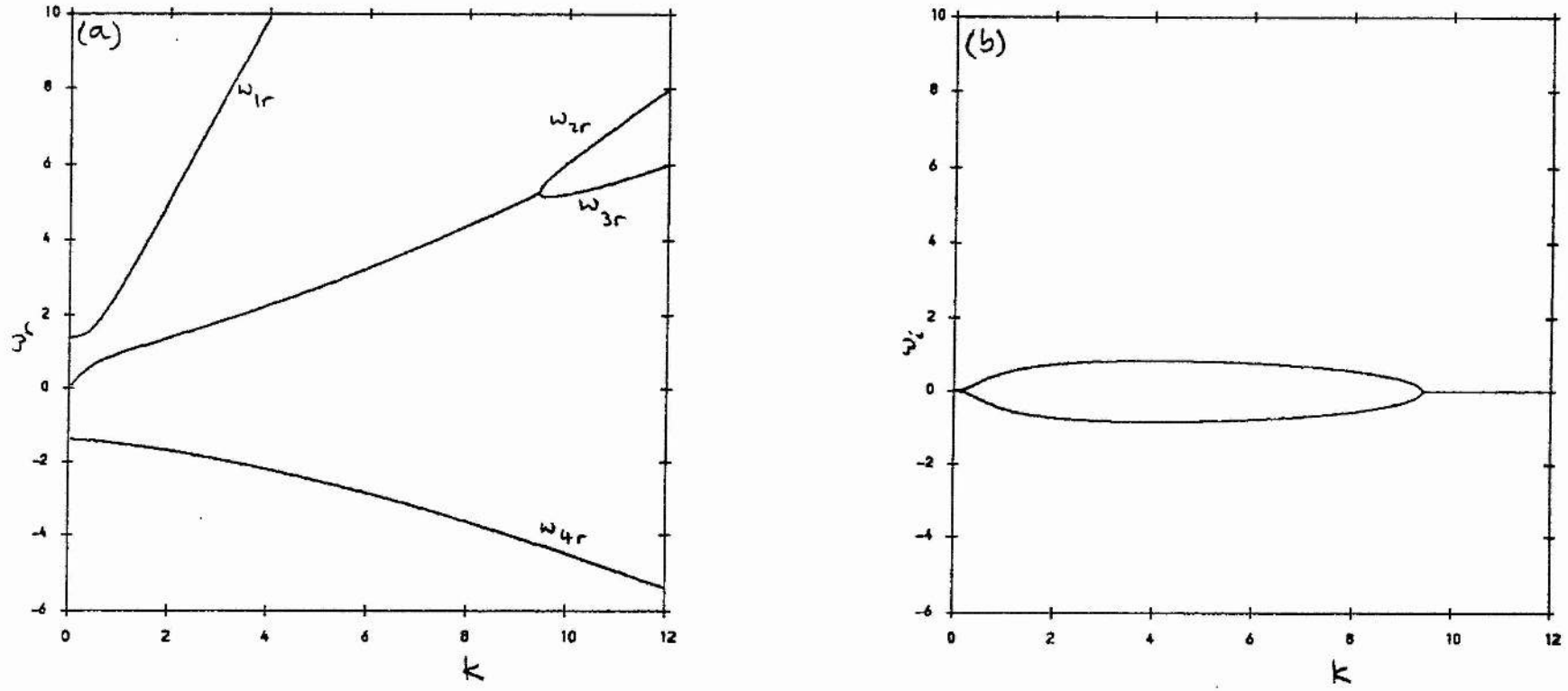

Figure 2.5 As Figure 1, except $h = 0.1$ m: coalescence of instabilities.

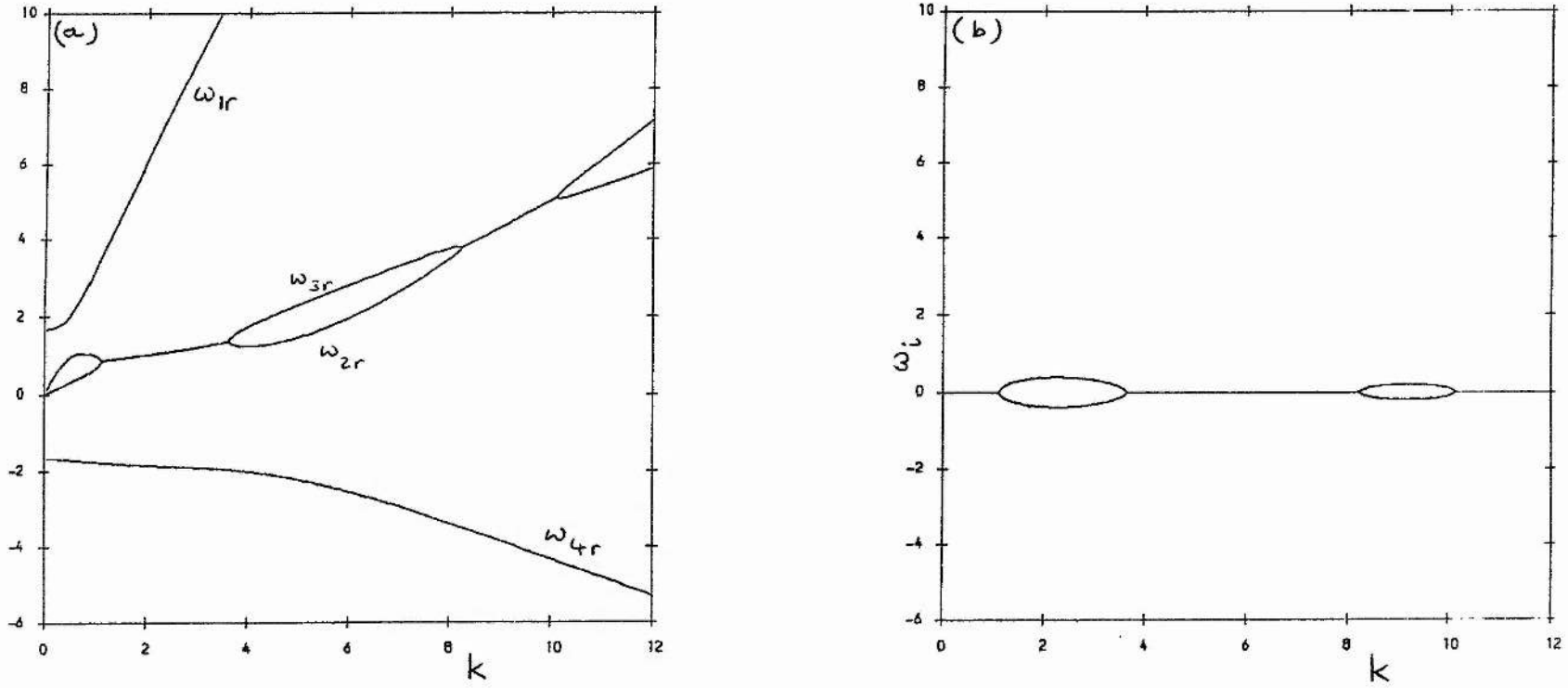

Figure 2.6 As Figure 1, except $h = 0.25$ m, $\rho^{-1}(\rho_s - \rho)=0.5$: unstable regions displaced to larger wavenumbers.

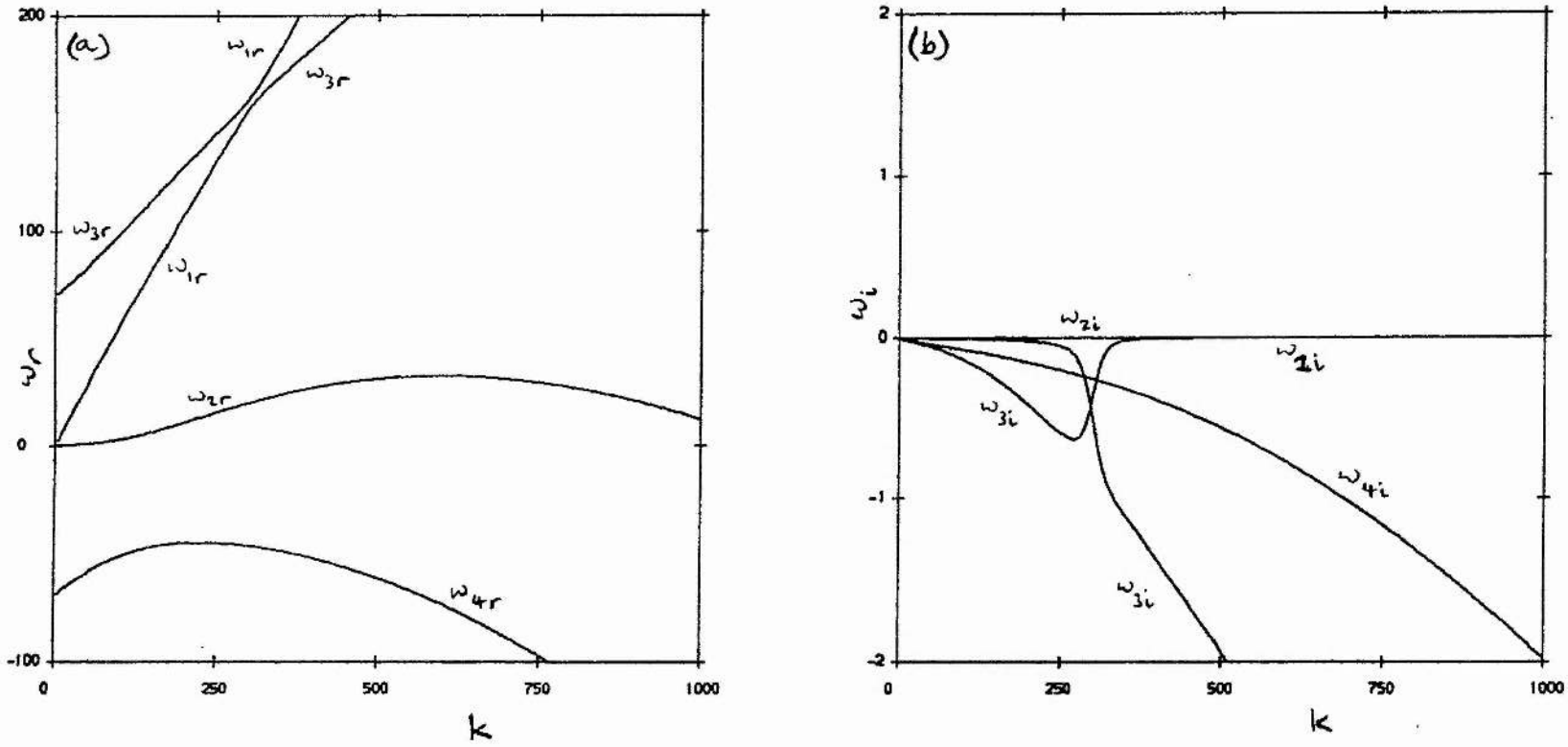

Figure 2.7 An example of damping producing instability of a negative energy wave in an otherwise neutrally stable system. $U = 0.3$ ms^{-1}, $\rho^{-1}m = 0.002$ metres, $c_0 = 0.31$ ms^{-1}, $h = 0.01$ m, $S = 6\rho g$: (a) ω_r for $l = 0$: $\omega_i = 0$ (neutral stability); (b) and (c) ω_i for $l = 0.01$ ms^{-1}, (b) showing exchange of identities of ω_{1i} and ω_{3i} at a point corresponding to exchange of identities of ω_{1r} and ω_{3r} (no observable difference in ω_r from case (a)), (c) showing amplification factor ω_{2i} (positive) and damping factor ω_{3i} (negative) with a greatly magnified vertical scale.

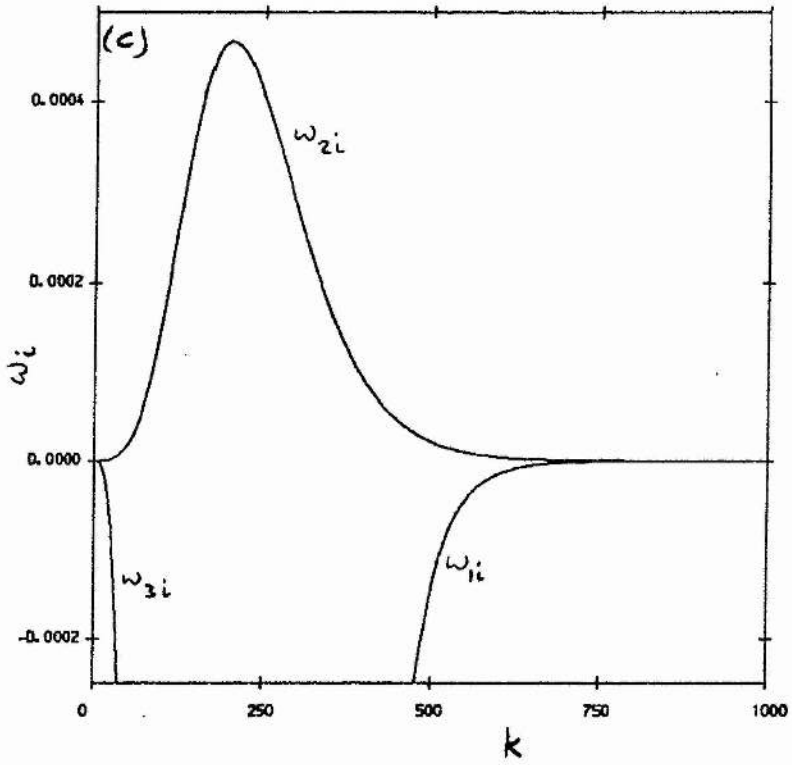
(c)
0.0004
0.0002
0.0000
-0.0002
ω_i
ω_{2i}
ω_{3i}
ω_{1i}
0
250
500
750
1000
k

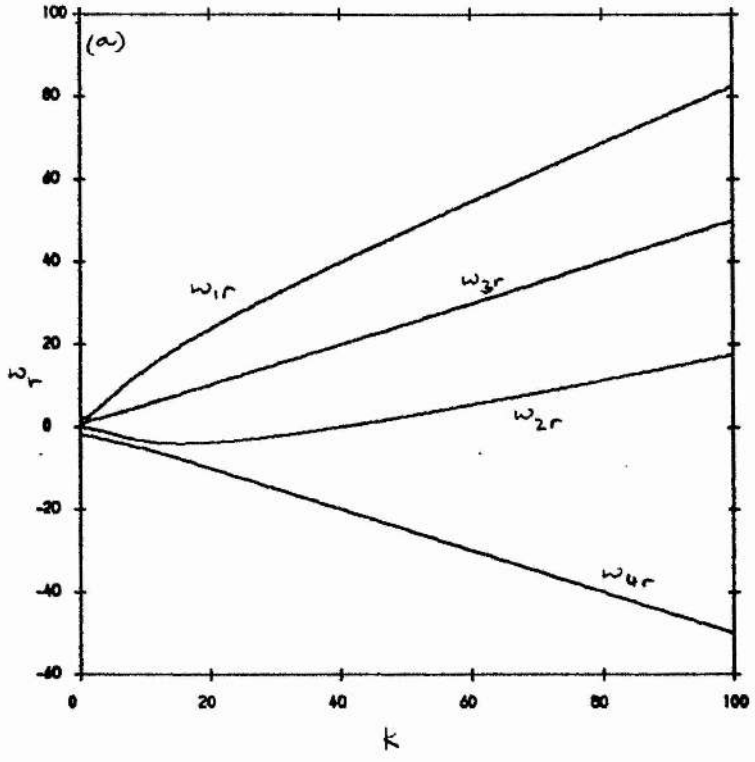

Figure 2.8 An example of damping producing instability of a negative energy wave in an otherwise linearly stable system. $U = 0.5$ ms^{-1}, $\rho^{-1}m = 5.0$ metres, $c_0 = 0.5$ ms^{-1}, $h = 0.1$ m, $\rho^{-1}(\rho_s - \rho)$=1.0: (a) ω_r for $l = 0$: $\omega_i = 0$ (no instability); (b) ω_r for $l = 10.0$ ms^{-1} (membrane modes are damped almost to zero); (c) ω_{2i} for $l = 10.0$ ms^{-1} (this is the only mode that has a positive growth rate).

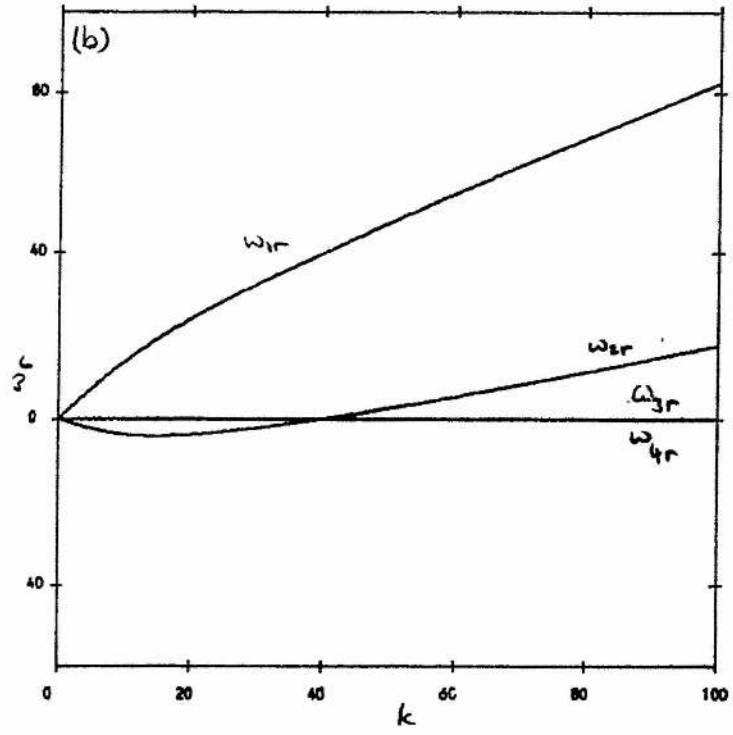
(b)
80
40
0
40
ω_r
ω_{1r}
ω_{2r}
ω_{3r}
ω_{4r}
0
20
40
60
80
100
k

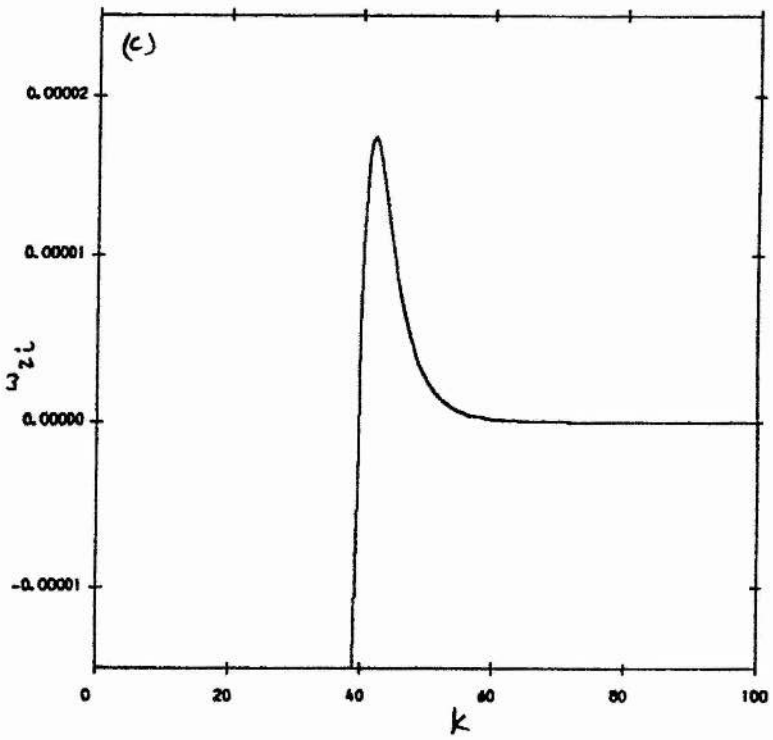
(c)
0.00002
0.00001
0.00000
-0.00001
ω_{2i}
0
20
40
60
80
100
k

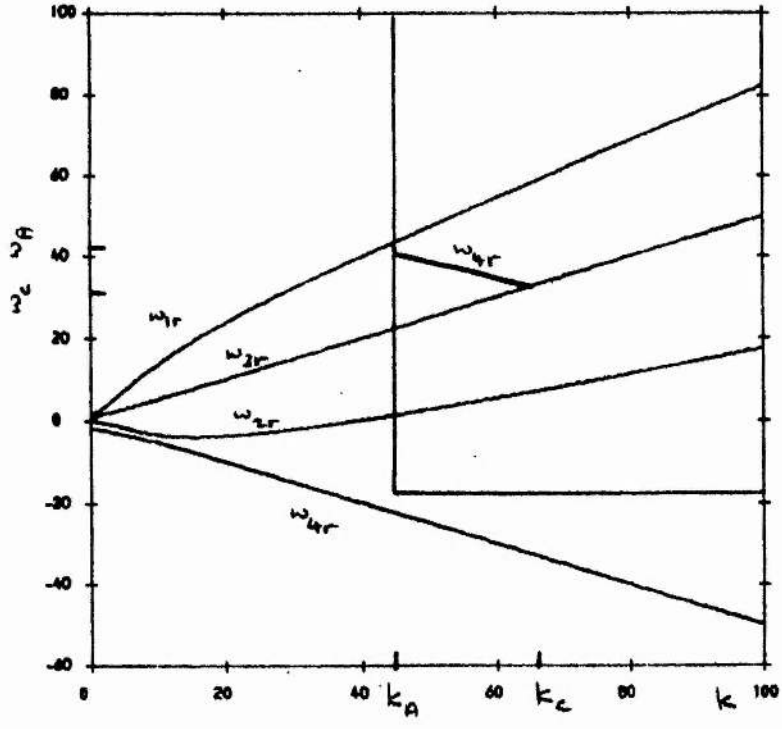

Figure 2.9 A graphical technique for finding the approximate location of resonant triads: here $k_A + k_B = k_C$, $\omega_A + \omega_B = \omega_C$.

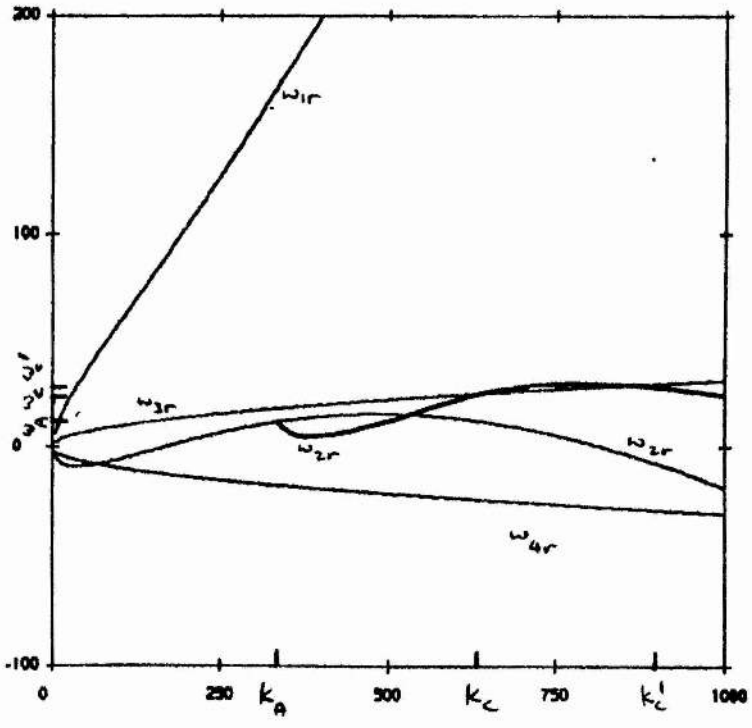

Figure 2.10 An example of explosive three-wave resonance. $U = 0.268$ ms^{-1}, $\rho^{-1}m = 5.0$ metres, $c_0 = k^{-1/2}$ ms^{-1}, $l = 0$ ms^{-1}, $h = 0.25$ m, $\rho^{-1}(\rho_s - \rho) = 1.0$.

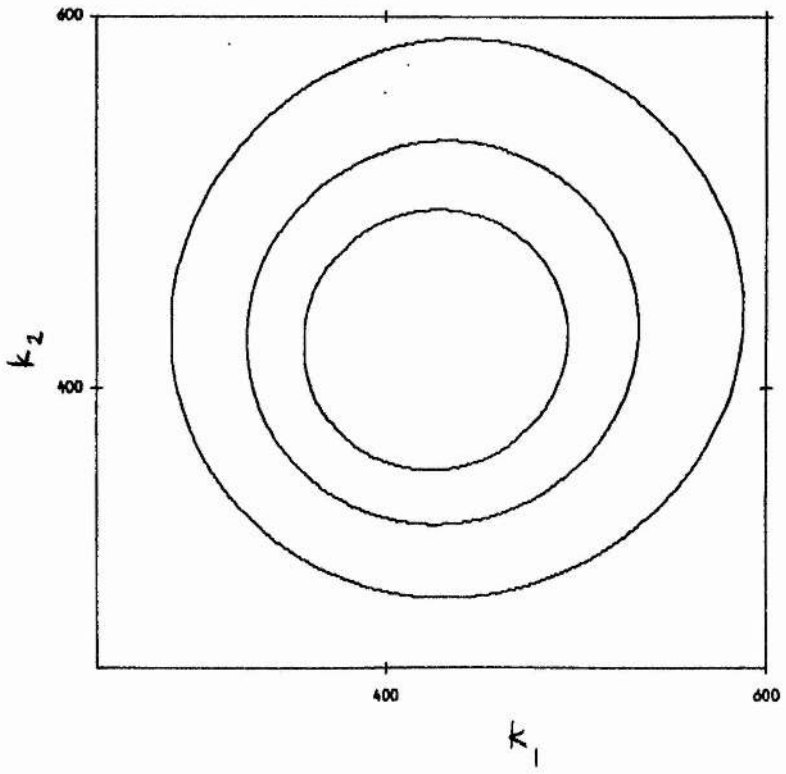

Figure 2.11 Wavenumbers k_1 and k_2 permitting exposive three-wave resonance, with $k_1 + k_2 = -k_3$, $\omega_1 + \omega_2 = -\omega_3$. Computed with $U = 0.27, 0.268, 0.265$ ms^{-1} for outer, middle and inner loops respectively. Other parameters:
$c_0 = 0$ ms^{-1}, $\rho^{-1}m = 5.0$ metres, $I = 0$ ms^{-1}, $S_0 = 2\rho g$, $S_1 = m$, $h = 0.25$ metres.

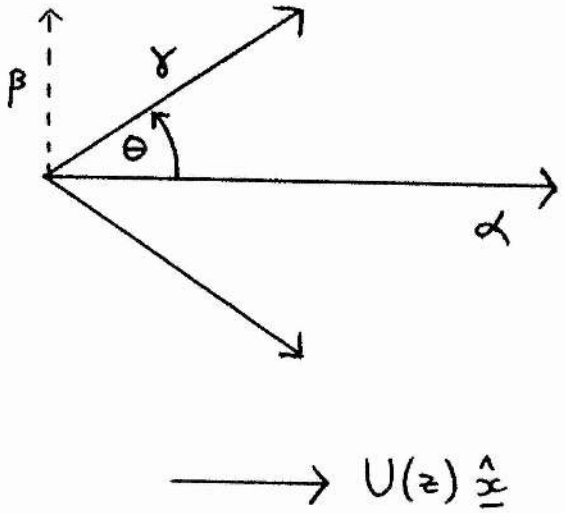

Figure 3.1 The model: resonant triad configuration.

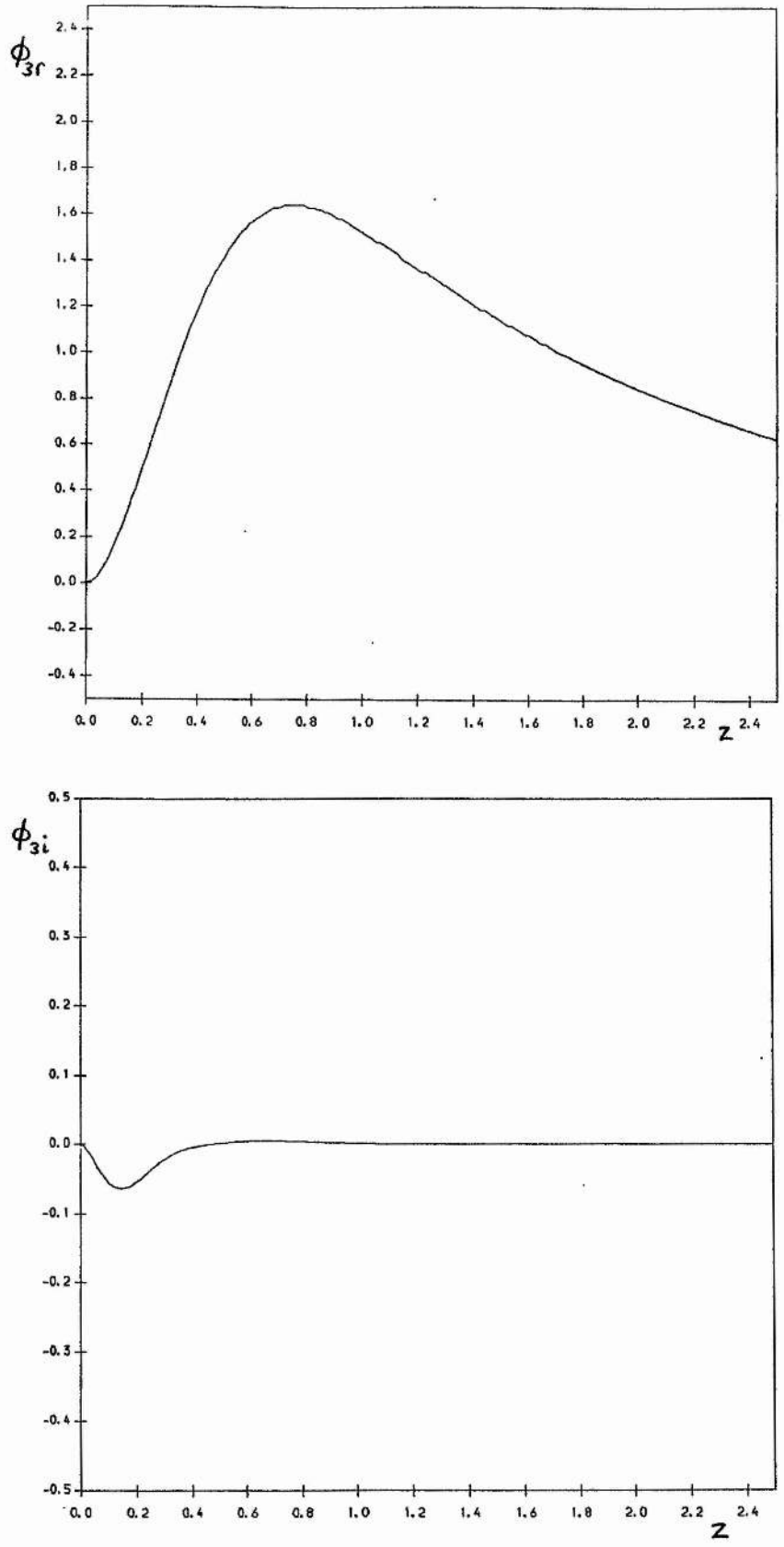

Figure 3.2 Rigid wall: $\alpha = 0.6$, $R = 2562.8$ (see Table 3.1).

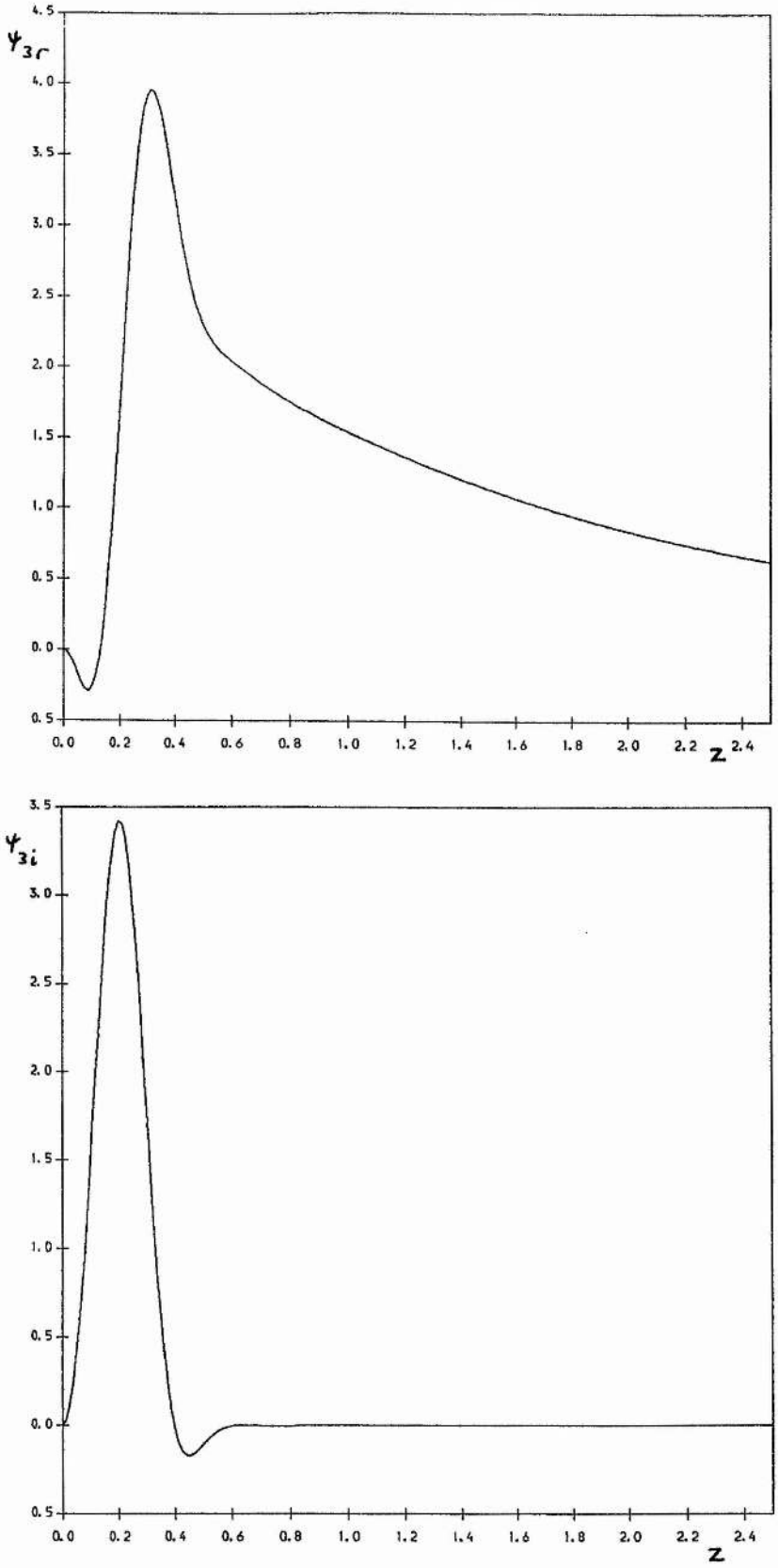

Figure 3.2 (contd.) Adjoint eigenfunction.

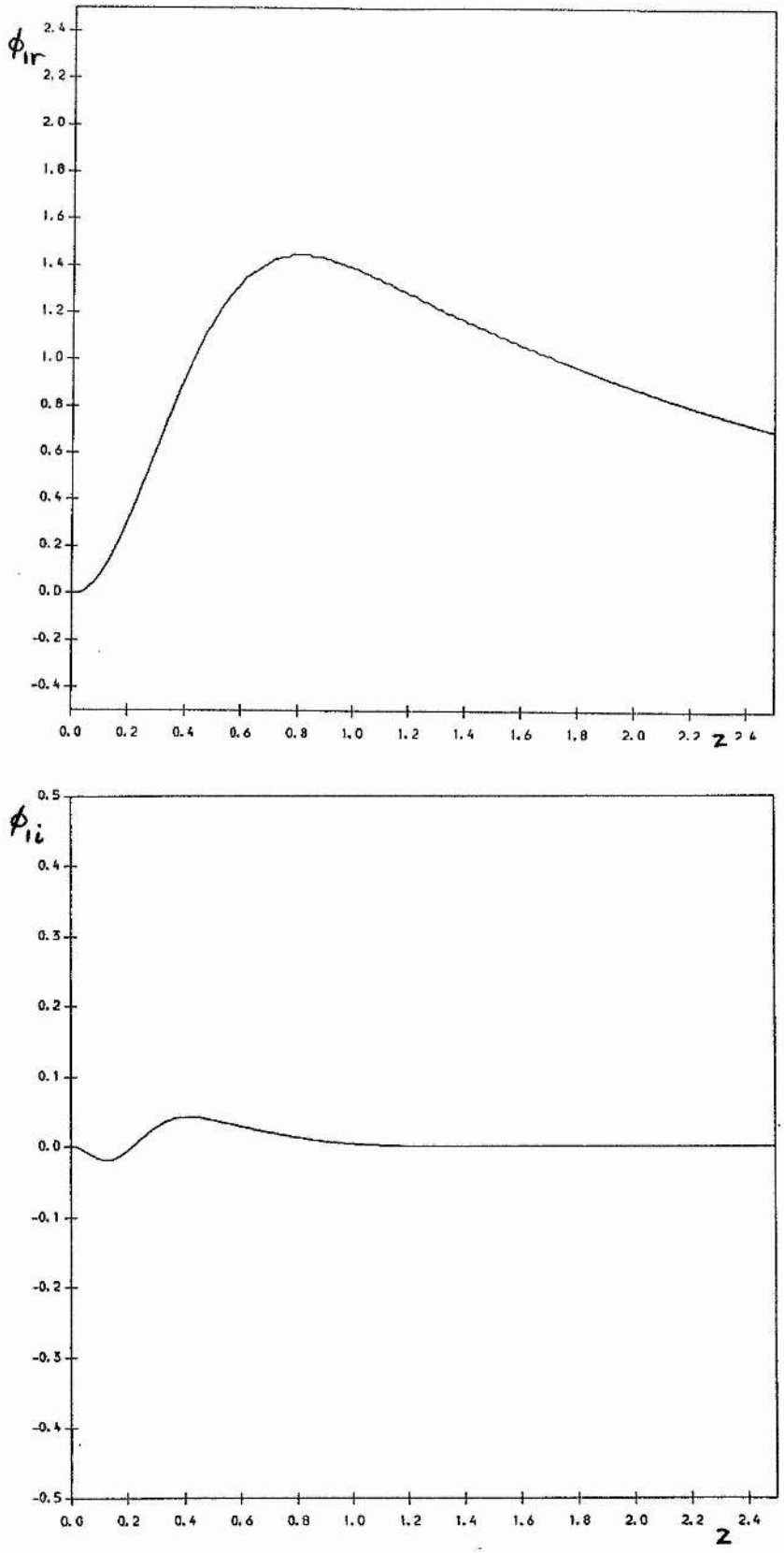

Figure 3.2 (contd.) Oblique eigenfunction.

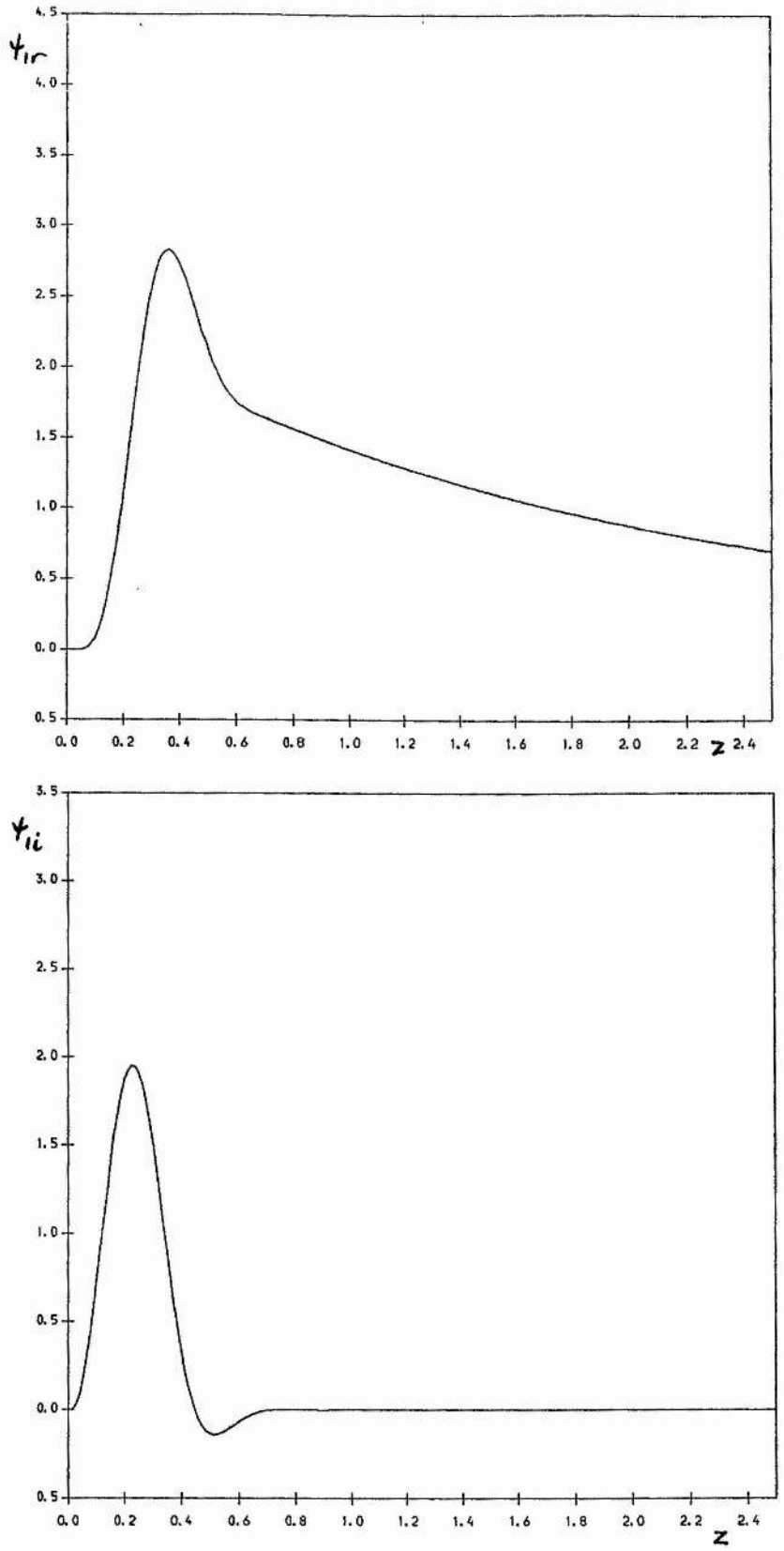

Figure 3.2 (contd.) Oblique adjoint eigenfunction.

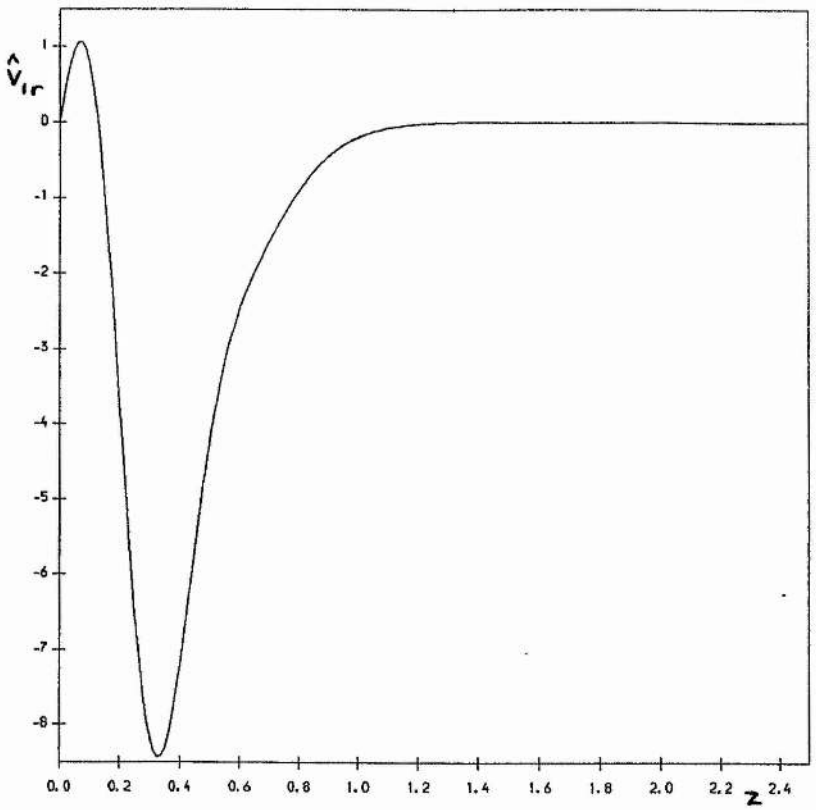

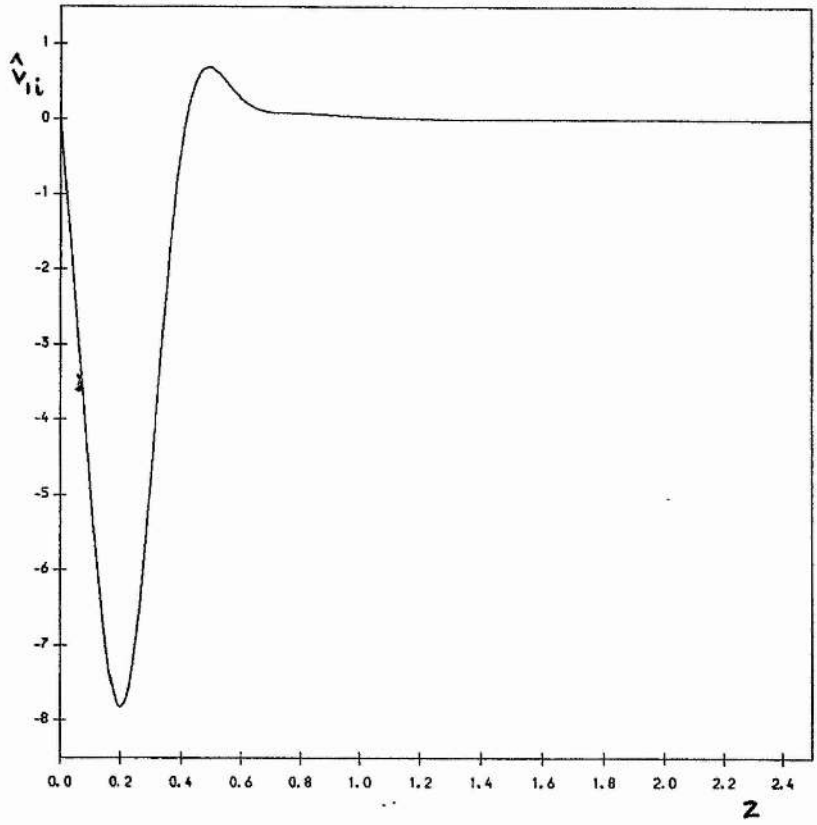

Figure 3.2 (contd.) Cross-flow velocity.

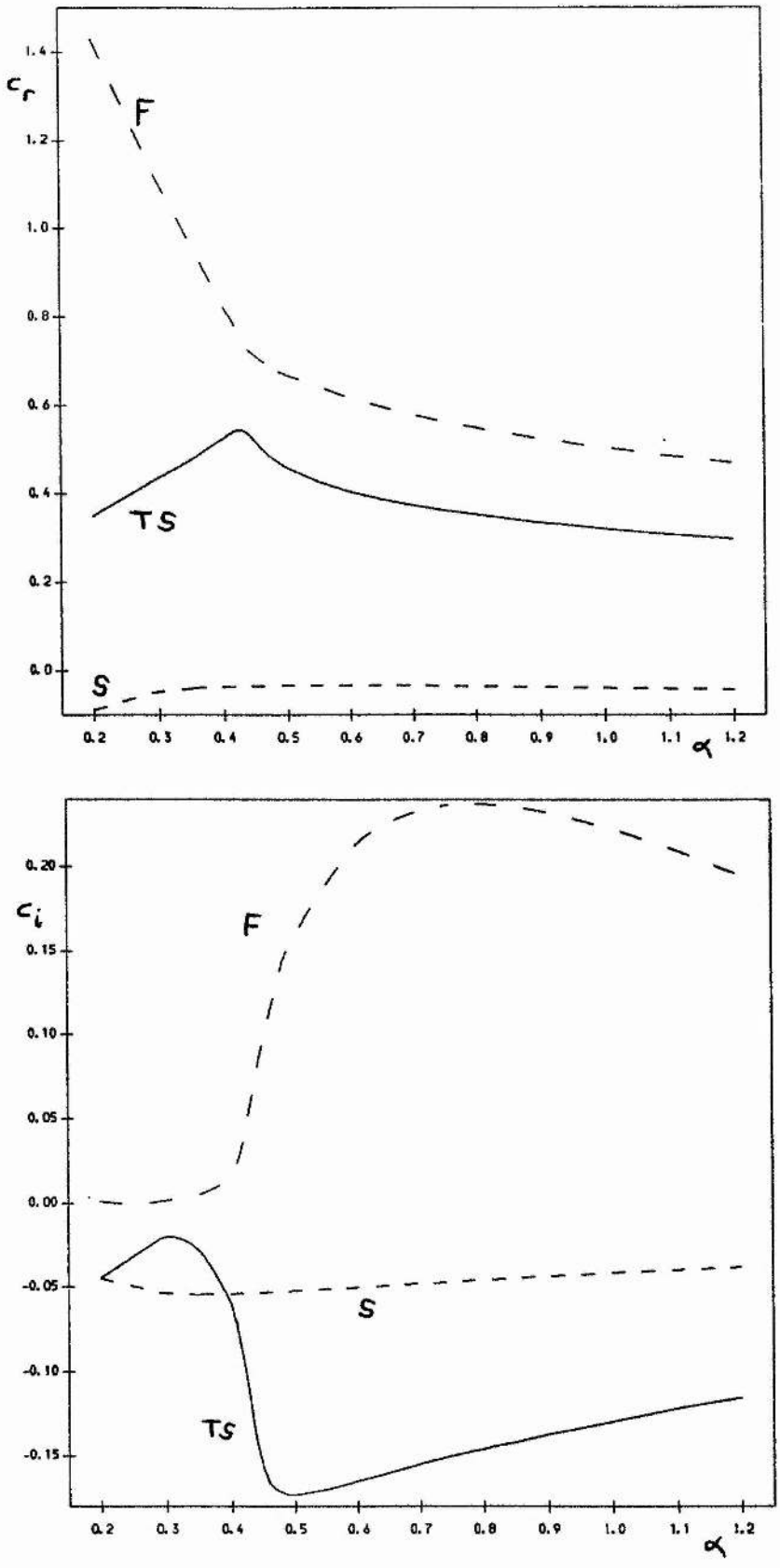

Figure 4.1 $m = 1.1$, $c_0 = 0.1$, $d = 0$, $S = 0.15$: $R = R_0 = 2562.8$ (see Table 4.1).

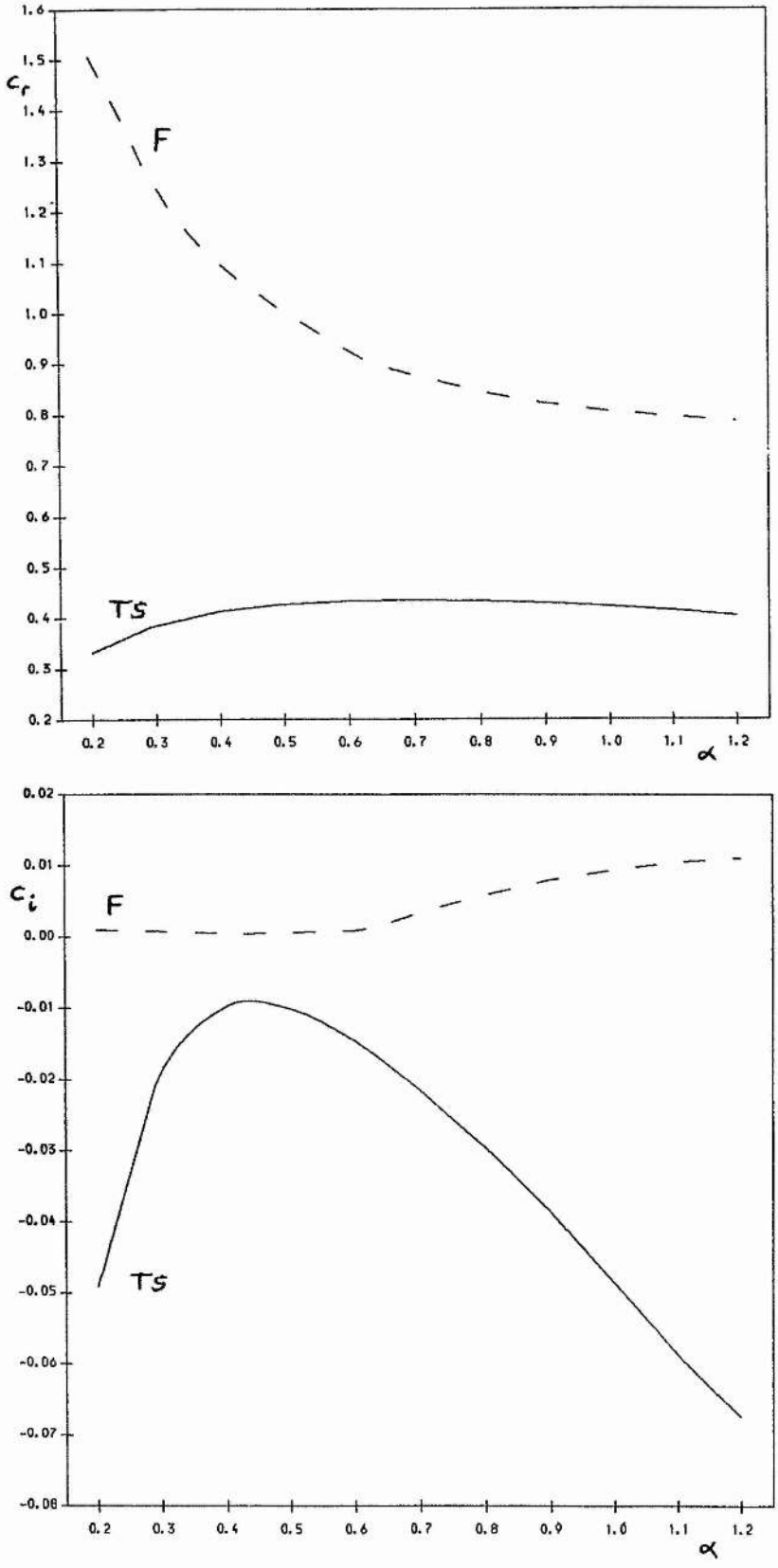

Figure 4.2 $c_0 = 0.8$, other parameters as Figure 4.1.

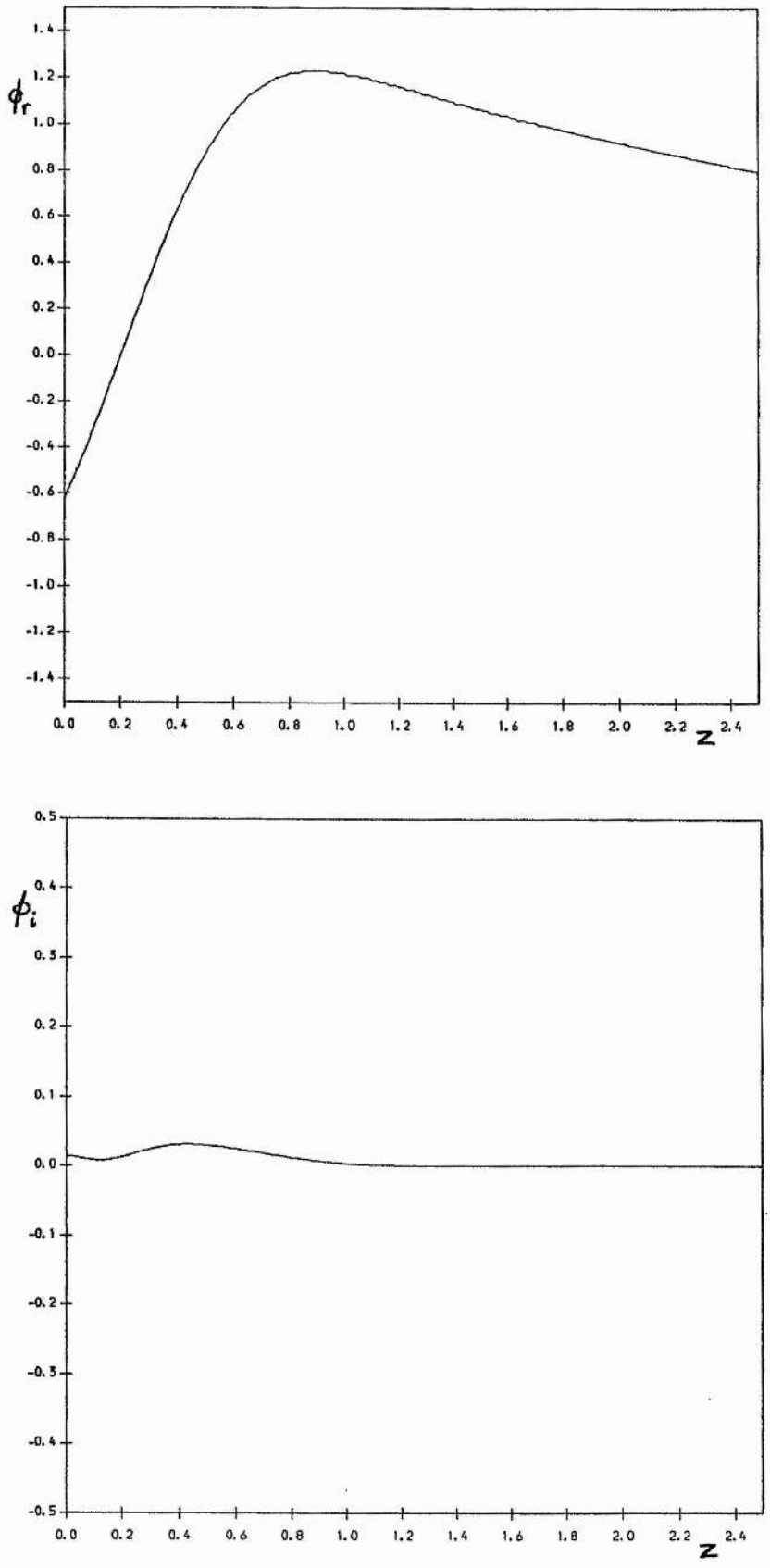

Figure 4.3 $m = 1.1$, $c_0 = 0.5$, $d = 0$, $S = 0.15$: $\alpha = 0.29056$, $R = R_0 = 2562.8$. TS mode: $c = (0.4071, -0.0198)$.

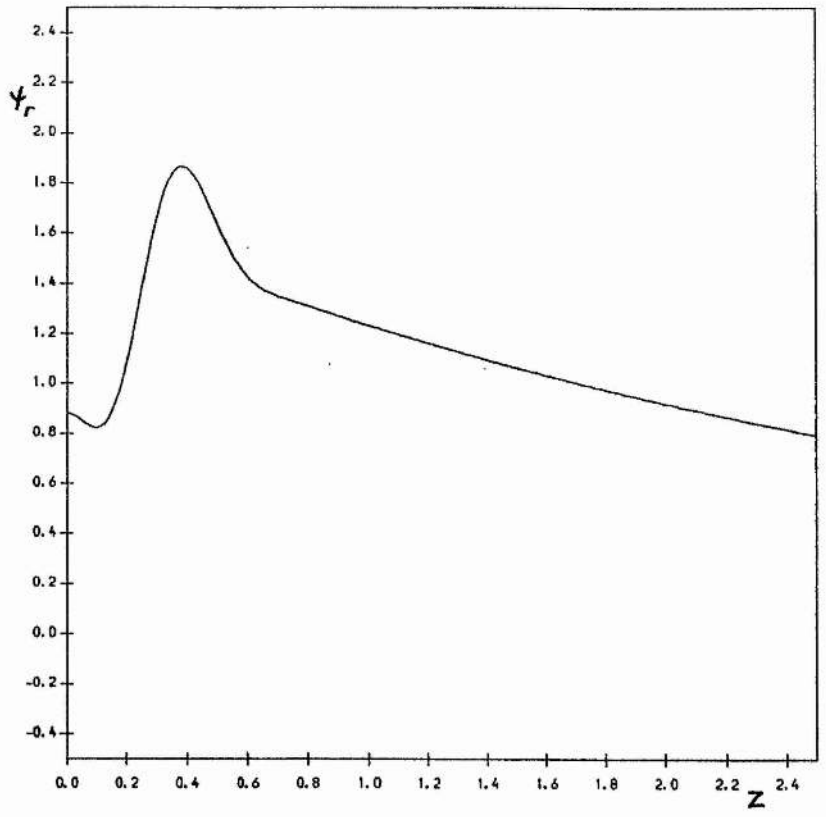

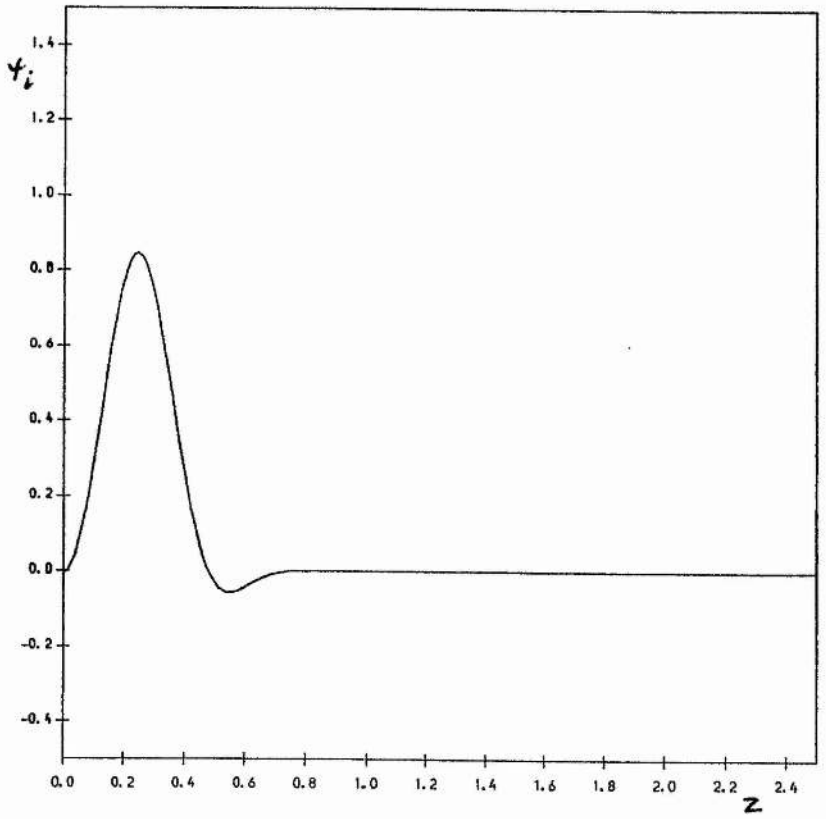

Figure 4.3 (contd.) Adjoint eigenfunction.

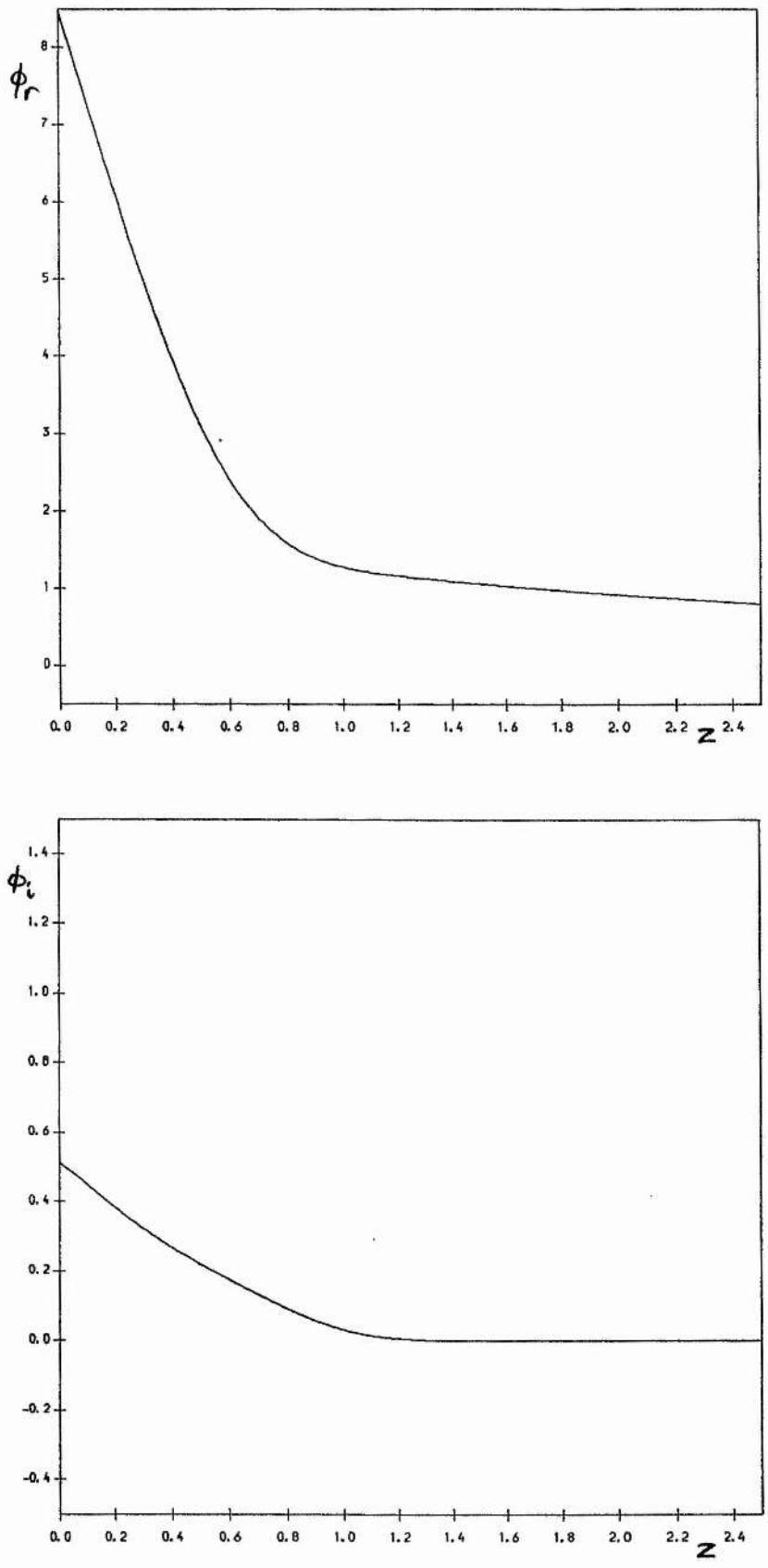

Figure 4.4 As Figure 4.3, but F mode: c = (1.1914, 0.0009).

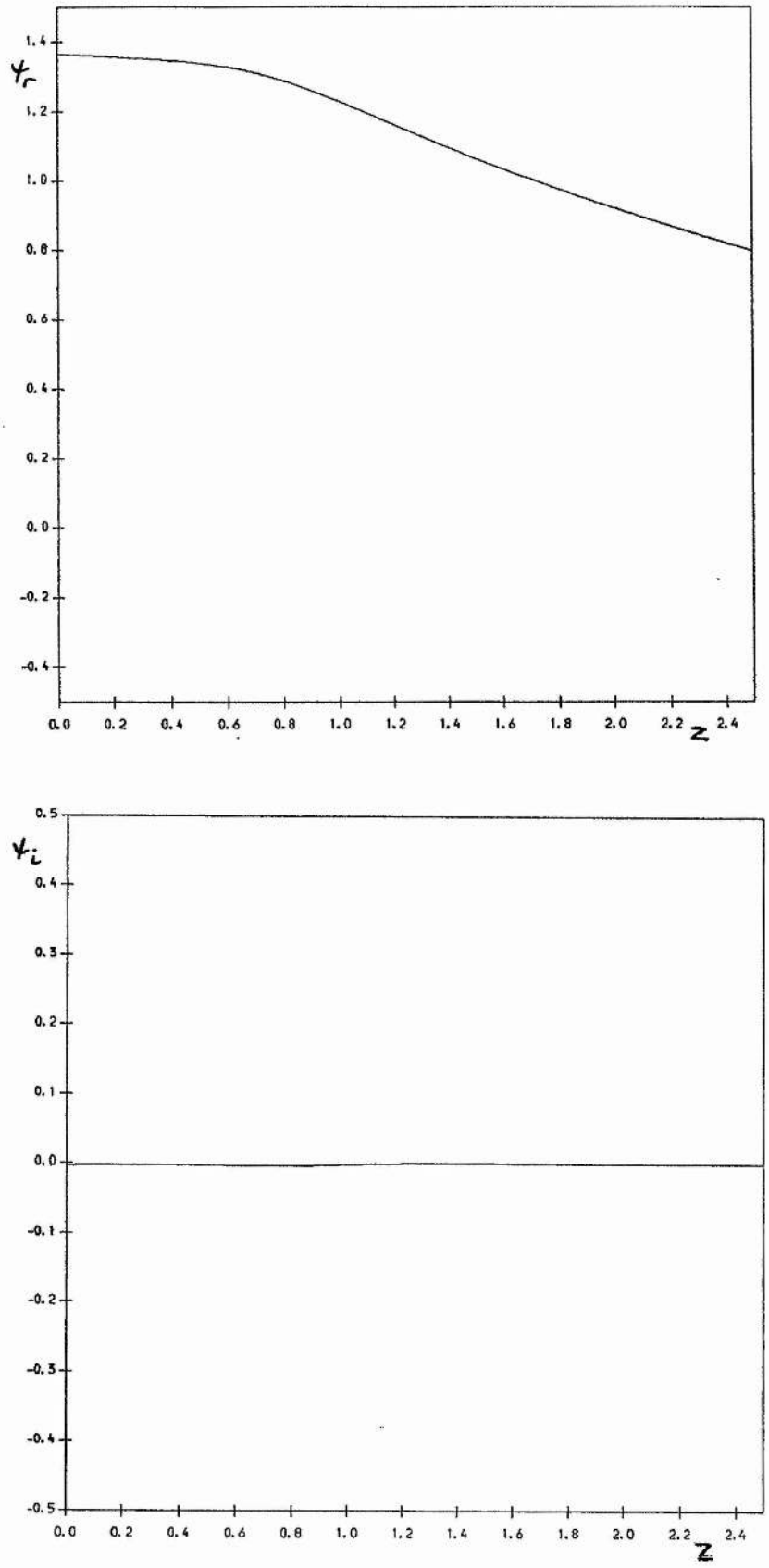

Figure 4.4 (contd.) Adjoint eigenfunction.

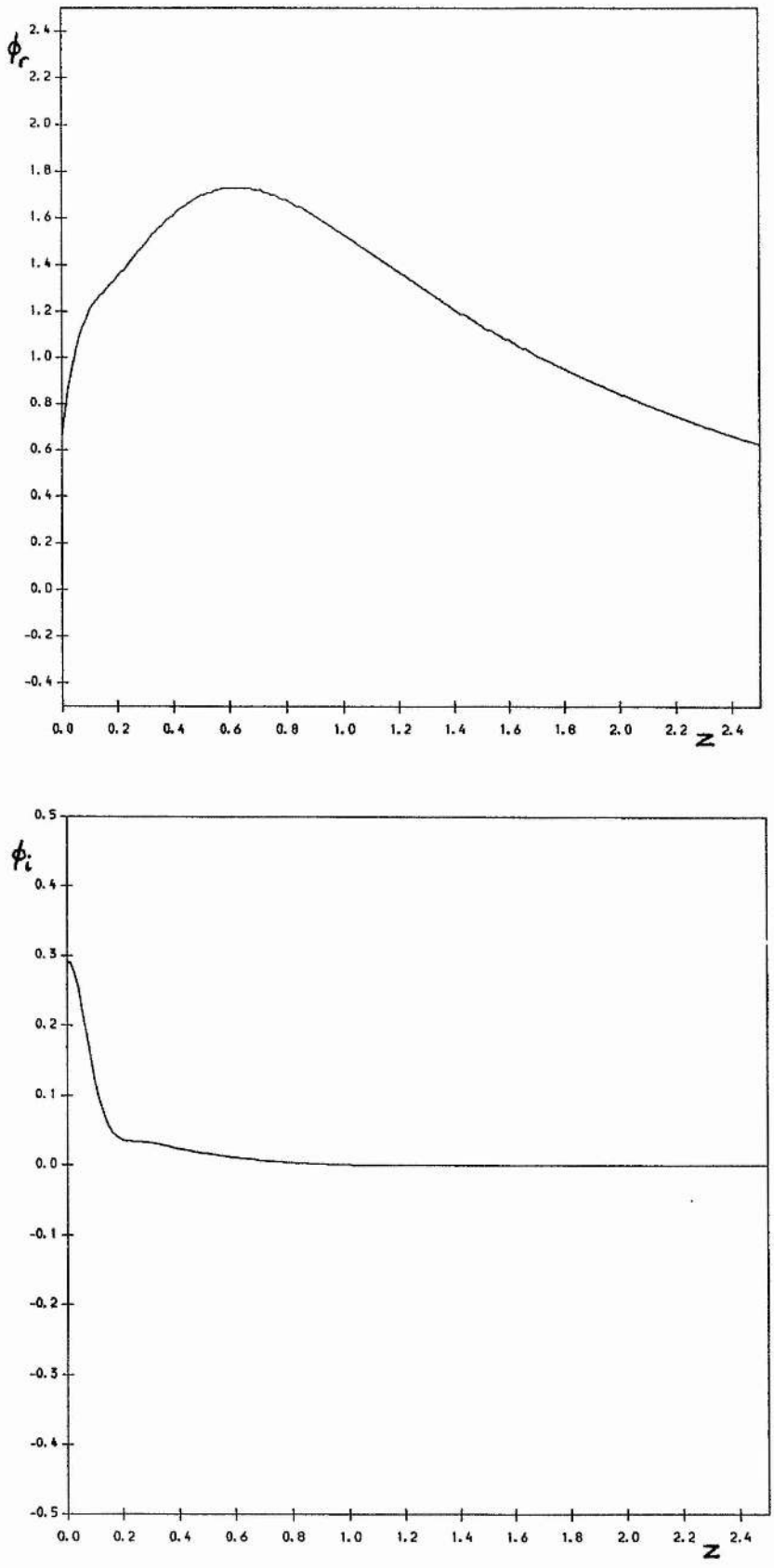

Figure 4.5 As Figure 4.3, but $\alpha = 0.6$. S mode: c = (-0.1122, -0.0413).

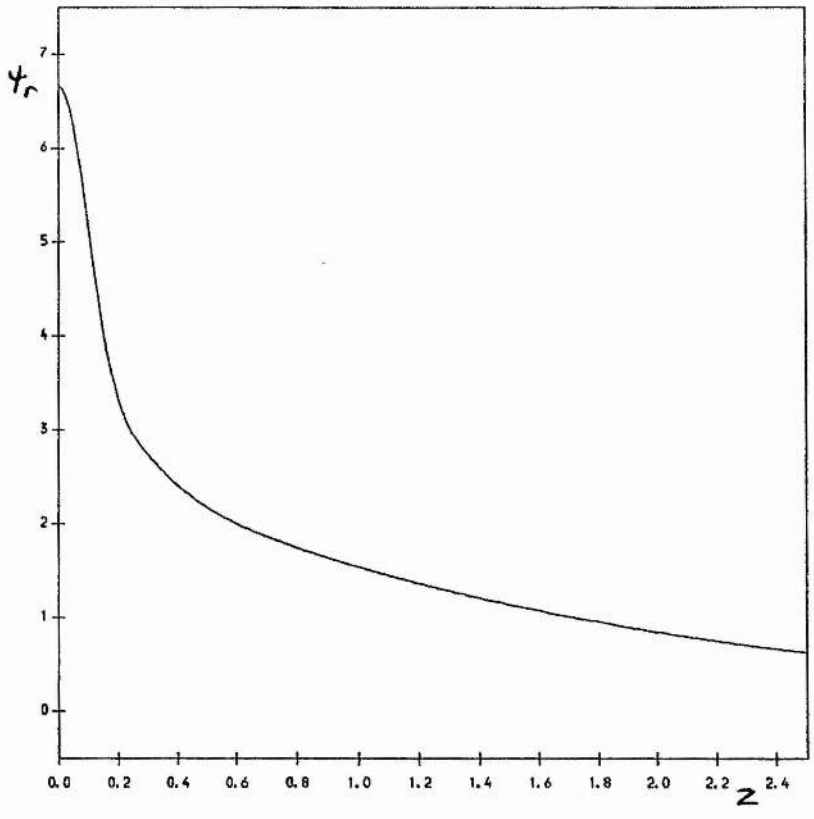

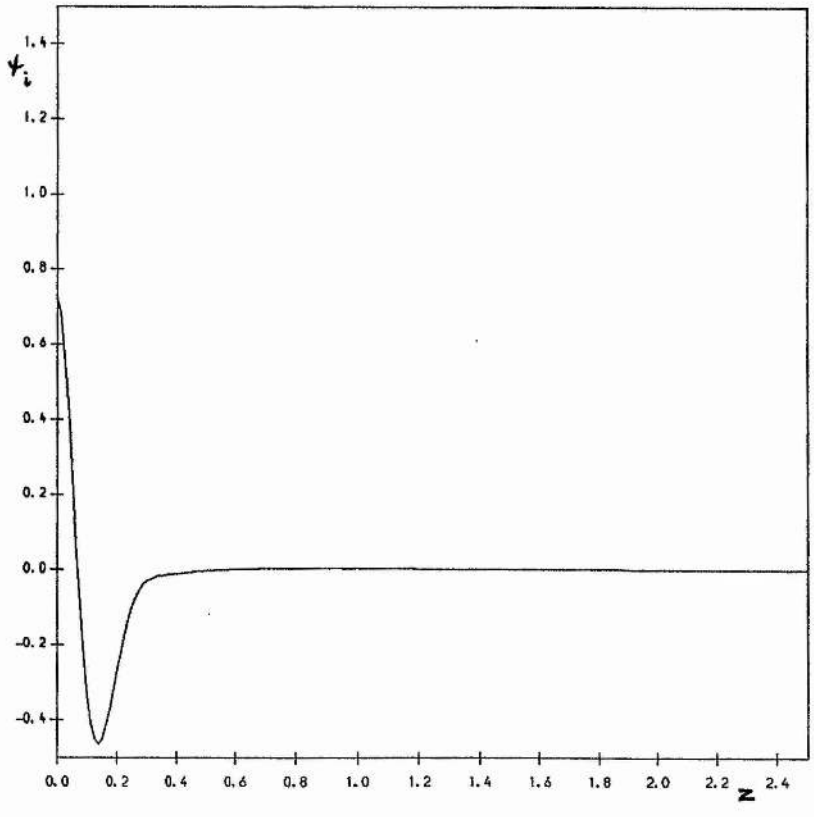

Figure 4.5 (contd.) Adjoint eigenfunction.

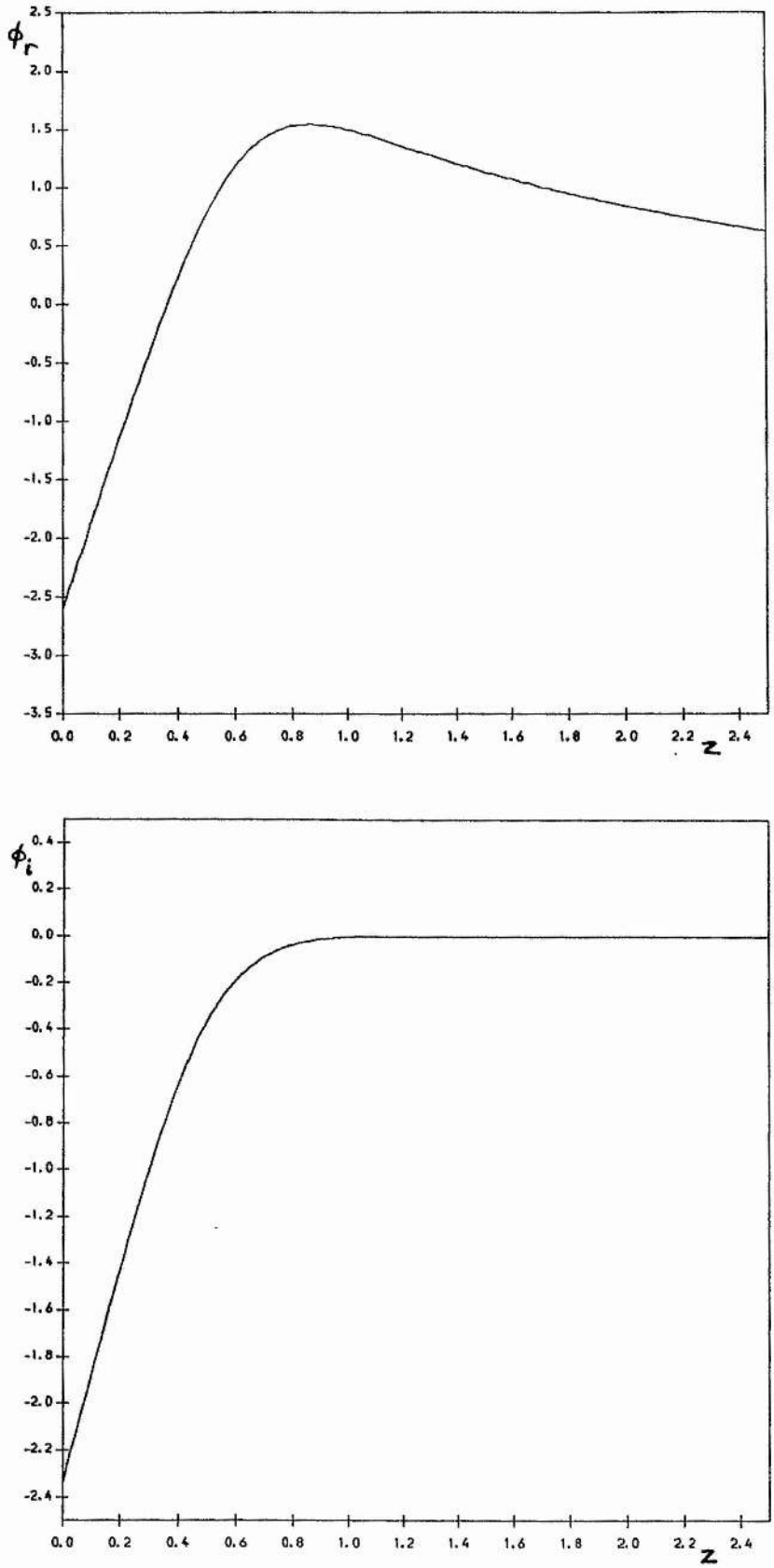

Figure 4.6 As Figure 4.5, but interacting F mode: c = (0.6846, 0.0856).

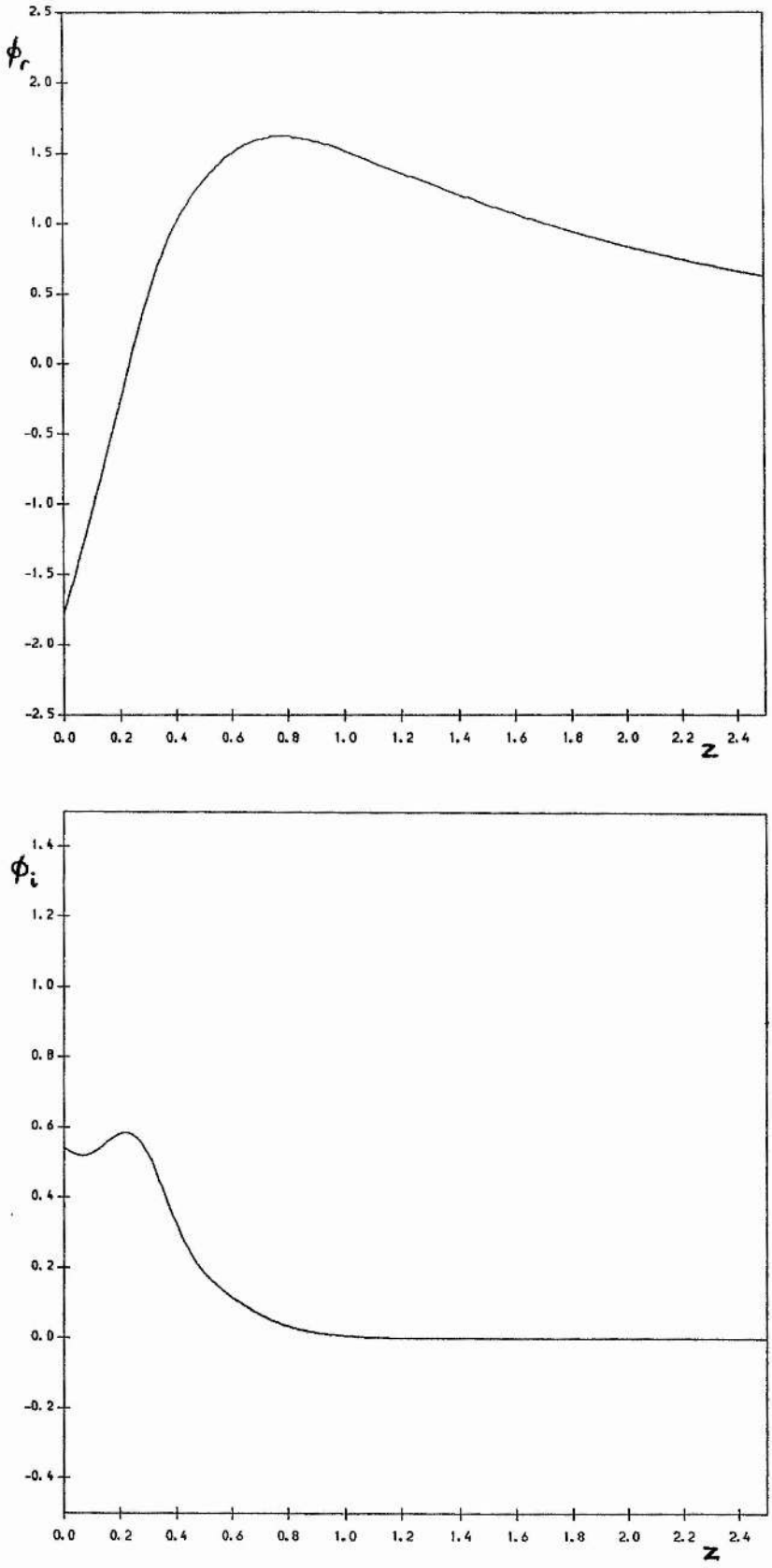

Figure 4.7 As Figure 4.5, but interacting TS mode: c = (0.4776, -0.1166).

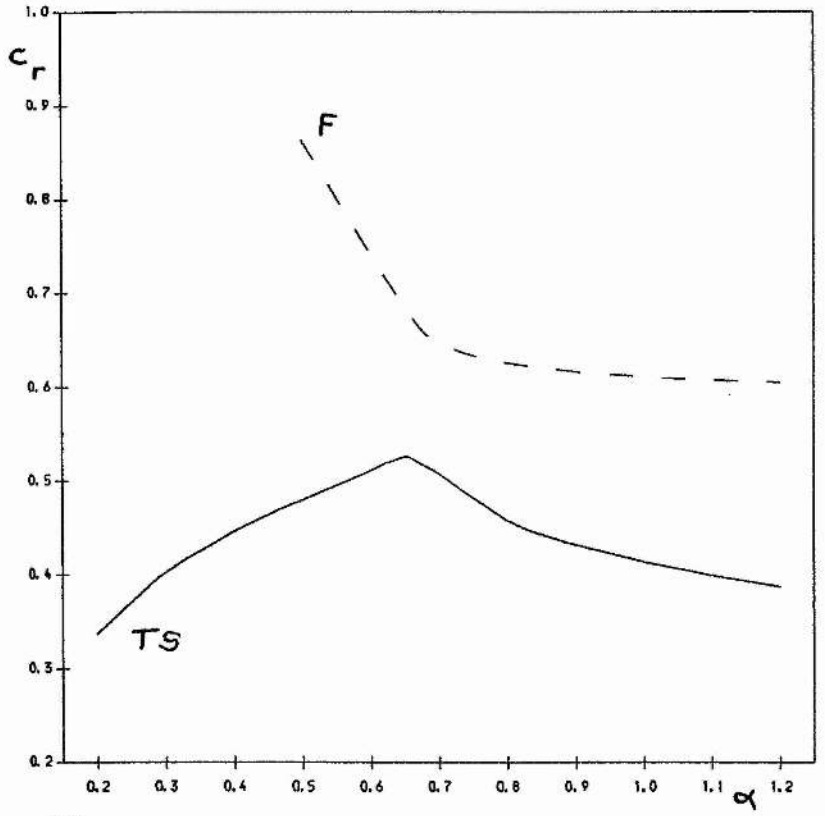

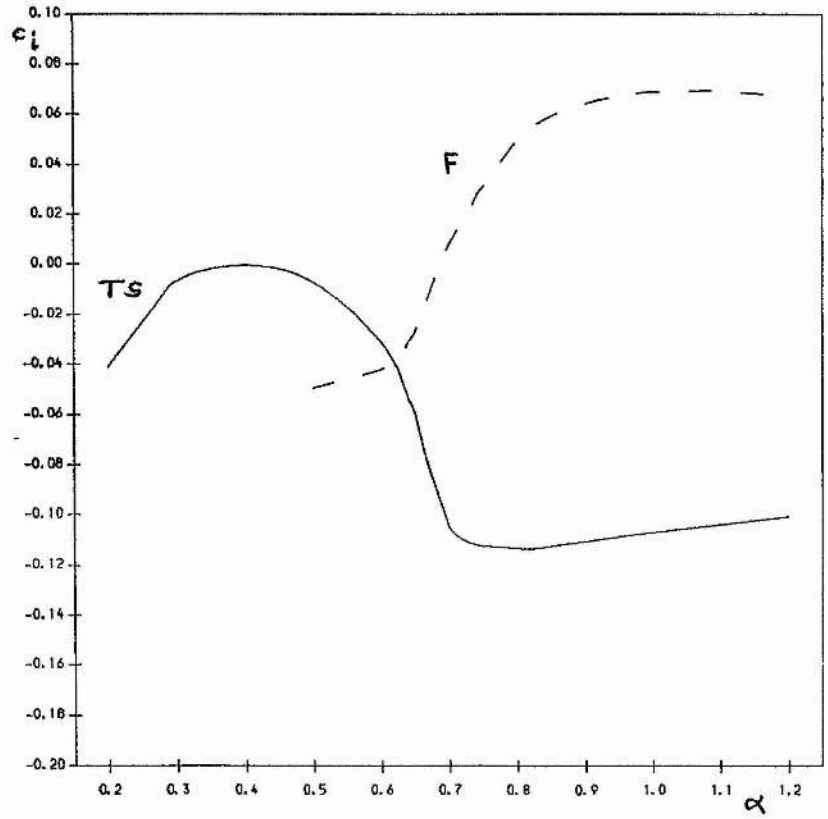

Figure 4.8 $m = 1.1$, $c_0 = 0.6$, $d = 0.05$, $S = 0.15$, $R = R_0 = 2562.8$.

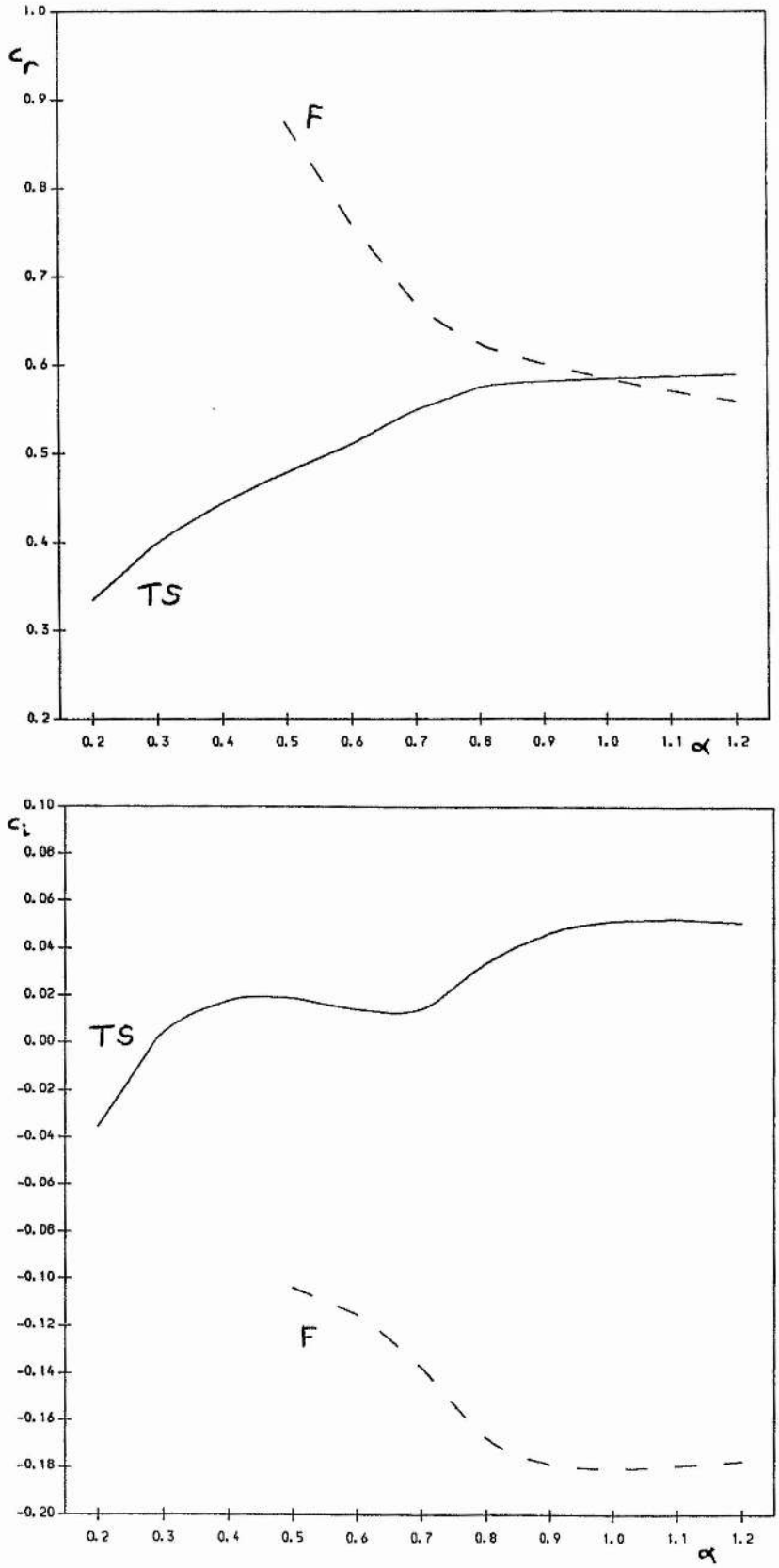

Figure 4.9 As Figure 4.8, but $d = 0.1$.

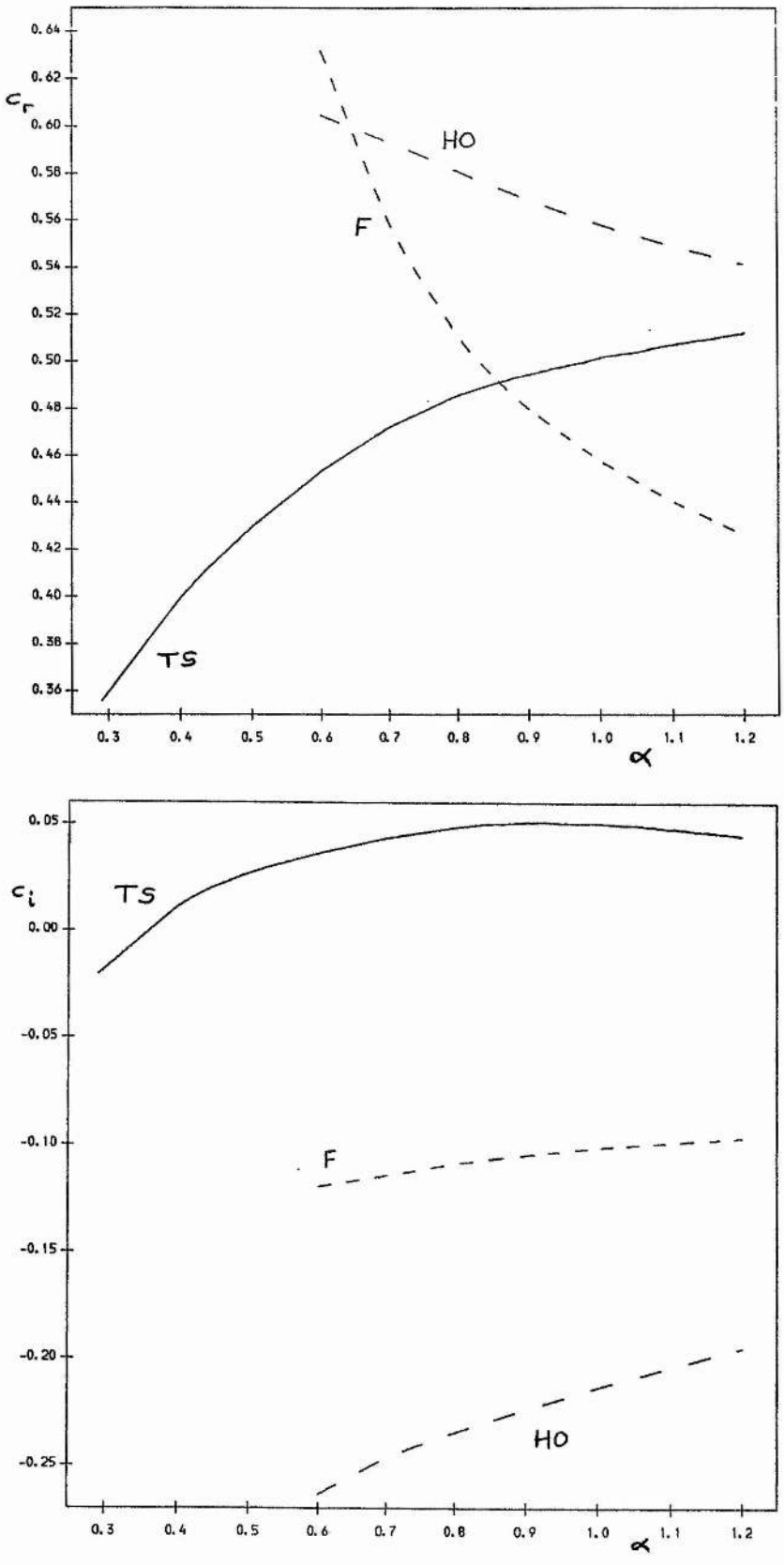

Figure 4.10 $m = 2$, $c_0 = 0.5$, $d = 0.2$, $S = 0.3$: $R = 2000$, $R_0 = 2562.8$.

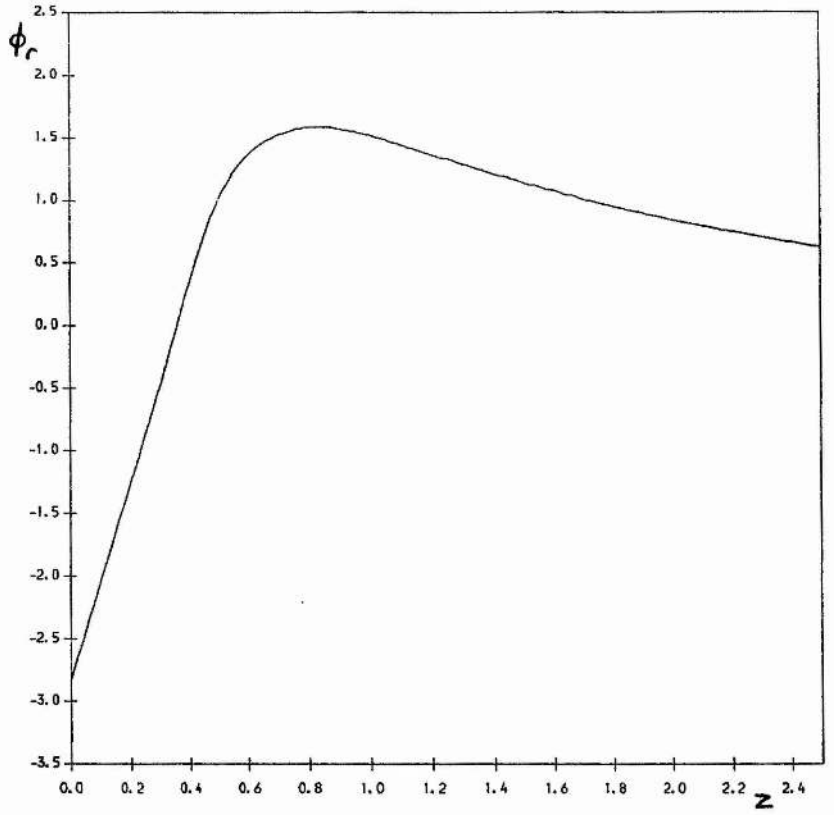

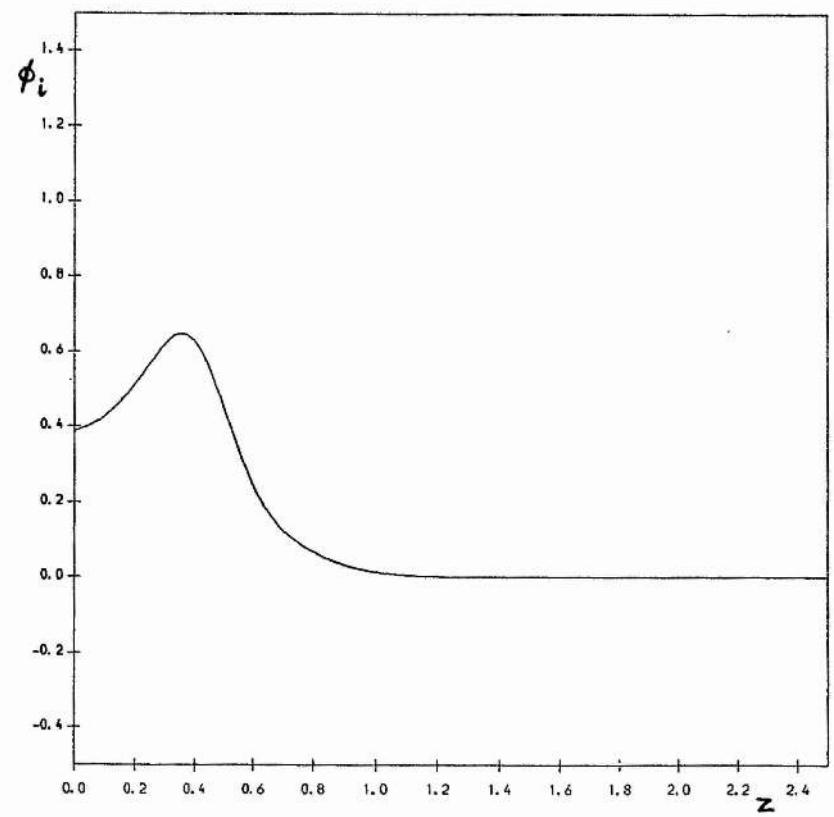

Figure 4.11 α = 0.6: other parameters as Figure 4.10. F mode.

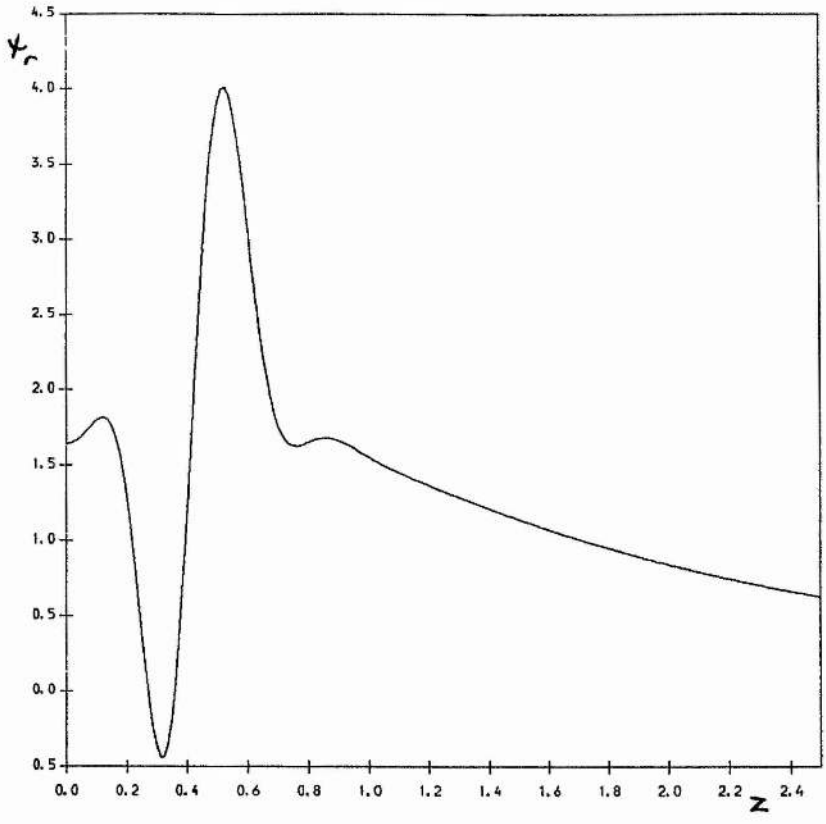

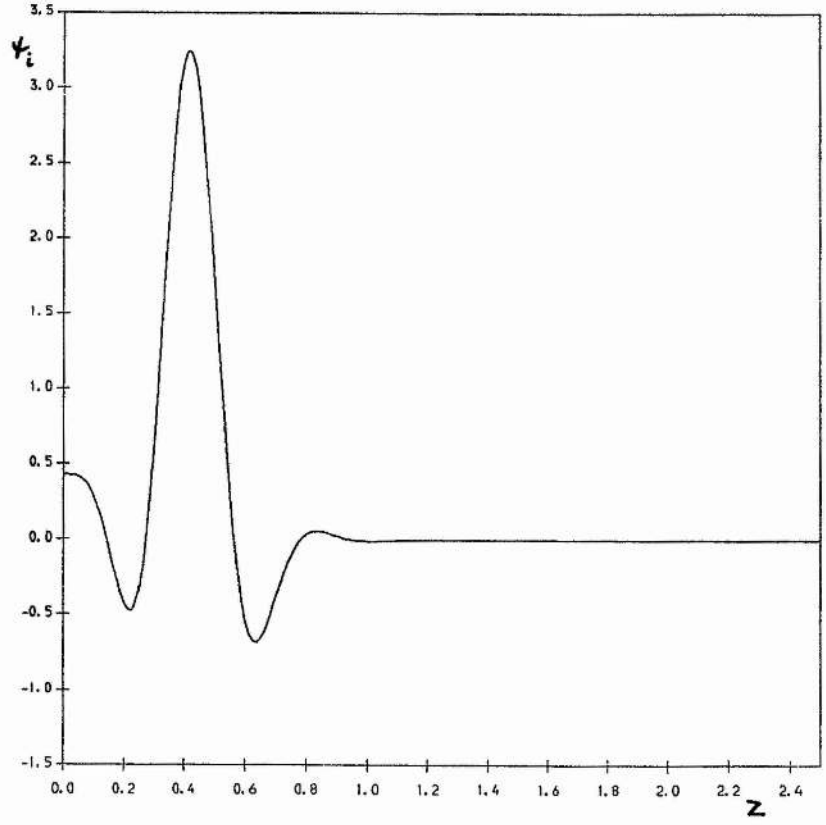

Figure 4.11 (contd.) Adjoint eigenfunction.

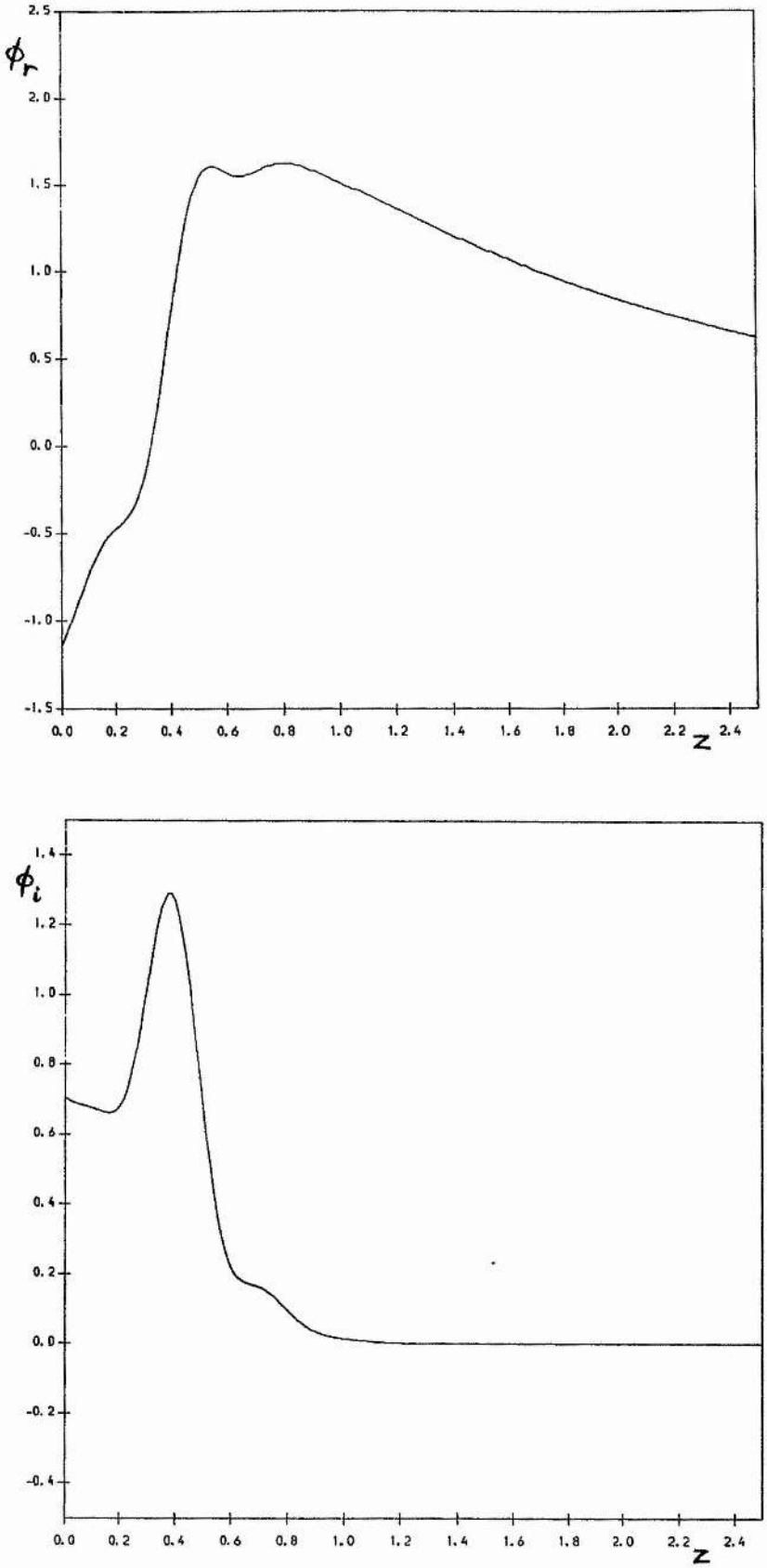

Figure 4.12 As Figure 4.11. Higher-order fluid mode.

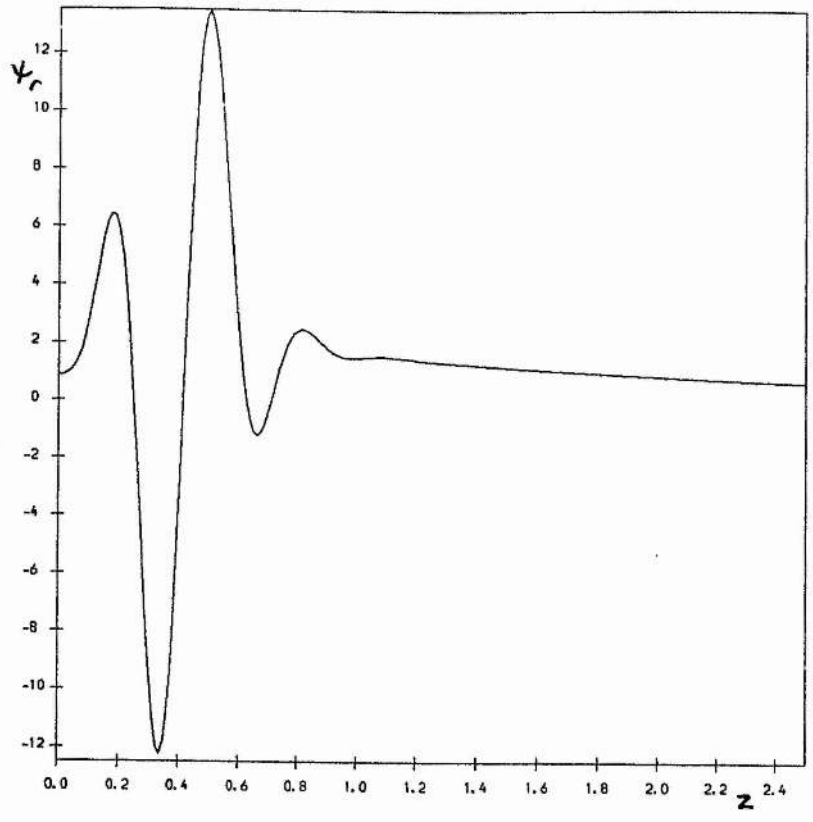

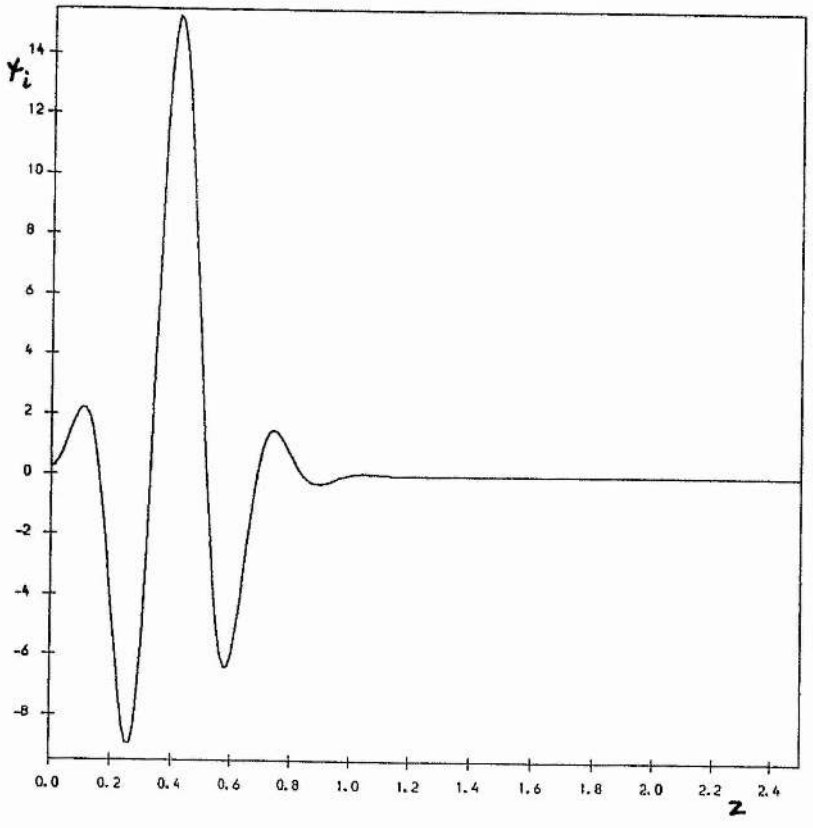

Figure 4.12 (contd.) Adjoint eigenfunction.

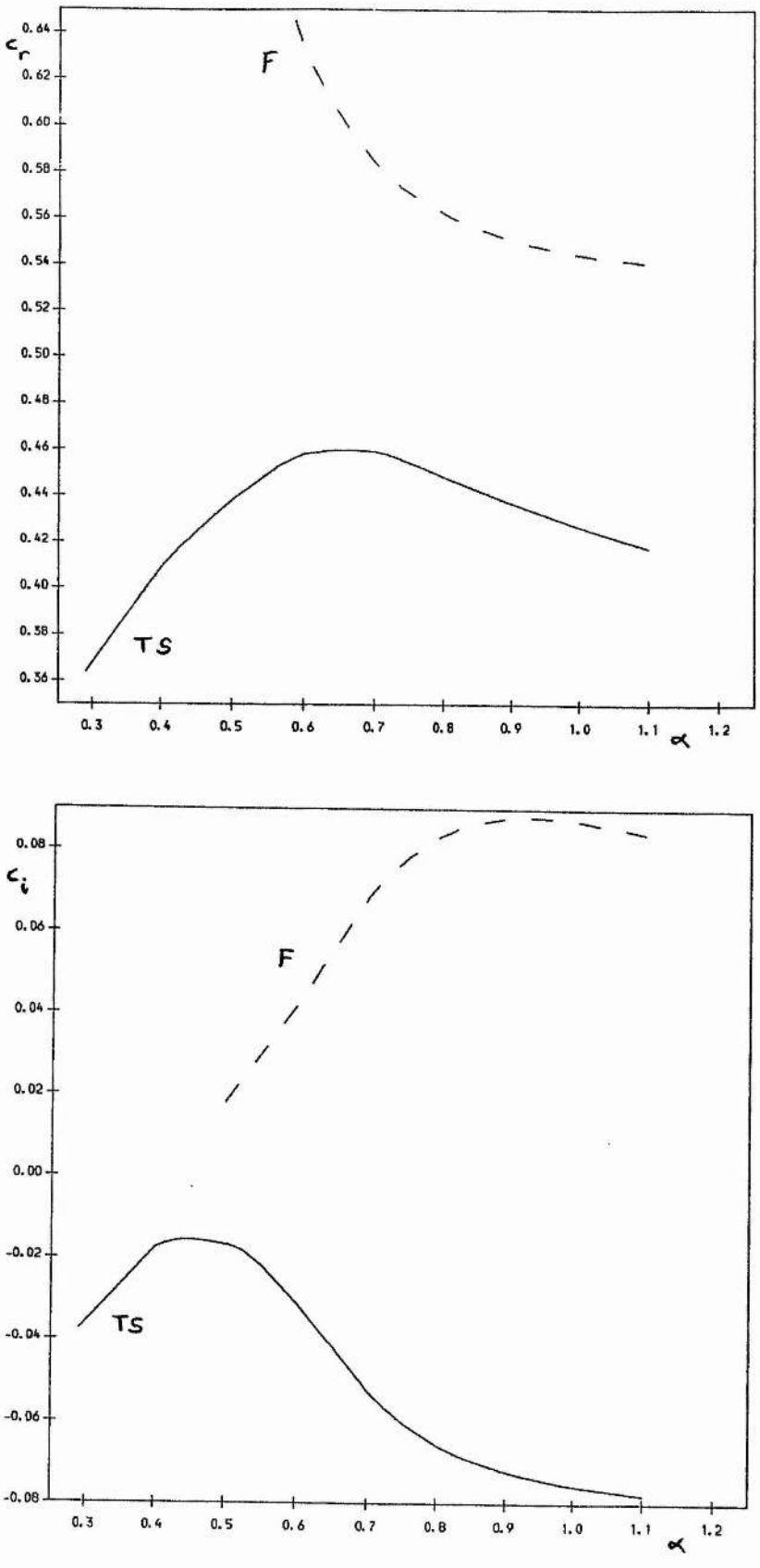

Figure 4.13 As Figure 4.10, but $d = 0$.

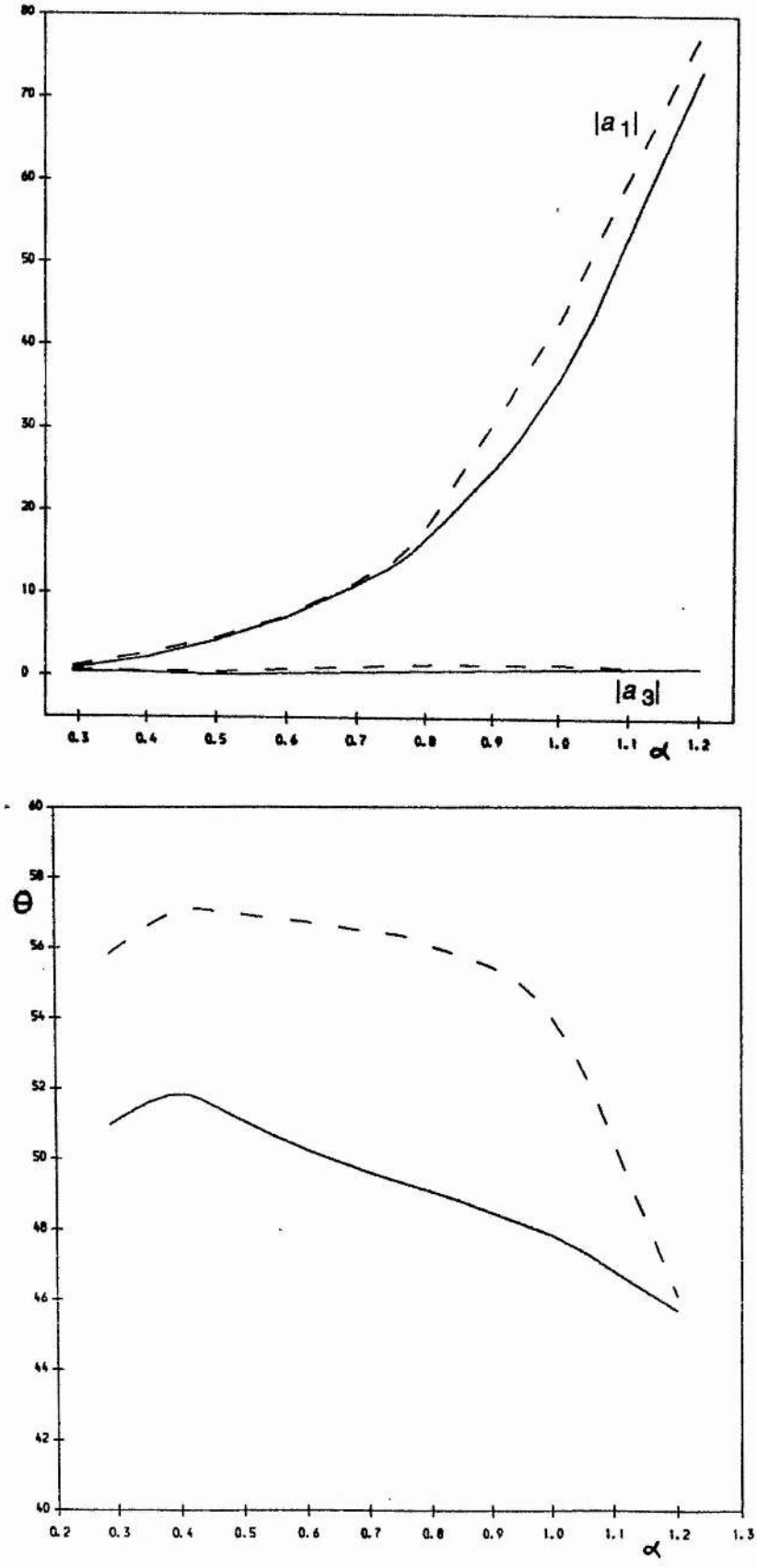

Figure 4.14 Quadratic interaction coefficients $|a_1|$, $|a_3|$ and oblique wave propagation angle θ (in degrees) versus wavenumber α : $m = 2$, $c_0 = 0.5$, $d = 0$, $S = 1$, $R = R_0 = 2562.8$. Triads comprise three TS modes. ——— , rigid wall; – – – , flexible wall.

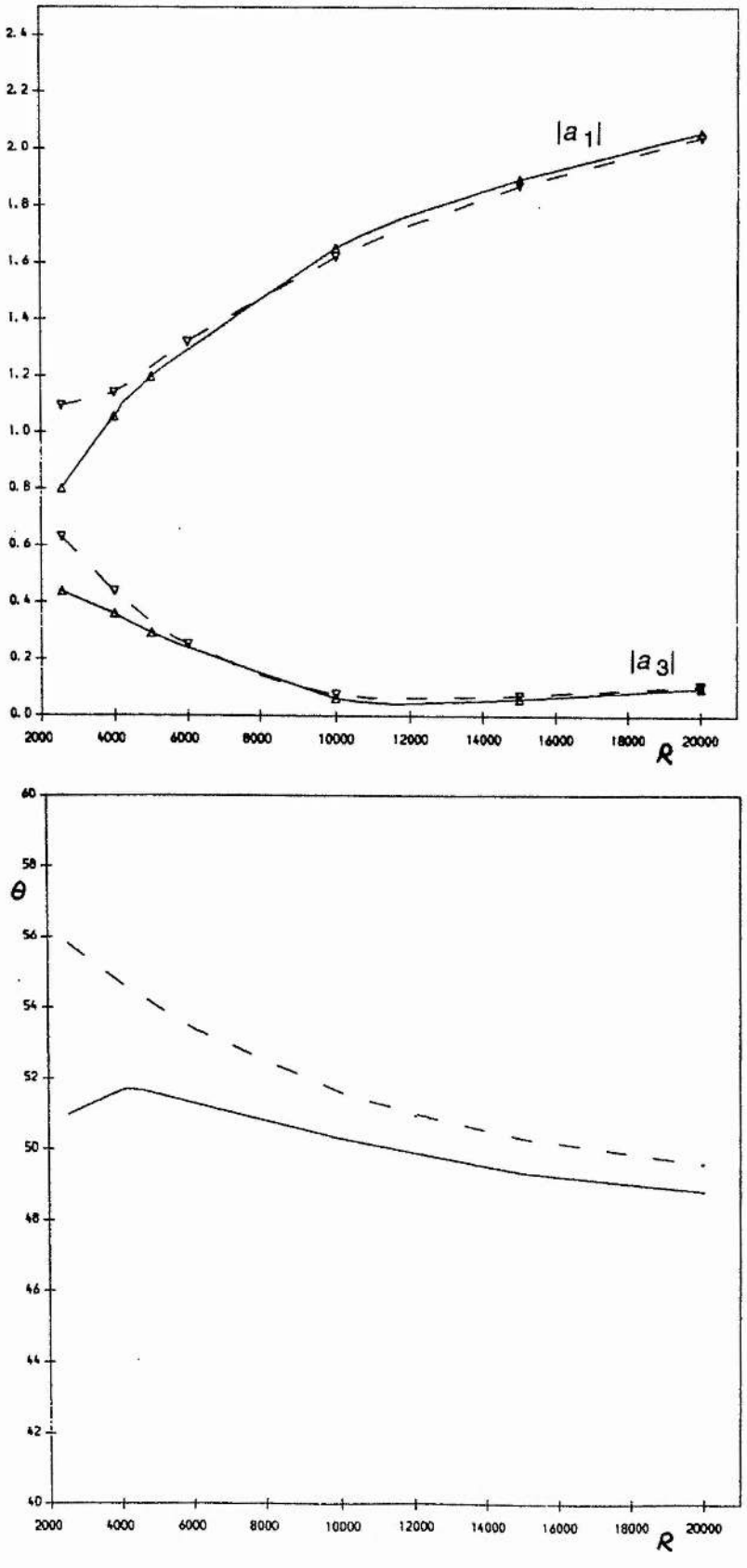

Figure 4.15 Quadratic interaction coefficients $|a_1|$, $|a_3|$ and oblique wave propagation angle θ (in degrees) versus Reynolds number R : $\alpha = 0.29056$, $R_0 = 2562.8$; wall parameters as Figure 4.14. Triads comprise three TS modes. ——, rigid wall; – – –, flexible wall.

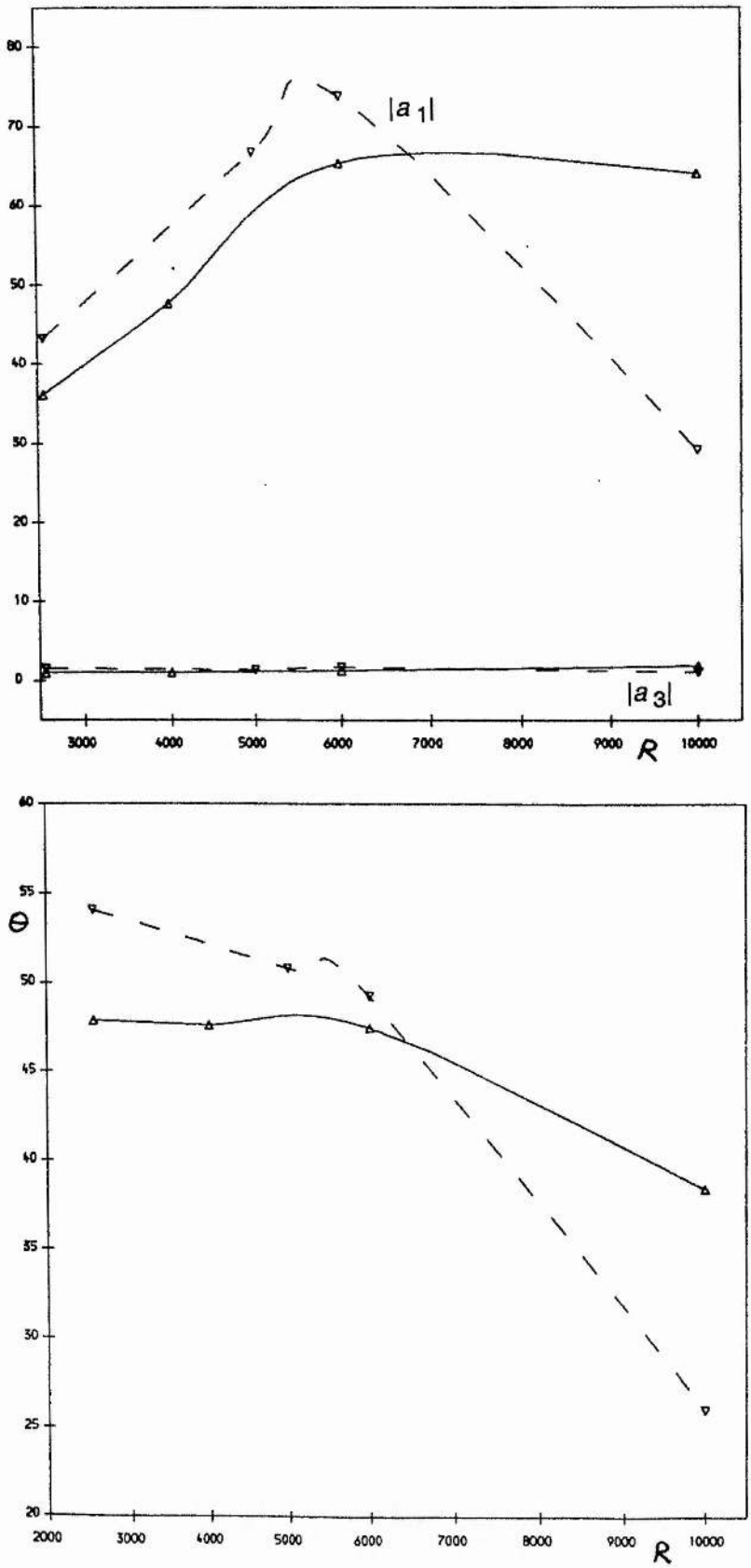

Figure 4.16 Quadratic interaction coefficients $|a_1|$, $|a_3|$ and oblique wave propagation angle θ (in degrees) versus Reynolds number R: $\alpha = 1.0$; other parameters as Figure 4.15. Triads comprise three TS modes. ——, rigid wall; – – –, flexible wall.

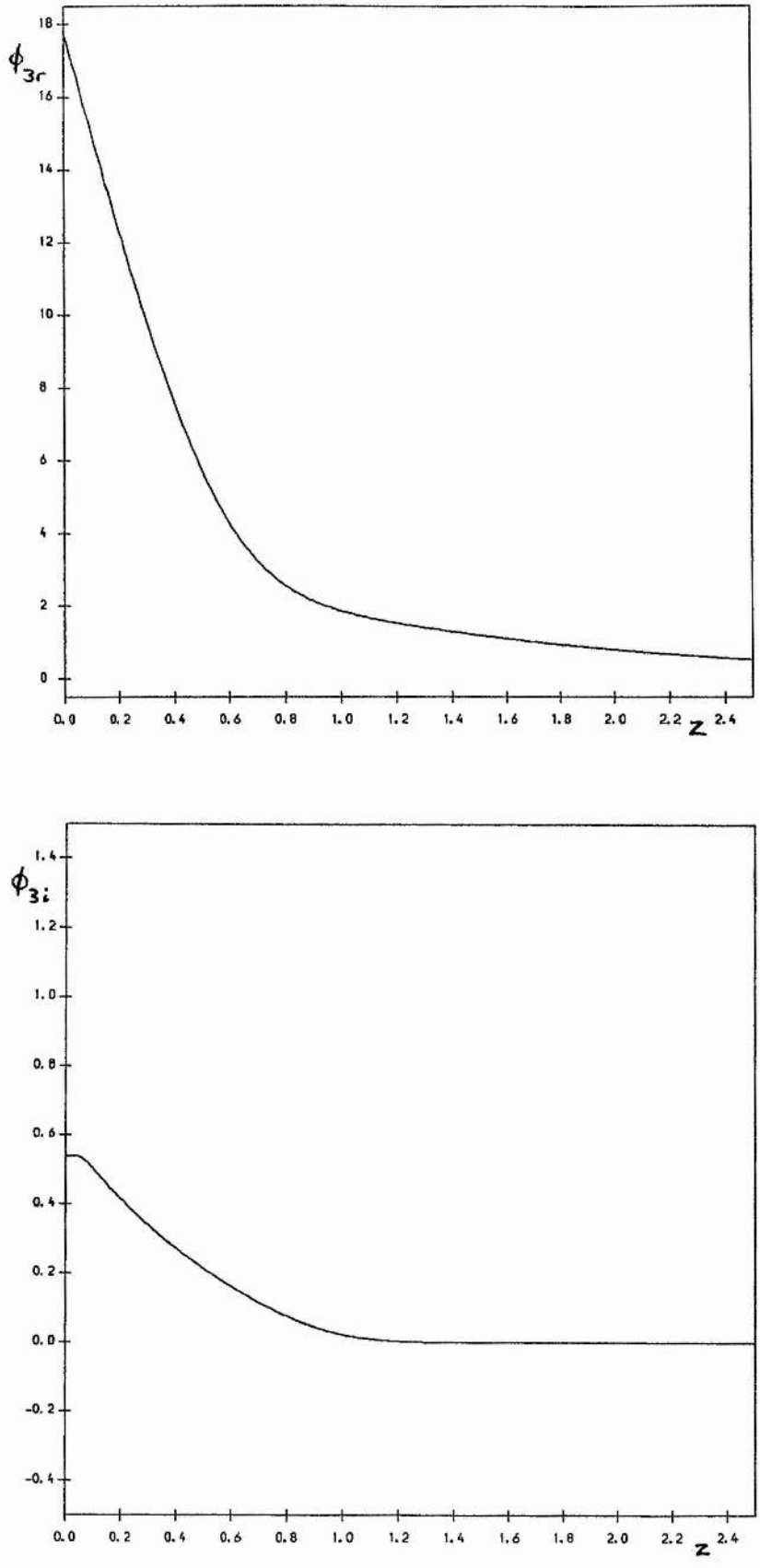

Figure 4.17 Triad comprising three wall modes: $\alpha = 0.8$, $R = R_0 = 2562.8$, $m = 2$, $c_0 = 1.2$, $d = 0$, $S = 0.1$.

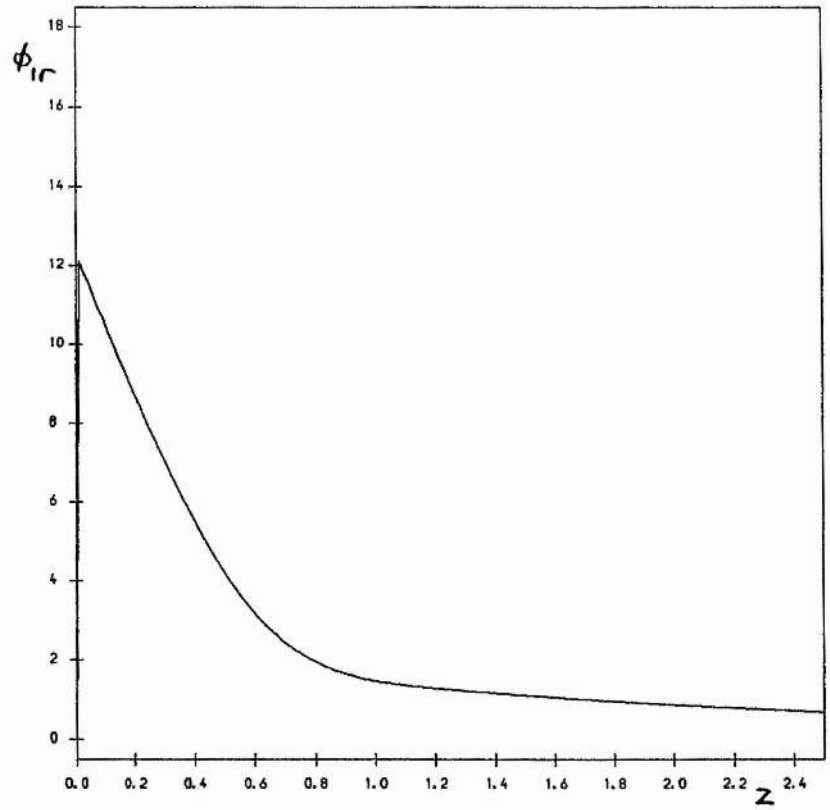

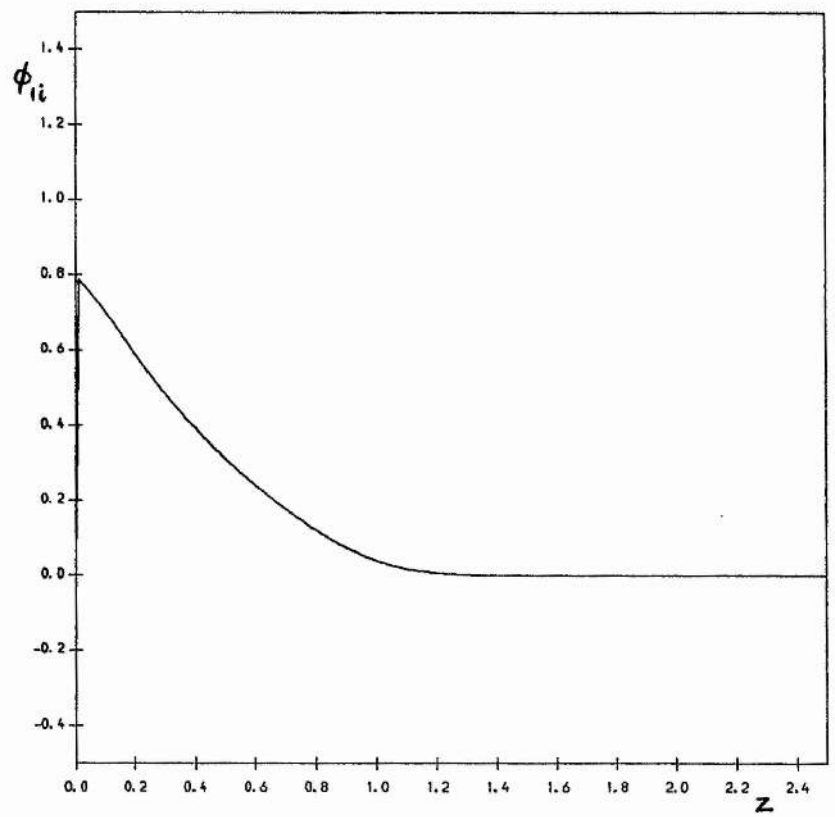

Figure 4.17 (contd.) Oblique eigenfunction.

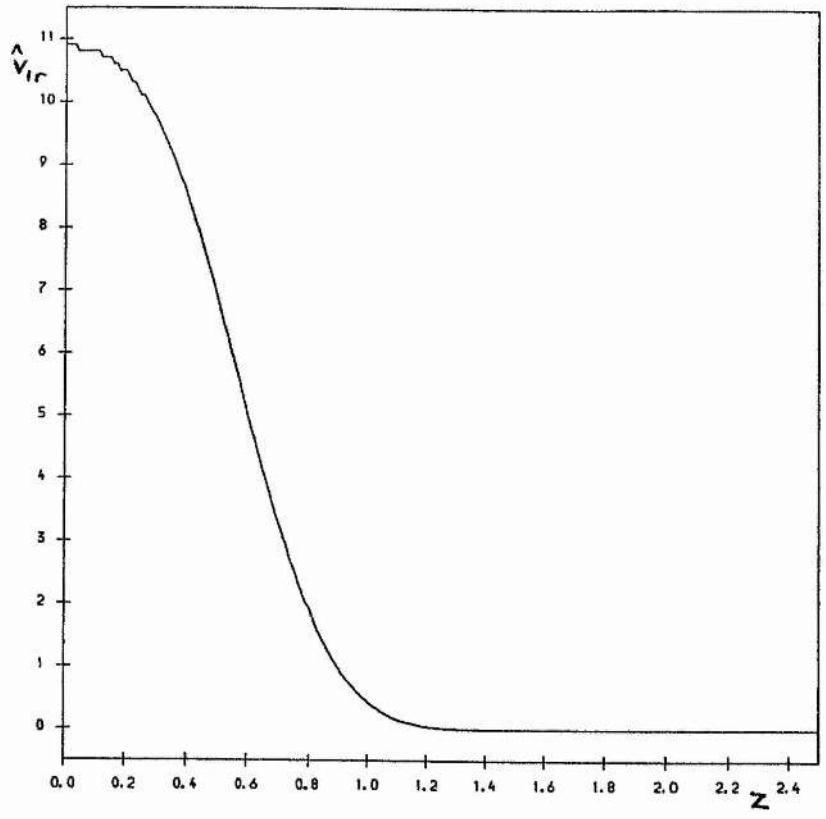

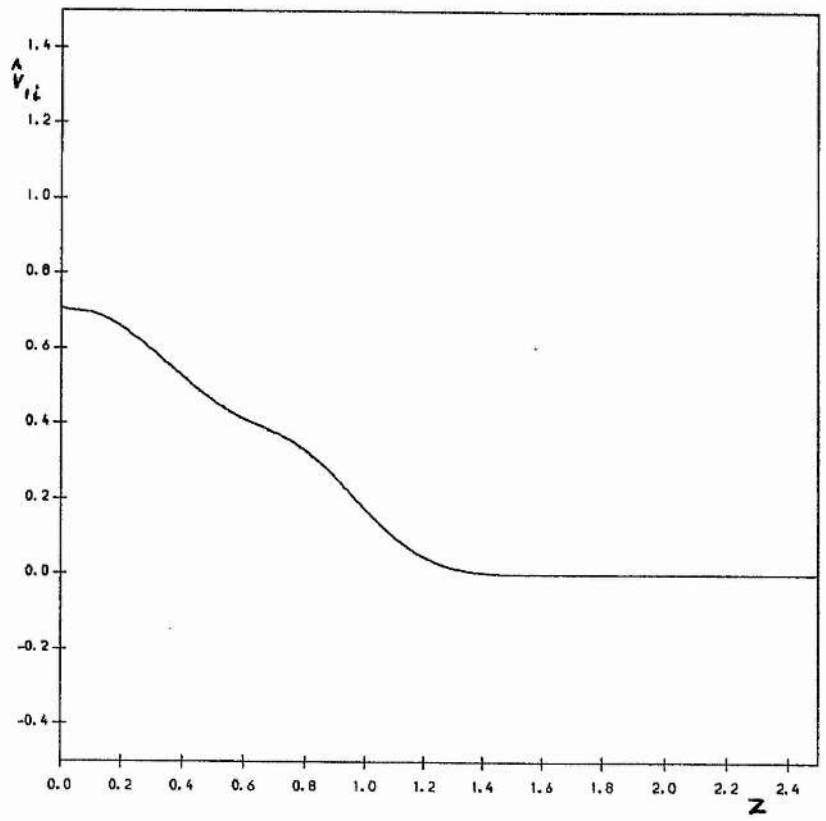

Figure 4.17 (contd.) Cross-flow velocity.

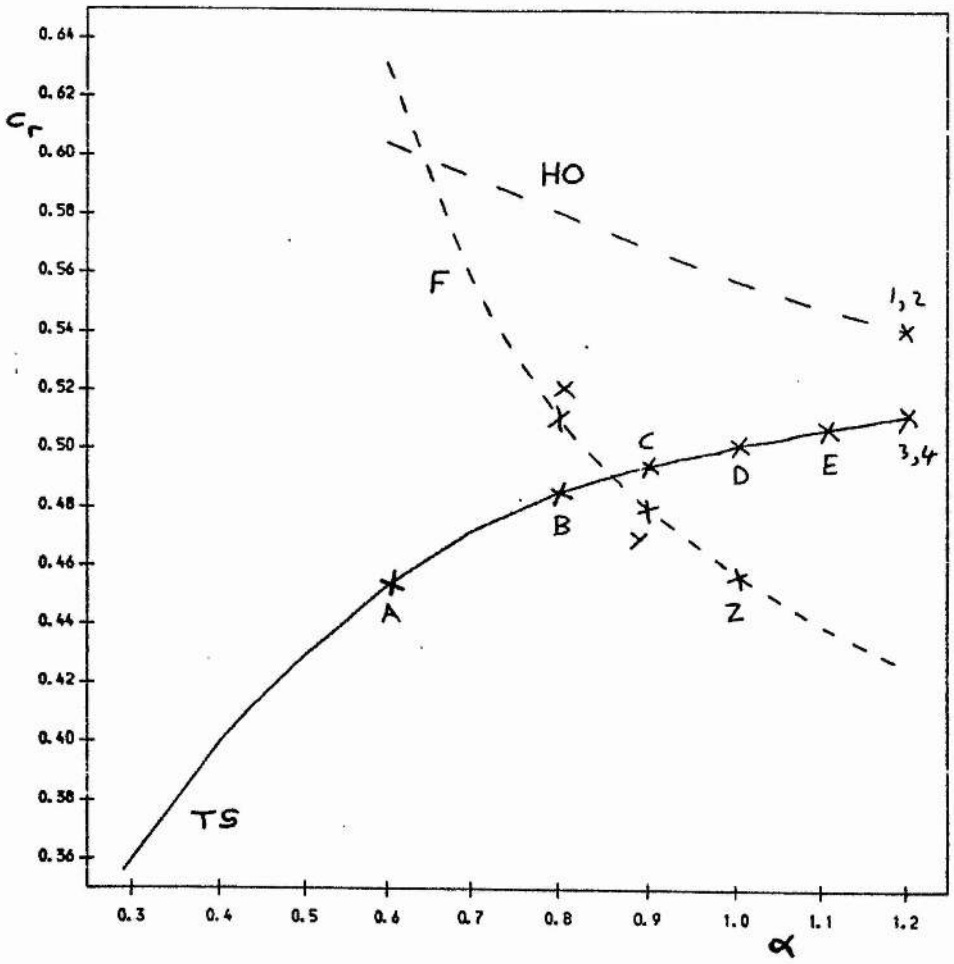

Figure 4.18 As Figure 4.10: marked points are the locations of streamwise constituents of resonant triads.

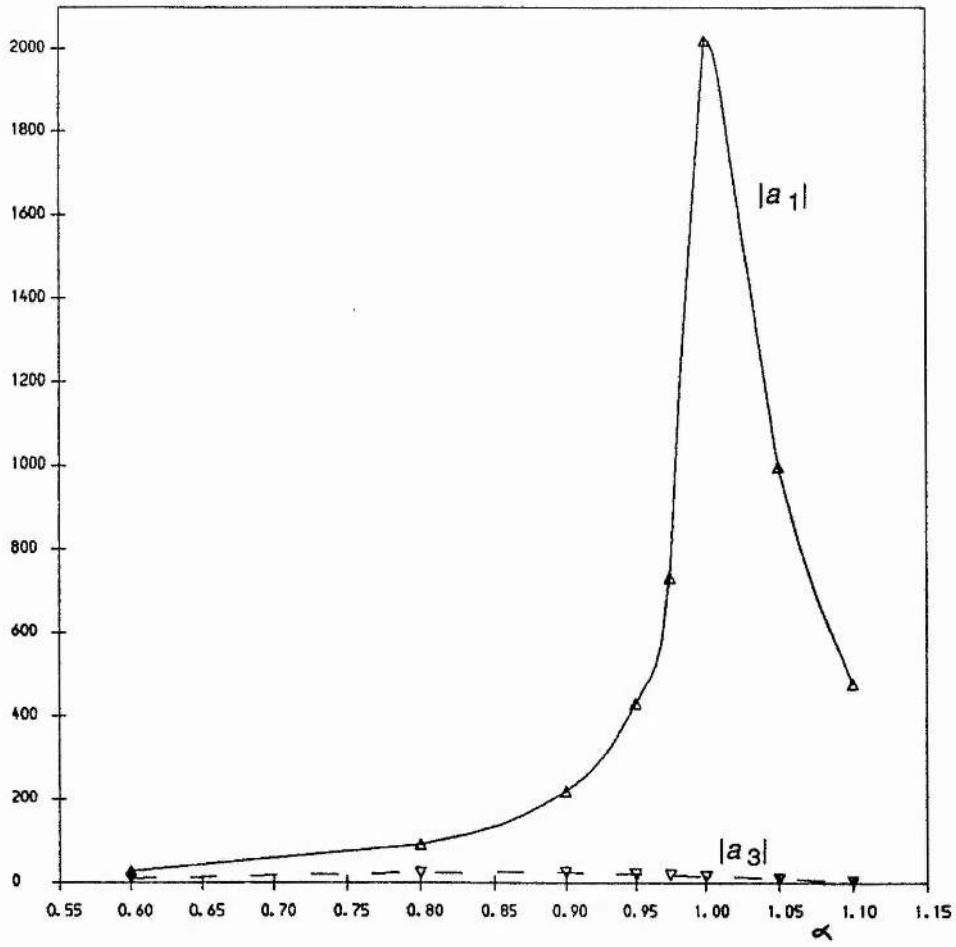

Figure 4.19 Quadratic interaction coefficients $|a_1|$, $|a_3|$ versus wavenumber α : parameters as Figure 4.10. Triads comprise three TS modes, linearly interacting with wall modes.

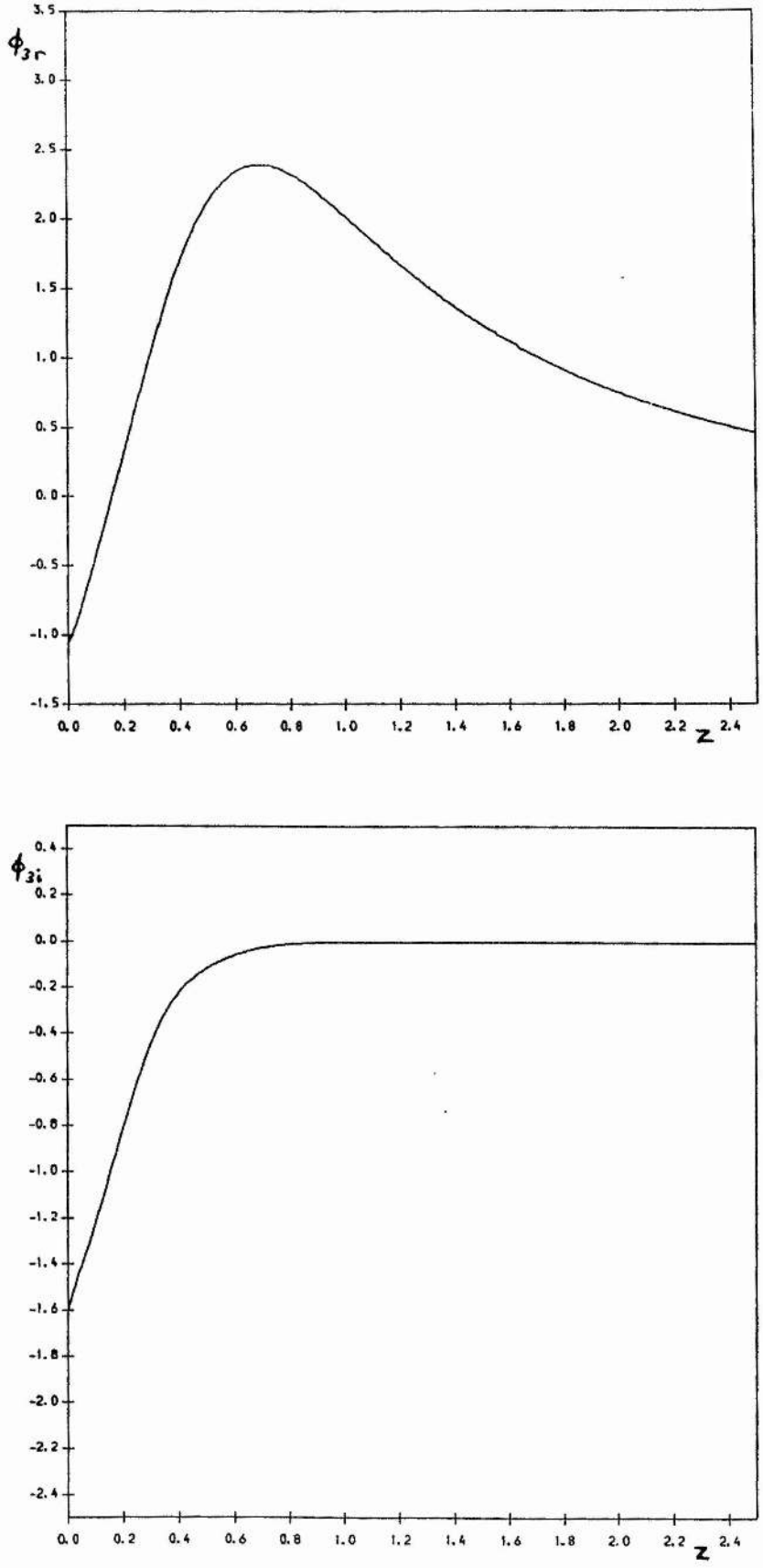

Figure 4.20 α = 1.0, other parameters as Figure 4.10; triad is located at spike of Figure 4.19.

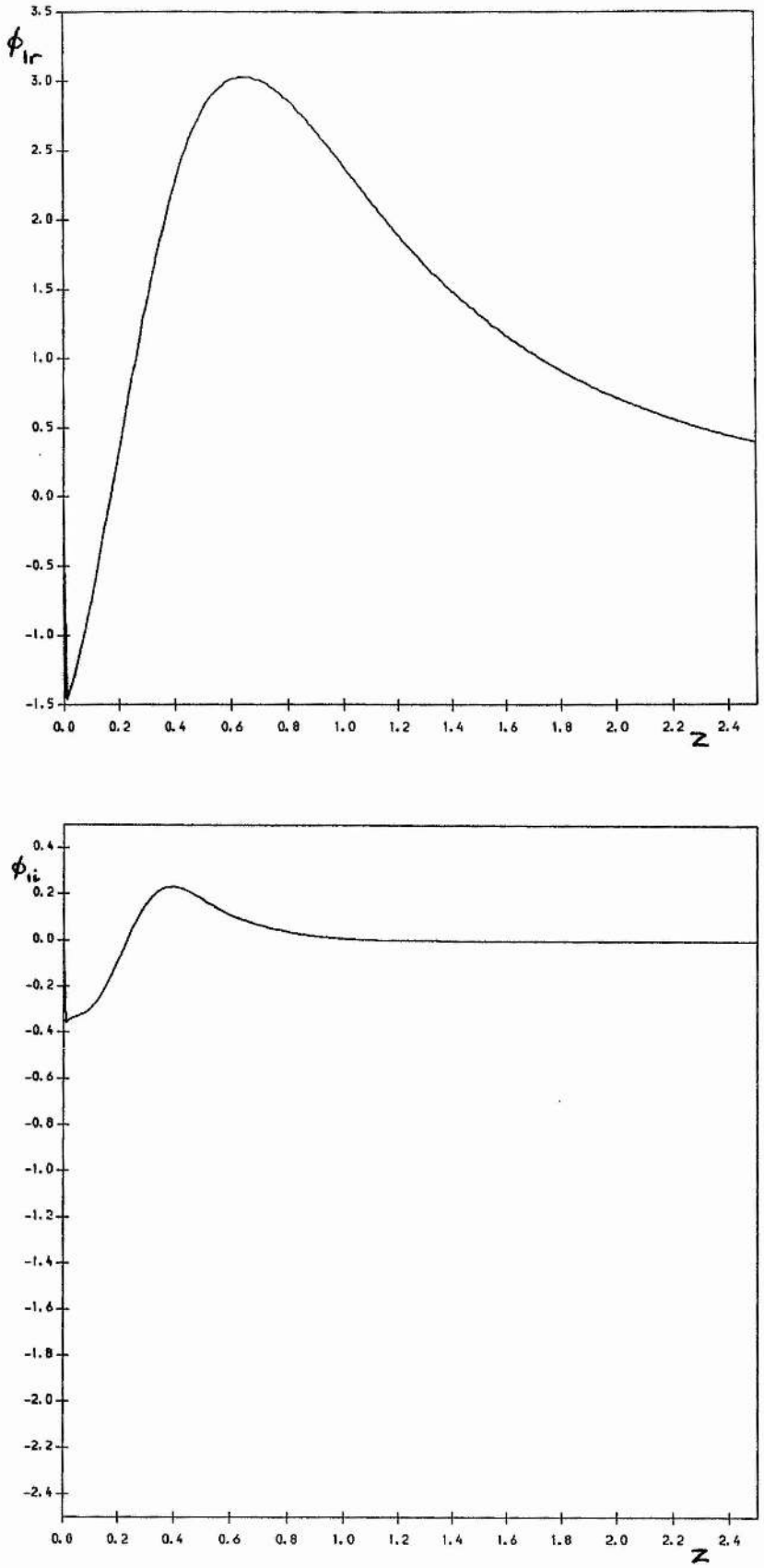

Figure 4.20 (contd.) Oblique eigenfunction.

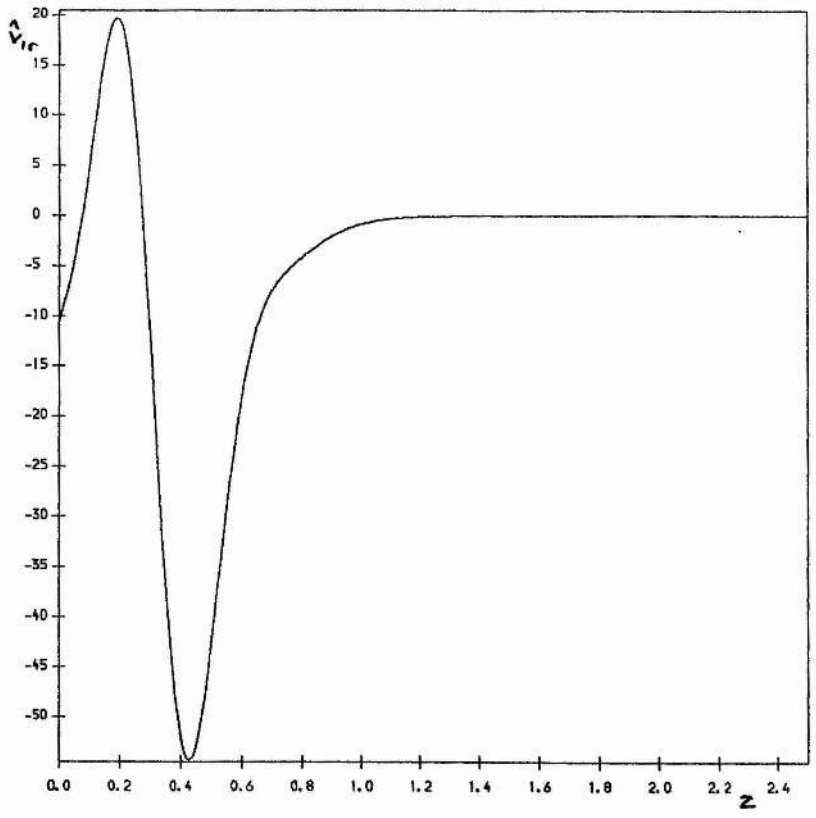

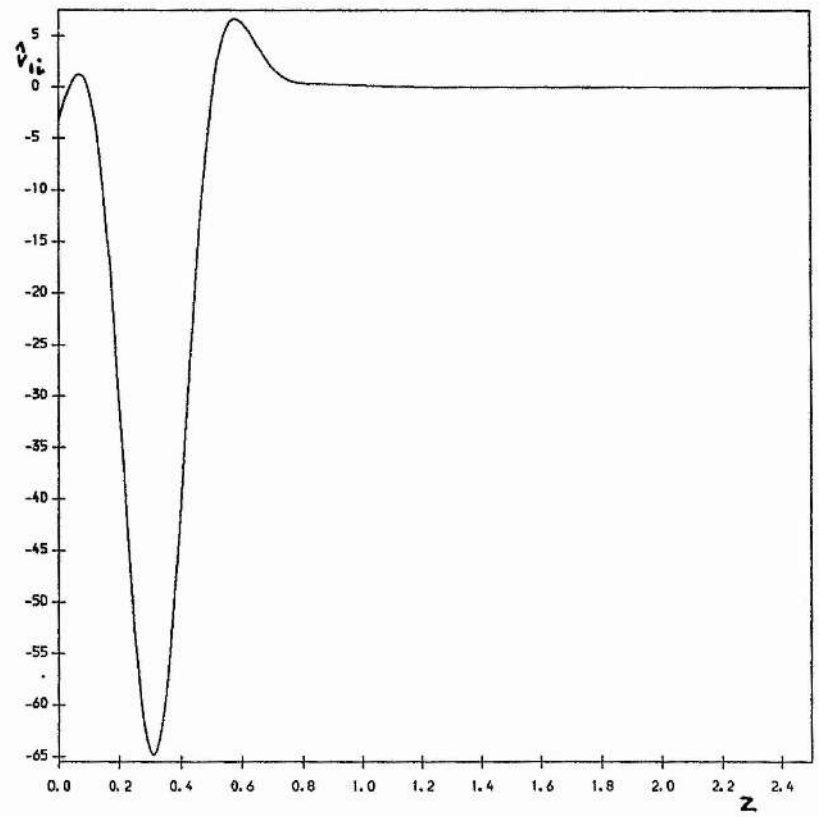

Figure 4.20 (contd.) Cross-flow velocity.

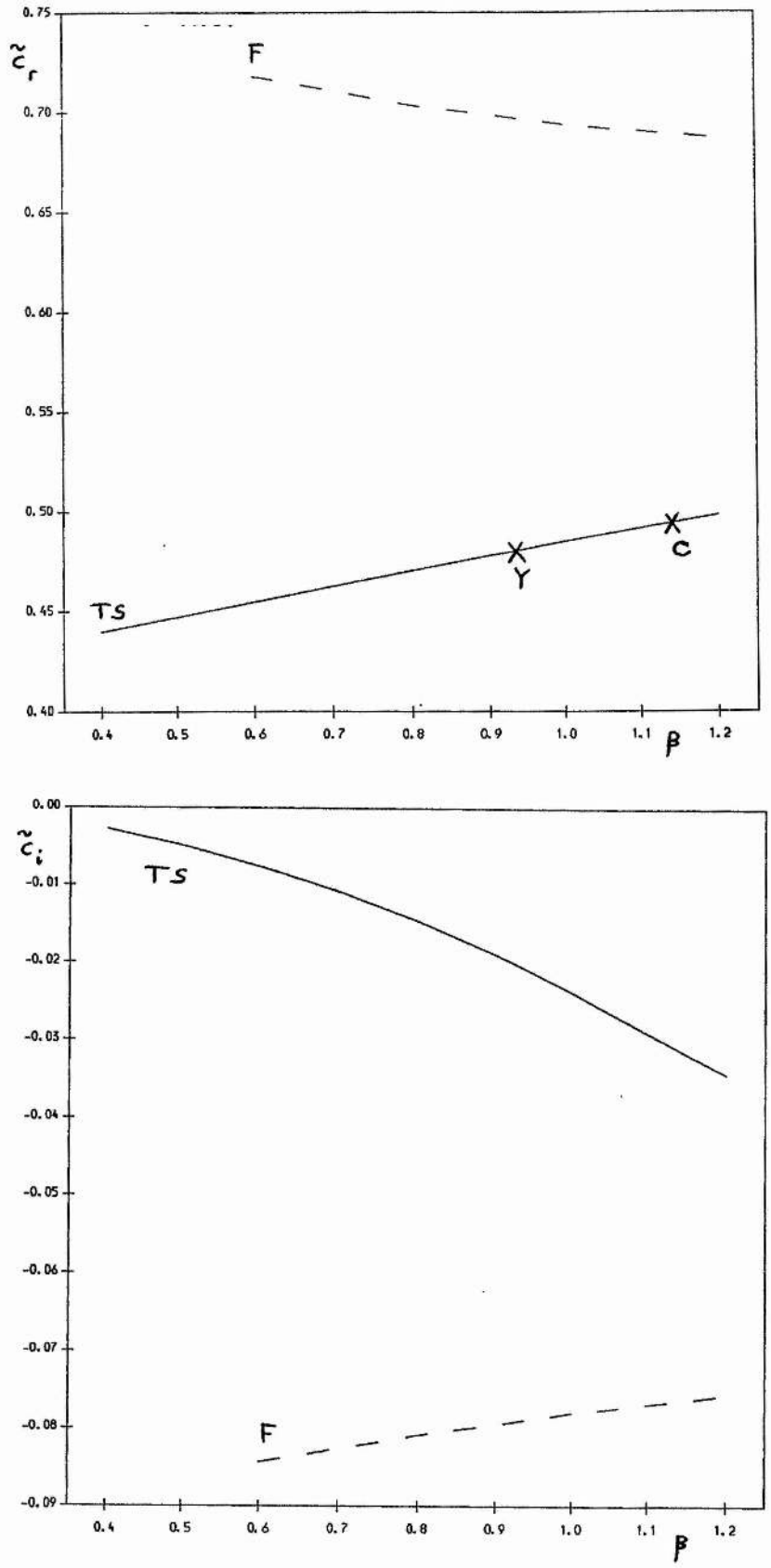

Figure 4.21 Eigenvalue variation of oblique triad constituent with transverse wavenumber β : parameters as Figure 4.10, except $\alpha = 0.9$.

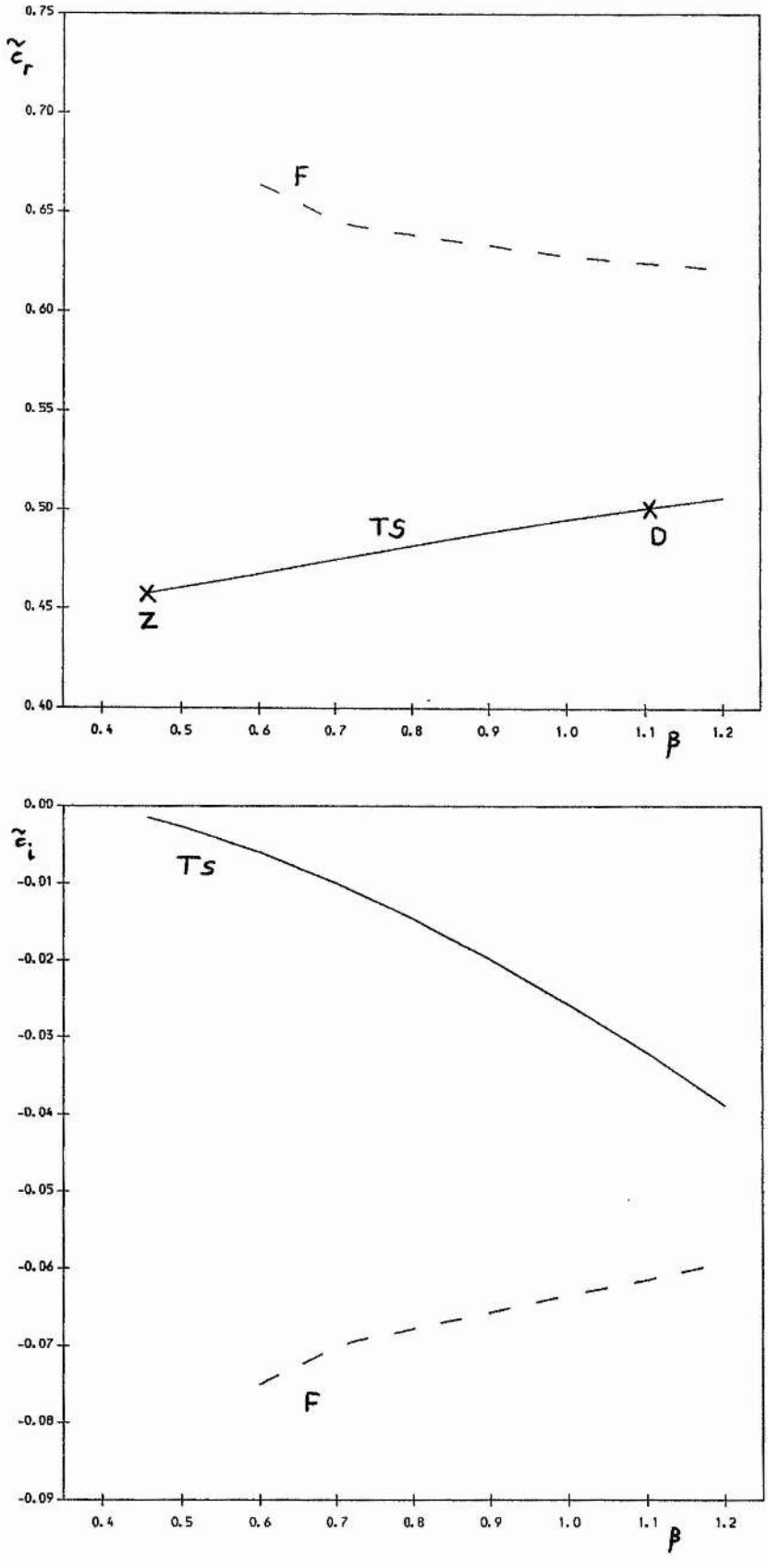

Figure 4.22 As Figure 4.21, except $\alpha = 1.0$.

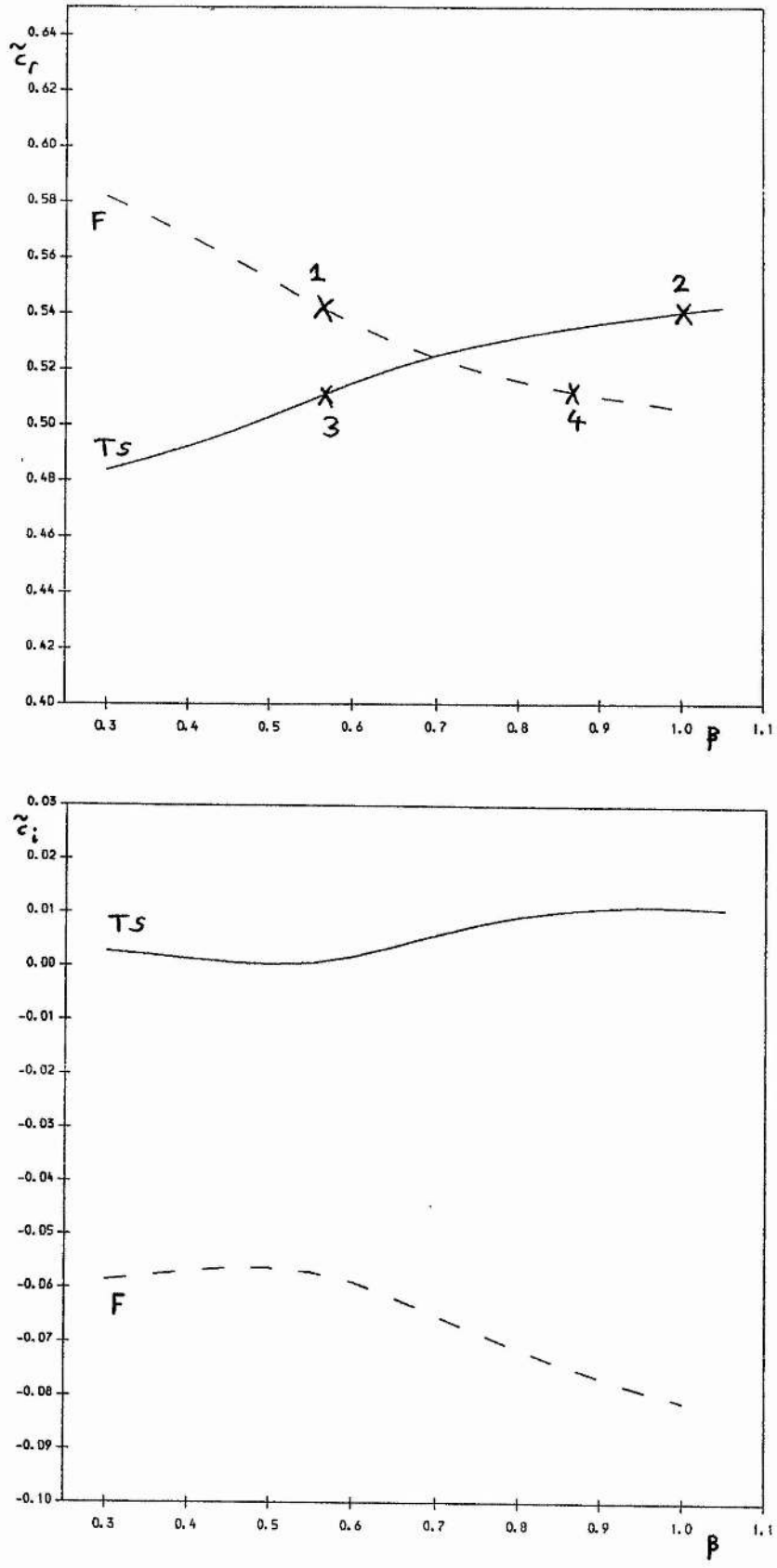

Figure 4.23 As Figure 4.21, except $\alpha = 1.2$.

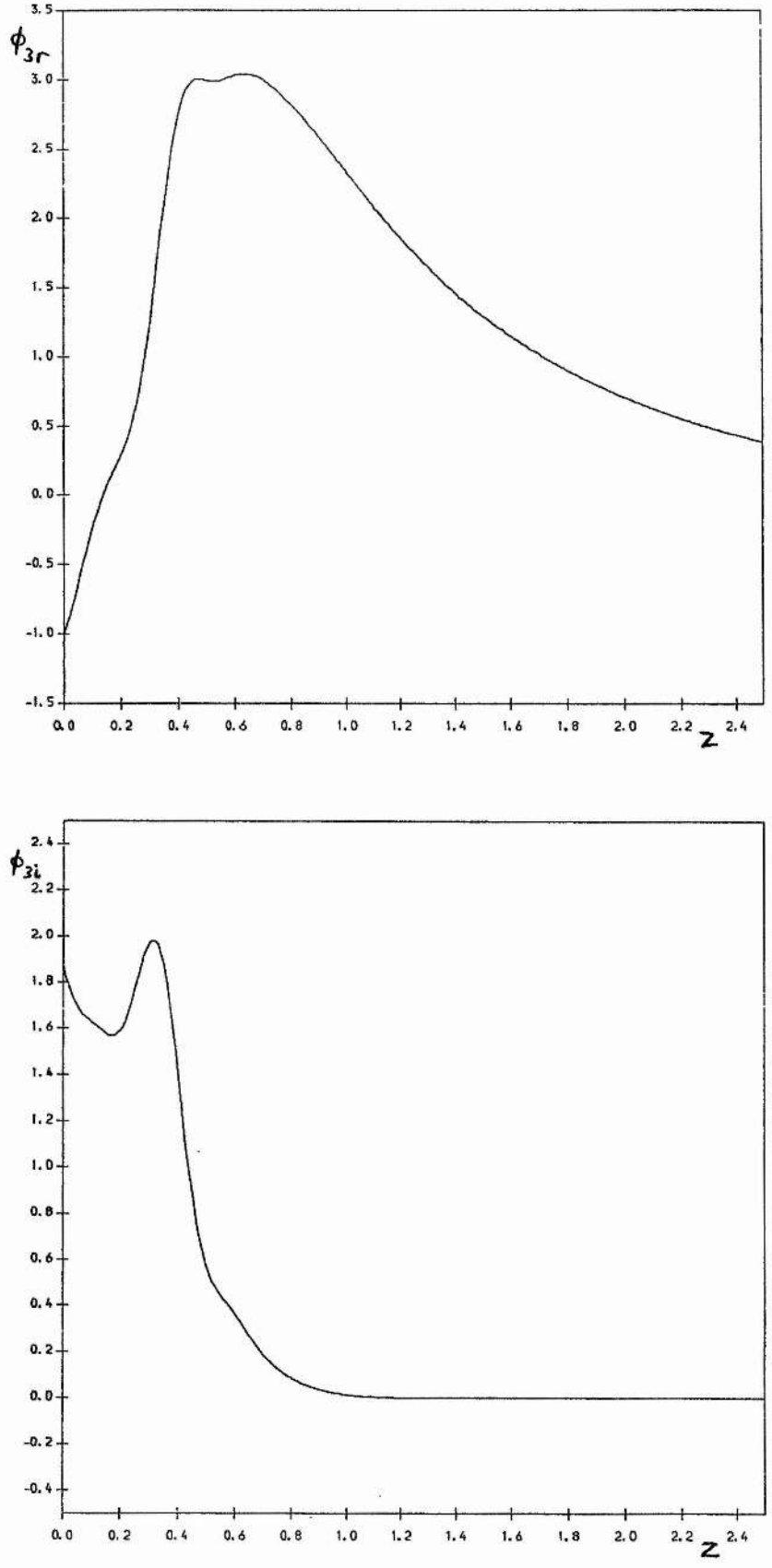

Figure 4.24 Eigenfunctions, etc. for triad at point 1 of Figure 4.18.

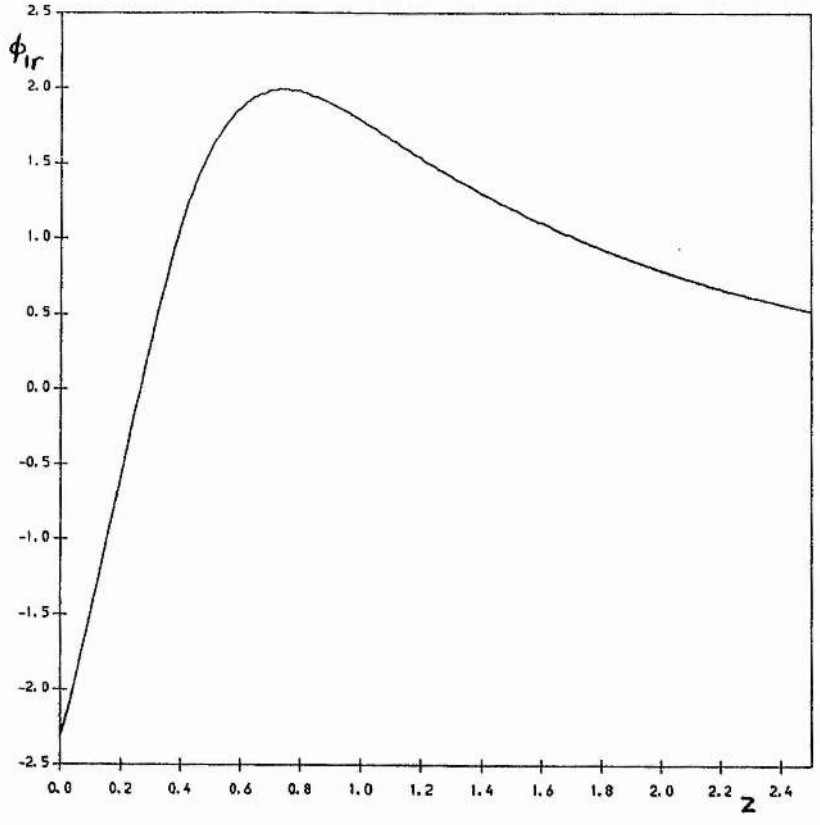

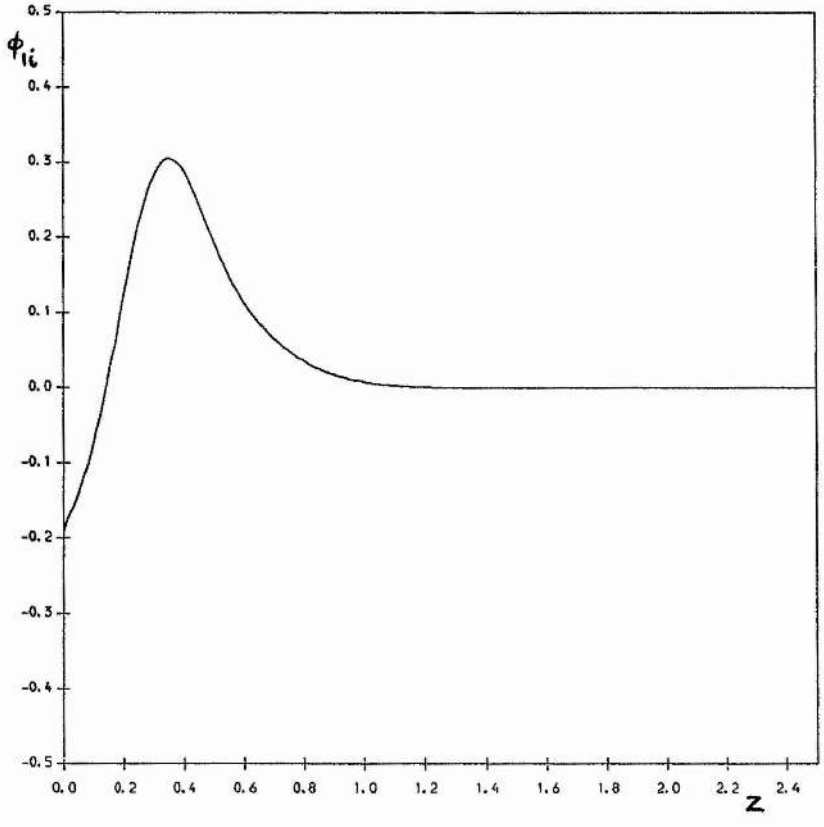

Figure 4.24 (contd.) Oblique eigenfunction.

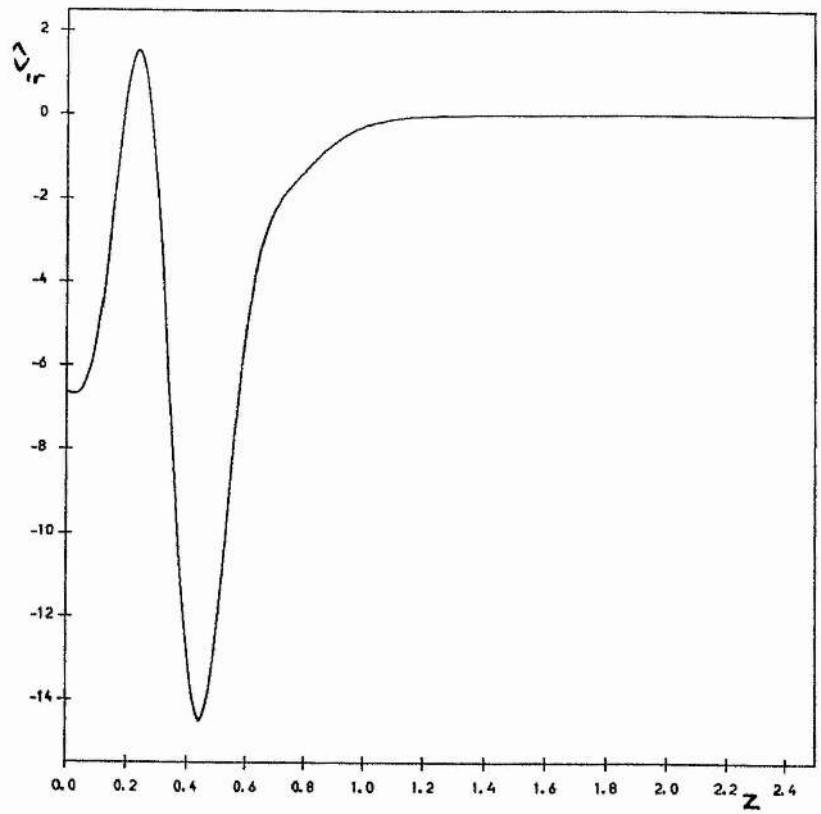

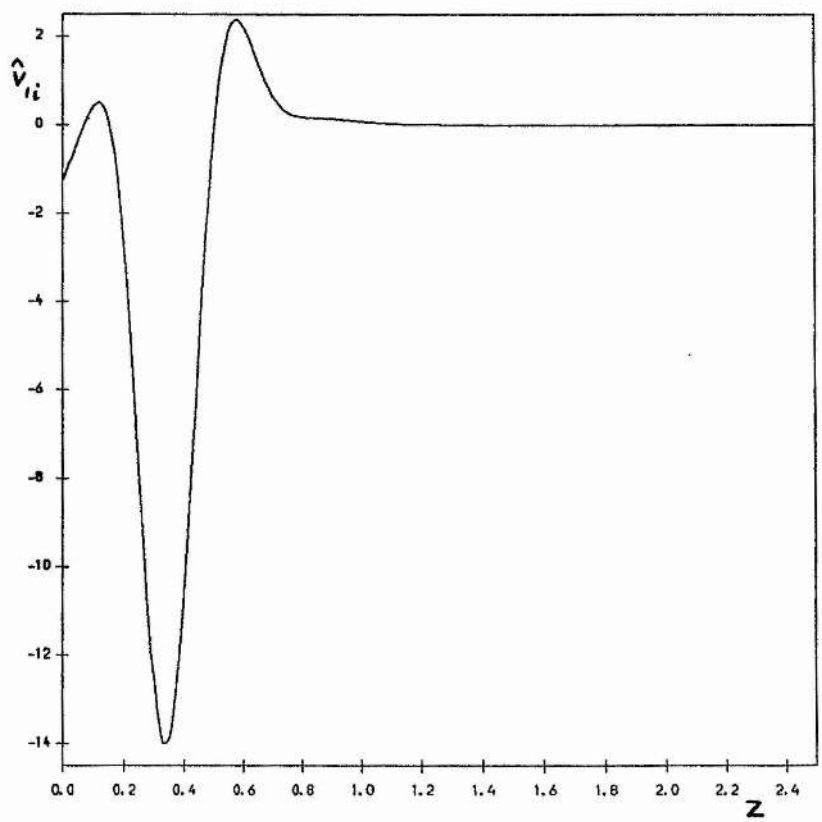

Figure 4.24 (contd.) Cross-flow velocity.

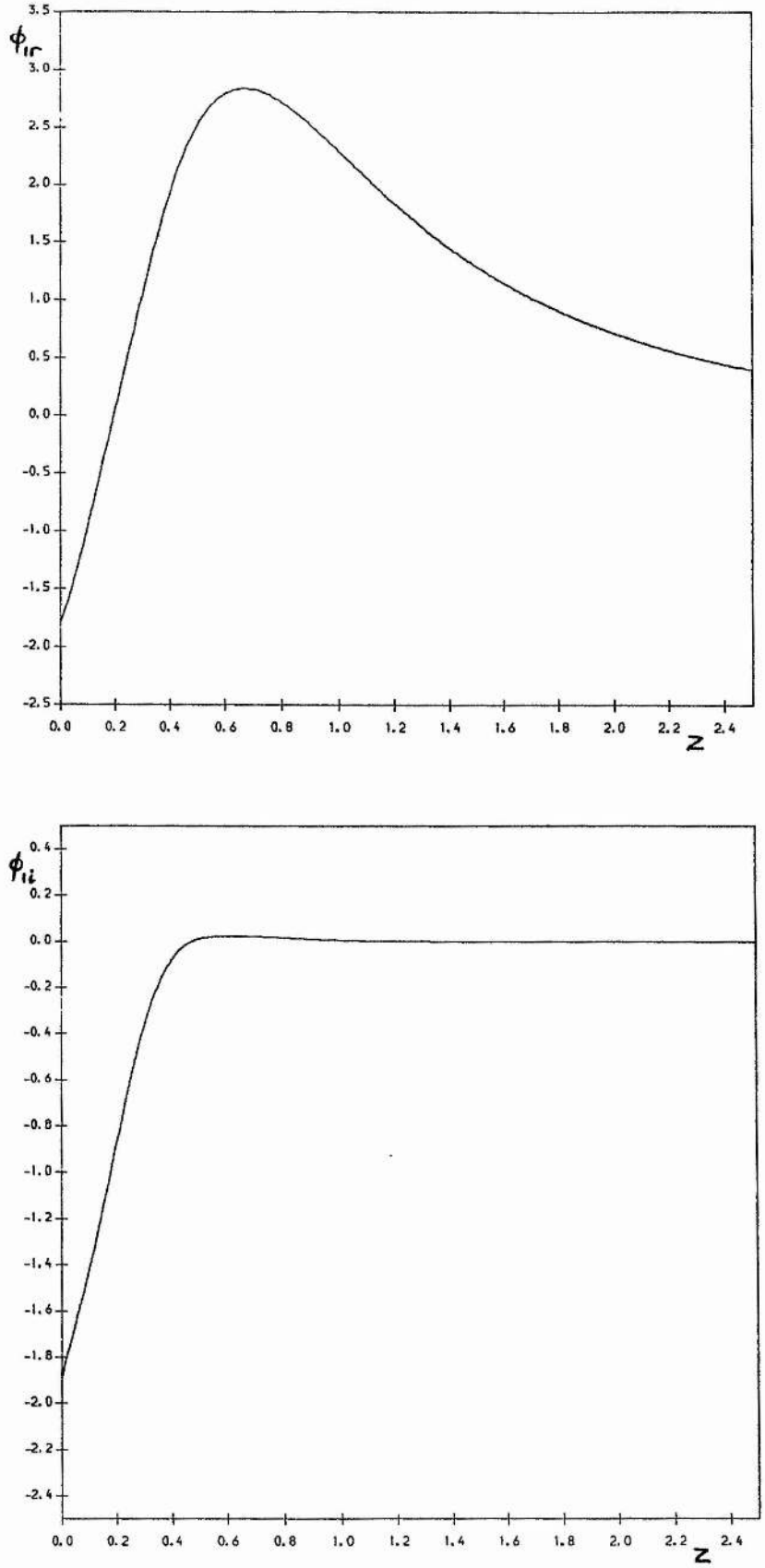

Figure 4.25 Oblique eigenfunctions, etc. for triad at point 2 of Figure 4.18: ϕ_3, ψ_3 as Figure 4.24.

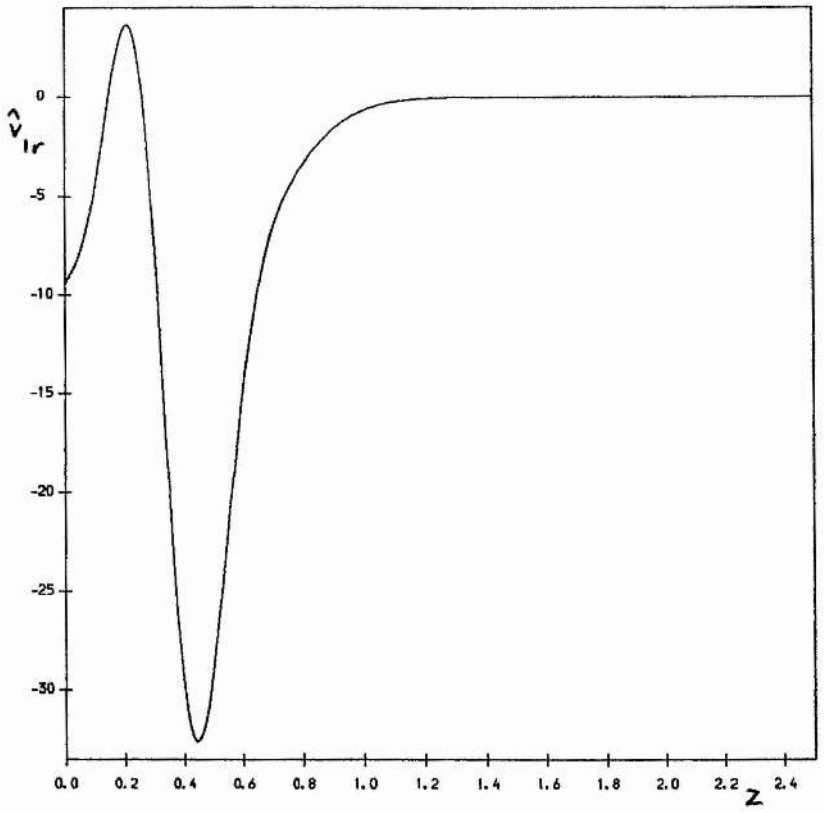

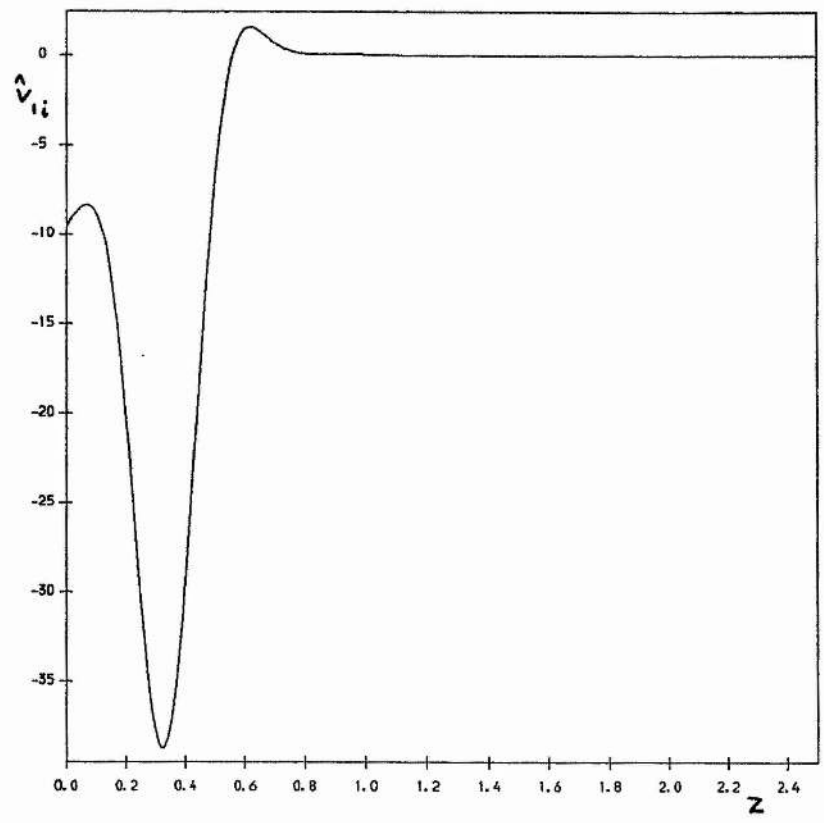

Figure 4.25 (contd.) Cross-flow velocity.

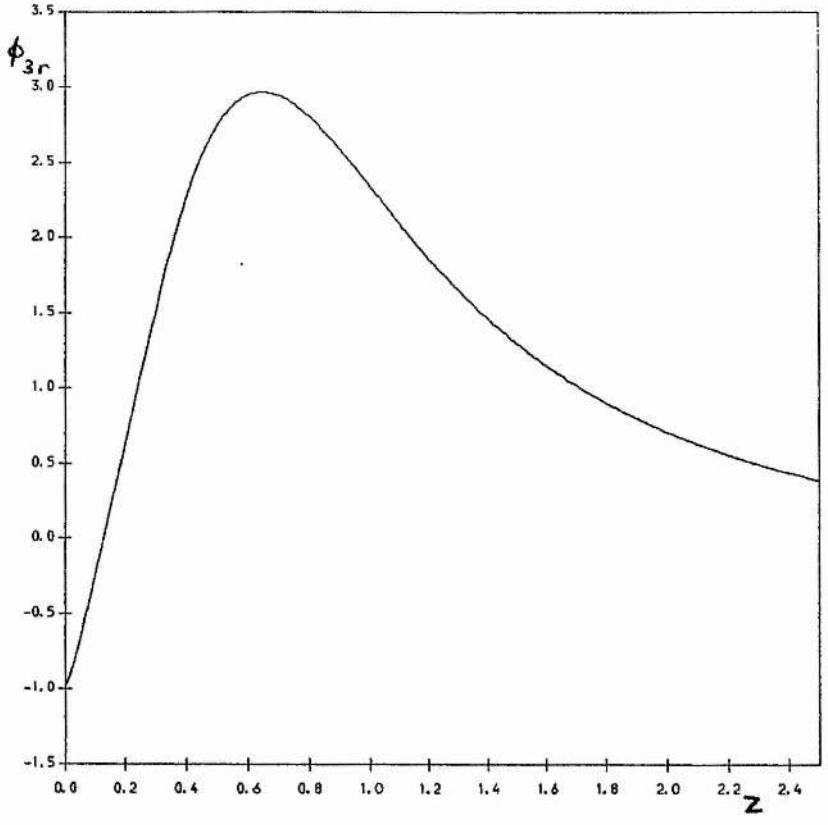

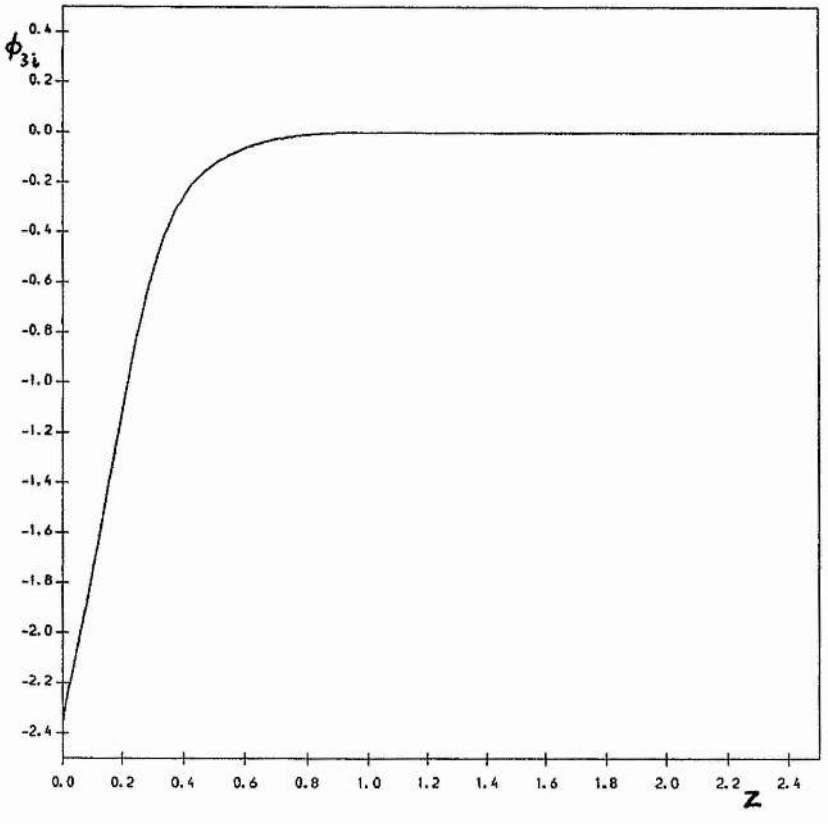

Figure 4.26 Eigenfunctions, etc. for triad at point 3 of Figure 4.18.

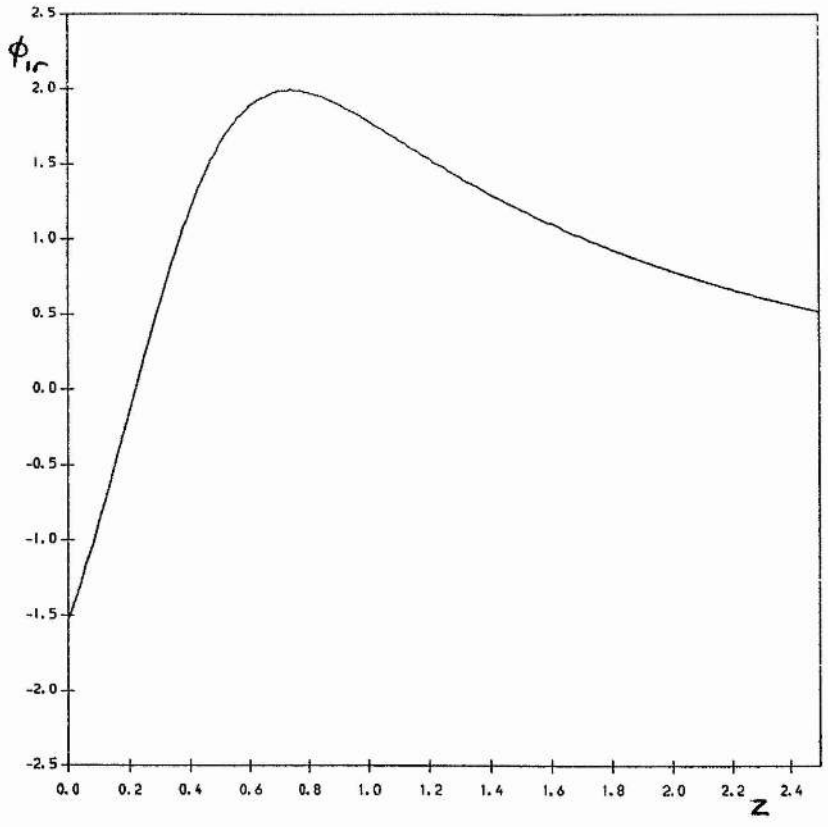

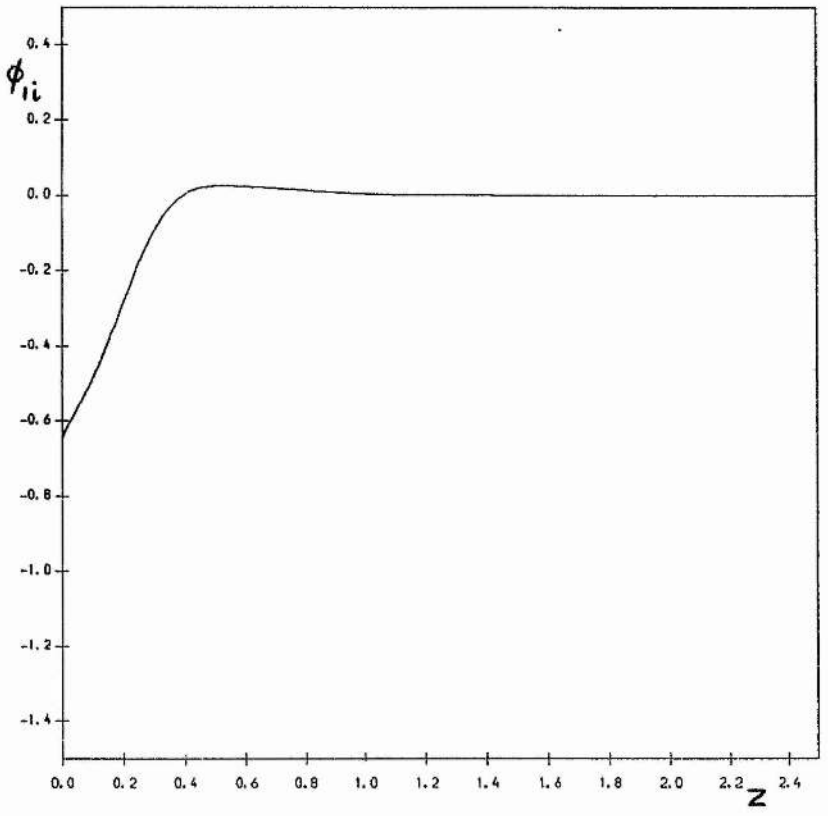

Figure 4.26 (contd.) Oblique eigenfunction.

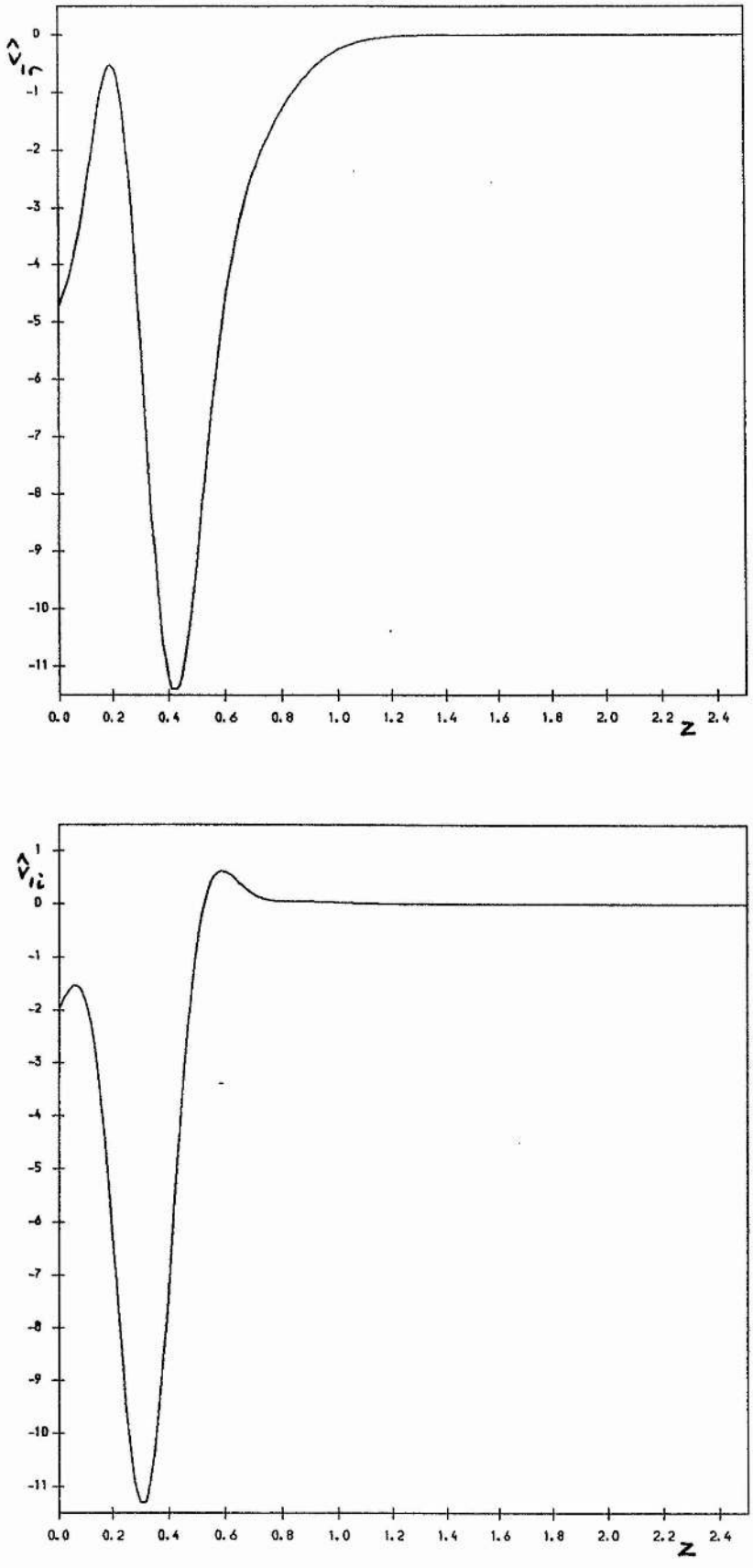

Figure 4.26 (contd.) Cross-flow velocity.

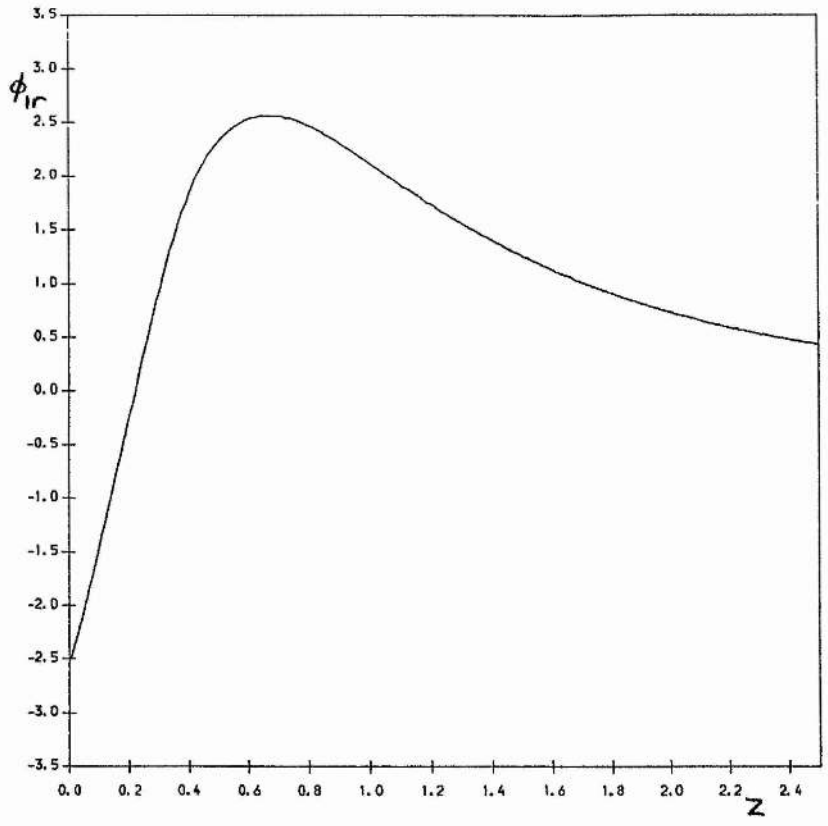

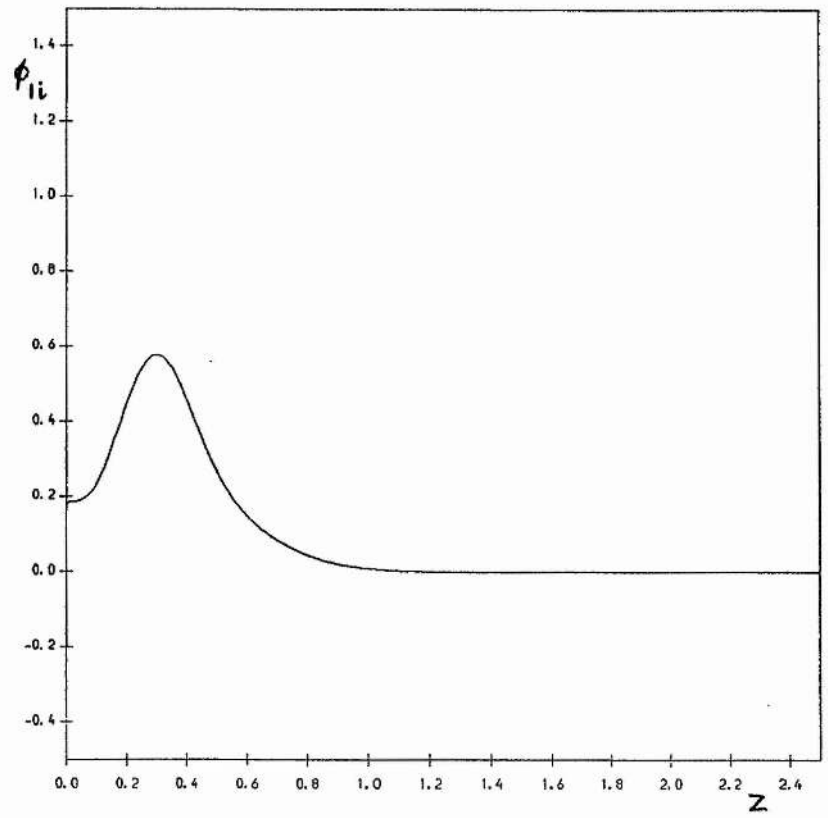

Figure 4.27 Oblique eigenfunctions, etc. for triad at point 4 of Figure 4.18: ϕ_3, ψ_3 as Figure 4.26.

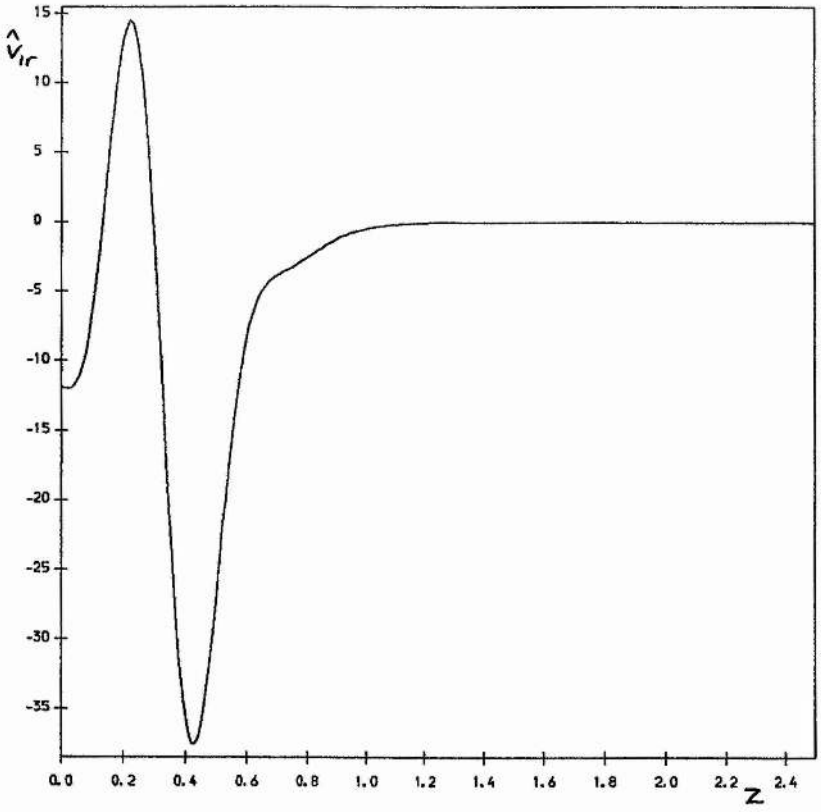

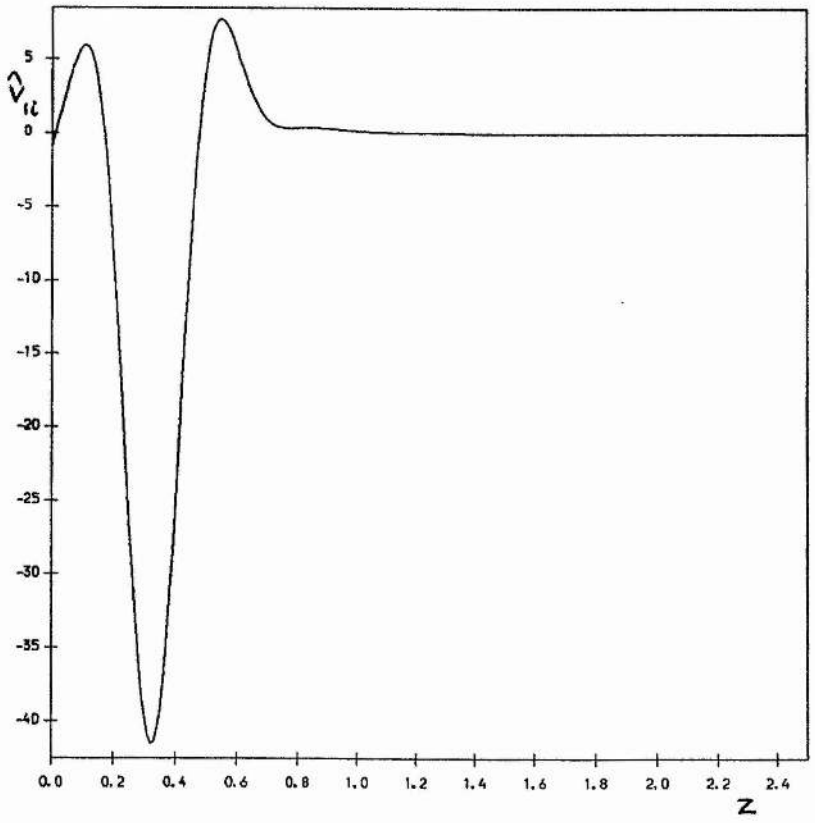

Figure 4.27 (contd.) Cross-flow velocity.

Supplement: the resonant-triad program

```
      PROGRAM OSCR53
C
C     THIS PROGRAM USES NEWTON-RAPHSON ON FIRST EIGENVALUE ESTIMATE,
C     AND REGULA FALSI FOR SUBSEQUENT ITERATIONS (SUBROUTINE EIGEN).
C     PRINCIPLE OF ARGUMENT ALSO AVAILABLE (SUBROUTINE EIGIT). BISECTION
C     IS USED ON BETA (TRANSVERSE WAVENUMBER). RESONANT TRIAD INTERACTION
C     COEFFICIENTS ARE CALCULATED. FINDS EIGENVALUE, THEN
C     THREE EIGENFUNCTIONS, THEN THREE ADJOINTS, THEN ONE TRANSVERSE
C     VELOCITY, AND FINALLY F1,F3. FIVE-/THREE-POINT CENTRAL
C     DIFFERENCE TECHNIQUES USED.
C
      IMPLICIT COMPLEX*16(A,G,H,S,X),REAL*8(B-F,O-R,T-W,Y,Z)
      DIMENSION UL(3201),ULP(3201),ULD(3201),ADS(3201,2),ADP(3201,2)
     1 ,ADD(3201,2),XVS(3201),XVP(3201),XVD(3201),XVT(3201)
     1,XJS(3201,2),XJP(3201,2),XJD(3201,2),XJT(3201,2),XJQ(3201,2)
      COMMON/RR/R,R0,R1,R2,RF,RL/MVL/UL,ULP,ULD
      COMMON/PP1/P1,P2,P3,P4,P5,P6,P7,P8/XFL/XVS,XVP,XVD,XVT
      COMMON/NNW/N,NM1,NP1,W,W2,W3,W4/ADJ/ADS,ADP,ADD
      COMMON/VV/VL,VL2,VL3,VL4,PR,PI/PHI/XJS,XJP,XJD,XJT,XJQ
      COMMON/COQ/AZ,AIO,ARL,ARL3,AC0,AC/IND/NK1,LLEV,NLEV,IPN
      COMMON/TF/AFF,RFF/RTD/BL,IBL,ITM/YMAX/YL/GAMM/XVL,XVL0
      COMMON/PAR/VL0,VL02,RR0,EPS,EPS1,DCR,DCI/XX/XB3,XB1
      COMMON/PROP/EM,C0,D,SS,ULP0/DET/DARG,DDARG,JR,JI,NARG,FCR,FCI
     1/PP2/RFV,P1V,P2V,P3V,P4V
C     YL-IS WIDTH OF Y-DOMAIN
C     N-IS NO. OF STEPS
C     IPN=0,1,2,---ORDER OF PRINT STATEMENTS
C     PROGRAM EXECUTION BEGINS
C
      WRITE(6,67)
67    FORMAT(1X//10X,'Program OSCRT'//1X,'Locates resonant triads
     1 in Blasius flow'///1X,'INC=0,1---linear,nonlinear problem;
     1 NLEV=0,1---rigid,compliant wall'//
     11X,'Enter: N,YL,INC,NLEV,IPN,ISET,LLEV,ITM'//)
      READ(5,*)N,YL,INC,NLEV,IPN,ISET,LLEV,ITM
      ISQ=0
      IF(LLEV.EQ.3) ISQ=1
      IF(LLEV.NE.1) GOTO 42
      WRITE(6,*) 'Adjoint iteration selected'
      WRITE(6,*)
42    IF(LLEV.EQ.3) WRITE(6,*) 'Squire mode problem selected'
      WRITE(6,44)
44    FORMAT(1X/1X,'Enter: EPS,EPS1;DCR,DCI (triad,eigenvalue search
     1tolerances;'/1X,'eigenvalue increments);NARG,JR,JI,FCR,FCI'/)
      READ(5,*) EPS,EPS1,DCR,DCI,NARG,JR,JI,FCR,FCI
      W=YL/N
      WRITE(6,10)YL,N,W
  10  FORMAT(/,10X,'YL=',F8.5,10X,'N=',I4,10X,'h=',F11.8/)
      NM1=N-1
      NP1=N+1
      R0=0.0D0
      R1=1.0D0
      R2=2.0D0
      NK1=0
C     LLEV=0
C
C     BLASIUS SOLN/MEAN-VEL CALCULATIONS BEGIN
```

```
      ETAL=5.0*YL/SQRT(2.0)
      WB=ETAL/N
      ETA=0.0D0
      F=0.0D0
      P=0.0D0
      Q=0.46959999904740314D0
      TR=0.0D0
      KB=1
      IF(IPN.NE.2)GO TO 23
      OPEN(3,FILE='MFLOW.DAT',STATUS='NEW')
      WRITE(3,21)
   21 FORMAT(4X,'Y',8X,'F',8X,'F`',8X,'F``',6X,'F```')
C  23 UI(KB)=F*(SQRT(2.0)/5.0)
23    UL(KB)=P
      ULP(KB)=Q*(5.0/SQRT(2.0))
      ULD(KB)=TR*12.5
      IF(IPN.NE.2)GO TO 26
      YY=(KB-1)*YL/N
      WRITE(3,24)YY,F,P,Q,TR
   24 FORMAT(2X,F4.2,2X,F8.5,2X,F8.5,2X,F8.5,2X,F8.5)
   25 FORMAT(2X,F4.2,2X,F8.5,2X,F8.5,2X,F8.5)
   26 DELF1=WB*P
      DELP1=WB*Q
      DELQ1=WB*(-F*Q)
      DELF2=WB*(P+DELP1/2.0)
      DELP2=WB*(Q+DELQ1/2.0)
      DELQ2=WB*(-(F+DELF1/2.0)*(Q+DELQ1/2.0))
      DELF3=WB*(P+DELP2/2.0)
      DELP3=WB*(Q+DELQ2/2.0)
      DELQ3=WB*(-(F+DELF2/2.0)*(Q+DELQ2/2.0))
      DELF4=WB*(P+DELP3)
      DELP4=WB*(Q+DELQ3)
      DELQ4=WB*(-(F+DELF3)*(Q+DELQ3))
      F=F+(DELF1+2.0*DELF2+2.0*DELF3+DELF4)/6.0
      P=P+(DELP1+2.0*DELP2+2.0*DELP3+DELP4)/6.0
      Q=Q+(DELQ1+2.0*DELQ2+2.0*DELQ3+DELQ4)/6.0
      TR=-(F*Q)
      ETA=ETA+WB
      KB=KB+1
      IF(KB.LE.NP1)GO TO 23
      IF(IPN.NE.2)GO TO 35
      WRITE(3,28)
   28 FORMAT(/,4X,'Y',7X,'UL',8X,'ULP',8X,'ULD',/)
C  29 FORMAT(/,4X,'Y',7X,'UI',8X,'UL',8X,'ULP',/)
      DO 30 J=1,NP1
      YY=(J-1)*(YL/N)
      WRITE(3,25)YY,UL(J),ULP(J),ULD(J)
   30 CONTINUE
      CLOSE(3)
C     BLASIUS SOLN/MEAN-VEL CALCULATIONS END
C
C     DATA GENERATION
   35 CONTINUE
C     VL--IS REAL ALPHA
C     R--IS REYNOLDS NUMBER
C     CR--IS REAL PART OF C (TRIAL VALUE)
C     CI--IS IMAGINARY PART OF C (TRIAL VALUE)
C
      ULP0=ULP(1)
```

```
      AZ=DCMPLX(R0,R0)
      AIO=DCMPLX(R0,R1)
C     W-IS STEP SIZE
C     W=YL/N
      W2=W*W
      W3=W2*W
      W4=W3*W
      RF=R1/360.0
      P1=R1/(R2*W)
      P2=R1/(12.0*W2)
      P3=R1/(R2*W3)
      P4=R1/W4
      P5=R1/(120.0*W)
      P6=R1/(15.0*W2)
      P7=R0
      P8=R2*W/45.0D0
      RFV=R1/6.0
      P1V=R1/(R2*W)
      P2V=R1/W2
      P3V=R1/(R2*W3)
      P4V=R1/W4
C     DCR=0.1D-05
C     DCI=0.1D-05
C     EPS=0.1D-06
      OPEN(4,FILE='RTRES.DAT',STATUS='NEW')
      WRITE(4,10) YL,N,W
      DCRR=DCR
      DCII=DCI
      DO 400 IAS=1,ISET
      DCR=DCRR
      DCI=DCII
      IF(IPN.EQ.0) GOTO 91
      IF(LLEV.LT.2) THEN
      OPEN(7,FILE='EIGF.DAT',STATUS='NEW')
      OPEN(8,FILE='ADJ.DAT',STATUS='NEW')
      ENDIF
      IF(INC.EQ.1.OR.LLEV.EQ.3) OPEN(9,FILE='XFLOW.DAT',STATUS='NEW')
91    WRITE(6,93)
93    FORMAT(1X/1X,'Enter: R0,Alpha,R,Cr,Ci,C1i,Beta,dBeta'//)
      READ(5,*) RREF,VL,R,CCR,CCI,C1I,BL0,DBL
      IF(NLEV.NE.1) GOTO 95
      WRITE(6,*) 'IOPT=0 for R=R(x);IOPT=1 for R=R(U)'
      WRITE(6,*) 'Enter IOPT,mass,c0,d,S'
      READ(5,*) IOPT,EM,C0,D,SS
C
      IF(R.NE.RREF.AND.IOPT.EQ.0) THEN
      WRITE(4,912) RREF,EM,SS
912   FORMAT(1X,'R=R(x)'//2X,'R0=',F8.1,4X,'m0=',F8.4,4X,
     1'S0=',2E11.4/)
      EM=EM*RREF/R
      SS=SS*R/RREF
      ELSEIF(R.NE.RREF) THEN
      WRITE(4,922) RREF,C0,D,SS
922   FORMAT(1X,'R=R(U)'//2X,'R0=',F8.1,2X,'c0(0)=',F8.4,2X,
     1'd0=',F8.4,2X,'S0=',2E11.4/)
      C0=C0*RREF/R
      D=D*RREF/R
      SS=SS*RREF*RREF/(R*R)
      ENDIF
```

```
C
      WRITE(4,94) EM,C0,D,SS
94    FORMAT(5X,'m',7X,'c0',6X,'d',13X,'S'
     1 //1X,3(F8.4),1X,2E11.4/)
95    CONTINUE
      VL0=VL
      VL02=VL*VL
      RR0=R
      ITR=0
      ITN=0
      THET=R0
      BL=R0
      IBL=1
      IF(INC.EQ.2) THEN
      BL=BL0
      IBL=2
      ENDIF
      KK2=0
      CALL EIGEN(CCR,CCI)
      CR0=CCR
      CI0=CCI
      AC0=DCMPLX(CR0,CI0)
      WRITE(6,1200) VL0,BL,RR0,CR0,CI0,RFF
      WRITE(4,1200) VL0,BL,RR0,CR0,CI0,RFF
C     IF(IPN.EQ.0)GOTO 1513
      NK1=1
      CALL MATSOL(CR0,CI0)
      IF(LLEV.EQ.3) GOTO 330
      IF(LLEV.EQ.0) THEN
      LLEV=1
      ELSE
      LLEV=0
      ENDIF
      ZADJ=FF(CCR,CCI)
C     CALL MATSOL(CR0,CI0)
      IF(LLEV.EQ.1) THEN
      WRITE(6,333) VL0,BL,RR0,CCR,CCI,ZADJ
      WRITE(4,333) VL0,BL,RR0,CCR,CCI,ZADJ
333   FORMAT(1X,'Adjoint:'/1X,F7.5,D17.10,F8.1
     1,3(1X,D15.8)/)
      LLEV=0
      ELSE
      WRITE(6,335) VL0,BL,RR0,CCR,CCI,ZADJ
      WRITE(4,335) VL0,BL,RR0,CCR,CCI,ZADJ
335   FORMAT(1X,'Phi:'/1X,F7.5,D17.10,F8.1,3(1X,D15.8)/)
      LLEV=1
      ENDIF
330   NK1=0
      IF(INC.NE.1) GOTO 420
      IBL=2
1513  ITR=0
C     CCI=C1I
1515  BL=BL0+ITR*DBL
      CCI=C1I
      CALL EIGEN(CCR,CCI)
      THET=CCR-CR0
      THMD=ABS(THET)
      IF(THMD.LT.EPS)GOTO 1535
      WRITE(6,1400) VL0,BL,RR0,CCR,CCI,THET
```

```
      WRITE(4,1400) VL0,BL,RR0,CCR,CCI,THET
1400  FORMAT(1X,F7.5,E17.10,F8.1,2(1X,E15.8),1X,E15.8)
C      IF(ITR.EQ.0.AND.THET.GT.R0) THEN
C      BL0=BL0-0.2D-1
C      DBL=0.1D-1
C      CCR=CR0
C      CCI=C1I
C      GOTO 1515
C      ELSEIF(ITR.EQ.0) THEN
C      GOTO 1526
C      ENDIF
      IF(ITR.EQ.0) GOTO 1526
      IF((THET*THETL).LT.R0)GOTO 1529
1526  THETL=THET
      BLL=BL
      ITR=ITR+1
      IF(ITR.GT.ITM)GOTO 400
      CCR=CR0
      GOTO 1515
1529  BLR=BL
1530  BL=(BLL+BLR)/2.0D0
      CALL EIGEN(CCR,CCI)
      THET=CCR-CR0
      THMD=ABS(THET)
      IF(THMD.LT.EPS)GOTO 1535
      WRITE(6,1400) VL0,BL,RR0,CCR,CCI,THET
      WRITE(4,1400) VL0,BL,RR0,CCR,CCI,THET
      IF((THET*THETL).GT.R0)GOTO 1533
      BLR=BL
      GOTO 1534
1533  BLL=BL
      THETL=THET
1534  KK2=KK2+1
      IF(KK2.GT.100)GOTO 400
      GOTO 1530
1535  WRITE(6,*)
      WRITE(6,*) 'RESONANT TRIAD LOCATED:'
      WRITE(6,1200) VL0,BL,RR0,CCR,CCI,THET
      WRITE(4,1200) VL0,BL,RR0,CCR,CCI,THET
1200  FORMAT(1X/1X,F7.5,D17.10,F8.1,3(1X,D15.8)/)
1210  FORMAT(1X/1X,'GAMMA=',F11.8,5X,'RPRIME=',F9.1//1X,'P=',
     1 2F12.6,5X,'P0=',2F12.6/)
C      IF(IPN.EQ.0)GOTO 400
      PR=CCR
      PI=CCI
      NK1=1
C      IBL=2
      CALL MATSOL(CCR,CCI)
      WRITE(6,1210) VL,R,XVL,XVL0
      WRITE(4,1210) VL,R,XVL,XVL0
C      IF(BL.GT.R0) THEN
      IF(LLEV.EQ.0) THEN
      LLEV=1
      ELSE
      LLEV=0
      ENDIF
      ZADJ=FF(CCR,CCI)
C      CALL MATSOL(CCR,CCI)
      IF(LLEV.EQ.1) THEN
```

```
      WRITE(6,423) VL0,BL,RR0,CCR,CCI,ZADJ
      WRITE(4,423) VL0,BL,RR0,CCR,CCI,ZADJ
423   FORMAT(1X,'Adjoint (oblique):'/1X,F7.5,D17.10
     1,F8.1,3(1X,D15.8)/)
      ELSE
      WRITE(6,425) VL0,BL,RR0,CCR,CCI,ZADJ
      WRITE(4,425) VL0,BL,RR0,CCR,CCI,ZADJ
425   FORMAT(1X,'Phi (oblique):'/1X,F7.5,D17.10,F8.1
     1,3(1X,D15.8)/)
      ENDIF
      LLEV=2
      CALL MATSOL(CCR,CCI)
      LLEV=0
      NK1=0
      CALL COEFF
C     ENDIF
420   IF(IPN.EQ.0) GOTO 400
      IF(ISQ.EQ.1) GOTO 773
      IPQ=1
      IPR=1
      IF(INC.GT.0) IPR=2
      IF(INC.EQ.2) IPQ=2
      DO 773 I=IPQ,IPR
       DO 776 J=1,NP1,4
C       IF(J.LT.51.OR.J.GT.(NP1-51))THEN
       WRITE(7,770) XJS(J,I),XJP(J,I),XJD(J,I),XJT(J,I),XJQ(J,I)
       WRITE(8,772) ADS(J,I),ADP(J,I),ADD(J,I)
C      ENDIF
776   CONTINUE
      WRITE(7,*)
      WRITE(8,*)
773   CONTINUE
      IF(INC.EQ.1.OR.ISQ.EQ.1) THEN
       DO 753 J=1,NP1,4
C      IF(J.LT.51.OR.J.GT.(NP1-51))WRITE(9,771) XVS(J),XVP(J),XVD(J),
C    1 XVT(J)
       WRITE(9,771) XVS(J),XVP(J),XVD(J),XVT(J)
753    CONTINUE
771    FORMAT(8E10.3)
       CLOSE(9)
      ENDIF
770   FORMAT(10E10.3)
772   FORMAT(6E12.5)
      IF(ISQ.EQ.1) GOTO 400
      CLOSE(8)
      CLOSE(7)
400   CONTINUE
406   CLOSE(4)
      STOP
      END
C
C
      SUBROUTINE EIGIT(TR,TI,NGAM)
C
C     TRACES CLOSED CONTOUR IN (CR,CI)-PLANE. EIGENVALUES LOCATED BY
C     PRINCIPLE OF ARGUMENT.
C
      IMPLICIT COMPLEX*16(A,G,H,S,X),REAL*8(B-F,O-R,T-W,Y,Z)
      COMMON/RR/R,R0,R1,R2,RF,RL/COQ/AZ,AIO,ARL,ARL3,AC0,AC
```

```
      COMMON/PAR/VL0,VL02,RR0,EPS,EPS1,DCR,DCI/TF/AFF,RFF
      COMMON/DET/DARG,DDARG,JR,JI,NARG,FCR,FCI
      COMMON/VV/VL,VL2,VL3,VL4,PR,PI/RTD/BL,IBL,ITM
      PI=3.141592654D0
      WRITE(4,180) VL0,BL,RR0
180   FORMAT(1X/1X,F7.5,E17.10,F8.1/)
      NIT=0
40    JMX=2*(JR+JI)
      JIR=JR+JI
      JIR2=JI+2*JR
50    CALL MATSOL(TR,TI)
      IF(RFF.LT.EPS1) GOTO 1000
      RMIN=RFF
      CRMIN=TR
      CIMIN=TI
      NGAM=0
      DARG1=DARG
      WRITE(6,200) TR,TI,RFF,DARG
C     IF(NIT.NE.0) GOTO 220
      WRITE(4,200) TR,TI,RFF,DARG
200   FORMAT(1X/1X,2(E15.8,1X),2(E13.6,1X))
      TR0=TR
      TI0=TI
220   DO 100 J=1,JMX
C
      IF(J.LE.JR) THEN
      TR=TR+DCR
      NWR=1
      ELSEIF(J.LE.JIR) THEN
      TI=TI+DCI
      NWR=2
      ELSEIF(J.LE.JIR2) THEN
      TR=TR-DCR
      NWR=1
      ELSE
      TI=TI-DCI
      NWR=2
      ENDIF
C
      CALL MATSOL(TR,TI)
      IF(RFF.LT.EPS1) GOTO 1000
      IF(RFF.LT.RMIN) THEN
      RMIN=RFF
      CRMIN=TR
      CIMIN=TI
      ENDIF
      DDARG=DARG-DARG1
C
      IF(DDARG.GE.PI) THEN
      NGAM=NGAM-1
      ELSEIF(DDARG.LE.(-PI)) THEN
      NGAM=NGAM+1
      ELSEIF(ABS(DDARG).GT.1.5D0) THEN
      WRITE(6,*) 'STEP SIZE MAY BE TOO LARGE:'
      WRITE(6,300) TR,TI,RFF,DARG,DDARG
      WRITE(4,300) TR,TI,RFF,DARG,DDARG
C      GOTO 95
      IF(NWR.EQ.1) THEN
      DCR=DCR/R2
```

```
      JR=JR*R2
      ELSE
      DCI=DCI/R2
      JI=JI*R2
      ENDIF
      IERR=IERR+1
      TR=TR0
      TI=TI0
      IF(JR.LT.80.AND.JI.LT.80) GOTO 40
      WRITE(6,*) 'TOO MANY POINTS; TERMINATING EXECUTION'
      WRITE(4,*) 'EXECUTION TERMINATED- TOO MANY POINTS'
      GOTO 1000
      ENDIF
C
      IF(J.EQ.JR.OR.J.EQ.JIR.OR.J.EQ.JIR2.OR.J.EQ.JMX) THEN
      WRITE(6,300) TR,TI,RFF,DARG,DDARG
      WRITE(4,300) TR,TI,RFF,DARG,DDARG
      ENDIF
300   FORMAT(1X,2(E15.8,1X),2(E13.6,1X),E12.5)
95    DARG1=DARG
100   CONTINUE
      IF(NGAM.LT.0) NGAM=-NGAM
      WRITE(6,400) NGAM
      WRITE(4,400) NGAM
400   FORMAT(1X/6X,I4,' EIGENVALUE(S)'/)
C
      IF(NGAM.NE.0) THEN
       WRITE(6,650) CRMIN,CIMIN,RMIN
       WRITE(4,650) CRMIN,CIMIN,RMIN
650    FORMAT(1X/1X,'CMIN=(',E12.5,',',E12.5,')   RMIN=',E12.5/)
      ENDIF
C      IF((DCR.LT.0.1D-3.AND.DCI.LT.0.1D-3).AND.NGAM.NE.0) THEN
C      IF(RFF.LT.0.2D-5.AND.NGAM.NE.0) THEN
      IF(NGAM.NE.0) THEN
       DELCR=DCR*JR
       DELCI=DCI*JI
C      IF((ABS(TR).GT.0.2D0.AND.DELCR.LT.0.1D-1.AND.DELCI.LE.
C     1  0.1D-1).OR.(DELCR.LE.0.1D-3.AND.DELCI.LE.0.1D-3)) THEN
       IF(DELCR.LT.FCR.AND.DELCI.LT.FCI) THEN
        DCR=0.1D-5
        DCI=0.1D-5
        GOTO 1000
       ENDIF
      ENDIF
C
      GOTO(500,600),NIT
      IF(NGAM.EQ.0.AND.NIT.EQ.0) GOTO 1000
500   IF(NGAM.EQ.0) TI=TI+JI*DCI
      DCR=DCR/R2
      NIT=2
      GOTO 50
600   IF(NGAM.EQ.0) TR=TR+JR*DCR
      DCI=DCI/R2
      NIT=1
      GOTO 50
1000  CONTINUE
      RETURN
      END
C
```

```
C
      SUBROUTINE EIGEN(CR,CI)
C
C     EIGENVALUE LOCATION BY NEWTON-RAPHSON/REGULA FALSI.
C
      IMPLICIT COMPLEX*16(A,G,H,S,X),REAL*8(B-F,O-R,T-W,Y,Z)
      COMMON/RR/R,R0,R1,R2,RF,RL/VV/VL,VL2,VL3,VL4,PR,PI
      COMMON/RTD/BL,IBL,ITM/COQ/AZ,AIO,ARL,ARL3,AC0,AC
      COMMON/PAR/VL0,VL02,RR0,EPS,EPS1,DCR,DCI/TF/AFF,RFF
      COMMON/DET/DARG,DDARG,JR,JI,NARG,FCR,FCI
C     EPS1=0.1D-09
      IF(BL.EQ.R0)GOTO 1010
      BLS=BL*BL
      RGAM=SQRT(BLS+VL02/4.0D0)
      R=(VL0/(2.0D0*RGAM))*RR0
      VL=RGAM
1010  VL2=VL*VL
      VL3=VL2*VL
      VL4=VL2*VL2
      RL=R*VL
      ARL=RL*AIO
      ARL3=VL2*ARL
      IF(NARG.NE.0) THEN
       NG=0
       CALL EIGIT(CR,CI,NG)
       IF(NG.EQ.0.OR.RFF.LT.EPS1) GOTO 930
      ENDIF
      Z1=FF(CR,CI)
      AC1=DCMPLX(CR,CI)
      AF1=AFF
C      IF(Z1.LT.EPS1)GOTO 930
      WRITE(6,275) VL0,BL,RR0,CR,CI,Z1
      VCR=DCR
      VCI=DCI
      C1=CR+VCR
      C2=CI+VCI
      Z2=FF(C1,CI)
      Z3=FF(CR,C2)
      ECR=(Z2-Z1)/VCR
      ECI=(Z3-Z1)/VCI
      DEN=ECR*ECR+ECI*ECI
      BCR=-Z1*ECR/DEN
      BCI=-Z1*ECI/DEN
      CR=CR+BCR
      CI=CI+BCI
      ZZPR=FF(CR,CI)
      AC2=DCMPLX(CR,CI)
      AF2=AFF
      IF(ZZPR.LT.EPS1)GOTO 930
      WRITE(6,275) VL0,BL,RR0,CR,CI,ZZPR
      ITC=0
 900  AC3=(AC1*AF2-AC2*AF1)/(AF2-AF1)
      CR=DREAL(AC3)
      CI=DIMAG(AC3)
      FF3=FF(CR,CI)
      IF(FF3.LT.EPS1)GOTO 930
      WRITE(6,275) VL0,BL,RR0,CR,CI,FF3
275   FORMAT(1X,F7.5,E17.10,F8.1,3(1X,E15.8))
      AC1=AC2
```

```
      AF1=AF2
      AC2=AC3
      AF2=AFF
      ITC=ITC+1
      IF(ITC.LT.ITM)GOTO 900
      WRITE(6,*) 'EIGENVALUE SEARCH NOT CONVERGING'
930   CONTINUE
      RETURN
      END
C
C
      FUNCTION FF(VR,VI)
      IMPLICIT COMPLEX*16(A,G,H,S,X),REAL*8(B-F,O-R,T-W,Y,Z)
      COMMON/TF/AFF,RFF
      CALL MATSOL(VR,VI)
      FF=RFF
      RETURN
      END
C
C
      SUBROUTINE MATSOL(CR,CI)
      IMPLICIT COMPLEX*16(A,G,H,S,X),REAL*8(B-F,O-R,T-W,Y,Z)
      DIMENSION A(3201,5),HP(3201)
      COMMON/IND/NK1,LLEV,NLEV,IPN/RTD/BL,IBL,ITM
      COMMON/MAT/A,HP/TF/AFF,RFF
      COMMON/NNW/N,NM1,NP1,W,W2,W3,W4
      COMMON/RR/R,R0,R1,R2,RF,RL
      COMMON/VV/VL,VL2,VL3,VL4,PR,PI
      COMMON/COQ/AZ,AIO,ARL,ARL3,AC0,AC
      AC=DCMPLX(CR,CI)
      CALL MATRIX
      CALL DIAG
      AFF=A(NP1,3)
      IF(LLEV.EQ.3) AFF=A(NP1,2)
      RFF=ABS(AFF)
      IF(NK1.EQ.0)GO TO 100
      CALL SOLN
 100  CONTINUE
      RETURN
      END
C
C
      SUBROUTINE MATRIX
      IMPLICIT COMPLEX*16(A,G,H,S,X),REAL*8(B-F,O-R,T-W,Y,Z)
      DIMENSION A(3201,5),UL(3201),ULP(3201),ULD(3201)
     1,HP(3201),XJS(3201,2),XJP(3201,2),XJD(3201,2),XJT(3201,2),
     1 XJQ(3201,2)
      COMMON/RR/R,R0,R1,R2,RF,RL/EE/HF1,HF2,HF3,HG1,HG2,HG3
      COMMON/PP1/P1,P2,P3,P4,P5,P6,P7,P8/VBC/XBB,XCC
      COMMON/NNW/N,NM1,NP1,W,W2,W3,W4/PROP/EM,C0,D,SS,ULP0
      COMMON/VV/VL,VL2,VL3,VL4,PR,PI/XX/XB3,XB1
      COMMON/COQ/AZ,AIO,ARL,ARL3,AC0,AC/PAR/VL0,VL02,RR0,
     1EPS,EPS1,DCR,DCI/RTD/BL,IBL,ITM/PHI/XJS,XJP,XJD,XJT,XJQ
      COMMON/IND/NK1,LLEV,NLEV,IPN/BCS/HBWA,HBWB,HBWC,HCWA,
     1 HCWB,HCWC/GP/GP0/GAMM/XVL,XVL0
      COMMON/MAT/A,HP/MVL/UL,ULP,ULD/PP2/RFV,P1V,P2V,P3V,P4V
      IF(NLEV.EQ.1.AND.IBL.EQ.1) THEN
       XB=(ARL*(EM*VL02*(AC*AC-C0*C0)+AIO*VL0*D-SS))/AC
       XB3=XB
```

```
      ELSEIF(NLEV.EQ.1.AND.IBL.EQ.2) THEN
       XB=(AIO*R2*VL2*RR0/(VL0*AC))*(EM*(VL02/4.0)*(AC*AC-(VL0*C0
     1 *C0)/(R2*VL))+(AIO*VL0*AC*D/R2)-SS)
       XB1=XB
      ENDIF
      A1=AZ
      IF(LLEV.LT.2) THEN
      A0=-VL4/ARL+VL2*AC
      A2=R2*VL2/ARL-AC
      A4=-R1/ARL
      A00=RF*A0
      A22=P2*A2
      A4=P4*A4
      ELSE
      A00=-RFV*(VL2-(ARL*AC))
      A2=DCMPLX(P2V,R0)
      A4=AZ
      ENDIF
      DO 50 J=1,NP1
      A0=A00-RF*VL2*UL(J)
      IF(LLEV.EQ.0) A0=A0-RF*ULD(J)
      IF(LLEV.GE.2) A0=A00-(RFV*ARL*UL(J))
      IF(LLEV.EQ.1) A1=P1*R2*ULP(J)
      IF(LLEV.LT.2) THEN
      A2=A22+P2*UL(J)
      A(J,1)=A0+A2+A4
      A(J,2)=A0*56.0+A2*8.0-A4*4.0-A1
      A(J,3)=A0*246.0-A2*18.0+A4*6.0
      A(J,4)=A(J,2)+R2*A1
      A(J,5)=A(J,1)
      HP(J)=AZ
      ELSE
      A(J,1)=A2+A0
      A(J,2)=-R2*A2+4.0*A0
      A(J,3)=A(J,1)
      HP(J)=AZ
      IF(LLEV.EQ.2) HP(J)=AIO*ULP(J)*BL*RR0*XJS(J,2)
      ENDIF
   50 CONTINUE
      GP0=AZ
      GP1=AZ
      GP2=AZ
C     WALL B.C.-S
      IF(LLEV.LT.2.AND.NLEV.EQ.0) THEN
      HBWA=AZ
      HBWB=R1
      HBWC=AZ
      HCWA=-246.0D0
      HCWB=-112.0D0
      HCWC=-R1
      ELSEIF(NLEV.EQ.0) THEN
CC    AV0=ARL*AC-VL2
C      HFV=AV0*P1
C      HFV1=P3+HFV
C      GD1=18.0*HFV1-6.0*P3-40.0*HFV
C      HBD=56.0*GD1-7.0*(9.0*HFV1+15.0*P3-157.0*HFV)
C      HBWA=-(114.0*GD1+392.0*HFV1)/HBD
C      HBWB=7.0*((9.0*HFV1+157.0*HFV-15.0*P3)-8.0*GD1)/HBD
C      HBWC=7.0*(18.0*HFV1+6.0*P3+40.0*HFV-GD1)/HBD
```

```
C       HBWD=14.0*HFV1/HBD
C       HCWA=-114.0/7.0-8.0*HBWA
C       HCWB=-8.0*(R1+HBWB)
C       HCWC=-(R1+8.0*HBWC)
C       HCWD=-8.0*HBWD
C       HDWA=56.0-18.0*HCWA-9.0*HBWA
C       HDWB=-9.0-18.0*HCWB-9.0*HBWB
C       HDWC=-18.0-18.0*HCWC-9.0*HBWC
C       HDWD=-R1-18.0*HCWD-9.0*HBWD
CC     HBWA=-11.0/R2
CC     HBWB=-R1
CC     HBWC=AZ
CC     HCWA=62.0D0
CC     HCWB=AZ
CC     HCWC=-R1
       HBWA=-4.0D0
       HBWB=-R1
       GP0=AZ
       ENDIF
       IF(NLEV.EQ.1.AND.LLEV.EQ.0) THEN
       HD1=ULP0*RF/AC
       HD2=3.0*VL2*P1
       HD3=XB*RF
       HCA=P3+HD3
       HBD=HCA*(56.0*HD1-P1)+HD1*(R2*P3+HD2-56.0*HD3)
       HBWA=HD1*246.0*(HD3-HCA)/HBD
       HBWB=(HD1*(R2*P3+HD2+56.0*HD3)-HCA*(56.0*HD1+P1))/HBD
       HBWC=HD1*(HD3-P3-HCA)/HBD
       HCX=P1-56.0*HD1
       HCWA=(-246.0*HD1+HCX*HBWA)/HD1
       HCWB=(HCX*HBWB-(56.0*HD1+P1))/HD1
       HCWC=(HCX*HBWC-HD1)/HD1
       ELSEIF(NLEV.EQ.1.AND.LLEV.EQ.1) THEN
       HD1=ULP0*P2/AC
       HD2=RF*((ULP0*VL2/AC)-XB)
       HBWA=AZ
       HBWB=R1
       HBWC=AZ
       HCD=P3-HD1-HD2
       HCWA=(246.0*HD2-18.0*HD1)/HCD
       HCWB=(16.0*HD1+112.0*HD2)/HCD
       HCWC=(P3+HD1+HD2)/HCD
       ELSEIF(NLEV.EQ.1) THEN
C       AV0=ARL*AC-VL2
C       AV1=-ARL*ULP0
C       HP0=R2*BL*ULP0*XJS(1,2)/(VL0*AC*RF)
      GP0=R2*BL*ULP0*XJS(1,2)/(VL0*AC*RFV)
      HBWA=-4.0D0
      HBWB=-R1
      ENDIF
      IF(LLEV.GE.2) THEN
      A(1,2)=A(1,2)+HBWA*A(1,1)
      A(1,3)=A(1,3)+HBWB*A(1,1)
      HP(1)=HP(1)-GP0*A(1,1)
      ELSE
      A(1,3)=A(1,3)+HBWA*A(1,2)+HCWA*A(1,1)
      A(1,4)=A(1,4)+HBWB*A(1,2)+HCWB*A(1,1)
      A(1,5)=A(1,5)+HBWC*A(1,2)+HCWC*A(1,1)
      A(2,2)=A(2,2)+HBWA*A(2,1)
```

```
      A(2,3)=A(2,3)+HBWB*A(2,1)
      A(2,4)=A(2,4)+HBWC*A(2,1)
      ENDIF
C     END OF WALL B.C.-S
C     VARIABLES REQD. FOR OUTER B.C.-S
      IF(LLEV.LT.2) THEN
      XVL2=VL2+ARL*(R1-AC)
      XVL=CDSQRT(XVL2)
      IF(IBL.EQ.1) XVL0=XVL
C     XVL=VL
C     XVL2=VL2
C     XBF1=P1/(XVL*RF)
C     XBF2=-P2/(XVL2*RF)
C     XCFM=(56.0+8.0*XBF2)/(R1+XBF2)
C     XCF=(246.0-18.0*XBF2)/(R1+XBF2)
C     XBB=-(56.0-XBF1-XCFM)/(56.0+XBF1-XCFM)
C     XCC=-(246.0-XCF)/(56.0+XBF1-XCFM)
C     XDD=-((56.0-XBF1)+(56.0+XBF1)*XBB)
C     XEE=-(246.0+(56.0+XBF1)*XCC)
C     XBB=EXP(-R2*VL*W)
C     XCC=XBB*XBB
      XA1=(XVL+VL)*P1
      XA2=XVL*VL*RF
      XA3=(XVL+VL)*P2
      XA4=XVL*VL*P1
      XC1=XA2+P2
      XC2=XA3+P3
      HFD=XC1*(8.0*XA3-R2*P3+XA4)-XC2*(8.0*P2+XA1+56.0*XA2)
      HF1=(XC2*(XA2+P2)-XC1*(XA3-P3))/HFD
      HF2=(XC2*(8.0*P2-XA1+56.0*XA2)-XC1*(R2*P3+8.0*XA3-XA4))/
     1  HFD
      HF3=(XC2*(246.0*XA2-18.0*P2)+XC1*18.0*XA3)/HFD
      HGC=-(8.0*P2+XA1+56.0*XA2)/XC1
      HG1=-R1+HGC*HF1
      HG2=(XA1-8.0*P2-56.0*XA2)/XC1+HGC*HF2
      HG3=(18.0*P2-246.0*XA2)/XC1+HGC*HF3
C     OUTER B.C.'S
      A(NP1,1)=A(NP1,1)+HF1*A(NP1,4)+HG1*A(NP1,5)
      A(NP1,2)=A(NP1,2)+HF2*A(NP1,4)+HG2*A(NP1,5)
      A(NP1,3)=A(NP1,3)+HF3*A(NP1,4)+HG3*A(NP1,5)
      A(N,2)=A(N,2)+HF1*A(N,5)
      A(N,3)=A(N,3)+HF2*A(N,5)
      A(N,4)=A(N,4)+HF3*A(N,5)
C     A(NP1,1)=A(NP1,1)+XCC*A(NP1,5)
C     A(NP1,2)=A(NP1,2)+XBB*A(NP1,4)
C     A(N,3)=A(N,3)+XBB*A(N,5)
C     A(NP1,1)=A(NP1,1)-A(NP1,5)
C     A(NP1,2)=A(NP1,2)+A(NP1,4)*XBB+A(NP1,5)*XDD
C     A(NP1,3)=A(NP1,3)+A(NP1,4)*XCC+A(NP1,5)*XEE
C     A(N,3)=A(N,3)+A(N,5)*XBB
C     A(N,4)=A(N,4)+A(N,5)*XCC
      ELSE
      XVL2=VL2+ARL*(R1-AC)
      XVL=CDSQRT(XVL2)
      SNN=XVL*RFV
      XBB=(P1V-SNN)/(P1V+SNN)
      XCC=-4.0*SNN/(SNN+P1V)
      A(NP1,1)=A(NP1,1)+XBB*A(NP1,3)
      A(NP1,2)=A(NP1,2)+XCC*A(NP1,3)
```

```
      ENDIF
C     END OF OUTER B.C.-S
      RETURN
      END
C
C
      SUBROUTINE DIAG
C
C     DIAGONALISATION OF MATRIX OF EQUATION.
C
      IMPLICIT COMPLEX*16(A,G,H,S,X),REAL*8(B-F,O-R,T-W,Y,Z)
      DIMENSION A(3201,5),HP(3201)
      COMMON/IND/NK1,LLEV,NLEV,IPN
      COMMON/NNW/N,NM1,NP1,W,W2,W3,W4
      COMMON/VV/VL,VL2,VL3,VL4,PR,PI
      COMMON/MAT/A,HP/DET/DARG,DDARG,JR,JI,NARG,FCR,FCI
      IF(LLEV.LT.2) THEN
      DO 40 J=1,NP1
      ZA=ABS(A(J,1))
      DO 37 K=2,5
      ZA1=ABS(A(J,K))
   37 IF(ZA.LT.ZA1)ZA=ZA1
C      IF(LLEV.GT.1) HP(J)=HP(J)/ZA
      DO 40 K=1,5
      A(J,K)=A(J,K)/ZA
40    CONTINUE
C     WRITE(6,*) A(1,4)
      DO 45 J=2,N
      XA=A(J,2)/A(J-1,3)
      XA1=A(J+1,1)/A(J-1,3)
C      IF(LLEV.GT.1) THEN
C      HP(J)=HP(J)-HP(J-1)*XA
C      HP(J+1)=HP(J+1)-HP(J-1)*XA1
C      ENDIF
      DO 45 K=4,5
      A(J,K-1)=A(J,K-1)-A(J-1,K)*XA
      A(J+1,K-2)=A(J+1,K-2)-A(J-1,K)*XA1
   45 CONTINUE
      XA=A(NP1,2)/A(N,3)
      A(NP1,3)=A(NP1,3)-A(N,4)*XA
C      IF(LLEV.GT.1) HP(NP1)=HP(NP1)-HP(N)*XA
      ELSE
      DO 140 J=1,NP1
      ZA=ABS(A(J,1))
      DO 137 K=2,3
      ZA1=ABS(A(J,K))
137   IF(ZA.LT.ZA1)ZA=ZA1
      IF(LLEV.EQ.2) HP(J)=HP(J)/ZA
      DO 140 K=1,3
      A(J,K)=A(J,K)/ZA
140   CONTINUE
      DO 145 J=2,NP1
      XA=A(J,1)/A(J-1,2)
      IF(LLEV.EQ.2) HP(J)=HP(J)-HP(J-1)*XA
C      DO 145 K=4,5
      K=3
      A(J,K-1)=A(J,K-1)-A(J-1,K)*XA
145   CONTINUE
C      XA=A(NP1,2)/A(N,3)
```

```
C       A(NP1,3)=A(NP1,3)-A(N,4)*XA
C       HP(NP1)=HP(NP1)-HP(N)*XA
        ENDIF
        IF(NARG.NE.0) THEN
        JG=3
        IF(LLEV.GE.2) JG=2
        GDET=A(1,JG)
        GDET=GDET/CDABS(A(1,JG))
        DO 80 J=2,NP1
        GDET=(A(J,JG)/CDABS(A(J,JG)))*GDET
80      CONTINUE
        DETX=DREAL(GDET)
        DETY=DIMAG(GDET)
        DARG=ATAN2(DETY,DETX)
        ENDIF
        RETURN
        END
C
C
        SUBROUTINE SOLN
C
C       CONSTRUCTION OF SOLUTION VECTOR.
C
        IMPLICIT COMPLEX*16(A,G,H,S,X),REAL*8(B-F,O-R,T-W,Y,Z)
        DIMENSION A(3201,5),G(3207),HP(3201),XJS(3201,2),XJP(3201,2)
       1,XJD(3201,2),XJT(3201,2),XJQ(3201,2),ADS(3201,2),ADP(3201,2)
       1 ,ADD(3201,2),XVS(3201),XVP(3201),XVD(3201),XVT(3201)
       1,XS(3201),XP(3201),XD(3201),XT(3201),XQ(3201),
       1 RAL(2),RAL3(2),UL(3201),ULP(3201),ULD(3201)
        COMMON/PHI/XJS,XJP,XJD,XJT,XJQ/ADJ/ADS,ADP,ADD/XFL/XVS,XVP,
       1 XVD,XVT/PROP/EM,C0,D,SS,ULP0/PAR/VL0,VL02,RR0,EPS,EPS1,DCR,
       1 DCI/MVL/UL,ULP,ULD/VBC/XBB,XCC
        COMMON/IND/NK1,LLEV,NLEV,IPN/RTD/BL,IBL,ITM
        COMMON/NNW/N,NM1,NP1,W,W2,W3,W4/EE/HF1,HF2,HF3,HG1,HG2,HG3
        COMMON/VV/VL,VL2,VL3,VL4,PR,PI/PP2/RFV,P1V,P2V,P3V,P4V
        COMMON/RR/R,R0,R1,R2,RF,RL
        COMMON/PP1/P1,P2,P3,P4,P5,P6,P7,P8
        COMMON/COQ/AZ,AIO,ARL,ARL3,AC0,AC/BCS/HBWA,HBWB,HBWC,
       1 HCWA,HCWB,HCWC
        COMMON/MAT/A,HP/YMAX/YL/GP/GP0
        DO 127 I=1,N+7
 127    G(I)=AZ
        G(NP1+3)=DCMPLX(R1,R0)
        IF(LLEV.GE.2) THEN
        IF(LLEV.EQ.2) G(NP1+3)=HP(NP1)/A(NP1,2)
        G(NP1+2)=(HP(N)-A(N,3)*G(NP1+3))/A(N,2)
        G(NP1+1)=(HP(NM1)-A(NM1,3)*G(NP1+2))/A(NM1,2)
        G(NP1+4)=XBB*G(NP1+2)+XCC*G(NP1+3)
        G(NP1+5)=AZ
        G(NP1+6)=AZ
C       AN=RFV*(G(NP1+1)+G(NP1+5)+56.0*(G(NP1+2)+G(NP1+4))+246.0*
C      1G(NP1+3))
C       AN=AN/EXP(VL*(1.7208-YL))
C       SUM=G(NP1+1)+G(NP1+2)+G(NP1+4)+G(NP1+5)
C       AN1=AN/SUM
C       CA=ABS(AN1)
C       IF(CA.GT.0.1D-09) G(NP1+3)=-(G(NP1+1)+56.0*(G(NP1+2)+
C      1G(NP1+4))+G(NP1+5))/246.0
C       G(N+4)=G(N+4)/AN
```

```
C       G(N+3)=(HP(N)-A(N,4)*G(N+4))/A(N,3)
        DO 450 J=1,N
        M=NP1-J
        G(M+3)=(HP(M)-A(M,3)*G(M+4))/A(M,2)
450     CONTINUE
C       G(N+5)=G(N+3)*XBB+G(N+4)*XCC
C       G(N+6)=-G(N+2)+G(N+3)*XDD+G(N+4)*XEE
        G(3)=HBWA*G(4)+HBWB*G(5)+GP0
C       G(2)=HCWA*G(4)+HCWB*G(5)+HCWC*G(6)+GP1
C       WRITE(4,*) G(2),G(3)
        DO 280 JJ=1,NP1
        J=JJ+3
C       IF(JJ.LE.8.OR.JJ.GE.(N-6)) WRITE(4,*) G(J)
        XVS(JJ)=RFV*(G(J-1)+G(J+1)+4.0*G(J))
        XVP(JJ)=P1V*(G(J+1)-G(J-1))
        XVD(JJ)=P2V*(G(J-1)+G(J+1)-R2*G(J))
        XVT(JJ)=AIO*BL*RR0*(ULP(JJ)*XJP(JJ,2)+ULD(JJ)*XJS(JJ,2))+
     1 ARL*ULP(JJ)*XVS(JJ)+(VL2+ARL*(UL(JJ)-AC))*XVP(JJ)
C       XVT(JJ)=P3V*(G(J+2)-G(J-2)-R2*(G(J+1)-G(J-1)))
280     CONTINUE
C       WRITE(4,*) G(N+5),G(N+6)
C       WRITE(4,*)
        ELSE
        G(NP1+2)=(HP(N)-A(N,4)*G(NP1+3))/A(N,3)
        G(NP1+1)=(HP(NM1)-A(NM1,4)*G(NP1+2)-A(NM1,5)*G(NP1+3))
     1/A(NM1,3)
C       G(NP1+4)=XBB*G(NP1+2)
C       G(NP1+5)=XCC*G(NP1+1)
C       G(NP1+4)=G(NP1+2)*XBB+G(NP1+3)*XCC
C       G(NP1+5)=-G(NP1+1)+G(NP1+2)*XDD+G(NP1+3)*XEE
        G(NP1+4)=HF1*G(NP1+1)+HF2*G(NP1+2)+HF3*G(NP1+3)
        G(NP1+5)=HG1*G(NP1+1)+HG2*G(NP1+2)+HG3*G(NP1+3)
        AN=RF*(G(NP1+1)+G(NP1+5)+56.0*(G(NP1+2)+G(NP1+4))+
     1 246.0*G(NP1+3))
        AN=AN/EXP((1.7208-YL)*VL)
C       IF(LLEV.EQ.2) GOTO 50
        G(N+4)=G(N+4)/AN
50      CONTINUE
        G(N+5)=AZ
        G(N+6)=AZ
        DO 250 J=2,NP1
        JJ=NP1-J+4
        K=NP1-J+1
        G(JJ)=(HP(K)-A(K,5)*G(JJ+2)-A(K,4)*G(JJ+1))/A(K,3)
250     CONTINUE
C       G(N+5)=XBB*G(N+3)
C       G(N+6)=XCC*G(N+2)
C       G(NP1+4)=G(NP1+2)*XBB+G(NP1+3)*XCC
C       G(NP1+5)=-G(NP1+1)+G(NP1+2)*XDD+G(NP1+3)*XEE
        G(NP1+4)=HF1*G(NP1+1)+HF2*G(NP1+2)+HF3*G(NP1+3)
        G(NP1+5)=HG1*G(NP1+1)+HG2*G(NP1+2)+HG3*G(NP1+3)
        G(N+7)=AZ
        G(3)=HBWA*G(4)+HBWB*G(5)+HBWC*G(6)
        G(2)=HCWA*G(4)+HCWB*G(5)+HCWC*G(6)
        G(1)=AZ
C       IF(LLEV.EQ.2) GOTO 350
        AN=RF*(G(N+2)+G(N+6)+56.0*(G(N+3)+G(N+5))+246.0*G(N+4))
        AN=AN/EXP((1.7208-YL)*VL)
        DO 300 J=1,N+7
```

```
D       IF(J.LE.10.OR.J.GE.(N-2))WRITE(4,*) G(J)
        G(J)=G(J)/AN
300     CONTINUE
        WRITE(4,*)
C350     CONTINUE
        DO 700 JJ=1,NP1
        J=JJ+3
        XS(JJ)=RF*(G(J-2)+G(J+2)+56.0D0*(G(J-1)+G(J+1))+
       1 246.0D0*G(J))
        XP(JJ)=P1*(G(J+1)-G(J-1))
        XD(JJ)=P2*(G(J-2)+G(J+2)+8.0*(G(J-1)+G(J+1))-18.0*G(J))
        XT(JJ)=AZ
        IF(LLEV.NE.1) XT(JJ)=P3*(G(J+2)-G(J-2)+R2*(G(J-1)-G(J+1)))
        XQ(JJ)=AZ
        IF(LLEV.EQ.0) XQ(JJ)=P4*(G(J-2)+G(J+2)-4.0*(G(J-1)+
       1 G(J+1))+6.0*G(J))
        IF(LLEV.EQ.0) THEN
        XJS(JJ,IBL)=XS(JJ)
        XJP(JJ,IBL)=XP(JJ)
        XJD(JJ,IBL)=XD(JJ)
        XJT(JJ,IBL)=XT(JJ)
        XJQ(JJ,IBL)=XQ(JJ)
D       IF(JJ.LT.10.OR.JJ.GT.(NP1-10))THEN
D       XERR=XQ(JJ)-(R2*VL2+ARL*(UL(JJ)-AC))*XD(JJ)+(VL4+ARL*
D      1
        ULD(JJ)+ARL3*(UL(JJ)-AC))*XS(JJ)
D       IF(JJ.EQ.1) WRITE(6,*) 'O.S. ERROR:'
D       WRITE(6,*) JJ,XERR
D       IF(JJ.EQ.NP1)THEN
D       XVL=CDSQRT(VL2+ARL*(R1-AC))
D       XERR1=XT(JJ)+(VL+XVL)*XD(JJ)+VL*XVL*XP(JJ)
D       XERR2=XD(JJ)+(VL+XVL)*XP(JJ)+VL*XVL*XS(JJ)
D       WRITE(6,*) 'BC ERRORS: ',XERR1,XERR2
D       ENDIF
D       ENDIF
        ELSEIF(LLEV.EQ.1) THEN
        ADS(JJ,IBL)=XS(JJ)
        ADP(JJ,IBL)=XP(JJ)
        ADD(JJ,IBL)=XD(JJ)
C        ELSEIF(LLEV.EQ.2) THEN
C        XVS(JJ)=XS(JJ)
C        XVP(JJ)=XP(JJ)
C        XVD(JJ)=XD(JJ)
C        XVT(JJ)=XT(JJ)
        ENDIF
700     CONTINUE
        ENDIF
        RAL(1)=VL0
        RAL(2)=VL
        RAL3(1)=VL0*VL02
        RAL3(2)=VL3
C        DO 800 J=1,2
C        XJP(NP1,J)=-RAL(J)*XJS(NP1,J)
C        XJT(NP1,J)=-RAL3(J)*XJS(NP1,J)
C800     CONTINUE
        RETURN
        END
C
C
```

```
      SUBROUTINE COEFF
C
C     NONLINEAR TERMS ON R.H.S.
C
      IMPLICIT COMPLEX*16(A,G,H,S,X),REAL*8(B-F,O-R,T-W,Y,Z)
      DIMENSION XJS(3201,2),XJP(3201,2),XJD(3201,2),XJT(3201,2),
     1 XJQ(3201,2),ADS(3201,2),ADP(3201,2),ADD(3201,2),XVS(3201)
     1,XVP(3201),XVD(3201),XVT(3201),HF(3201,2),
     1 RAL2(2),SV(3201,2),HFA(3201,2),SVA(3201,2)
      COMMON/PHI/XJS,XJP,XJD,XJT,XJQ/ADJ/ADS,ADP,ADD/XFL/XVS,XVP
     1,XVD,XVT/XX/XB3,XB1/PROP/EM,C0,D,SS,ULP0
     1/IND/NK1,LLEV,NLEV,IPN/RTD/BL,IBL,ITM/VV/VL,VL2,VL3,VL4,PR,
     1PI/RR/R,R0,R1,R2,RF,RL/COQ/AZ,AIO,ARL,ARL3,AC0,AC
     1/PAR/VL0,VL02,RR0,EPS,EPS1,DCR,DCI
     1/NNW/N,NM1,NP1,W,W2,W3,W4
C
      RAL2(1)=VL02
      RAL2(2)=VL2
      DO 100 J=1,NP1
C
      HF(J,1)=AIO*(VL0/R2)*((3.0D0-(VL02/VL2))*XJP(J,2)*
     1(XJD(J,2)-(VL2*XJS(J,2)))+XJS(J,2)*(XJT(J,2)-(VL2*
     1XJP(J,2)))+R2*(VL0*BL/VL2)*(XVS(J)*(XJD(J,2)-(VL2*
     1XJS(J,2)))+(XJP(J,2)*XVP(J)))-4.0D0*(BL*BL/VL2)*
     1(XVS(J)*XVP(J))-R2*(BL/VL0)*(XJD(J,2)*XVS(J)+
     1R2*XJP(J,2)*XVP(J)+XJS(J,2)*XVD(J)))
C
      HF(J,2)=AIO*(VL0/4.0D0)*(((VL02/VL2)-R2)*XJS(J,1)*
     1DCONJG(XJT(J,2)-(VL2*XJP(J,2)))+((VL02/VL2)-3.0D0)*
     1XJP(J,1)*DCONJG(XJD(J,2)-(VL2*XJS(J,2)))-R2*
     1DCONJG(XJP(J,2))*(XJD(J,1)-(VL02*XJS(J,1)))-
     1DCONJG(XJS(J,2))*(XJT(J,1)-(VL02*XJP(J,1)))-R2*BL*
     1(VL0/VL2)*(XJS(J,1)*DCONJG(XVD(J))+XJP(J,1)*
     1DCONJG(XVP(J))+VL2*XJS(J,1)*DCONJG(XVS(J))))
C
      DO 90 I=1,2
      SV(J,I)=XJD(J,I)-(RAL2(I)*XJS(J,I))
      SVA(J,I)=SV(J,I)*ADS(J,I)
      HFA(J,I)=HF(J,I)*ADS(J,I)
90    CONTINUE
100   CONTINUE
C
      CALL INTEGR(HFA,XN3,XN1)
      CALL INTEGR(SVA,XD3,XD1)
C
      IF(NLEV.GT.0) THEN
      AETA1=-R2*(VL/(ULP0*VL0))*XJP(1,2)
      AETA3=-XJP(1,1)/ULP0
C
      HPREP1=(VL0/R2)*VL*AC*XJS(1,2)-AIO*(VL/RR0)*SV(1,2)
      HPREP3=VL02*AC0*XJS(1,1)-AIO*(VL0/RR0)*SV(1,1)
C
      XMU1=(AETA1/VL)*(BL*XVP(1)-(VL0/R2)*XJD(1,2))
C
      XMU2=AIO*VL0*AETA1*((BL/VL)*XVS(1)-(VL0/(R2*VL))*XJP(1,2)
     1 -(ULP0/R2)*AETA1)
C
      XMU3=AIO*(VL0/(R2*VL))*AC*AETA1*((VL0/R2)*XJD(1,2)-BL*
     1 XVP(1))-AIO*(VL0/R2)*AETA1*HPREP1+(AETA1/(VL*RR0))*((VL0
```

```
     1 /R2)*(XJQ(1,2)-VL2*XJD(1,2))-BL*(XVT(1)-VL2*XVP(1)))+AIO*
     1 (BL/VL)*ULP0*AETA1*(BL*XJP(1,2)+(VL0/R2)*XVS(1))-(AIO/VL2)
     1 *(((VL0*VL02/8.0)-(VL0/R2)*BL*BL)*XJP(1,2)*XJP(1,2)+VL0*
     1 BL*BL*XVS(1)*XVS(1)+BL*(BL*BL-(3.0/4.0)*VL02)*XJP(1,2)*
     1 XVS(1)-VL*XJS(1,2)*((VL0/R2)*XJD(1,2)-BL*XVP(1)))
C
      XMU4=-AETA1*HPREP1-AIO*(AETA1/RR0)*((3.0*VL02+4.0*BL*BL)*
     1 (XJD(1,2)/VL)-VL0*(BL/VL)*XVP(1)+VL*((VL02/4.0)-BL*BL)*
     1 XJS(1,2))
C
      XKA1=-(AETA3/(R2*VL))*((VL0/R2)*DCONJG(XJD(1,2))-BL*
     1 DCONJG(XVP(1)))-DCONJG(AETA1)*(XJD(1,1)/R2)
C
      XKA2=(AETA3/(R2*VL))*(BL*DCONJG(XJD(1,2))+(VL0/R2)*
     1 DCONJG(XVP(1)))
C
      XKA3=-AIO*(VL0/4.0)*(ULP0*AETA3*DCONJG(AETA1)-R2*(BL/VL)*
     1 AETA3*DCONJG(XVP(1))+XJP(1,1)*DCONJG(AETA1)+((VL02-R2*VL2
     1 )/(VL*VL0))*AETA3*DCONJG(XJP(1,2)))
C
      XKA4=-(R1/R2)*(AETA3*DCONJG(HPREP1)+HPREP3*DCONJG(AETA1))
     1 +AIO*VL*AETA3*DCONJG(XJD(1,2))-AIO*VL0*XJD(1,1)*
     1 DCONJG(AETA1)-AIO*(VL0/(R2*VL))*AETA3*((VL0/R2)*
     1 DCONJG(XJD(1,2)+VL2*XJS(1,2))-BL*DCONJG(XVP(1)))+AIO*
     1 (VL0/4.0)*DCONJG(AETA1)*(XJD(1,1)+VL02*XJS(1,1))
C
      XKA5=AIO*(VL0/4.0)*(AETA3*DCONJG(HPREP1)-R2*HPREP3*
     1 DCONJG(AETA1)-AETA3*(VL0/(R2*VL))*DCONJG(AC*XJD(1,2))+
     1 BL*AETA3*DCONJG(AC*XVP(1))+R2*AC0*XJD(1,1)*DCONJG(AETA1))
     1 -(AIO/(R2*VL))*((VL02/4.0)*XJP(1,1)*DCONJG(XJP(1,2))-VL0*
     1 (BL/R2)*XJP(1,1)*DCONJG(XVS(1))+VL2*XJD(1,1)*
     1 DCONJG(XJS(1,2))-(VL02/R2)*XJS(1,1)*DCONJG(XJD(1,2))+VL0*
     1 BL*XJS(1,1)*DCONJG(XVP(1))+BL*ULP0*AETA3*(DCONJG(XJP(1,2))
     1 *BL+(VL0/R2)*DCONJG(XVS(1))))-(R1/(R2*RR0))*(DCONJG(AETA1)
     1 *(XJQ(1,1)-VL02*XJD(1,1))+(AETA3/VL)*((VL0/R2)*DCONJG(
     1 XJQ(1,2)-VL2*XJD(1,2))-BL*DCONJG(XVT(1)-VL2*XVP(1))))
C
      XKA6=AIO*(VL0/(4.0*VL))*(AETA3*DCONJG(AC)-R2*XJS(1,1))*
     1 DCONJG(BL*XJD(1,2)+(VL0/R2)*XVP(1))-(AETA3/R2)*(AIO*BL*
     1 DCONJG(HPREP1)+(BL/(VL*RR0))*DCONJG(XJQ(1,2)-VL2*XJP(1,2)
     1 )+(VL0/(R2*VL*RR0))*DCONJG(XVT(1)-VL2*XVP(1)))
C
      GV63=(ADD(1,1)+(VL02+AIO*VL0*RR0*AC0)*ADS(1,1))/RR0
      GV53=ADS(1,1)/RR0
      GV61=(ADD(1,2)+(VL2+ARL*AC)*ADS(1,2))/R
      GV51=ADS(1,2)/R
C
      XD3=XD3+GV63*(XJP(1,1)/(AIO*VL0*AC0))-GV53*(XJP(1,1)/ULP0
     1 )*(AIO*VL0*RR0*(R2*AIO*VL0*AC0*EM-D)+(XB3/(AIO*VL0)))
C
      XN3=XN3+GV53*RR0*(AIO*VL0*AC0*XMU1+ULP0*XMU2+XMU3-AIO*VL0
     1 *XMU4+(XB3/(AIO*VL0*RR0))*XMU2)-GV63*(XMU1+(ULP0/(AIO*VL0
     1 *AC0))*XMU2)
C
      XD1=XD1+GV61*R2*(XJP(1,2)/(AIO*VL0*AC))-R2*(VL/(VL0*ULP0))
     1 *GV51*(AIO*VL*RR0*(AIO*VL0*AC*EM-D)+(XB1/(AIO*VL)))*
     1 XJP(1,2)
C
      XN1=XN1-(GV61/VL)*((VL0/R2)*XKA1+BL*XKA2+(ULP0/(AIO*AC))
```

```
     1 *XKA3)-(RR0/VL)*GV51*(AIO*VL2*XKA4-(VL0/R2)*XKA5-BL*XKA6-
     1 AIO*(VL0/R2)*((VL0/R2)*AC*XKA1+BL*AC*XKA2-AIO*ULP0*XKA3)+
     1 AIO*(XB1/RR0)*XKA3)
C      WRITE(4,*) XMU1,XMU2,XMU3,XMU4,XKA1,XKA2,XKA3,XKA4,
C      1 XKA5,XKA6,GV63,GV53,GV61,GV51
       ENDIF
       WRITE(4,*) 'HF3,HF1,SV3,SV1 (N,NP1):'
       WRITE(4,*) HF(N,1),HF(N,2),SV(N,1),SV(N,2)
       WRITE(4,*) HF(NP1,1),HF(NP1,2),SV(NP1,1),SV(NP1,2)
       WRITE(4,*) 'PHI,PSI,3,1:'
       DO 988 J=1,4
       K=J
       IF(J.GT.2) K=N+J-3
       DO 999 I=1,2
       WRITE(4,*) K,',',I,XJS(K,I),XJP(K,I),XJD(K,I),XJT(K,I),
     1 XJQ(K,I),ADS(K,I),ADP(K,I),ADD(K,I)
999    CONTINUE
       WRITE(4,*)
988    CONTINUE
       WRITE(4,*) 'V,VP,VD,VT:J=1,...,5;N-3,...,NP1'
       DO 1047 J=1,10
       K=J
       IF(J.GT.5) K=NP1-10+J
       WRITE(4,*) XVS(K),XVP(K),XVD(K),XVT(K)
1047   CONTINUE
       WRITE(4,*) 'ETA3,ETA1,PRESSURES:'
       WRITE(4,*) AETA3,AETA1,HPREP3,HPREP1
C
       XLAM1=XN1/XD1
       XLAM3=XN3/XD3
       BLAM1=ABS(XLAM1)
       BLAM3=ABS(XLAM3)
       XLAM1A=-AIO*XLAM1*1.7208/(5.0*VL0)
       XLAM3A=AIO*XLAM3*1.7208*VL0/(5.0*VL2)
       BLAM1A=ABS(XLAM1A)
       BLAM3A=ABS(XLAM3A)
       WRITE(6,200) XLAM3,XLAM1,XLAM3A,XLAM1A
       WRITE(4,200) XLAM3,XLAM1,XLAM3A,XLAM1A
200    FORMAT(1X/1X,'Interaction coefficients:',//1X,'a3=',2D15.8,
     12X,'a1=',2D15.8,' (wrt delta)'//1X,
     1'a3=',2D15.8,2X,'a1=',2D15.8,' (wrt delt*)'/)
       WRITE(6,210) BLAM3,BLAM1,BLAM3A,BLAM1A
       WRITE(4,210) BLAM3,BLAM1,BLAM3A,BLAM1A
210    FORMAT(1X/1X,'Moduli:'//1x,'a3=',D11.4,2X,'a1=',D11.4,
     12X,'a3(delt*)=',D11.4,2X,'a1(delt*)=',D11.4/)
       RETURN
       END
C
C
       SUBROUTINE INTEGR(XI,XR1,XR2)
C
C      SOLVABILITY CONDITION.
C
       IMPLICIT COMPLEX*16(A,G,H,S,X),REAL*8(B-F,O-R,T-W,Y,Z)
       DIMENSION XI(3201,2)
       COMMON/PP1/P1,P2,P3,P4,P5,P6,P7,P8/
     1NNW/N,NM1,NP1,W,W2,W3,W4/COQ/AZ,AIO,ARL,ARL3,AC0,AC
C
       XR1=AZ
```

```
      XR2=AZ
      DO 70 I=1,2
      DO 50 J=3,NM1,4
C
      XA=7.0D0*(XI(J-2,I)+XI(J+2,I))+32.0D0*(XI(J-1,I)+XI(J+1,I))
     1 +12.0D0*XI(J,I)
C
      IF(I.EQ.1) XR1=XR1+XA
      IF(I.EQ.2) XR2=XR2+XA
C
50    CONTINUE
70    CONTINUE
      XR1=XR1*P8
      XR2=XR2*P8
      RETURN
      END
```